

The University of Nottingham

UNITED KINGDOM · CHINA · MALAYSIA

DEPARTMENT OF CHEMICAL & ENVIRONMENTAL ENGINEERING

A STUDY INTO THE EFFECTS OF INTRODUCING HYDROTHERMAL CARBONIZATION AS A PRE-TREATMENT STEP IN PRODUCING ACTIVATED CARBON FROM STRAWBERRY, COFFEE, AND SEWAGE WASTES

By

Lewis Tuck

April 2023

Abstract

This study focuses on the activation of wet waste organics, by utilizing hydrothermal carbonization (HTC) as a treatment before steam activating the hydrochars to form activated carbons (AC). The demand for AC is growing which has led to research exploring new carbon-based precursors, like biomass. Wet biomass wastes are an underutilized resource because the drying requirements are expensive and energy intensive. HTC has been highlighted as a treatment solution because it will treat the waste in its current state. HTC produces hydrochars which have a similar structure and composition to coal, the traditional precursor for AC. The hydrochar is anticipated to be a more suitable precursor for activation than the raw biomass.

In this report, the theory has been tested on strawberry pomace (SP), coffee grounds (CG) and sewage sludge (SS). These wet wastes have not previously been converted to hydrochars and physically activated. SP and SS were activated in an industrial HTC pilot plant. The activation of such hydrochars is the first of its kind. Physical activation was selected, as it is the standard industrial approach, to match the scale of production. Steam activation of hydrochars is not well reported and needs more research in this context.

The experimental plan sets out to produce commercial grade AC from the three waste streams, while optimising the reaction conditions to report an operating range. The research produced two successful AC products, with contrasting porosities. SP was found to produce mesoporous carbons. The most successful sample, SP-HTC-ACT-800-1, has a surface area of 1008 m^2/g and pore volume of 0.72 cm^3/g. During a process water sorption study, the material had a higher removal of total organic carbon (51 %) and organic compounds in the UV-visible spectra (99 %) than a commercial coal derived AC. CG was found to produce highly microporous ACs. The highest quality sample, CG-HTC-ACT-850-1, had a surface area of 1344 m^2/g and pore volume of 0.52 cm^3/g. These samples had a 95 % carbon purity and a low ash content. SS was unable to produce samples recognised as ACs. The material is still recommended for HTC. The study has compared the activation pathways of raw and pre-treated samples and concluded that HTC pre-treatment does produce a higher quality AC and it is necessary to effectively activate the materials.

As a treatment method, the steam activation of hydrochar was found to be effective in producing activated carbon. The key parameters have been evaluated and optimised throughout this paper. The balance is ensuring a quality activated carbon was produced, indicated by high surface area and pore volume, while minimising the losses associated with the process to maximise the yield. The concept of hydrothermal carbonization followed by steam activation provides value and sustainability for wet waste.

Acknowledgements

Firstly, I would like to acknowledge the funding provided by the UKEPSRC. Special thanks to Professor Colin Snape, for his guidance, knowledge, and patience in the completion of the project. I am deeply indebted to Dr. Lee Stevens for his efforts and support during the critical stages of the project. I believe the project would not have been successful without your endeavours. I would like to thank all the staff at UoN who tirelessly worked throughout the COVID-19 pandemic to keep the university open and facilitate research like this. I'd like to express thanks to my colleagues Dr. Xin Liu and Mr. Adrian Quinn at the ETB for their assistance and practicality.

I'm grateful for the team at Antaco for their financial support and entrusting me with their project. I hope this research adds value to your mission. Thanks also goes to the University of Surrey Chemical Engineering department, particularly Dr. Judy Lee, for accommodating me. There I had the pleasure of collaborating with Dr. Oliver Crossley and Dr. Bethany Campbell.

I'd like to express gratitude to my family. Without their encouragement, motivation, and the stability they provided, I would not have been equipped to pursue a project of this nature.

Finally, to my partner Lucy, thank you for everything. It's over. Now we can start our life.

Table of Contents

1 Introduction 1
1.1 The Broader Context 1
1.2 Changing Our Perspective on Waste 1
1.3 Disposal Mechanisms for Biomass 2
1.4 Defining the Problem 3
2 Aims and Objectives 4
2.1 Statement of Novelty 6
3 Literature Review 7
3.1 Activated Carbon 7
3.1.1 What is Activated Carbon? 7
3.1.2 The Building Blocks of Activated Carbon 7
3.1.3 Varieties of Commercially Available Activated Carbon 12
3.1.4 Modern Applications of the Product 14
3.1.5 The Global Market 18
3.1.6 Activation: The Formation Process 19
3.1.7 Core Methods of Activation 21
3.1.8 Activation Parameters: The Impact of the Conditions 23
3.1.9 Importance of the Precursor Materials 24
3.2 Hydrothermal Carbonization 25
3.2.1 What is Hydrothermal Cabonization? 25
3.2.2 Background of the Chemical Process 26
3.2.3 The Hydrochar Product 27
3.2.4 Applications of Hydrochar 29
3.2.5 The Array of Precursor Materials 31
3.2.6 The Crucial Carbonization Mechanism 33
3.2.7 Process Parameters: The Impact of the Conditions 36
3.3 The Introduction of Activated Hydrochar 39
3.4 Materials in this Body of Work 41
3.4.1 Coffee Grounds 43
3.4.2 Sewage Sludge 46
3.4.3 Strawberry Pomace 49
3.4.4 Summary 50
4 Methodology 52

4.1 Sample Selection 52
4.1.1 Strawberry Pomace (SP) 52
4.1.2 Coffee Grounds (CG) 53
4.1.3 Sewage Sludge (SS) 54
4.1.4 Sample Key 54
4.2 Hydrothermal Carbonization 54
4.2.1 The HTC Pilot Plant 54
4.2.2 The Laboratory Scale HTC Reactor 56
4.3 Horizontal Tube Furnace 58
4.3.1 Activation Process 58
4.3.2 Activating Agent 58
4.3.3 Activation Conditions 59
4.3.4 Apparatus 60
4.3.5 Test Variations 62
4.4 Characterization Techniques 64
4.4.1 Textural Characterisation 64
4.4.2 Thermogravimetric Analyser (TGA) 70
4.4.3 Elemental Analysis (EA) 71
4.4.4 Helium Pycnometry 71
4.4.5 Mercury Intrusion Porosimetry (MIP) 73
4.4.6 X-Ray Photoelectron Spectroscopy 74
4.4.7 Scanning Electron Microscopy (SEM) 75
4.4.8 Transmission Electron Microscopy (TEM) 75
4.4.9 Adsorption of Organic Material from HTC Process Water with AC 75
4.4.10 Bomb Calorimeter 76
5 Results & Discussion 78
5.1 Strawberry pomace 78
5.1.1 SP HTC Pre-Treatment 78
5.1.2 SP Independent Pyrolysis Tests 80
5.1.3 SP Activation Tests 82
5.1.4 SP Activation Yield 83
5.1.5 SP Chemical Composition 89
5.1.6 SP Textural Properties 96
5.1.7 SP Raw Activation Tests 104
5.1.8 SP Key Samples Detailed Characterization 108
5.1.9 Summary 124

5.2 Coffee Grounds 127
5.2.1 CG HTC Pre-Treatment 127
5.2.2 CG Independent Pyrolysis Tests 130
5.2.3 CG Activation Yield 130
5.2.4 CG Chemical Composition 136
5.2.5 CG Textural Properties 140
5.2.6 CG Raw Activation Tests 146
5.2.7 HTC Pre-Treatment Temperature Alteration 150
5.2.8 CG Key Sample Detailed Characterization 152
5.2.9 Summary 162
5.3 Sewage Sludge 164
5.3.1 The Context for Sewage Sludge Research 164
5.3.2 SS HTC Pre-Treatment 164
5.3.3 SS Activation Analysis 165
5.3.4 SS Textural Analysis 169
5.3.5 SS Detailed Characterization 175
5.3.6 SS Summary 177
5.4 Application Test: Adsorption of Organic Material from HTC Process Water with Activated Hydrochars 180
5.5 Discussion 182
5.6 Closing Remarks 194
6 Conclusion 195
7 Further Work 196
7.1 Narrow experimental range for optimisation 196
7.2 The impact of the HTC pilot plant versus the batch reactor 196
7.3 HTC pre-treatment temperature adjustment 196
7.4 The role of sample preparation through pelletization 196
7.5 Test raw materials at less severe conditions (Chemical Activation) 196
8 References 197
9 Appendix 224

1 Introduction

1.1 The Broader Context

Life creates waste, through actions, consumption, and degradation. It has always been this way, but a combination of rapid urbanization, population growth, and changed behaviour towards disposal, has accelerated the quantity of waste produced annually. The infrastructure to deal with such volumes has not kept up with the growth (Singh et al., 2014). Therefore, resource management is key in becoming more sustainable and rectifying this problem. This was acknowledged by the UK government who enforced recycling laws in 2003. According to a 2020 report from the UK department for Environment, Food & Rural Affairs, in 2016 the UK alone produced 221 million tonnes of waste, a 1.5 % annual growth trend despite efforts to manage it (DEFRA, 2020). The issue is global and not all countries have the resources to focus on waste management. During 2016 the global production of municipal solid waste (MSW) was 2.01 billion tonnes, and it was estimated that at least a third was unmanaged. Recent predictions expect the global output to be greater than 3.4 billion tonnes by 2050. Currently, the waste per capita varies widely between 0.11 kg per day against 4.54 kg per day, with an imbalance in high income nations producing greater amounts of waste (Kaza et al., 2018). There is a correlation between economic growth and waste production. Therefore, it is an issue we must address now, as more nations develop this may exacerbate the issue further.

The manufacture of a desired product will usually form side products during production, transportation, packaging, or usage. In some cases, a secondary product can be utilised independently. As an example, coal fired power stations will create greenhouse gases, fly ash and boiler slag, but the liberated heat is the useful product. Fly ash can be repurposed for gypsum and cement, despite not being the intended product. But often by-products are redundant. Overall, only 40 % of the waste from this process can be recycled as usable products (Telesca et al., 2013). Improving a procedures efficiency can reduce the output of unwanted materials but ultimately, the formation of waste is inevitable. Without a specific use, the waste must be disposed. If the material poses a threat, due to toxicity or biologically active pathogens, the waste must undergo treatment processes before it can be legally released. Upon treatment, much of the waste is disposed of in landfill. Currently 24.4 % of UK waste is sent to landfill (DEFRA, 2020). This occupies valuable space, as the amount of waste continues to accumulate and degrade slowly. Overall, it is a costly process which disposes of the material but retrieves minor value from the material.

1.2 Changing Our Perspective on Waste

Materials considered to be waste is a broad spectrum. They can be classified based on the original source such as industrial wastes, agricultural waste, construction waste, MSW, electrical waste, medical waste, among others (Demirbas, 2011). This study will focus on organic waste materials. Almost 50 % of the total global waste is organic material (Pawar et al., 2021). That is waste derived from living matter which is biodegradable such as food waste, garden waste, manure, slaughterhouse waste or paper waste. The term ‘waste’ is defined as being substance or object which the holder discards, intends to discard or is required to discard (Che, 2002). This is usually after the primary use has rendered it worthless or defective. The definition shows the label is affixed to an object based on the holding party’s consensus of value. Therefore, the definition of waste is flexible and can change based on perspectives governed by the user’s priorities. Thus, the vast quantities of waste can be viewed as a resource. Waste streams need to be managed to identify waste

materials which have greater value than initially perceived so it can be recovered and utilized.

Waste is a potential feedstock for energy recovery, construction materials, fertilizer, carbon sequestration or complex polymerised materials (He, Sun & Han, 2013), (Su, 2020). Utilising the material is effectively protecting the environment and health of those nearby to the waste disposal site, as well as recovering valuable resources. The incentivisation of repurposing waste will promote careful disposal and educate holders to recognise the value within a waste stream. Promoting reuse, recovery, and recycling moves closer towards a circular economy. This is where the value of a product, material, or resource is maintained in the economy for as long as possible, and the generation of waste is minimised (Van Ewijk & Stegemann, 2020). The aim is that resources are repeatedly used, as opposed to consumed, and permanently retain their value. Small cycles can begin through the continual reuse of materials but implementing this system on a large scale requires commitment at all levels of society, re-evaluating values by changing consumer behaviours and business models (Rosiek, 2020). This study has identified three organic waste materials with the potential to be repurposed as higher value products.

1.3 Disposal Mechanisms for Biomass

There are many processes for the disposal of organic waste. Waste can be sent to landfill, although this is unlikely for organic materials. It is more likely to be composted where it can be used as a fertilizer. The degradation process naturally releases carbon dioxide to the atmosphere. Biomass is often used for energy production. The most obvious solution is direct combustion. This is usually practiced on wood, agricultural residues, and animal waste. The process forms heat which can be used to generate electricity. The composition of biomass can vary greatly, leading to unstable burning conditions. The peak temperature and ignition temperatures are much lower than coal. Unfortunately, the material has a high volatile content, a low bulk density and offers a relatively low heating value, contributing to a less successful burn. The pollutants emitted are much lower than coal, however it does emit fly ash and more particulate matter. The remaining ash causes issues of corrosion, slagging and fouling from contaminants in the raw material (Demirbas, 2005). Materials can be compressed to increase density or cofired with coal to reduce emissions.

Thermo-chemical conversion processes can be used to enhance biomass as a fuel prior to combustion. Pyrolysis is the thermal decomposition of organic materials in the absence of oxygen. This can be used to create solid, liquid, and gaseous fuels. Conventional pyrolysis occurs between 300 – 800 °C and flash pyrolysis can happen above 1000 °C, using a faster heating rate (Demirbas & Arin, 2010). Slower pyrolysis will favour gas production, consisting of hydrogen and carbon monoxide. Both fast and flash pyrolysis produce a greater liquid fraction, known as a bio-oil. The remaining char is carbonized, meaning it has a much greater carbon percentage (Dhyani & Bhaskar, 2018). The process is like torrefaction and is best carried out on materials with high lignin content i.e., wood. Torrefaction increases the carbon fraction in wood at milder temperaturae than pyrolysis and is used when prioritising the yield of solid product (Van der Stelt et al., 2011). Gasification is another fuel conversion technique. It is performed at higher temperatures than pyrolysis, to partially oxidise the biomass. This produces a gaseous product rich in hydrogen and methane which can be used as a fuel, known as syngas. The fuel stream can be polluted by sulphur and nitrogen compounds as well as contaminants like alkali metals, adding the need for more cleaning stages (Liu, Chmely & Abdoulmoumine, 2017). All these thermo-chemical processes require

the material prerequisite in a dry state. Wet material will not spontaneously react, and combustion efficiency will be lower and so it must be dried before processing, which is costly and energy intensive. Hydrothermal carbonization (HTC) is an emerging thermo-chemical conversion technique which uses the moisture content in a closed system to increase the pressure and conversion takes place at a relatively low temperature.

There are other technologies for high moisture wastes. Biochemical conversions accept the material as a wet waste. One such example is fermentation which produces bioethanol. This can use fermentation agents such as yeast to ferment the starch in biomass and bacteria break down the cellulose fraction (Hossain, Zaini & Mahlia, 2017). Materials high in sugars and starch are ideal for this process. Another biochemical conversion is anaerobic digestion. This process converts the biomass to biogas, a mixture of methane and carbon dioxide. This is aided by anaerobic bacteria in the absence of oxygen (Saidur et al., 2011). The process also creates a great deal of thermal energy which can be utilized. This technology is perfect for material such as sewage sludge and algae which have a very high liquid content (Ward, Lewis & Green, 2014). Drawbacks to these processes is that they are time consuming and requires large amounts of space to complete the reactions.

1.4 Defining the Problem

It is known that large quantities of waste are being produced annually and the trend is set to increase. In an effort to stop waste accumulating and conserve resources, many treatment options have been developed and are being executed continuously. However, wet waste sources have often been overlooked for conversion into higher value products. This is because of the energy requirements for drying, and the fiscal costs associated, are too high to be economically feasible. The energy recovered from these materials is often countered by the drying process itself. Current wet waste treatment options are available, but drawbacks include long residence times and large space requirements.

Hydrothermal carbonization (HTC) has been identified as a key technology for treating wet waste. Respective to other treatment techniques it offers a fast, effective, cheap, and low energy handling option for all forms of biomass. If used optimally it could be a long-term solution for the diversion of organics from landfill and the creation of energy from waste. It can be utilized specifically to target the wet waste bracket. The resulting product, known as hydrochar, is an effective coal substitute, but as a highly carbonaceous substance it has many other uses. One of the issues facing hydrothermal carbonization is the production and contamination of process water. Before it can be discharged, it must be thoroughly cleaned to remove contaminants and pollutants. This is done through various filtration techniques. A commonly used adsorbent in this instance is activated carbon.

The production of activated carbon is a vast and growing market. One issue presently encountered by the industry is that it is hindered by production costs. It is typically made from fossil coal, an expensive, finite resource which requires destructive extraction techniques. Following this, organic waste is being investigated as an alternative precursor, due to its carbonaceous nature. If the hydrochar can be a substitute for coal, then surely activated carbon is an ideal higher value product to convert the hydrochar into. Thus, it is proposed that wet organic waste materials will be converted into activated carbon for the treatment of HTC process water. This will form an insular circular economy, where the activated carbon product can be used to treat the by-product formed during the HTC treatment stage.

2 Aims and Objectives

This research project aims to produce consumer grade activated carbon from major sources of wet organic waste which have been pre-treated with HTC. This is with a view that the methodology could conceivably be scaled and applied post HTC as a direct use for hydrochar. This work aims to promote HTC as a more desirable solution to the growing problem of waste disposal. The work will build upon the existing knowledge of activating hydrochars, with unused combinations of materials and production methods. The purpose of the activated carbon product is twofold. It will have potential to serve as a secondary market for the HTC manufacturers. Alternatively, it could be applied in treating the wastewater produced as a by-product from the HTC process. The project expects to show the benefits of using HTC as a pre-treatment far outweigh the drawbacks.

The major research objectives in this study are listed below:

- **To produce hydrochar samples from a continuous HTC process using the patented process and plant of Antaco Ltd.**

- **To validate the effectiveness of physical activation by producing consumer grade activated carbon. This will be decided by detailed analysis and comparison with commercial grade activated carbons**

- **To find an optimum window for the activation process conditions, balancing the product quality with the material losses by altering the key parameters**

- **To show the activation process is enhanced by the introduction of an HTC pre-treatment by activating with and without the HTC step**

- **To identify and characterize the material types created in the experimentation**

- **To demonstrate the commercial viability of the process through the application of the activated carbon as an adsorbent, mass balances and basic technoeconomic studies**

Scope of works:

The scope of the methodology will focus the study on the parameters which are deemed to have the most impact on activation: time and temperature. Additional variables would not be possible under the time constraints. The time and temperature will be varied across a range considered suitable for activation. A total of four materials were tested and three have been included in this thesis.

Due to the industrial nature of the sample collection, it would not be possible to accurately vary the HTC pre-treatment phase. So, a single condition will be used, and the samples will all be collected at the same time.

The analysis of the produced samples will concentrate on characterization methods showing surface area, pore volume, material density, chemical constituents and structure, as these are integral in understanding the type and quality of activated carbon produced.

Due to constraints imposed by the 2020 pandemics, a select group of samples were used for all analysis.

The literature will be reviewed in Chapter 3, from the larger aspects narrowing down to specifics, which encompasses activated carbon and the HTC process. This will describe the structure of the materials, the production methods, mechanisms, and process parameters. This will incorporate real-world applications and the wider value. The chapter will then move on to describe the materials selected, how they were sourced and previous examples of studies on them, including the knowledge gaps.

Chapter 4 will introduce the methodology, equipment used and testing matrix. This will specify the sample origins, pre-treatment processes and activation. Beyond that, Chapter 5 will present the results before a discussion on the findings, including potential uses, reviewing the method and selecting the optimum activation conditions. The conclusions in Chapter 6 will decide whether the hypothesis has been proven correct and Chapter 7 will review the process and show what is next for the study through a future work section.

Firstly, a prologue to the literature review which shows all the aspects which make this work novel.

2.1 Statement of Novelty

Hydrothermal carbonization is an old technology which has recently gathered attention for its potential application in the energy from waste sector. As a burgeoning industry, there are very few commercial scale HTC plants in the world. One of these large-scale systems will be operated to produce hydrochar samples for this project. This will be considered as a pre-treatment step. This project will be the first to use industrially sourced hydrochar samples as a precursor for activation.

Throughout the study, it has been noted that there is limited work on hydrochars as precursors to activated carbon. Due to the broad categorisation of wet waste and the differing characteristics of each material, many specific waste sources are yet to be tested in HTC activation. Based on the gaps in the literature, three materials have been identified to have the potential to be successful in the HTC activation process. Each has certain desirable qualities as a feedstock for both HTC and activation. An important area that has not been examined is the use of physical activation on these samples. Following an established method previously practiced on raw biomass, and introducing an HTC pre-treatment, could lead to a significantly improved activation process for the biomass.

Physical activation with steam is the most direct activation treatment which is already used at scale in industry. Despite physical activation being the primary method for virtually all commercially produced activated carbon, there is a tendency for laboratory studies of activating hydrochars to favour using chemical activation, due to the superior yield and surface areas demonstrated. This study intends to focus on physical activation with the vision that the activation process could be set up directly after an industrial HTC plant, if the study is deemed to be successful. So, this study aims to show physical activation as a viable technique for converting the selected wet wastes into activated carbon.

Following on from this, it has been acknowledged that there is a lack of activation condition studies when activating hydrochar using physical activation. Process parameters, such as time and temperature, have a direct effect on the quality of activated carbon produced, outlined in section 2.1.9. The consideration will account for carbon losses and the activated carbons functionality. For this, the project will introduce a systematic testing regime to optimise and assess the key parameters and report on the most effective. The testing matrix designed can be found in Section 4.3.3.

Overall, from the literature reviewed, HTC combined with activation is an emerging topic. Thus far, there are few detailed studies which have compared the difference between activating biomass with and without an HTC pre-treatment step. This study will establish a carbon yield across the whole process to indicate whether the added step is more efficient overall. It will also determine whether a higher quality activated carbon can be developed using the technique.

3 Literature Review

3.1 Activated Carbon

3.1.1 What is Activated Carbon?

Activated carbon is a form of highly porous material. The fine structure is comprised of approximately 90 % carbon on a dry basis (Cecen, 2014). It is commonly created through the activation of carbonaceous materials such as anthracite, bitumen and other forms of charcoal, lignite, peat, wood, and coconut shells (González-García, 2017). More alternative materials have been trialled such as agricultural and industrial waste streams. These are selected for their low cost, abundance, and lack of applications. Examples include bagasse, fruit stones, nut shells and bones among other biomasses, as environmentally conscious prospects (Heidarinejad et al., 2020). An activated carbon can be formed as a powder, granule, rod, sphere, or fibre. The most commonly used varieties are powdered activated carbon (PAC) and granular activated carbon (GAC). They are selected for their simple manufacturing process, ease of use and versatility in adsorbing liquid and gas contaminants from different phases. The most desirable part of an activated carbon is the porosity. These voids are formed internally between pseudo-graphitic domains. They exist in the raw material but are developed more during the activation process. The amorphous carbon material is comprised of a network of openings which interconnect inside the substance. These pores have a non-uniform shape and can have effective diameters lower than 1 nm. Based on this, activated carbons are known to have a surface area per unit weight which far exceeds the exterior surface area (Kaneko et al., 1992). The large surface area gives the material functionality for a diverse range of applications including adsorption, absorption, filtration, and storage. The inner surface becomes an active site for chemical reactions and attractive forces. The pore size distribution affects the performance of the product and the applications it is suitable for.

The properties of the final product are dictated by the selected starting material, the activation conditions and choice of activation agent. The materials quality is measured by surface area, pore volume and pore size distribution, because they are strong indicators of the adsorptive capacity. Commonly used commercial activated carbons have a specific surface area between 800 to 1500 m^2/g. However, experiments have shown materials that exceeded 3000 m^2/g in some instances (Kierzek et al., 2004), (Otowa, Tanibata & Itoh, 1993). It is also reported that standard activated carbons possess a total pore volume of 0.20 to 0.60 cm^3/g. Again, experimental procedures have recorded materials which have a much larger volume, with some exceeding 1.0 cm^3/g (Bansal & Goyal, 2005). Other factors to impact the functionality include pore texture, surface functionality, bulk density, and skeletal density (Stevenson, Leckie & Eliassen, 1972). The variation between different activated carbons makes them a fascinating material to explore.

3.1.2 The Building Blocks of Activated Carbon

3.1.2.1 The Elemental Balance

The composition of activated carbon primarily carbon. This constituent tends to make up 85 to 95 % of the material mass, although this is influenced by a combination of the oxygen and ash content. It is desirable to have a high carbon fraction, which gives a greater potential for porosity and a strong, well-connected structure. The carbon atoms make up the pore walls to form a disorganised structure. The second largest component is oxygen, at around 5 %.

During activation, oxygen, among other heteroatoms, can bond to the AC to form functional groups which are essential in the adsorptive properties of the material (Gottipati, 2012). The rest is made up of small fractions of hydrogen, nitrogen, sulphur, and ash. The ash content will differ depending on the precursor. Ash is not removed during activation; instead, the mass fraction will increase as the other components are removed (Bansal & Goyal, 2005). Thus, precursors for high quality activated carbons will have a low initial ash content; creating a final product which has a higher carbon purity. He et al. (2012) proved coal tar pitch to be a strong precursor for quality activated carbon because of a high fixed carbon content and a low initial ash content. A high percentage of the original carbon was retained in the final product, leading to a high carbon yield. Many of the non-carbon impurities were removed and the ash fraction began very low so the proportion in the final product was not significant. The final composition is a direct result of the starting material and any treatments undergone before or during activation.

3.1.2.2 The Physical Structure

Carbon can form multiple allotropes based on the bonding orientation. The overall shape and arrangement of carbon atoms is an identifying feature are distinguished in Figure 3.1. Firstly, a graphene layer can be seen, this is recognized by the sp2 bonding structure. Each carbon atom bonds to 3 other carbon atoms through σ-bonds or π-bonds, creating a regular hexagonal structure. Fullerenes follow a similar bonding pattern but create spheres or tubes instead of sheets. Oppositely, the presence of a bond in the third (c-) direction leads to tetrahedral structures of diamond, where all outer electrons are bonded, which is characteristic of a graphitic carbon. (Rodriguez-Reinoso & Sepulveda-Escribano, 2001). The physical structure of an activated carbon is integral to its adsorption properties and separates it from other solid carbon allotropes. It was first noted by Rosalind Franklin (1951) that the structure of carbons formed during pyrolysis is not only dependent on the temperature, but to a large extent, the structure of the starting material. She distinguished that carbon materials formed by pyrolysis can be separated into two distinct and well-defined classes: graphitizing carbons and non-graphitizing carbons, which can be seen on the left following on from graphite in Figure 3.1.

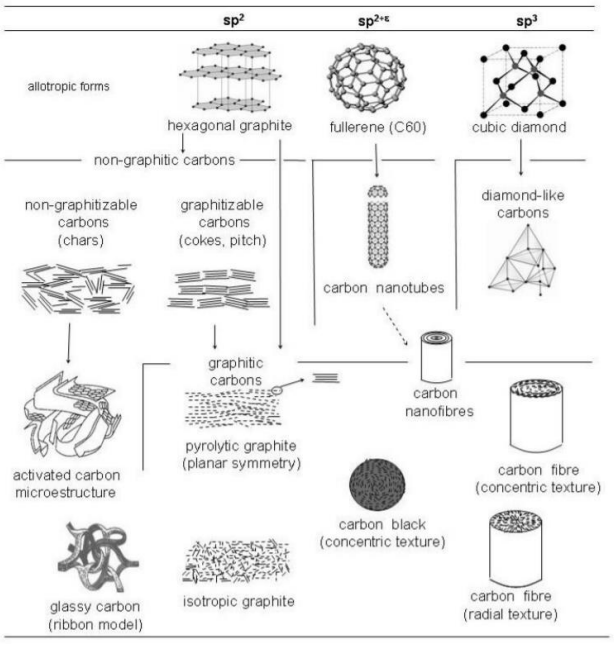

Figure 3.1 Infographic demonstrating the classification of carbon materials (Diaz & Martin-Gullon, 2006)

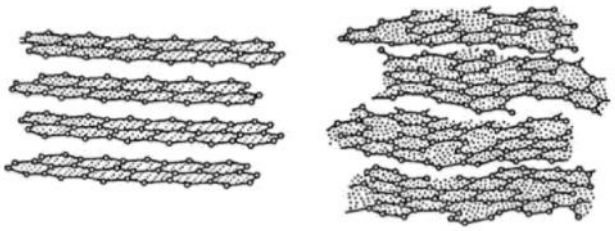

Figure 3.2 a) Elementary graphene crystal, b) Turbostratic carbon (Jurkiewicz, Pawlyta & Burian, 2018)

The arrangement of the graphene layers can differ between materials based on the level of disorder between layers. This is demonstrated in the image above, where in Figure 3.2a is arranged in an orderly formation, whereas the Figure 3.2b is less ordered. Graphite is well ordered and shows parallel stacking, as seen in the left image. The layers are held in the third direction through weak Van der Waal forces. This is termed as an elementary graphite crystal. This makes the structure soft, dense, and non-porous. In contrast, the layers in chars cover a smaller area and they tend to be more randomly orientated, overlapping in irregular patterns. This can be seen in the image on the right. The layers in chars are disrupted by other carbon structures, heteroatoms, and impurities such as hydrocarbons, oxygen, and ash. This is termed as a turbostratic arrangement (Bansal & Goyal, 2005). The difference in organisation can be seen through the interlayer spacing. Graphite has 0.335 nm between layers but in chars it is larger, ranging between 0.34 – 0.35 nm, leaving greater space for other materials or porous gaps (Diaz & Martin-Gullon, 2006).

Non graphitic carbons have graphite layers in parallel groups but are not oriented in the crystalline structure of graphite. Non-graphitic carbons are separated into graphitizable and non-graphitizable carbons. The difference is seen in the structure as heat is applied to the material, particularly in the early phases of carbonization. In non-graphitizing carbons a strong system of cross-linking forms which unites the crystallites. This leads to a random orientation of the crystallites in a ridged unit. The voids between the crystalline structure hereby become the pores in the activated carbon. At higher temperatures the growth is impeded by both the strong cross-linking between neighbouring crystallites and by their random orientation, forming hard carbons. Non-graphitizing, isotropic, carbons are distinguishable as being hard, having a low density and displaying high levels of porosity (Marsh & Rodriguez-Reinoso, 2006). When comparing the images in Figure 3.3, the right image has more gaps which translates to a greater porosity. Some materials will not produce graphite no matter the temperature applied to them, and under no temperature can a non-graphitizing carbon be transformed into crystalline graphite.

However, graphitizing, anisotropic, soft carbons can be transformed into crystalline graphite by heating to temperatures up to 3000 °C. In graphitizing carbons, the cross linking is seen to be much weaker than in non-graphitizing carbons, and the structure is more compact. Based on this starting position of layer planes, they can gradually be displaced, causing crystallite growth. So as the material is heated the adjacent crystallites have a strong tendency to lie in nearly parallel orientation, which shows similarity with to the structure of graphite. The regular stacking begins to exhibit a three-dimensional structure.

Where the three-dimensional graphite structure is partially formed, the material is known as a graphitic carbon.

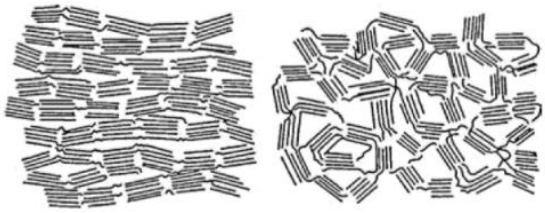

Figure 3.3 left) Graphitizing carbon, right) non-graphitizing carbon (Franklin, 1951)

Therefore, it is established that activated carbons are non-graphitic, turbostratic, and non-graphitizing carbons. The carbon structure inside activated carbon present in two forms. The first is a non-crystalline, amorphous carbon which is characteristically disorganised. This is interspersed between a microcrystalline aromatic structure which is well ordered. These planes are arranged randomly in space, so despite the uniformity of these aromatic rings, the overall structure has a highly disordered microcrystalline structure with the voids between the small pseudo-graphitic nanodomains. These voids are known as pores and this very nature causes the material to exhibit porosity.

3.1.2.3 The Porous Nature

Pores are formed from the voids between the carbonaceous framework. The porosity in activated carbon allows it to perform many actions such as adsorption, separation, and storage. These pores can be categorised by size. The main classifications are microporous, mesoporous and macroporous. A pore diameter is the average width between the pore walls, as they are not always uniform in shape. The classification and size can be seen below in Table 3.1.

Table 3.1 Effective pore diameter classification (Thommes et al., 2015)

Classification	Macropore	Mesopore	Micropore	Super-micropore	Ultra-micropore	Sub-micropore
IUPAC (2015)	> 50 nm	2 – 50 nm	< 2 nm	0.7 – 2 nm	< 0.7 nm	< 0.4 nm

Micropores are the smallest pores. They have an effective diameter less than 2 nm. Sub denominations of micropores exist and can be broken down into super-micropores (2 – 0.7 nm), ultra-micropores (< 0.7 nm) and sub-micropores (< 0.4 nm). Adsorption in micropores takes place through micropore filling. The pores are molecular sized, so they bulk fill with adsorbate. This is known as physical adsorption (Gregg & Sing, 1982). The pores are so small that the adsorption is equivalent to a monolayer. The micropores can contribute up to 95 % of the internal surface area. The mesoporous region, less than 50 nm but greater than 2 nm, is a site of adsorption due to the strong attractive forces, although they are weaker than those exhibited in micropores (Dubinin, 1989). Mesopores contribute the largest part of the internal volume. Adsorption happens here through capillary condensation, filling monolayered at first then multi-layered thereafter. In larger mesopores the accumulation of adsorbate forms a condensate (Fomkin & Petukhova, 2020). Mesopores also act as a transport route for the adsorbate to the entrance of micropores. The largest pore sizes are macropores. These pores are greater than 50 nm. They impact the adsorption kinetics and predominantly act as transport networks. They direct molecules toward the smaller channels and voids, thus controlling the diffusion rate (Lehmann & Joseph, 2009).

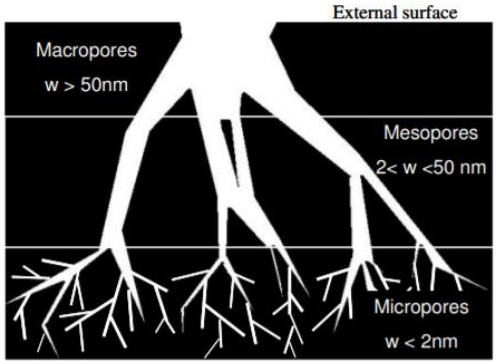

Figure 3.4 Cross section of pores (Diaz & Martin-Gullon, 2006)

Usually, the pores connected to the external surface structure are macropores. Deeper into the structure they branch into mesopores. Beyond this, micropores are offshoots from the mesopores. This network is demonstrated in Figure 3.4. There can be closed pores within the internal structure which have no connection to the outer surface. In powdered activated carbons, the micropores are positioned closer to the surface which increases the adsorption rate. Micropores are useful for adsorbing small molecules like gases and vapours. Adsorption in a micropore occurs at a low relative pressure due to the narrow pore diameter and proximity between the adsorbate and the pore walls when it enters the pore. Alternatively, mesopores are useful for adsorbing solutes from solution (Marsh & Rodriguez-Reinoso, 2006). It is understood that a varied distribution of interconnected pores is required to maintain the transportation of the adsorbate throughout the structure (Kyotani, 2003). It also allows a porous medium to adsorb a wider range of molecule sizes. The pore size range of an adsorbent can be tailored depending on the size of the target adsorbate. For high performance electrodes in supercapacitors an effective combination of micropores and mesopores is needed (Negara et al., 2019). The various pore sizes are also categorised by shape. As per the Kaneko classification shown in Figure 3.5 (Kaneko, 1994), pore geometry is varied and exist as cylinders (a), cones (b), slits (c) ink bottles (d) and spherical pores (e). Ink bottle shaped pores can also develop within slit and cone shaped openings.

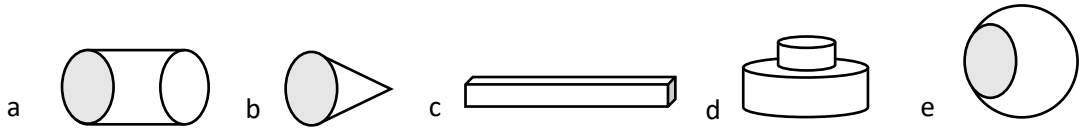

Figure 3.5 Pore shapes (Kaneko, 1994)

3.1.2.4 The Surface Functionality

The adsorption properties of an activated carbon can be influenced by the surface chemistry. The non-carbon constituents present on the external surface can improve functionality, for example in surface reactions or catalysis, with constituents such as platinum, nickel and iron (Jüntgen, 1986), (Kang, Bae & Lee, 2005), (Lam et al., 2017). Carbon atoms positioned at the edge of the broken microcrystalline sheets, as described in Section 2.1.2.2, have unpaired electrons which are highly reactive. They will interact with heteroatoms like oxygen, hydrogen, nitrogen, and sulphur during the activation. These elements can come from the precursor or can be added through a doping agent. The resulting groups are known as surface complexes.

Oxygen is the most abundant heteroatom. It reacts to create groups such as carboxyls, phenols, lactones, quinones and carbonyls, among others (Rodriguez-Reinoso & Sepulveda-Escribano, 2001). The additional complexes can influence surface behaviour, wettability, electrical and catalytic properties (Gottipati, 2012). Most oxygen surface species are acidic, such as carboxyls and lactones. These can partake in surface reactions, which are complex and heavily influenced by the surface chemistry and adsorbate. For example, the acidic surface oxides allow the material to interact with polar and ionic absorbates like heavy metals, which it previously could not react with. It also reduces the hydrophobic nature of activated carbon, allowing it to bond with hydrogen atoms in water (Cecen, 2014). However, acidic functional groups are found to reduce the adsorption of materials such as phenols. Carboxyls were found to hinder p-nitrophenol adsorption whereas carbonyls enhanced it. Without the presence of oxygen, a carbon can form basic sites through delocalised electrons, which are greater at adsorbing phenolic groups (Tessmer, Vidic & Uranowski, 1997). Nitrogen heteroatoms can also form surface functional groups. This also influences the surface characteristics and affinities for certain substances. These functional groups can attract hydrogen sulphide (Travlou et al., 2016). So, although these additional complexes are minor in terms of quantity, they can improve adsorption capacity by targeting new adsorbates that would otherwise be unable to be adsorbed. However, it can also block the adsorption of other adsorbates.

3.1.3 Varieties of Commercially Available Activated Carbon

3.1.3.1 Powdered Activated Carbon (PAC)

The powder form is identified by having a particle size less than 0.1 mm. The average size tends to be 0.015 to 0.025 mm (Diaz & Martin-Gullon, 2006). In PACs the micropores are closer to the surface, which increases the adsorption rate and allows the process to achieve equilibrium faster (Negara et al., 2019). The pressure-drop required for adsorption increases when smaller particles are targeted. The geometry and capacity of PAC particles tends to be more homogenous than GAC particles. It is commonly used for dye removal, wastewater treatment and flue gas cleaning. It can be used in both batch and continuous processes. PAC is small enough to be mixed or elutriated into a contaminated medium to maximise contact time, as opposed to being held in a fixed bed. In this process the PAC is filtered out at the end for disposal or recovery.

3.1.3.2 Granular Activated Carbon (GAC)

The granular form has a particle size between 1 to 5 mm (Diaz & Martin-Gullon, 2006). In GACs the micropores are offshoots from the mesopores, which in turn connect to the macropores, as seen previously in Figure 3.4. It requires all three pore types to transport the adsorbate medium to the active sites (Rodriguez-Reinoso & Sepulveda-Escribano, 2001). The typical application is in gas adsorption, but it can be used in liquids as well. It is used in continuous processes and is held in place by a fixed or packed bed. The adsorption in GAC requires a lower pressure drop than PAC. The particles are generally stronger than PAC and have the benefit of a regeneration process to prolong use. Upon manufacturing GAC, particles which are smaller than 1 mm are regarded as broken GAC and can be crushed into PAC (Gottipati, 2012).

3.1.3.3 Extruded & Pelletized Activated Carbon (EAC)

These are variations of GAC where the product has been formed in specific shapes. The extruded form is elongated and shaped into long cylinders. The pelletised form is pressed into tablets. It is often formed with a combination of binders to hold the desired shape

during activation (Gottipati, 2012). Natural binders such as resins, waxes or cellulose can be utilized for this application. They are beneficial as sustainable low-cost materials with few pollutants (Bueno et al., 2021). However, binders made from polymers and polymerised ionic liquids have been synthesised for specific purposes due to their versatile physicochemical properties. This opens the scope of potential applications such as enzymatic reactions, thermally driven vapour adsorption and capture and separation of CO_2 (Pal et al., 2017). One example used graphene oxide as a binder in a supercapacitor. The graphene was able to hold the material in place, but also assisted the application through its conductive nature (Galhena et al., 2018).

3.1.3.4 Activated Carbon Fibres (ACF)

The fibre alternative is formed by in a similar way to carbon fibre. It is commonly made from carbon fibre precursors such as rayon, cellulose fibres and polyacrylonitrile for insulation and filtration (Jäger et al., 2010). The fibres are first spun before being heat treated in an oxidizing atmosphere to stabilize the material. It then undergoes a carbonisation and activation phase like other AC manufacturing. It is an area of interest for its flexibility, fast adsorption rate, high thermal and electrical conductivities (Suzuki, 1993). ACFs are also used for common activated carbon applications like gas separation, recovering solvents and as a catalyst support (Marsh & Rodriguez-Reinoso, 2006). The fabric has a higher contact area than GACs and is predominantly microporous with low mesoporosity and no macroporosity (Diaz & Martin-Gullon, 2006). The thin fibre shape aids fast intraparticle adsorption kinetics compared to GAC or PAC, but the mechanical properties can be limited by the activation conditions and precursor. The cost associated with the production and precursor is much higher than other microporous materials which has limited the widespread usage (Won et al., 2020).

3.1.3.5 Other Forms of Activated Carbon

Bead activated carbons (BAC), activated carbon cloths (ACC), spherical activated carbons (SAC), and activated carbon monoliths, are produced for more niche applications (Rodriguez-Reinoso & Sepulveda-Escribano, 2001). BACs are highly microporous with a low angle of internal friction, which indicates strong flow properties for adsorbents. Therefore, they are known to be highly effective adsorbents in multi-layer adsorption applications in packed bed reactors or fixed bed columns (Hung et al., 2011). SACs are similar to BACs, and come in the form of small spheres, but they have a more uniform shape and size. The shape means SACs offer a high surface area to volume ratio and robust mechanical strength making them more resistant to abrasion and are popular for their low resistance to liquid diffusion (Oh et al., 2009). The shape can be formed through several methods such as polymerization reactions, agglomeration, or hydrothermal synthesis. The spheres are then activated through a typical activation process applied to GACs or PACs (Amorós-Pérez et al., 2018) SACs are used for water treatment, chemical purification, and gas adsorption such as carbon capture (Wickramaratne & Jaroniec, 2013). ACCs are versatile electrode materials which offer both flexibility and mechanical stability (Zhang et al., 2019). ACCs are fibres, fabrics or substrate cloths which have been impregnated with activated carbon (Macías Pérez et al., 1997). These are similar to ACFs but less brittle. The cloths can easily be shaped to fit filters. Activated carbon monoliths are formations of activated carbons which are compressed together after activation and heated to form ridged shapes such as cylinders. The functionalities and pore size distribution are highly tuneable (Pirmoradi et al., 2020). It is a dense material hosting a huge internal structure with a bimodal pore distribution, including micropores for adsorptions and macropores for transportation. It is effective for

fuel storage and adsorb gases such as hydrogen and methane (Lozano-Castello et al., 2002), (Jorda-Beneyto et al., 2008).

3.1.4 Modern Applications of the Product

The variation between different activated carbons allows them to perform a wide spectrum of functions. Presently activated carbons are commonplace in the purification of medicine, wastewater, and flue gases as well as a key component in supercapacitors. In the future they may be capable of overcoming challenges such as carbon sequestration and energy storage which makes them vital for our endeavours in environmental protection (Beguin & Frackowiak, 2009). The material is popular for its operational simplicity and versatility. It is employed in liquid-phase and gas-phase applications. The predominant use is for liquid adsorption, accounting for 80 % of cases (Diaz & Martin-Gullon, 2006). GACs are mainly used in gas purification and tend to have a specific surface area ranging from 800 to 1500 m^2/g. Both PACs and GACs are used in water treatment and their surface areas range from 500 to 1500 m^2/g (Cecen, 2014). The following section expands on the specific uses of activated carbons.

3.1.4.1 Adsorption

Activated carbon possesses powerful adsorptive properties and can adsorb substantial amounts due to the large surface area. For scale, using the standard methyl blue adsorption test, an AC derived from reeds was able to capture 704.23 mg/g (Zhou et al., 2017). Adsorption phenomena works through gradients and forces. The concentration of a liquid or gas at the solid interface of the adsorbent is more concentrated than in the bulk of the matter. The adsorbate, the contaminant being removed, will move through the internal structure of an AC until a suitable unsaturated site is found. The process of adsorption is exothermic. The adsorbate is held on the surface by physical forces, such as Van Der Waals, or through chemical bonds with surface complexes. The bonds formed in chemisorption are much stronger than those formed in physisorption. The adsorption kinetics are dictated by concentration gradients and pore size distribution. An equilibrium is formed when the rate of adsorption equals that of desorption. The rate at which this is met can be plotted as an isotherm, which will show the concentration adsorbed across the contact time. This process only occurs at the interface between two phases. Impurities can be removed from both gaseous and liquid phases. Contaminants include SO_2, NO_x, H_2S, volatile organic compounds (VOC), natural organic matter (NOM), phenols and heavy metals like Cd, Cr, Cu, Hg, Ni, Pb and Zn (Danish & Ahmad, 2018).

The predominant applications for AC are filtration and purification. It can be seen in the treatment of drinking, municipal and industrial wastewaters to remove dyes, pesticides, odours, taste, organics, and inorganics. It is also employed in flue gas scrubbing, pharmaceuticals, cosmetics, food, and beverage industries (Ukanwa et al., 2019). Producing potable water is a global challenge and GAC is a proven filtration media for removing impurities from drinking water (González-García, 2017). Deployed for its low maintenance and simple process operation, AC reduces the need for chemical disinfection. Piai et al. (2020) demonstrated the longevity of GAC when used as a polishing step for drinking water. GAC was installed to remove micropollutants which were present after the initial treatment stages. The material showed a high adsorption capacity for the tested micropollutants. After the equivalent of 100,000 bed volumes of effluent, the adsorption capacity of the GAC was comparable to fresh GAC. In another example, Golea et al. (2020) demonstrated GAC as the final treatment step in a wastewater treatment setup. AC produced form multiple precursors

were tested on two liquid samples. One water sample had been processed through a standard wastewater treatment plant (WWTP) and a comparison sample had been treated with a sand filter. The GAC was used to filter NOM from the wastewater. Initially 94 % of contaminants were removed from the sand filter sample and it demonstrated no selective removal traits. This caused pore blockages through the adsorption of larger molecules and at the end of the test, the removal efficiency had reduced to 27 %. The sample which had undergone the WWTP pre-process was reduced to 50 % capacity, as the WWTP was more effective at removing the large molecules. Figure 3.6 shows how the pore diameter can affect adsorption. The close-up shows that the micropores can accept the smaller blue molecules. However, the pore diameter is too narrow to allow other molecules in, such as the yellow molecule, which is how blockages could occur. The blockages will interfere with the total surface area available for adsorption. In Golea's experiment, the materials tested had varied pore size distributions. One coal variant was able to process twice as much water than another coal sample, due to the varied pore sizes which influenced the ability to adsorb more of the smaller molecules. This coal sample was able to reach environmental limits, even for the sand filter sample, whereas many materials could only hit this target for the pre-processed water. It shows that the GAC technology is not an immediate fix to the issues of pollution but fits as an integral part to the overall WWTP which can be tailored to the pollutant's removal needs.

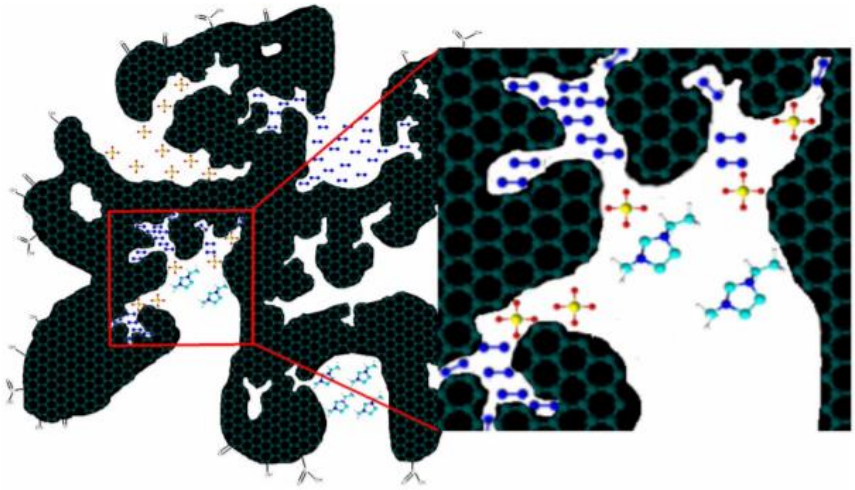

Figure 3.6 Internal structure of an activated carbon during adsorption (MacDermid-Watts, Pradhan & Dutta, 2020)

Toxins and micropollutants such as pesticides, herbicides, and dyes are routinely released by industry. These pollutants are often discharged by WWTPs due to the need for high frequency detection, which can impact aquatic life. An investigation into removing trace organic pollutants from pharmaceutical processes with ozone treatment, Tang et al. (2020) used GAC to collect the dissolved toxins post-decomposition. Wood and coconut shell based GAC were tested. It was found that the functional groups present on the materials was the performance differential which separated the materials. The presence of carboxyl, lactone and phenolic hydroxyl groups improved the adsorption capacity in coconut shell GAC and removed 82 % of the trace organic pollutants, highlighting the impact of surface functional groups.

3.1.4.2 Catalysis & Catalyst Support

Activated carbon can act as a catalyst by offering reaction sites and participating in reactions. The ability and uses are dependent on the surface properties and functional groups present. Using AC is highly efficient because of the large accessible surface area, so many catalytic sites can be used simultaneously. Examples include oxidation catalyst for glyphosate manufacture (Pinel et al., 1999), zinc-oxygen polarisation (Cecen, 2014), in batteries and iron oxide/H_2O_2 oxidation (Bach & Semiat, 2011). Su et al. (2020) used hydrothermal carbonization pre-treatment on pine wood to create a highly carbonaceous material. This was subsequently activated to create a material boasting a high surface area with a large surface oxygen content. When used in a gasification reaction designed to liberate syngas, the presence of the AC increased the gas yield by providing reaction sites via the oxygen containing functional groups. The catalysts presence made the reaction possible at 500 °C, compared to the standard practice at 800 – 1000 °C. The oxygen containing functional groups reacted with superheated moisture to produce acidic surface sites which became proton donors. This promoted the dehydration and decarbonylation reactions to proceed ahead of others, producing more CH_4 and H_2. Furthermore, the remaining biochar was analysed and showed further promise as an AC itself.

Additionally, due to the strength and structure of the material it can also act as a catalysis support. Catalysts can be impregnated onto the AC surface and used in pharmaceutical or chemical industries (Jüntgen, 1986). They are seen as ideal support materials because the carbon is not reactive and has potentially useful physical properties like hydrophobicity and polarity, which can be adjusted during activation. The materials are demineralised with methods like acid washing, to make the material as pure as possible and to avoid contamination or side reactions (Iwanow et al., 2020). While it is an effective support, it must be tailored to the application as structure can impact the catalysts performance, pore size distribution can impact the rate of transport and surface complexes can influence the activity (Albers et al., 2003). One set up used commercial grade AC as a pre prepared support for a variety of monometallic and bimetallic catalysts to remove nitrates from water through catalytic reduction. The experiments created 23 different catalysts through the wetness method, with different variations of metallic catalysts, showing the versatility of the material. The catalysts were compared with a previous experiment using similar metals with an alumina support. The AC support was effective and showed comparable activity to the alumina supports, but the surface area was not maximised by the method and showed a slower rate reaction. The AC did have the benefit of providing additional adsorption of the micropollutants and easy recovery of the metals by burning (Soares et al., 2008).

3.1.4.3 Reduction

Activated carbon can be used as a reducing agent. In Section 2.2.2. it was stated that carbon atoms on the edge of the graphene sheets are unsaturated and highly reactive. In the reduction process, a radical carbon will transfer a free electron to a positively charged molecule. A typical example of this process would be the removal of excess free chlorine from water. The carbon is oxidised during the dichlorination, completing the redox reaction, seen below in Equation 3.1.

$$C^* + HOCl \rightarrow CO^* + H^+ + Cl^-$$

Equation 3.1 (Suidan, Snoeyink & Schmitz, 1977)

Another useful example is increasing the efficiency of fuel cells. An oxygen reduction reaction occurs within a fuel cell which reduces the rate of electron transfer. An activated carbon has been used as an intermediate which facilitates high catalytic activity of the oxygen reduction reaction (Iwazaki et al., 2009), (Lv et al., 2018).

3.1.4.4 Separation

The material can be used for gas separation and solvent recovery. The adsorbate is adsorbed and held until it can be recovered afterwards through desorption. The recovery of an adsorbate can be facilitated through temperature and pressure swing adsorption units. In this instance, an alternate way to view the activated carbon is as a molecular sieve (Beguin & Frackowiak, 2009). This can be demonstrated in the decontamination of natural gas or syngas. These fuels are often found mixed with impurities like carbon dioxide. By using the activated carbon to selectively adsorb carbon dioxide, the fuel is purified. The carbon dioxide can be removed at elevated pressure and sent for storage (Grande et al., 2013). A similar situation is found with a gaseous mix of nitrogen and methane. The selection of an adsorbent relies on the separation factor and an adsorbent will often show a greater affinity for certain impurities. Activated carbon was used by Yang et al. (2020) to capture methane gas from a methane-nitrogen mix, until the adsorbent was saturated. A mixture of 20/80 methane to nitrogen was used. Through a single pass, 80 % of the methane could be removed successfully. The material is also useful for separating liquid-solid mixtures. Precious metals such as gold can be recovered from solutions. Shahrivar & Gharabaghi (2020) demonstrated this case by collecting gold after a common cyanide leaching process. The activated carbon was coated with graphene, outperforming the pure material due to a faster uptake, ultimately removing 60 mg/g. The conclusions showed the performance was heavily influenced by conditions, such as contact time, pH and temperature. This influenced the rate of removal and overall adsorption capacity. So, despite the ACs separation ability, the optimal performance must be coerced by external factors. Away from separating useful materials to collect a product, it can also be used for environmental control issues. Examples include long-term issues like immobilizing heaving metals in leachate from landfills or deploying fast acting protection for incidents like oil spills (Mohan & Nair, 2020), (Shokry, Elkady & Salama, 2020).

Activated carbons can also be used as solid adsorbents in carbon capture, utilisation, and storage (CCUS). The premise uses adsorption and desorption loops to separate and purify flue gas in order to mitigate the release of CO_2. The mechanism can be enforced pre-combustion or post-combustion for the cleaner burn of coal, releasing fewer pollutants. CCS can capture > 90 % of the CO_2 produced (Moore et al., 2009). The captured CO_2 is then transported to storage sites such as abandoned oilfields (Neele et al., 2011). The CO_2 is not returned to the atmosphere thus removing CO_2 from the carbon cycle and reducing the atmospheric content.

3.1.4.5 Chemical and Electrical Storage

The characteristics of activated carbon lend themselves as storage alternatives. For example, they can be used as a viable alternative to holding fuels in pressurised tanks. Hydrogen and natural gas have both been shown to adsorb to selected activated carbons (Noh, Agarwal & Schwarz, 1987), (Sircar, Golden & Rao, 1996). The process can offer storage at ambient conditions, although capacity is currently limited. It could be a safer alternative by offering storage at reduced pressures. Recently Dogan et al. (2020) used activated carbons synthesised from tangerine peel to store hydrogen. The chemical

activation used KOH and $ZnCl_2$ to synthesize AC. Higher ratios of activation agent resulted in a greater hydrogen uptake, although this would be correlated with a higher surface area. The hydrogen was found to adsorb using Van der Waals interactions. Elsewhere there have been examples of HTC pre-treated hydrogen storage. Sultana et al. (2022) used chemical activation with KOH to synthesize activated hydrochar made from loblolly pine. The product boasted a surface area of 1700 m^2/g with a total pore volume of 0.73 cm^3/g. The particularly microporous samples were superior at H_2 adsorption, where it is easier for the H_2 molecules to agglomerate. The highest recording was almost 55 mg/g. In terms of the HTC pre-treatment, the highest temperature sample (260°C) retained the highest carbon content and ultimately produced the best results. The study found multifunctional use for the material, also showing CO_2 capture capacity and electron storage. The 220 °C HTC sample performed best in the electrochemical tests, with the highest specific capacitance due to the high mesopore to macropore volume and high surface area.

The electrical conductivity and stability of the material makes it a prominent candidate as a long-term solution for supercapacitor electrodes. These are highly robust, able to withstand over 100,000 charging cycles. Activated carbon can provide high power densities for a long lifecycle, two key parameters for electrodes (Sevilla & Mokaya, 2014). Typically, energy storage devises are made from non-renewable or destructive materials, so there is interest in finding an environmentally friendly, low-cost alternative. An example of this is from Sevilla & Fuertes (2016) who used glucose derived hydrochar to form supercapacitor electrodes. The study explored the use of $KHCO_3$ as an alternative to the more widely used, and more corrosive, KOH activating agent. The results show KOH to produce the highest pore volume and surface area at 1.3 cm^3/g and 2670 m^2/g respectively, but the $KHCO_3$ samples were still high measuring 1.1 cm^3/g and 2230 m^2/g. However, the $KHCO_3$ samples produced a superior yield and had better packing properties through the retention of the hydrochar spherical morphology. The $KHCO_3$ samples ultimately provided greater storage and a greater supercapacitor performance than the KOH sample in some cases. The test with and without HTC treatment provided the best and worst results respectively, providing evidence that effective supercapacitors can be made from biomass and benefit from the introduction of HTC.

3.1.5 The Global Market

The value of the activated carbon global market is reportedly $5 billion USD, as of 2020. (RAM, 2020) This sizable industry is helped by the growing demand for activated carbon products in the industrialization of developing nations and in the emerging sector of environmentalism. It is estimated that the current global consumption of activated carbon is approaching 2 million tonnes per annum (GIA, 2021). Current trends point to steady annual growth rates in the next 10 years, primarily from an increased use of activated carbon in the wastewater treatment sector. This growth is expected to continue at 10 % year on year (Román et al., 2013). PAC currently has a 60 % market share, which is expected to increase due to growth in wastewater treatment sector (GVW, 2019). GAC use will see too an increased uptake in food, beverage, and pharmaceutical practices.

Commercially activated carbons can be highly profitable. It is expected that an average material will fetch 1000 USD / tonne. Those used in wastewater can range from 500 USD / tonne to above 2000 USD/ tonne, depending on the quality, which is dictated by surface area (Ľudmila et al., 2015), (Alhashimi & Aktas, 2017). The going rate is high, but it must balance

the mass losses originating in the production, a high temperature treatment phase and the precursor value.

3.1.6 Activation: The Formation Process

The activation mechanism for producing activated carbon comprises of two steps; the carbonization followed by the activation. The structural arrangement of the precursor is the template for the basic structure. The pores develop during the carbonization phase and are defined during the activation phase.

3.1.6.1 Primary Phase: Carbonization

To increase the carbon fraction in the material, precursors undergo thermal treatment in an inert atmosphere. This tends to happen over the range 400 to 1000 °C (Sevilla & Mokaya, 2014). The result will remove nonessential components and focus on retaining the char. Firstly, residual moisture will be removed up to 150 °C. Then a dehydration reaction will occur up to 240 °C to remove bonded hydrogen and oxygen. The process will progress to devolatilization above 250 °C. Weakly bonded aliphatic hydrocarbons are removed, resulting in the release of tars, CO, CO_2, and H_2O. Above 400 °C aromatization begins within the char in locations where hydrogen molecules have been gasified. This forms stable hexagonal graphene structures which are orientated randomly. As the temperature reaches the set point of > 800 °C, gaseous products are liberated which include CH_4 and H_2 (Beguin & Frackowiak, 2009). The material is outgassed, leaving a char which is dominated by fixed carbons which have been further aromatized. The remaining composition is un-gasified heteroatoms and ash. The level of porosity has increased, but not sufficiently to be classed as an active carbon. This is displayed in Figure 3.7 between phase A and B. It shows the hydrocarbons have been removed, which has created more space within the material, but the fixed carbon structure has barely changed. Many of the micropores are inaccessible to the surface and mesopores can be blocked by soot and tar depositions. The heating rate of the carbonization will impact features on the char. Faster heating rates create a rapid release of volatile matter which ultimately creates a more dense and hard structure without improving the microporous volume, creating an activated carbon with a lower surface area and total pore volume. Whereas with a slower heating rate, the volatiles experience a controlled release over a longer period, leading to a greater defined microporous structure, at the sacrifice of density, abrasion number, and hardness (Lua et al., 2004). Therefore, a balance must be achieved.

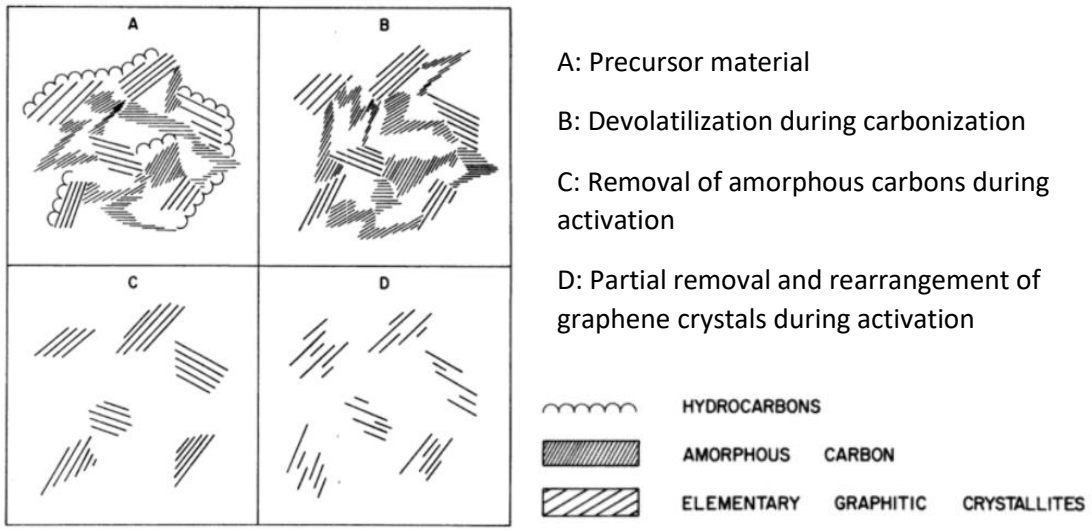

Figure 3.7 Stages of carbon removal (Stevenson, Leckie & Eliassen, 1972)

3.1.6.2 Secondary Phase: Activation

An activation agent promotes the growth of pores and initiates surface modifications by the gasification of individual carbon atoms inside the carbonaceous material. Not all carbon atoms are equally reactive. The microcrystalline graphene sheets are more resistant than the amorphous carbon found between them, so the less organised carbon is removed first. This action increases porosity areas which are not fully developed, by removing blockages and widening pores. Once the amorphous carbon is removed, the next action targets the edges of the microcrystalline structure. Ultra-micropores are opened into micropores, micropores grow into mesopores and mesopores grow into macropores (Beguin & Frackowiak, 2009). This development continues until the reaction is stopped and temperature is reduced. The calculated liberation of carbon atoms leaves the strong disorganised graphene sheets packed in an infinite number of ways leaving evacuated spaces between them known as pores. In Figure 3.7, the difference between phase B and D shows the full effect of the activation process. Amorphous carbon is removed leaving gaps between the graphitic structure. The difference between phase C and D demonstrates the pore development in the microcrystalline structure and carbon atoms are removed. If the process was to continue to a phase E, the graphitic structure would continue to be removed until there was no carbon remaining, resulting in no structure with only ash remaining.

Across the activation process much of the starting mass will be lost. It is common to experience > 85 % loss in an activation process (Stevenson, Leckie & Eliassen, 1972). An experiment by José Paras, et al., showed how the adsorption capacity of a carbon increased with activation losses. The longer the experiment ran for the greater the loss of carbon. This was associated with a higher degree of activation because more pores had been developed, exposed and widened, which is the purpose of activation. The conclusion was that at a low burnoff, there were only narrow micropores, but as it progressed they would widen and even develop mesoporosity (Parra et al., 1995). There would be an optimal moment, and beyond that, the microcrystalline structure would be destroyed, pore walls would collapse which would destroy the porous effect. Additionally, the resulting yield would be too low.

3.1.6.3 The Impact on the Final Product

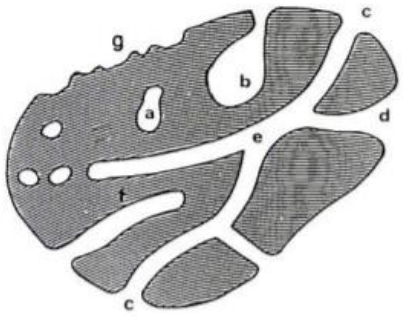

Figure 3.8 Generic final pore structure (Zdravkov et al., 2007)

Pores which are present in the char, before the activation phase, are known as structurally intrinsic pores. Pores which are created during the activation are described as injected intrinsic pores. Finally, pores which are formed by the liberation or reaction of an implanted activation agent are known as extrinsic pores. Figure 3.8 shows a cross sectional schematic of an activated carbon product. Section (a) shows a closed pore. This does not tabulate into the total surface area and cannot contribute towards adsorption, but it does add mechanical strength. This feature shows the activation is incomplete as it is not connected to the

network or the external surface. Section (b) shows an ink bottle pore. Both section (b) and (f) are open at one end, which are categorised as blind pores. Sections (c), (d) and (e) are open at both ends, categorised as through pores. All (b), (c), (d), (e) and (f) are in contact with the external surface, labelling them open pores (Zdravkov et al., 2007).

3.1.7 Core Methods of Activation

There are two well established techniques for activation, physical activation, and chemical activation. In order to commence the reaction, it must be subjected to an elevated temperature for a sustained period and combined with an activating agent. This section will explore the production methods further.

3.1.7.1 Physical Activation

Physical activation, sometimes referred to as thermal activation, happens in two stages. The stages can be completed one after another in series for a 'direct activation' with the correct equipment, which saves time and energy. The first phase, carbonization, is initiated on a raw material to intensify the carbon content. A char is formed. The second phase, activation, is performed on the intermediate material in an inert atmosphere and heated to a temperature above 700 °C. The system is exposed to an oxidising agent, causing a partial gasification reaction on the char. This essentially 'activates' the material. Agents which can create an oxidising atmosphere include air, steam, and CO_2. The controlled introduction of oxygen allows the more reactive sites to be removed first and clear a porous network. On the surface, reactions take place with oxygen from the activation agent or existing heteroatoms to form surface complexes.

Reactions with air are problematic due to the exothermic nature of oxidation. As a result, steam and CO_2 are preferred as activation agents because they are easier to control. The primary reactions when applying these agents are displayed below. These are endothermic which prevents runaway reactions. Multiple secondary reactions are also present (Stevenson, Leckie & Eliassen, 1972), (Rodriguez-Reinoso & Sepulveda-Escribano, 2001), (Cecen, 2014), (Diaz & Martin-Gullon, 2006).

$$C + H_2O \leftrightarrow H_2 + CO$$

$$\Delta H = 132kJ/mol$$

Equation 3.2

$$C + 2H_2O \rightarrow 2H_2 + CO_2$$

$$\Delta H = 75kJ/mol$$

Equation 3.3

$$C + CO_2 \rightarrow 2CO$$

$$\Delta H = 159kJ/mol$$

Equation 3.4

3.1.7.2 Chemical Activation

In chemical activation, the material must be impregnated with an activating agent before it is subjected to heat treatment. The pre-treatment requires precursor material to be mixed with an activation solution, forming a homogenous substance. Once dried the material is ready for activation. A key parameter is the ratio between precursor and activation agent,

which generally ranges from 4:1 to 1:1. A higher ratio of activation agent usually leads to a higher surface area (Gao et al., 2020). Chemical additives include KOH, NaOH, $ZnCl_2$ and H_3PO_4, which offer oxidative, dehydration and structural properties. The material is subjected to an inert atmosphere and heated to temperatures between 400 and 800 °C, depending on the reagent requirements (Marsh & Rodriguez-Reinoso, 2006). The chemical is present to catalyse the activation, reduce shrinkage, remove hydrogen and oxygen by promoting dehydration, prioritise char yield and minimise tar formation. The post process requires the activated carbon to be washed. The removal of the activation agent leaves additional voids which benefits the overall porosity.

Chemical activation is preferred for PAC and physical activation for GAC. Nevertheless, both methods can produce both PAC and GAC. The advantage of using chemical activation is the reduced carbon losses (< 70 %) (Rodriguez-Reinoso & Sepulveda-Escribano, 2001), and comparatively low process temperatures. There is a greater packing efficiency within the synthesized chemical structure than that of the original raw material because there is less space wasted. Some experiments have produced results exceeding 3000 m^2/g using KOH as an activation agent (Hsu & Teng, 2000). The chemical activation process will require pre and post treatment for the impregnation and removal of activation agent. The use of chemicals at high ratios will prove costly and the leachate may have environmental implications. Physical activation treatments are harsher and produce a lower carbon yield, but the parameters allow for more control over pore size (Prauchner & Rodríguez-Reinoso, 2012).

3.1.7.3 Industrial Production

In industry, physical activation the preferential method of production. Physical activation is a tried and tested method at scale, it has fewer treatment stages both before and after the activation and the reagents cost less. It is typically the disadvantages of chemical activation which is why there are no large-scale commercial plants in production. Without the additional impregnation and cleaning steps, the chemicals used as activation agents can cause corrosion and pollution (Gao et al., 2020). The manufacture of activated carbon can be carried out in continuous rotating kilns, multiple hearth furnaces and fluidized beds. All are designed to meet multiple temperature requirements and distribute the temperature. The plants can operate in continuous or in batch production (Sevilla & Mokaya, 2014). There are instances of success where both chemical and physical activation have been combined simultaneously for the benefits of both. This can also prove useful in removing the chemical but also compounds the losses of both techniques.

3.1.7.4 Regeneration & Reactivation

Upon saturation, the activated carbon is spent and is no longer an efficient adsorbent. The material can be replaced, regenerated or in some cases reactivated. The relatively high cost of activated carbon means reuse is an attractive option. In regeneration, the material can be subjected to temperature or pressure swing adsorptions, to remove the adsorbed material from the saturated activated carbon (Salvadora & Jiménez, 1996). Studies show materials can be regenerated to 95 % of the original absorbent capacity. New activated carbons can be made through reactivation by treating spent material with activation agents in a variant of physical, chemical, or biological activation. However, carbon losses will still be present in the process through oxidation and attrition (Cecen, 2014). For example, Khok et al. (2020) took spent activated carbon from the common process of gylcerine purification and reactivated it through both chemical and physical means. Standard

activation agents of CO_2, steam, H_2SO_4, $ZnCl_2$, KOH, and NaOH, found in the activation process are also used for reactivation. The different techniques were shown to be effective at removing different contaminants. Those adsorbates bonded to the adsorbent through chemisorption were more successfully removed with chemical treatment whereas physisorbed molecules responded better to physical treatment. The results showed a need for balance between yield and reactivation efficiency, to avoid poor quality products and too greater loss. A physically reactivated sample demonstrated the greatest performance, in line with the original sample, but also suffered a 30 % mass loss upon reactivation. However, the optimum sample only removed two thirds the contaminant that the original sample did. Therefore, there is much work to make reactivation a viable option. It can be a costly process, due to the conditions required, equipment and the release of the captured contaminants. The field is developing in response to this. Narbaitz & Karimi-Jashni (2012) tested the use of electrochemical activation, which appears to offset material losses. During the process it was found that when reactivation efficiencies were lower, the mass of activated carbon recovered increased. However, a relatively minimal mass loss was encountered. Overall, with lower losses but lower reactivation efficiency, the technology is level economically with the standard physical reactivation. Future optimisation may improve the efficiency, improving the viability of the technology. The variation of technologies show there are many options available to improve the current performance.

3.1.8 Activation Parameters: The Impact of the Conditions

Temperature and time are seen to be the most influential factors in the production of activated carbon. However, these are just two of many other parameters at play, which manipulate the material. This section shows the impact key parameters have on the reaction and final product.

3.1.8.1 Temperature

Temperature follows the rule that, as temperature is increased, the mass removal is also increased. The increased temperature increases the porosity and pore volume, up to a point where pore collapses take place. It can also have a positive effect on mesoporosity, indicating the action of pore widening (Bergna et al., 2020). This would signal a more effective process, but temperature has the potential to cause the greatest losses and must be balanced with residence time. If the conditions are too harsh, only the mineral matter will remain. So, despite the improved losses at higher temperatures, a balance must be struck to confirm the losses are improving the quality while producing an acceptable yield. A lower temperature range is required for chemical activation, but still shows the same general trend (Bansal & Goyal, 2005).

3.1.8.2 Holding Time

Time follows the tendency where with increased time comes increased mass removal. The increased time also delivers increased surface area and pore volume. It has a positive effect on mesoporosity. The increased time will allow more opportunity for pores to develop, for reactions to progress further and to successfully remove amorphous carbon and parts of the microcrystalline structure. A shorter holding time is required in chemical activation (Gottipati, 2012). This is due to the reagents catalysing the reactions. Overall, the time is dependent on other factors present, such as temperature.

3.1.8.3 Activating Agent

An increased concentration of agent will increase the rate carbon is removed from the material and the number of side reactions because more oxygen molecules are present. In

physical activation this can be diluted by an accompanying gas, either nitrogen or argon. Results from Linares-Solano et al. (2000) showed that during the activation of bituminous coal char, better pore development was attributed to steam activation than CO_2 activation, despite a proportional mass loss. However, in a conflicting report it is stated that CO_2 is more effective at an equal burn off, when activating coffee endocarp (Nabais et al., 2008). Reports also indicate that steam activated samples favour microporous development over CO_2, which shows higher development in mesoporous regions (Rodríguez-Reinoso, Molina-Sabio & González, 1995). The differences can be attributed to different sample materials. However, the overall concentration of gasifying agent makes a minor difference, and most experiments are completed in excess due to the small sample sizes (Chang, Chang & Tsai, 2000). For chemical activation the ratio has a much larger influence on the quality of activated carbon. The ratio will have a large influence on the pore size distribution and overall surface area. Pore size will increase with the increased use of activation agent. Trials tend to use ratios between 4:1 to 1:3 (Danish & Ahmad, 2018). There is evidence that some agents when present in high concentrations are effective at reducing material shrinkage by holding the shape under thermal stresses (Cecen, 2014). Additional pores are created upon the removal of the chemical. However, a higher ratio will require more washing treatment after the reaction to remove the material. The resulting solution will require more post treatment to recover the chemical because many reagents are pollutants and will damage the environment. They are also costly, so recovery is preferred. Therefore, a higher ratio of chemical activation agent will significantly increase the operational cost associated with the method (Ukanwa et al., 2019).

3.1.8.4 Other Factors

Of lower significance is the holding gas flow rate, heating rate and the total mass being treated. J. Pallares et al., researched the effect of doubling the heating rate from 5 °C /min to 10 °C /min which had a positive impact, slightly increasing the final surface area and pore volume. 10 °C /min appears to be the peak as other reports show a reversed affect at greater temperature gradients. Ultimately temperature and time are the most influential factor on the raw materials development. Although the trend of increasing the time and temperature parameters create a greater activated carbon product, they produce a broader pore size distribution. The losses associated with higher temperature and longer time mean it is not feasible. An optimum point would sacrifice additional porosity for a greater yield.

3.1.9 Importance of the Precursor Materials

Activated carbon is traditionally derived from fossil coal. Coal is favoured because of its consistent structure and high carbon content (Gao et al., 2021). The material has already undergone carbonization, creating a natural microporosity and does not require this stage of treatment. The scope of precursors is expanding with a shift in reliance away from fossil materials and a focus on repurposing and recycling. Using non-fossilized organics is not a new field of research. There is evidence of activated carbons being created from coconut shell in 1865 and papermill waste in 1868 (Dąbrowski, 2001). Common base carbons include wood, peat, grasses, husks, and shells. Each primary carbon will have a unique composition and internal structure, which is why the end products can vary so much. Cellulose based materials tend to produce highly microporous materials and lignin is more associated with developing macropores (Gottipati, 2012). The starting material will have effective surface area < 100 m^2/g which can grow to > 3000 m^2/g with effective treatment (Stevenson, Leckie & Eliassen, 1972). Theoretically any carbonaceous material could be

considered a parent material for activated carbon, however a series of features make certain organics desirable and other unfit for purpose.

3.1.9.1 Characteristics

Firstly, the organic needs to be a non-graphitizable carbon. Coking coals and thermoplastic wastes are not suitable for this reason, they will lose their initial porous shape upon heating (Diaz & Martin-Gullon, 2006). The initial structure is the blueprint for the activated carbons porosity and must remain intact. The criteria also require materials to have a high concentration of fixed carbon. The aim is to create an almost pure carbon structure, so a greater initial content will promote a higher carbon yield. This means a material with lower quantities of volatile matter is preferential because hydrocarbons are removed and lost during pre-treatment. Another compositional requirement is low ash content. Aside from any washing or pre-treatment, the mineral matter in the base material is not removed during activation. Thus, the weight percentage of the ash will grow because of the removal of other species. For the manufacture of GAC, the materials hardness is a factor. Finally, the materials configuration should be consistent and reproducible between batches and sites to avoid fluctuations in product quality (Diaz & Martin-Gullon, 2006).

3.1.9.2 Economics

It is important for the primary material to be low cost and have a stable market. The precursor material will ideally have a low moisture content, to reduce unnecessary mass and drying, which is energy intensive and costly. Activation is synonymous with mass loss. In some instances, there are ten-fold losses of the starting material. Coal is an expensive primary carbon compared with sawdust or bagasse. From this perspective, it explains why there is such interest in finding new sources from industrial and municipal waste supplies. Many streams of waste have high potential by offering a low cost, continuous supply of carbon rich material. High moisture waste materials are often neglected due to the cost and energy involved in drying the material. Hydrothermal carbonization (HTC) has recently garnered attention for its efficient disposal of wet waste and subsequent production of fuel. The product, a replica of coal, can be seen as a feedstock for activation. As so, an innovative development of HTC has harnessed the technology as a pre-treatment in the production of activated carbons.

3.1.9.3 Logistics

Availability of the precursor material is crucial. It must be easily accessed and have a consistent supply. Seasonal wastes are therefore not ideal. The material must be abundant in one location, to avoid transporting the material far, incurring more costs (Marsh & Rodriguez-Reinoso, 2006). Transporting the material far is not recommended due to the high moisture content. An HTC plant is best suited in a location which is a hub for wet wastes. Drying for transport and rehydration would defeat the purpose. Due to the losses and demand for the material, the scale of operation will require tonnes of precursor.

3.2 Hydrothermal Carbonization

3.2.1 What is Hydrothermal Cabonization?

Hydrothermal carbonization (HTC) is a process which increases the carbon content of a biomass precursor. The process produces a mixture of solid, liquid and gas products. Hydrochar is the primary solid product of HTC. The properties of hydrochar strongly resemble that of fossil coal, specifically brown coal (Sadish et al., 2019). Compared to the biomass precursor it is a darker, denser, more thermally energetic material (Krylova &

Zaitchenko, 2018). Dissecting the terminology, 'hydrothermal' means to be heated in aqueous conditions and it is the main premise of the technology. The precursor is prepared as a high moisture slurry. It is subjected to temperatures between 180 to 250 °C. The temperature bracket is seen as relatively low compared to other carbonization techniques, such as pyrolysis (Wang et al., 2018). Other practices were mentioned in Section 1.3, and Table 3.2 expands upon this by comparing the pros and cons.

The properties of subcritical water permit the conversion reactions to take place at a much lower temperature. As the temperature is increased in the closed system, the pressure naturally rises. This results in a highly pressurised and heated environment. The elevated pressure allows the water to remain in liquid phase throughout the conversion, despite the elevated temperature. HTC will take place between 2 – 20 bar (Libra et al., 2011). The mixture is held at these conditions for a matter of hours. Both batch and continuous methods are practical, both having strengths and weaknesses dependant on the scenario. The reaction happens in a thermochemical transformation which carbonizes the feedstock into a material that is chemically and structurally like fossilized coal. It can easily imitate brown coal but through optimisation the final product can provide a heating value greater than 30 MJ/kg (Khan et al., 2019). The process essentially replicates the natural coalification process in a fraction of the time. Typically, HTC will range from 1 to 12 hours, but there are examples of treatments as fast as 15 minutes (Zheng et al., 2020). The product can then be marketed and used as a fuel, as well as a soil remediation and carbon sequestration. With minimal retrofitting it can be used as a coal substitute in traditional coal fired power plants. The primary by-product formed is water, however this must still be treated for high levels of pollutants.

Table 3.2 A comparison of biomass waste utilization methods (Wang et al., 2018)

Biomass Utilization	Advantages	Disadvantages	Detail
Pyrolysis	Efficient & flexible	Feedstock must be dry	Heating in inert atmosphere Slow, fast, or flash variants Produces biochar, biooil & gases (CO, CO_2, CH_4, H_2)
Hydrothermal	Applied directly to wet biomass	Products require separation and lots of equipment	Carbonization, liquefaction & gasification Produces hydrochar, biooil and gases (CO, CO_2, CH_4, H_2)
Biological conversion	Low process energy	Long duration	Fermentation & anaerobic digestion Products include bioethanol & biogas
Densified solid fuel	Low transport costs	Low energy content	Mechanical dewatering and pelletization or briquetting, for combustion

3.2.2 Background of the Chemical Process

Hydrothermal carbonization has received much attention in the past decade for its low cost, low energy treatment of wet organic materials. The commercialization process of HTC process is only in its infancy, but it was first discovered over a century ago. Over the years HTC has been known as other synonyms including wet pyrolysis, wet torrefaction, aqueous

carbonization, compressed or subcritical water treatment and hydrothermal treatment (Dinjus, Kruse & Tröger, 2011), (Wang et al., 2018). The process was initially reported by German chemist Friedrich Bergius in 1913 but fell into relative obscurity after his initial discovery. (Funke & Ziegler, 2010) His intention was to create a synthetic liquid or gaseous hydrocarbon fuel from Germany's vast coal stores (Stranges, 2000). His hydrogenation experiments were conducted under high pressures and temperatures and yielded 85 % conversion of coal to petroleum.

Based on the knowledge of biomass's natural coalification process he transferred the method to cellulose combined with water. By conceptualizing the benefits of executing the reaction in a liquid state, he allowed the exothermic reaction of cellulose to take place without uncontrolled decomposition, owing to water having a large heat capacity and thermal conductivity. He retained the matter in a liquid state by balancing the temperature and pressure to allow the reaction to take place above the STP boiling point of water. This process replicated the coalification phenomena on a much faster scale, without the formation of coke. The product was a black powder, containing 84 % carbon which on further analysis proved to be soft coal formed directly from cellulose. He concluded that the limited pressure conditions meant he could not improve the process further to create a material to rival natural coal (Bergius, 1913), (Child, 2014). Due to the increasing demand for liquid hydrocarbons and the low calorific value of the product, there was no further research into the hydrochar. He had however, demonstrated the first HTC reaction and the discovery was a milestone towards his goal of liquefying coal (Bergius, 1932). Work by Berl and Schmidt in 1932 expanded the knowledge base of the HTC process by varying the source materials and testing conditions between 150 and 350 °C (Krishnan et al., 2014). Later the concept was picked up by Schuhmacher et al. to test the effect of the pH level on the final product; concluding that rates of coalification were accelerated by 10^6 to 10^9 in slightly acidified environments. There is little evidence of HTC being used beyond these examples and remained relatively untouched; resigned to the aforementioned papers.

Credit is attributed to Markus Antonietti of the Max Planck Institute of Colloids and Interfaces for rediscovering the effectiveness of the HTC process in 2006 (Titirici et al., 2007). The resurrection of the technology included research into increasing the decomposition rate with the use of metal ion catalysts, optimizing the conditions, and understanding how the starting material composition affects the hydrochars thermal value and physicochemical properties. Titirici, Thomas & Antonietti, 2007 calculated that converting 8.5 % of the world's biomass would completely compensate for the CO_2 emissions from oil. This revelation brought much attention to harnessing the optimum efficiency out of biomass.

3.2.3 The Hydrochar Product

Hydrochar is the solid product formed in HTC. As a material it is chemically and structurally similar to brown coal, in both the elemental composition and bonding patterns. It behaves similarly to coal in thermal processes (Nizamuddin et al., 2017). It is often converted to a durable pellet or briquette for ease of storage and transportation. It has many improvements over the raw biomass it is derived from, including a higher calorific value, increased dewaterability, increased energy density, material density and a greater degree of porosity. The final composition of the hydrochar very much depends on the precursor constituents and the treatment conditions. The carbonization guarantees a higher concentration of carbon in the hydrochar. It is expected that > 60 % of the original carbon

from the biomass can be carried over and if optimised properly that figure can exceed 80 % (Wang, Chang & Li, 2019), (Nizamuddin et al., 2017). During HTC, oxygen and hydrogen concentrations are reduced through the reaction mechanisms. The amount of nitrogen, sulphur and phosphorous are also reduced, primarily by dissolving into the water medium. Other fractions of the material are made up of mineral matter present in the source material.

Hydrochar is most suited as a fuel. The carbonization process has condensed the fixed carbon fraction in the material. Hydrochars derived from lignin-based materials like wood will have a high degree of aromaticity. This contributes to the high heating value of the material. It is known that 60 % of carbons present in hydrochar are cross linked in aromatic structures (Baccile et al., 2009). Volatile matter has decreased during HTC which increases the fuel ratio. This means the material will be ignited at higher temperature compared to the raw biomass and is more effective for power generation. This can be defined as having an improved combustion efficiency. With reduced hydrogen and oxygen content the heating value is densified. The H/C and O/C ratios are a good indicator of the HTC reaction severity. It is also a good quantification for comparing a hydrochar with grades of fossil coal. Reducing other impurities such as nitrogen and sulphur means the combustion emissions are cleaner and produces less pollution (Afolabi et al., 2020).

The structure of the material can be manipulated in the HTC process. The porosity of a hydrochar is relatively poor; however, it increases the surface area compared to the precursor. The conditions of HTC can be altered to maximise the potential. For instance, high temperature HTC tends to limit the formation of porosity and can reduce it by collapsing networks and forming blockages. If managed correctly it can reach > 30 m^2/g (Mumme et al., 2011). This is greater than the precursor but lower than materials which have undergone pyrolysis. When an organic material is treated at a significantly higher temperature using pyrolysis, the surface area can be 10 times greater compared the same sample prepared with HTC (Fuertes et al., 2010). They are suitable as an adsorbent, but post treatment activation creates a more effective material.

The elimination of hydroxyl and carboxyl groups also affects the materials wettability. Reducing these components reduces the materials hydrophilic nature, which ultimately makes it easier to dewater. Sevilla & Fuertes (2009) were the first to point out that hydrochars exhibit the structure of a hydrophobic core with a hydrophilic shell. The results showed the O/C ratio to be similar between the shell and core. However, the functional groups on the surface contain more active functional groups like hydroxyls, carbonyls, carboxylic and esters. Whereas the internal is an aromatic nucleus of stable groups such as ether, quinone and pyrone. Studies have also evidenced the shell-core relationship such as Gao et al. (2012) and Kambo & Dutta (2015). The liberation of bound water during the HTC process reduces the materials final moisture content. This feature makes the drying process more effective and less energy intensive. It can also be seen as a positive outcome with respect to material storage, as hydrochars are less likely dampen and grow mould. The polarity allows hydrogen bonding to organic adsorbates. It also increases the ionic capacity and facilitates complex reactions between oxygen groups and inorganics (Román et al., 2018).

The main by-products of the HTC process are water, carbon dioxide and soluble organics. Other gases can be formed such as carbon monoxide, methane, and hydrogen, providing the conditions allow it. The liberated water, as well as the original reaction medium, will

require treatment to remove the dissolved organics before it meets environmental release regulations. This can be done through methods such as recirculation, membrane filtration and wet air oxidation (Reza et al., 2016), (Urbanowska et al., 2020). Additionally, nutrients such as nitrogen and phosphorous can be recovered (Shen, 2020).

3.2.4 Applications of Hydrochar

3.2.4.1 Energy

Fossil fuels are directly linked to climate change and are a leading factor in the accumulation of atmospheric greenhouse gases. Predictions based on our current fossil fuel reliance show that the planets ambient temperature could increase 4 °C by 2050, if no action is taken (Zetterberg & Chen, 2015). This has catastrophic consequences for ecosystems and mankind. Investments have been made in renewable energy sources like solar, wind and tidal or different fuels such as hydrogen. The infrastructure for fossil fuel combustion is already developed, so it is essential to utilize this as our reliance decreases. Hydrochar can be utilized in this regard as a biofuel. Biofuels have the advantage of being a sustainable resource, renewable and releasing lower emissions.

The hydrochar combusts in a similar way to fossil coal so its most obvious use is as a fuel. It burns at a high temperature for a long duration when compared weight for weight against the raw biomass precursor. The hydrochar material is dense and packed with aromatic carbons. The high density of the material overcomes one of the challenges of raw biomass, which is the low energy density. Hydrochar has proven to be multiple times denser in its natural form than mechanically compressed biomass (Fang et al., 2017). The HTC process devolatilizes the material, whilst increasing the fixed carbon fraction which gives the hydrochar a higher fuel ratio. The lack of impurities also increases the energy density. The aromatic carbon structure is like that of fossil coal, and the reduced H/C and O/C ratio is more in line with that of fossil coal. All of this contributes to an overall greater higher heating value (HHV), making it a desirable fuel source.

Hydrochar is hydrophobic by nature making it easier to dewater and less likely to absorb moisture during storage. HTC has the opportunity to reduce the acidic and alkaline metals present in biowastes. Some of these elements are leached into the process water which reduces the content in the hydrochar. Compared to combusting the raw biomass, the hydrochar, with its reduced ash content, will have fewer issues with slagging, fouling, scaling, and corrosion (Kambo & Dutta, 2015). Additionally, issues of SOx and NOx in the flue gas of combusted hydrochar is reduced from the HTC treatment. Overall, it burns as a much cleaner fuel than the precursor. Zhu et al. (2019) converted cotton stalk through HTC to test the combustion performance. When the hydrochar was tested directly against the raw biomass, the hydrochars peak combustion temperature was 552 °C compared to 320 °C. It was also found to have much improved combustion kinetics. The combustion characteristics were proven to be more in line with coal and therefore energy used in the HTC process was justified in the improved HHV output of 25 MJ/kg.

Hydrochar can effectively be cofired with coal, to reduce the fossil coal emission. Beyond this there is argument for using HTC in localized energy grids, where locally sourced biomass can be converted to power to reduce energy transport losses (Steurer & Ardissone, 2015). HTC can also be the first stage in creating other fuels. If the desired product is gas, then the hydrochars can act as a precursor to syngas. This is achieved through gasification, where the material is heated in an atmosphere devoid of oxygen, to

capture hydrogen and methane. The condensed hydrochar matter, now with a higher carbon content and a good fraction of oxygen and hydrogen is a good precursor for this process, which is conventionally practiced on coal (Peng, Gai & Peng, 2020). The hydrothermal process can also directly create fuels in other phases. By increasing the reaction conditions, namely temperature, the process can produce a liquid fuel through hydrothermal liquefaction, typically between 280 to 370 °C (Gollakota, Kishore & Gu, 2018). At temperatures beyond the critical point of water, 374 °C, hydrothermal gasification can be achieved (Okolie et al., 2020).

Aside from being a fuel, hydrochars can act as a fuel carrier. Carbon materials can be successful components for energy storage such as electrodes in supercapacitors. The carbon acts as a medium for converting and storing energy. The materials offer benefits such as longer cycle life compared to current materials, such as nickel oxide and manganese oxide (Iro, Subramani & Dash, 2016). Corn straw was used by Liu et al. (2020) to prepare HTC electrode materials. The hydrochar was upgraded using microwave assisted activation, achieving 1781 m^2/g. This developed a more ordered pore structure similar to graphene which improve the specific capacitance and rate performance. There is a long way to go to match current supercapacitors, but this offers a low cost, environmentally sound option for a future with a heavy reliance on batteries.

3.2.4.2 Soil Remediation

The porous structure of the hydrochar helps aerate soils which is beneficial to the microorganisms that inhabit them, increasing their activity and the soils fertility. The hydrochar also influences the nutrient retention and moisture capacity of the soil (Kambo & Dutta, 2015). This will enhance the benefit of fertilizers by avoiding losses in surface runoff. The hydrochar can adsorb the fertilizer and release it over time (Fang et al., 2017). It will also retain water, which is useful in sandy soils which are unable to retain moisture. If the soil pH is too high, the acidic nature of hydrochar can be used to balance alkaline soils.

Hydrochar itself is generally low in soil nutrients but it can still have a beneficial effect on the soil environment, providing it does not disturb the microorganisms. If the ratio of soil to hydrochar is balanced incorrectly it can damage the environment through toxicity and soil pollution (Saqib et al., 2019). When the hydrochar is present in the soil it can adsorb and retain toxic substances in the soil. Most of all, the presence of hydrochar has a positive effect on plant growth (Islam et al., 2021). Xia et al. (2019) demonstrated the effectiveness of using hydrochar to remove soil contamination. Heavy metals in the form of lead and cadmium were reduced by adding 5 wt% hydrochar to the polluted soil. It was able to remove 54 % of lead and 27 % of cadmium. For agricultural use, an experiment conducted by Eibisch, Schroll & Fuß (2015) showed that soil treated with 5 wt% HTC corn, miscanthus and wood chip hydrochars were all capable capturing, storing, and releasing pesticides in a controlled manor. This made the pesticide more effective, and the soil required less frequent treatment.

3.2.4.3 Carbon Sequestration

Hydrochars can be used as a carbon abatement technology. HTC is a carbon neutral process and if the material is used to store carbon it can create a net negative carbon emission effect. During the HTC process, much of the CO_2 which the biomass has captured through photosynthesis is retained in the solid char, thus removing CO_2 from the carbon cycle. The hydrochar contains a high carbon content, which if combusted would release CO_2 to atmosphere. The biomass would have decomposed naturally and released that level of CO_2,

so it only releases CO_2 already present in the carbon cycle, albeit at a much faster rate. But if it remains stable, the carbon can stay sequestered for many years. The structural properties and lack of volatiles mean it is not prone to autoignition and can sequester the carbon for long periods of time. The premise is based on the Terra Preta soils found in the Amazon rainforest. The soil there contains a significant portion of carbon in the form of char. Over many years Amazonians packed chars into the ground making a carbon rich soil. The chars have remained stable and retained the carbon for thousands of years (Kambo & Dutta, 2015). However, when applied to soil, hydrochar has been found to be less effective at sequestration than similar materials such as biochar, from the pyrolysis process. Hydrochar is less stable than biochar and contains a higher volatile fraction. Naisse et al. (2015) compared the performance of hydrochar against biochar, both originating from maize silage. The carbon losses were calculated through simulated weathering. It was found the carbon half-life in hydrochar was approximately 10 years, whereas the biochar was approximately 75 years, providing to be the better sequestration technique. To rectify the poor stability, hydrochar can undergo a post process carbonization phase, such as pyrolysis, which although seemingly counter intuitive, would avoid the drying process for direct pyrolysis (Fang et al., 2017). On a separate note, the HTC process creates very few harmful GHGs during its production. The temperature is kept relatively low which does not accelerate the reactions producing gaseous products.

3.2.4.4 Adsorbent

The surface area of hydrochar is poor, but the surface oxygen functionalities mean it has a higher than originally anticipated adsorption capacity. This adsorption is selective of adsorbates. It can be used to remove heavy metals from effluent and aid wastewater treatment. The process can capture contaminants in liquid and gaseous form. However, it must be noted that the volatile component of the hydrochar could dissolve into the water and introduce new contaminants (Román et al., 2018). As environmental limits become stricter; more adsorbents will be required to treat effluent more thoroughly and effectively. There is an interest in utilizing waste in this industry, which has increased the scope of feedstocks. This offers hope for producing sustainable methods of producing drinking water anywhere, especially in developing nations.

It has been found that during HTC, a low temperature treatment over a shorter duration is the best way to maximise the porosity of hydrochar. Post process treatments can also be applied to improve the porosity, surface area, capacity, or functionality of the hydrochar (Zhu et al., 2015). Hydrochar can be activated through conventional chemical or physical activation processes, described in section 2.8. He et al. (2020) were able to use HTC shrimp shell to remove methyl orange from solution. The surface area was found to be just 13 m^2/g but it was capable of an adsorption capacity of 755 mg/g. This was possible by the presence of surface functional groups, including long aliphatic chains rich with nitrogen. Different starting materials will produce hydrochar with various functional groups which each have specific functionalities. Hydrochar is viewed positively as a precursor because it is structurally like coal while being renewable and low cost. This has been selected as the ideal use in this thesis.

3.2.5 The Array of Precursor Materials

HTC can be applied directly to any carbonaceous material. Waste biomass is seen as an ideal feedstock because it is carbon based, low value, renewable, abundant, readily available in all habitable areas and has few uses. Being a form of waste, it has not been

specifically grown for HTC and therefore it does not compete for land space with food crops, although some wastes will be formed from the production of foodstuffs. Many materials require a treatment process regardless before they can be sent to landfill, so HTC provides this intermediate step and creates a useful product in the process. The phenomena can be applied to wet or dry feedstock. The material used in HTC begins as a liquid slurry, so materials in a wet form are more desirable for the process. Biomass is known generally for having a high moisture content, lending itself as an ideal source material. The benefit of this is that a costly or energy intensive drying process is not required. Feedstocks can be mixed and processed in one slurry (Hitzl et al., 2015). Commonly recycled dry biomass such as wood or bagasse, can be used by adding water. A bigger potential market makes use of highly wet wastes which wouldn't be considered suitable feedstocks for other techniques. Wet waste is considered to have > 30 % moisture content and includes sewage sludge, algae, and municipal solid waste (Kambo & Dutta, 2015), (Wang et al., 2018).

The proportion of lignocellulosic components will dictate which conditions are needed to decompose the biomass. Feedstock properties such as chemical composition, volatile matter, moisture content, particle size and energy content play an important role in the hydrochar yield and the heating value of a char (Libra et al., 2011). For example, precursor materials with a greater carbon content tend to produce a greater hydrochar yield (Lu & Berge, 2014). The composition of ash in the precursor is also an indicator of the final hydrochar ash content. Elements such as Al, Fe and Ca have a low solubility during the HTC process and will remain in the hydrochar (Mäkelä, Fullana & Yoshikawa, 2016). Experimentation has shown that higher temperatures increase the solubility of water and remove greater quantities of minerals, but it also has a diminishing effect on the hydrochar yield (Reza et al., 2013). Precursor materials which are commonly used for HTC include wood, garden waste, food waste, municipal solid waste, sewage sludge and algae (Aragon-Briceno et al., 2021). Table 3.3 shows multiple feedstocks treated with HTC in various conditions. The results vary widely based on this treatment and the composition of the initial feedstock.

Table 3.3 Example biomass precursors and results with varying degrees of success

Material	Temp. (°C)	Time (hours)	Hydrochar yield (%)	Carbon yield (%)	O/C	H/C	Surface area (m^2/g)	HHV (MJ/kg)	Reference
Bamboo	200	1	64.8	56.0	-	-	9	-	(Choe et al., 2019)
Corn Stover	250	4	36.0	57.0	0.27	0.94	4	-	(Fuertes et al., 2010)
Dry leaves	240	0.5	67.0	-	-		2	20.0	(Saqib et al., 2017)
Lime peel	220	1	52.1	11.2	-	-	-	17.8	(Shafie, Al-atta & Zainal, 2018)
Miscanthus	250	1	43.0	43.0	0.22	0.85	-	26.1	(Smith et al., 2018)
Microalgae	250	1	27.6	41.0	0.28	-	-	22.3	(Brown et al., 2020)
Olive waste	120 - 250	0.5	97.1 – 48.0	-	0.25 – 0.45	0.99 – 1.45	-	19.8 – 27.6	(Volpe & Fiori, 2017)

Pig manure	200	2	58.8	33.8	0.33	1.5	-		(Gascó et al., 2018)
Sewage sludge	190 – 260	1 – 24	-	-	0.17 – 0.06	1.17 – 1.64	3 – 17	16.7 – 18.3	(Jin-Hong, Qi-Mei & Xiao-Rong, 2014)
Sewage Sludge + Corn Cob	300	1	48.0	50.2	0.04	0.91	-	21.3	(Zhai et al., 2017)

3.2.6 The Crucial Carbonization Mechanism

HTC mimics the natural coalification process of biomass. The premise is the materials are thermochemically altered through decomposition reactions and reformed into aromatic structures. Many reactions happen in parallel to produce the carbonizing effect, including hydrolysis, dehydration, decarboxylation, condensation, polymerisation, and aromatisation. The temperature is controlled to keep the water in a subcritical state, integral to HTC. The conditions make the material unstable, and it begins to decompose. The subcritical conditions facilitate an acceleration of the natural coalification process, so it only takes a matter of hours. The aqueous conditions reduce the activation energies required for bond cleavage allowing reactions to take place at a significantly lower temperature than they would without the presence of compressed water. Hemicellulose begins to break down between 180 – 200 °C and cellulose is affected above 220 °C (Sevilla & Fuertes, 2009). Lignin is more complex and occurs over a wider range of temperatures (Pauline & Joseph, 2020). Lignin will begin to decompose between 180 – 220 °C but can require temperatures greater than 260 °C. This is due to its cross linked, high molecular weight polymers with high numbers of ether bonds. Weaker bonds are broken early on, and the stronger cleavage bonds proceed to break with under an elevated temperature (Libra et al., 2011). The temperature also effects many characteristics of the water medium such as density, viscosity, and solubility. The process contributes to a large dehydration in the material through the destruction of oxygen rich functional groups hydroxyl and carboxyl. It is also noted that reduction of O/C is much greater than the reduction of H/C, showing HTC to effectively be an oxygen removal process (Wang, Chang & Li, 2019). The entire process is governed by the reaction conditions used. The reaction mechanisms are described below.

3.2.6.1 Hydrolysis

Hydrolysis is the first reaction to commence because it has the lowest activation energy. The reaction depolymerises the biomass down into smaller molecules which facilitate other reactions. Hemicellulose is hydrolysed first, due to its weak amorphous structure, followed by cellulose and then lignin. Lignin only partially hydrolyses because temperatures greater than the HTC region are required for complete homogeneity, often super critical conditions (> 300 °C) (Wang et al., 2018). The high temperature reduces the water density, decreasing the dielectric constant, thus weakening hydrogen bonds in the biomass. This enhances dissociation and produces iconic products hydronium ($H3O^+$) and hydroxide (OH^-) (Wang, Chang & Li 2019). The increased proton dissociation increases the concentration of H^+ and OH^- which enhances acid catalysed and base catalysed reactions respectively. The water phase behaves like a solvent, becoming a highly reactive medium with increased solubility. It favours ionic reactions of non-polar organic compounds and aids hydrolysis and bond cleavage reactions. The temperature also affects the viscosity of water. This allows it to enter the biomass pores more effectively and promote reactions throughout the medium (Reza et al., 2014).

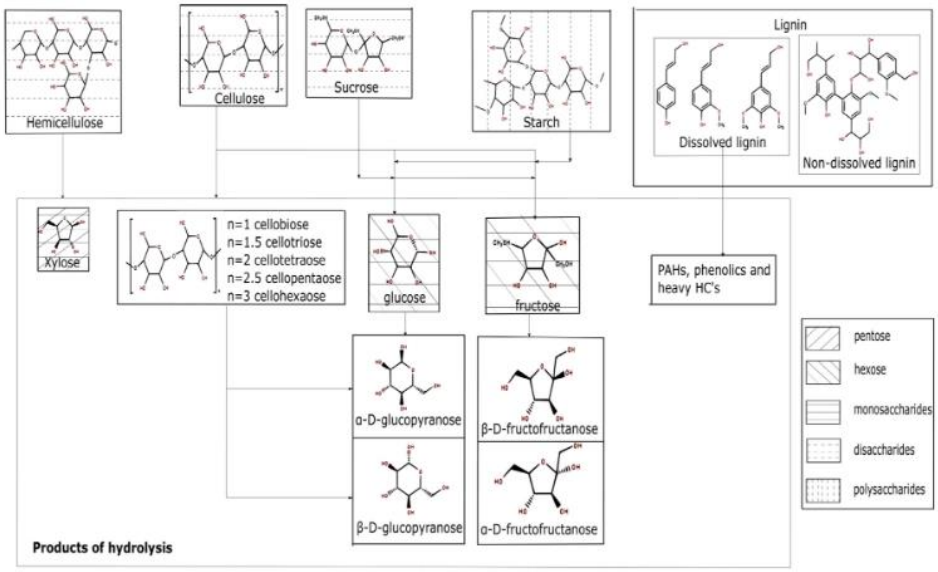

Figure 3.9 Reaction pathways and the products formed during hydrolysis (Pauline & Joseph, 2020)

A basic flowchart of the hydrolysis reactions is exhibited in Figure 3.9, which shows the products of hydrolysis. The process reduces the molecules size. For example, the process reduces the hemicellulose into xylose. Cellulose is converted into water soluble oligomers of various lengths and then further into glucose and fructose. Disaccharides and polysaccharides are broken down into monosaccharides. Lignin is reduced to phenol and other phenolic derivatives. The fragments are highly reactive and precipitate through condensation reactions. The materials become more stable by reacting with one another, for example hemicellulose fragments will react with lignin fragments to form more soluble aromatic structures (Funke & Ziegler, 2010).

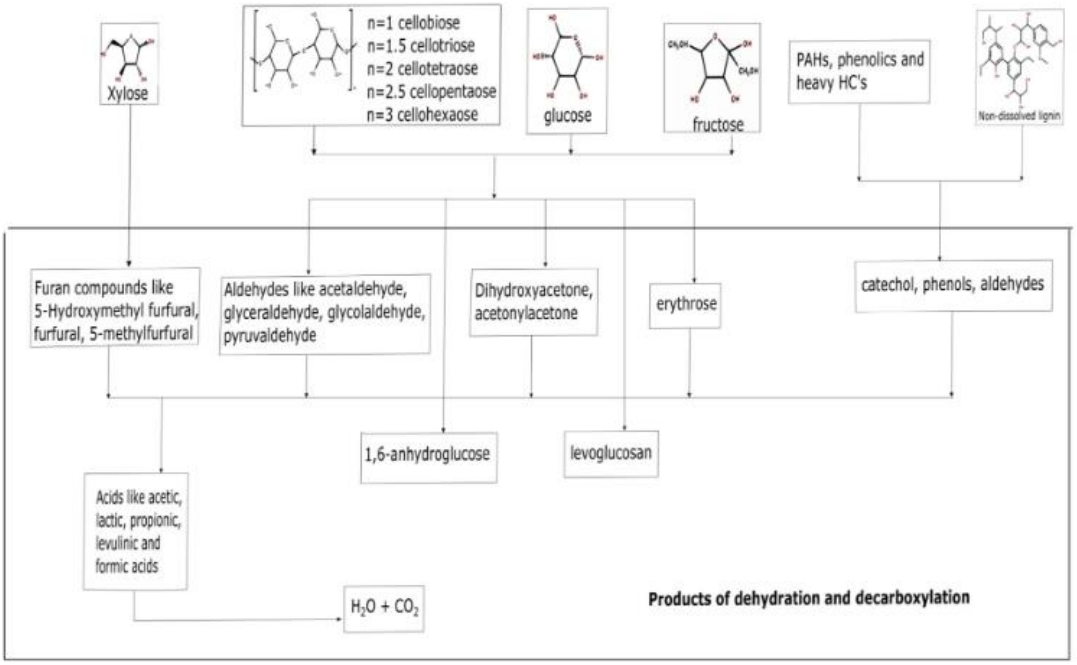

Figure 3.10 Intermediate routes during dehydration and decarboxylation reactions (Pauline & Joseph, 2020)

3.2.6.2 Dehydration

The dehydration phase occurs after hydrolysis. Monomers from hydrolysis decompose to form organic acids, reducing the pH. The acidity further degrades the remaining biomass, other intermediates and begins to influence other reactions as a catalyst, such as the dehydration process. Dehydration removes hydroxyl groups, which continues to fragment the biomass into reaction intermediates (Wang et al., 2018). An example of this action would be the dehydration of cellulose, seen below in Equation 3.5.

$$4(C_6H_{10}O_5)_n \leftrightarrow 2(C_{12}H_{10}O_5)_n + 10H_2O$$

Equation 3.5 (Sevilla & Fuertes, 2009)

The dehydration reaction continues and liberates more water and creates many intermediate products. Key intermediates such as furfural and 5-hydroxymethylfurfural (5-HMF) are common examples of soluble intermediate products. They are highly influential in hydrochar heating values and surface area (Kambo & Dutta, 2015). They are highly reactive and will readily undergo condensation or polymerisation through aldol-condensation. During the recombination, there is intermolecular dehydration which releases more water to form hydrochar (Saqib et al., 2019). It is the most effective way of reducing the H/C and O/C ratio in the hydrochar. During the HTC process the decarboxylation takes place at a similar time to dehydration. The reaction can be activated from 150 °C (Saqib et al., 2019). But despite this, the rate does not increase it until the dehydration reaction has progressed sufficiently. The ratio of decarboxylation to dehydration is always in favour of dehydration. Figure 3.10 demonstrates some of the pathways which intermediates can follow to produce water and carbon dioxide.

3.2.6.3 Polymerisation

During this stage, many of the intermediate monomers formed from the previous reactions join to form a solid precipitation polymer chain. It can be referred to as a recondensation phase. Unsaturated intermediates from the elimination of carboxyl and hydroxyl groups are highly reactive, so they are easily polymerised through aldol-condensation. They form carbon-carbon double bonds. When molecules combine, it forms a bigger molecule and releases a small molecule, which is usually water, through intermolecular dehydration (Heidari et al., 2019). Many molecules will combine to create a random cross-linked structure. The process is fast at high temperatures but can continue for months at room temperature (Funke & Ziegler, 2010).

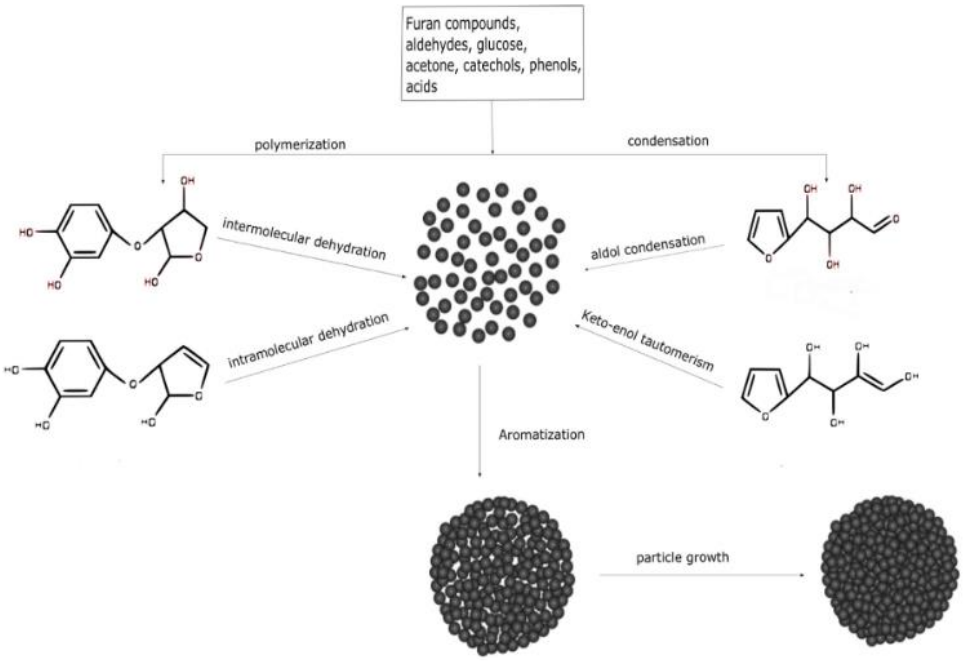

Figure 3.11 Particle growth of hydrochar during condensation, polymerization, and aromatization reactions (Pauline & Joseph, 2020)

3.2.6.4 Aromatisation

This process creates the basic building block of the hydrochar. They are made from the decomposition and further dehydration of the oligomers and monosaccharides formed in the hydrolysis. They appear through the subsequent condensation of the aromatized molecules. As the concentration of aromatics increase in the aqueous environment, they begin to cluster and build outwards. When a critical saturation point is reached, a burst nucleation process takes place, where chemical species present in the solution are attracted to the nuclei, thus growing the particle (Sevilla & Fuertes, 2009). Ether bonds are formed, and the particle becomes stabilized. The functional groups become the reactive surface, and the aromatic structures are the hydrophobic nuclei. The process can be visualised in Figure 3.11. The process is optimised in alkaline conditions (Pauline & Joseph, 2020).

3.2.7 Process Parameters: The Impact of the Conditions

3.2.7.1 Temperature

The HTC zone is 180 – 250 °C, the optimum range for promoting the production of solid hydrochar. The temperature provides the heat of decomposition to the biomass to fragment the bond linkages and initiate carbonization reactions which creates new combinations of molecules (Akhtar & Amin, 2012). The temperature range is important to keep the water in the subcritical region, influencing factors such as phase, reaction rate, density, and viscosity; all which promote reactivity. The operating temperature is influential as to which reactions progress and therefore, which materials are degraded. The HTC reaction is exothermic, which adds thermal energy to the mixture. At the start of the reaction, the hydrolysis reaction is initiated above 180 °C, as seen in section 2.2.5.1. At temperatures greater than this, dehydration and decarboxylation reactions occur. Beyond this, condensation reactions tend to happen between 230 – 250 °C which reduces the hydrogen and oxygen fractions in the hydrochar. An elevated temperature is necessary to release volatile matter which will aid dehydration and elimination reactions (Sharma et al.,

2020). Reductions in hydrogen and oxygen molecules are necessary to increase the carbon fraction in the hydrochar. Lower temperatures are shown to maximise the solid yield. It is reported in some works that reaction conditions greater than 200 °C reduce the hydrochar yield (Nizamuddin et al., 2017). At this point the rate of solubilisation is greater than the rate of char production (Pauline & Joseph, 2020). At even higher temperatures, the reaction is more severe and has a greater degradation of the biomass, often stimulating secondary char reactions. This favours liquid and gaseous products. Above the HTC temperature range is known as hydrothermal liquefaction which is useful when targeting a biooil product. This is material dependant, for instance, Sevilla & Fuertes 2009, showed the yield of hydrochar derived from saccharides increases with temperature, and is highest at 240 °C, due to the material sufficiently undergoing HTC. Overall, can be concluded that temperature has the single biggest governing effect on the HTC process.

3.2.7.2 Residence Time

It has been observed that an increase in time increases the reaction severity and conversion rate, allowing more condensed products with a lower O/C and H/C ratio. Combined, time and temperature are considered the most influential parameters in HTC, although temperature is more so. It is key in making the hydrochar stable. Sevilla & Fuertes (2009) showed that the yield of cellulose was always higher in the 4-hour samples, compared to the 2-hour samples. There does seem to be a point where the time begins to negatively impact the yield. Experiments performed on multiple HTC feedstocks, including cellulose, from 6 hours to 48 hours showed that as time progressed, the hydrochar yield peaked and decreased gradually. In the same experiments, the carbon content rose during the yield decline, while the hydrogen and oxygen content dropped. (Simsir, Eltugral & Karagoz, 2017). It is also noted that HHV increases with time. An increased reaction time is necessary for feedstocks with more complex components such as lignin and lignocellulosic biomass to break down. Longer times will promote the propagation of demethoxylation and alkylation reactions (Shen, 2020). A higher residence time also encourages the hydrolysis reactions to continue, increasing the liquid fragment which becomes polymerised over time.

The total time also has an impact on the physical structure and surface characteristics. Materials subjected to an hour of treatment show signs of surface cracks and trenches. Beyond 6 hours, the presence of carbon microspheres can be noted, and at 24 hours the microspheres aggregate together (Wang et al., 2018). This creates a more defined porous structure and increases surface area and pore volume (Nizamuddin et al., 2017). The residence time is specifically the time which the reaction takes place at the temperature set point, disregarding the heating rate and cooling period. However, Román et al. (2018) noted a discrepancy in results, where some report the entire duration and some just the reaction period.

3.2.7.3 Pressure

The pressure increase is autogenous during the process. It is induced by the increased temperature within a sealed system. Pressure is paramount in keeping the water in a subcritical state. This influences the liquid phase density and viscosity, making the medium part of the reactions and penetrating further into the biomass structure. When higher temperatures are introduced, the pressure increases proportionally to maintain equilibrium (Pauline & Joseph, 2020). Tests have been conducted to vary the pressure within the vessel while keeping other parameters constant. The results showed little effect on the hydrochar

structure, except a minor increase to the pore volume at higher pressures. Although, any impacts would not be experienced at autogenous pressures (Heidari et al., 2019). Pressure is the main consideration when selecting an operating temperature. At the chosen set point, providing the pressure is above the saturation pressure of water, the conditions are fit for the HTC process.

3.2.7.4 pH

The solution pH has a measurable effect on the process. A weakly acidic environment is reported to enhance the coalification process (Pauline & Joseph, 2020). The addition of an acid will catalyse the process, facilitating the hydrolysis and dehydration reactions. The increased proton availability will increase the rate of reaction. The acidic conditions facilitate the breakdown of hemicellulose and will also have a significant impact on the degradation of cellulose, which will have a positive impact on the HHV (Saqib et al., 2019). The opposite effect happens when a basic catalyst is used, which promotes the liquid fraction so the hydrochar yield is reduced. Some experiments have produced materials with greater adsorption capacities when pre-treated with acid catalysts, such as hydrochloric acid (Flora et al., 2013).

3.2.7.5 Moisture Content

The reaction is only possible because the carbonaceous material is in water, as explained in section 2.2.5, which differentiates it from pyrolysis. Water is efficient at heat transfer medium, which helps keep a homogeneous temperature throughout the mixture and avoids local overheating which can stem from the exothermic reactions. The moisture content must be great enough so that the biomass can be completely wetted. A higher moisture content is reported to improve physical properties like porosity, which is ideal for an activated carbon precursor (Heidari et al., 2019). These conditions are found to favour decarboxylation and hydrolysis reactions (He et al., 2015). It can also reduce the number of impurities, such as nitrogen, phosphorous and ash, in the final hydrochar product (Li et al., 2019). But at the same time there is more liquid for organics to dissolve into, which will reduce the hydrochar product. Studies generally report that as moisture content increases in the initial feedstock, the solid yield decreases in the final product (Román et al., 2018). Instead, a higher carbon fraction is found in the liquid and gaseous phases. From an environmental standpoint, it should be considered that a lower liquid fraction would reduce the overall volume that is needed to be heated, reducing time and energy usage. Finally, bound moisture is released during the process, which will increase the process water output slightly. Overall, it can be seen that the moisture content is required for the reaction mechanisms, but it should be balanced with the dry solid content based on which product is desired.

3.2.7.6 Heating Rate

This parameter has a big impact on the final product phase. A rapid heating rate can impede the hydrochar formation. By allowing a slow heating rate, for example 5 °C /min, the hydrolysis reactions, which begin at 150 °C, have time to create the intermediate properties and the conditions needed for carbonization before other reaction activation energies are hit (Wang, Chang & Li, 2019). Flash or fast pyrolysis promotes liquid products, which is also correct for HTC. A low heating rate is linked to lower oxygen and hydrogen fractions in the hydrochar. This also results in a greater HHV if the hydrochar was used as a fuel (Wang et al., 2018).

3.3 The Introduction of Activated Hydrochar

Using hydrochar as a feedstock for activated carbon is an emerging field. Studies in the area have shown the potential of activating hydrochar. The first to report this combination were Sevilla, Fuertes & Mokaya, 2011 who converted a range of organic materials into hydrochars before activating with KOH. The surface areas surpassed 2000 m^2/g and reported pore volumes upwards of 1 cm^3/g. The products showed a high affinity for hydrogen storage, with a higher specific hydrogen uptake than previous AC examples. In doing so they proved hydrochar is an ideal precursor for high performance ACs. Since then, many more experiments have been conducted using chemical activation methods, including: HTC green waste and HTC municipal solid waste activated with KOH which showed adsorption characteristics similar to commercial activated carbon (Puccini et al., 2017), HTC coconut shell activated with $ZnCl_2$ which increased the mesoporous region by 80 % and improved the adsorption capacity of phenol (Jain, Balasubramanian & Srinivasan, 2015), HTC sawdust activated using $FeCl_3$ to produce high performance granular activated carbon (Yu et al., 2020), HTC corn cob activated with H_3PO_4 to produce a high surface area (2192 m^2/g) with a high pore volume (1.27 cm^3/g) (Chen et al., 2017) and HTC algae activated with KCO_3 to evaluate the process variables, among many other studies. The focus of this work will be on physical activation studies.

An early experiment conducted by Román et al., (2013) showed the potential of physical HTC activation. Lignocellulosic wastes such as walnut shell, sunflower stems, and olive stones, underwent HTC treatment in the form of 5 % dry solids at 220 °C for 20 hours. The harsh conditions were necessary for a greater severity of carbonization due to the complex nature of the lignocellulosic materials. They were treated with CO_2 and air in separate activations. Both proved successful, offering different benefits. CO_2 activation was seen to decrease the oxygen surface groups whereas air kept the acidic surface characteristics. Air produced a lower yield across the materials due to the uncontrolled burn off. So, CO_2 proved to be the greater value activation agent, showing higher surface area development with fewer mass losses. Throughout the study it emphasised the benefits of using HTC for pre-treatment because it increases the final carbon yield and offers more control over the porosity distribution in the product. In turn it was concluded that there is a future for the method of producing activated carbons through HTC pre-treatment, which can be tailored for specialised applications like adsorption or storage.

In one procedure, HTC sugarcane bagasse was physically activated using steam. The goal was to decolourise syrup which had been produced from the sugarcane. Despite being one of the most conventional approaches for activation, there are few studies which have used steam for the physical activation of HTC biomass. The hydrothermal carbonization followed a matrix of temperatures and times between 180 – 240 °C and 30 – 90 minutes, to find the optimum conditions. The methodology was strong and reproducible. The material entered at 15 % dry solids and was heated at a rate of 4 °C /min. As indicated in the literature, increased time and temperature resulted in lower hydrochar yields. The activation was performed in a vertical low-pressure autoclave and where steam was injected. The heating rate used was 10 °C /min. The preheated steam entered at a rate of 1.1 L/min. As expected, longer residence times decreased activated carbon yield. Interestingly, higher HTC treatment temperatures produced better activated carbon yields than low temperature HTC, despite having a lower initial hydrochar yield, due to a higher fixed carbon content. The activated carbons were rich in mesopores and micropores. In general, the high temperature HTC and activation performed best in creating porosity. Whereas there is only

a minor increase when activation is set at 700 °C. Although the highest value of surface area was only 390 m^2/g, the steam activation was effective enough to alter the internal structure (Congsomjit & Areeprasert, 2020).

In a separate study, sucrose was treated with HTC for 5 hours at 190 °C before an activation phase. The steam activation was only trialled at 800 °C for 1 hour. The purpose of the experiment was as a control to show the superior chemical activations, using KOH and K_2CO_3. The chemical activated samples proved to have higher adsorption capacities and surface areas. The steam activation was still useable and reached a surface area of 814 m^2/g, which is well within the limits of a commercially viable activated carbon. The results found that the highest carbon retention and overall percentage was in the steam activated sample (Mestre et al., 2015). There is much potential with the simpler and more sustainable route of physically activating without any toxic chemicals. The conditions could also be fluctuated to improve the physically activated carbons performance to try and closer match the chemical counterparts.

One method used by Antero et al. (2019) utilized moisture entrainment to carry the activation agent through the vessel. A vertical tube furnace was assembled with a moisture vessel connected to the inlet. The water remained heated at 80 °C and nitrogen was bubbled through it before entering the reaction vessel. This carried a proportion of moisture through the reaction chamber to facilitate the activation, which was carried out at 700 °C across 3 hours. HTC Magonia Pubescens bark was used as a precursor. The HTC pre-treatment was 170 – 190 °C for 5 hours. The result produced a surface area of 441 m^2/g. The aim was to remove bisphenol-A from water after the production of plastics. The activated carbon had a removal efficiency of 50 % which was close to the AC used as comparison. The activation was successful, but the surface area was not as large as would be expected over 5 hours of treatment. This amounted to a 53 % burn off, which is a good balance. However, due to the energy required to heat the reaction for 5 hours, the elutriation mechanism may not be efficient enough for scale up. Injecting preheated steam appears to be a much more successful technique.

There are multiple activation agents available for use in physical activation to oxidise the material other than steam. One study used corn stigmata as the base material to study the ability of an adsorbent prepared with and without HTC pre-treatment. The practice used physical CO_2 activation to produce the activated carbons. In the results of the activation, the material which had undertaken HTC proved to have a higher carbon yield, greater carbon content and a much greater surface area. The highest result was 1111 m^2/g, which was twice that of the non-HTC equivalent and a significant improvement from the raw material, originally measuring 47 m^2/g. The activation residence times used were 0.5, 1, 2, and 3 hours. Some of the higher temperature conditions were acknowledged to be too aggressive when subjected for a duration of an hour onwards. Some of which returned yields as low as < 7 %. Some of the remainder would simply be ash (Mbarki et al., 2019). Overall, the method demonstrated that using HTC pre-treatment before physical activation had a positive influence. Lower carbon losses were recorded for the HTC sample during activation. However, the losses reported only consider those caused during activation. Both the HTC and non-HTC samples are weighed out as an equal mass before activation, for a direct comparison. Due to losses associated with the HTC process, this sample would represent a greater quantity of the original raw material. This should be mentioned, factored into the results, or tested against the equivalent non-HTC sample mass.

One study followed an unconventional sample preparation route on grey alder wood. The hydrothermal treatment was not done under pressure, instead it was held at 180 °C in a saturated steam atmosphere, a process known as autohydrolysis. The treatment was optimised at 2 hours. The author cited that the material underwent similar reaction mechanisms which are present in HTC, namely hydrolysis. The aim was to create a mechanically strong GAC, so the pellets were pressed after the autohydrolysis stage in preparation for activation, like the extruded activated carbon described in section 2.1.3.3. The carbonization and activation steps were treated as separate events. In total, the pellets were steam activated for 90 minutes at 850 °C. The pre-treatment process showed to only affect the hemicellulose, leaving the cellulose and lignin structures in place to bolster the pellets strength. Hemicellulose products also acted as a binder. The resulting material had a surface area of 1338 m^2/g, showing that steam activation was a successful treatment path. Although it met the intended purpose, under HTC autogenic pressures, the carbon fraction could have been increased more. Using HTC as a pre-treatment method would target more hydrogen and oxygen fractions in cellulose and lignin (Rizhikovs et al., 2012).

Another variation of the process used a chemical additive during the HTC phase. $ZnCl_2$ doped coconut shell underwent HTC at a high dry solids content of 30 % for 12 hours at 180 °C. The material was then activated in 3 ways, physically with steam, chemically with KOH, and through direct pyrolysis in 5 % hydrogen conditions. Both the physical and chemical activations retained and developed surface functional groups as well as a strong aromatic core. They were both found to be highly microporous, with similar surface areas, 483 m^2/g for physical and 499 m^2/g for chemical. Usually, chemical activations lead to much higher surface areas than physical activations. The discussion does not acknowledge that the initial $ZnCl_2$ doping could play a part in each of the activation processes. So, the physical activation was actually a hybrid of physical and chemical activation, which would explain the similarity between them in chemical and physical textural properties. The direct pyrolysis was preferred for the application as a fuel cell, due to a reduction in surface functional groups and a greater mesoporosity for the platinum catalyst. But the experiment showed another example of a successful HTC activation (Schonvogel et al., 2019). A different study showed a direct comparison between chemical and physical HTC activation of the same precursor. Also using coconut shell, the material was HTC treated at 275 °C for 20 minutes. The material was either physically activated with CO_2 or chemically activated with $ZnCl_2$, producing surface areas of 712 m^2/g and 1652 m^2/g respectively. Both materials showed improvements from their not HTC treated counterparts, as expected (Jain et al., 2013). This result was to be expected, which demonstrates the unusuality of the result produced by Schonvogel et al.

3.4 Materials in this Body of Work

This study will use waste organic matter. Biomass has been defined as “the biodegradable fraction of products, waste and residues from biological origin from agriculture, forestry and related industries including fisheries and aquaculture, as well as the biodegradable fraction of industrial and municipal waste” (Rakowski, 2015). This includes wood, sawdust, straw, bagasse, crops, nut shells, fruit stones, algae, seaweed, sewage, and much more. The potential energy within biomass is formed from sunlight during photosynthesis. The energy is fixed and stored in the plant. The energy is carried up the food chain as it is consumed until it is applied or returned through excrement. This chain of events make biomass a renewable resource.

Biomass is a generic term encapsulating organic materials, and each type is made from differing proportions of organic components and minerals. Some kinds of raw biomass are wet materials, and the moisture can be one of the highest weight fractions in the material. The core structure of lignocellulosic materials constitutes of cellulose, hemicellulose, and lignin, such as wood and herbaceous biomass. Together they represent the largest mass fraction in biomass on a dry basis and the most abundant organic renewable resource on earth (Saidur et al., 2011). They are also made up of lower quantities of proteins, lipids, sugars and starches. Completing the material balance is an inorganic fraction of various elements, including Ca, Cl, K, Mg, Na, P & Si. This will vary depending on the material and source environment. Materials primarily containing lipids, proteins, starch, inorganics, and minerals are known as non-lignocellulosic biomass, including sewage sludge or aquatic biomass (Anukam & Berghel, 2021).

Biomass possesses the potential to be a very useful material. One of the biggest natural examples is that all fossil fuels are derived from biomass. In the instance of forming coal, the process began millions of years ago when carbonaceous materials such as plant matter began to degrade in an aerobic process above ground or by anaerobic bacteria below ground. This removed the softer components, and the material was subsequently buried. The coalification process is a physiochemical degradation which happens below the surface, subjecting the material to elevated temperature and pressure. The process removes moisture and CO_2 to leave a carbonized substance rich in aromatic carbon (Marsh & Rodriguez-Reinoso, 2006). The coalification process is what the pre-treatment step in study aims to artificially replicate.

Biomass wastes are formed as low value by-products during many applications, including harvesting, forestry, and food preparation. The waste can be utilized in a circular economy. A benefit of using biomass is that it is hugely abundant. There is a great deal of materials at our disposal both on land and in the water, hosting 1.8 trillion tons and 4 billion tons respectively (Tursi, 2019). These materials would otherwise actively need treating and would be released to environment, so recycling to create a useful product is arguably better. By allowing the material to degrade naturally would release CO_2, in the same way that combustion would, albeit in a much shorter timeframe. This works toward achieving the carbon offset target of carbon neutrality. The greenhouse gas emission can be reduced significantly because the biomass does not contribute additional CO_2 into the carbon cycle (Tursi, 2019). The most economical reason to use biomass waste is that it is very cheap, often free and in some cases the recipient will receive a gate fee for processing the waste.

One of the main issues facing biomass as a recyclable material today is the high moisture content. A high moisture fraction in the material makes it more difficult to handle and increases the weight which must be transported. Another factor is the low-density nature of many biomass materials, which make these processes less efficient. Considering most upcycling processes will require a dry precursor, there will be considerable cost and energy requirements to prepare the material to be suitable. The material also has a high volatile fraction and a low higher heating value (HHV), which doesn't translate into being a successful fuel. When combusting, the material has a low burn temperature and due to the low energy density, burns out quickly. Another drawback is the heterogeneity of the material. This means characteristics could change depending on the date of harvest, source location, among other factors. The material may also have a high ash content and have issues with contaminants. In a more practical sense, there may be issues with storage, as

the material will begin to decompose. This can result in the release of odours or the potential for leaching hazardous materials (Pauline & Joseph, 2020).

So, biomass has the benefits of being an abundant and cheap carbonaceous precursor, which is available wherever life is present. Many sources of biomass are considered waste and are of no particular use in their current state. As previously mentioned, this study will focus on wet biomass, a category of waste which is often overlooked due to the drying costs necessary to prepare the material. This moisture fraction is key for the HTC pre-treatment. The following sections will introduce three wet biomass wastes which have been selected for the study.

3.4.1 Coffee Grounds

Coffee is a valuable commodity, both for its trade worth and psychoactive properties. It is the most exported product in many developing nations, in a global industry worth over $30bn USD, in 2018 according to the OEC report. It is a staple beverage worldwide and over 2 million cups of coffee are consumed per day (Nieber, 2017). This invariably creates a lot of waste during the harvest, manufacture, and consumption. Coffee grounds are the remains of spent coffee beans after brewing the hot drink. It is collected as a moist powder, once the coffee beans have been strained, filtered, or pressed. They are also prevalent in the remains of instant coffee capsules. This is commonly found in households, offices, and restaurants but predominantly in cafes and coffee outlets. It is reported that 2 kg of wet coffee grounds are produced for every 1 kg of soluble coffee (Mussatto et al., 2011). This resulted in a total of 6.5 million tonnes of coffee ground waste being produced globally in 2018, with the trend set to increase (Massaya et al., 2021).

Table 3.4 Comparison of fuel outputs, coal against hydrochar (Bergius, 1932) (Richards et al., 2021)

Coal Grade	**Heating value (MJ/kg)**
Low Volatile Bituminous	33
Anthracite	30
High Volatile Bituminous	25
Biochar	**18-30**
Sub Bituminous	20
Lignite	16

This poses a problem for disposal. It is a problematic material to landfill due to its high levels of organic matter requiring a lot of oxygen to decompose, which would release greenhouse gases to the atmosphere. It raises additional environmental concern because it is acidic and contains some toxic compounds such as caffeine, tannin and polyphenols which can leach into soil and ground water (Silva, 1998). Some uses have already been trialled for the waste. The material is rich in fatty oils which can be recovered and repurposed as biodiesel (Dang and Nguyen, 2019). Products such as ethanol and glycerine have also been extracted from the material (Kondamudi et al., 2008). However, this can be

time consuming and energy intensive. Instead, coffee grounds can be used for direct combustion, as demonstrated by *Bio-bean*, who dry and compress the material into a dense solid fuel. However, the heating value is 20 MJ/kg, similar to sub bituminous coal, as seen in Table 3.4, and it has issues with emissions from particulates and NOx (Cervera-Mata et al., 2021). Coffee grounds have also been used as composites in bricks and plastic substitutes, but it is still deemed an underutilized resource (McNutt, 2018). Presently only direct combustion has a commercial market. However, all these methods require a drying process and do not use the coffee grounds in their raw form.

Table 3.5 Dry basis coffee ground composition (Haile, 2014)

Material	Cellulose	Hemicellulose	Proteins	Lignin
Spent Coffee Grounds	8.6 – 13.8 %	30 – 40 %	10 – 20 % (oil)	25 – 33 %

Table 3.5 displace the expected constituents of coffee grounds. The largest fraction is hemicellulose which is the first to degrade in HTC. Coffee grounds have the potential to create high calorific fuels. Table 3.5 shows the composition, which is rich in organics and oils. Due to this it has recently gained attention in the field of HTC. A series of studies have tested a wide range of HTC parameters: adjusting residence time (1 – 12 hours), temperature (175 – 260 °C), dry solids content (10 – 50 %), and total volume (0.3 – 2 L). (Afolabi et al., 2020), (Cervera-Mata et al., 2021), (Massaya et al., 2021), (Zhang et al., 2020b) The results between the studies often show disagreements. These minor discrepancies have been attributed to the variable nature of the feedstock. The major findings from the studies listed are summarised as follows:

- Coffee grounds have an extremely low ash content (< 2%). Ash is removed during the HTC process, but higher temperature treatments suppress the demineralization action.
- Calorific values of coffee ground based hydrochars ranged from 26 to 33.5 MJ/kg.
- Temperature and residence time have the biggest effects on the hydrochars calorific value. Temperature has the greatest effect compared to residence time. Increasing the temperature from 180 to 220 °C resulted in a + 6 MJ/kg rise, while increasing the duration from 1 to 5 hours only had a +2 MJ/kg impact. The low temperature samples may not have completed the reactions necessary to undergo HTC, hence the lower calorific value.
- The fixed carbon increased with temperature and residence time. This also raised the fuel ratio of fixed carbon to volatile matter. Temperature had the greatest influence overall.
- Based on the experiments run, temperature and residence time have the biggest effects on hydrochar yield. The higher the temperature and the longer the residence time the lower the yield. Temperature is a more significant factor compared to residence time. When the temperature was increased from 180 to 220 °C the hydrochar yield dropped -15.5 wt%. When at 220 °C, the duration was increased from 1 to 5 hours, which dropped the yield - 8.3 wt%. However, at lower temperatures of 190 °C, the time has a negligible effect. The low temperature samples may not have completed the reactions necessary to undergo HTC, hence the higher yield.

- The surface of the hydrochar was rich in oxygen functional groups (carboxyl, hydroxyl, etc.).
- It was observed that hydrochar has a greater porosity than the raw material. Increased time favours the formation of a larger pore volume and BET surface area. However, not significantly enough to be considered as an activated carbon.

To summarise, a low to mid temperature combined with a long residence time appears to create the best precursors for activated carbon. Despite high temperatures leading to more fixed carbon, it also decreases the overall hydrochar yield. There is also less ash content at lower temperatures. Conversely, at temperatures below 200 °C, a longer residence time does not harm the hydrochar yield and there are greater signs of porosity development. This will provide a framework for this studies activation methods.

In addition, coffee grounds have already been trialled as a successful activated carbon precursor. Most successful trials have used chemical activation as a means of production, for use as CO_2 capture (Plaza et al., 2012) and adsorption of contaminants such as dyes, organic pollutants, phenols (Namane et al., 2005) and metal ions (Ching et al., 2011). The consensus is the material has a high capacity for adsorption. Table 3.6 shows the results of previous studies into activated carbon derived from coffee grounds.

Table 3.6 Successful activation techniques carried out on coffee grounds

Activating Agent	BET surface area (m^2/g)	Activation temperature (°C)	Application	Reference
H_2SO_4	225	600	Iron adsorption	(Ching et al., 2011)
H_3PO_4	950	600	Dye removal	(Namane et al., 2005)
H_3PO_4	830	600	Phenol adsorption	(Lamine et al., 2014)
H_3PO_4	910	600	Pesticide removal	(Bouchenafa-Saïb et al., 2014)
K_2CO_3	950	800	Phenol adsorption	(Castro et al., 2011)
KOH	1082	700	CO_2 capture	(Plaza et al., 2012)
KOH + CO_2	1865	800	Methyl blue removal	(Laksaci et al., 2017)
$ZnCl_2$	640	600	Dye removal	(Namane et al., 2005)
$ZnCl_2$	617	600	Salicylic acid adsorption	(Khenniche & Aissani, 2009)
$ZnCl_2$	682	600	Heavy metal (Cd, Pb) removal	(Boudrahem et al., 2011)
$ZnCl_2$	831	500	Heavy metal (Cu) removal	(Jutakridsada et al., 2016)
$ZnCl_2$	1039	500	Bisphenol-A removal	(Alves et al., 2019)

There are, however, gaps in the literature for the physical activation of coffee grounds. Examples from Castro et al. (2011) and Alves et al. (2019) showed activated carbons with 620 and 400 m^2/g respectively from steam facilitated activation. Both methods have not reached the full potential of coffee grounds as an activated carbon because the activation temperature reaches a maximum of 550 °C which is below the 700 °C threshold established earlier in Section 2.1.8.1. Also, both trials were run in parallel with a chemical activation under the same conditions. In both scenarios the chemical variant was the preferred option due to superior textural properties and less carbon loss. (Plaza et al., 2012) It is believed in this study, that by activating the material at a higher temperature, combined with the carbonization effect of HTC, the activated carbon produced will be far superior and more in line with the chemical variants.

3.4.2 Sewage Sludge

Dry solids removed from wastewater is one of the largest streams of waste worldwide. It is the true definition of waste, and it is prevalent in all places which host life. It is reported that over 330 km^3 per year of municipal wastewater is accounted for globally. It is expected this load will increase considerably as the population grows. Presently only 60 % of that is treated, which is a cause for environmental concern (Mateo-Sagasta et al., 2015). In the European union alone, the output of dried sewage sludge is estimated to be more the 10 million tonnes of per year (Grobelak & Jaskulak, 2019). Sewage sludge is considered as the concentrated solid resulting from household liquid wastes (Eid et al., 2018). The dry solid content is varied in sewage sludge, typically 1 % but it can range up to 12 % (Nguyen et al., 2021). Many characteristics of the slurry will change depending on the sample location, the origin source and treatment processes, making it unpredictable. The constituents in sewage sludge can be seen in Table 3.7. This demonstrates the fluctuation which can happen between batches based on the origin. Drying the material is highly energy intensive. The treatment, drying and disposal of the sludge currently accounts for 60 % of the total operational costs in wastewater treatment, despite it only being applied to a small fraction of the total wastewater volume treated (Murray, Horvath & Nelson, 2008).

Table 3.7 Dry basis sewage sludge composition (Grobelak & Jaskulak, 2019) (Fan et al., 2020)

Material	Organic matter	Organic Carbon	Nitrogen	Phosphorus	Mineral Matter
Sewage Sludge	9.5 – 85 %	12 – 63 %	0.1 – 8.4 %	0 – 4.2 %	10 – 75 %

As an unavoidable waste source that has been around for centuries, many uses have been found. The most common options are combustion and soil amendment. The nitrates and phosphorous content make it a natural fertilizer. In 2010 it was reported that across the EU, 39 % dry solids recovered from wastewater treatment processes were utilised in the agricultural industry (Lamastra et al., 2018). The uses vary greatly between countries, based on their needs and limitations. In the UK, there is a drive to utilize the waste because of a lack of space. Due to this and the heavily farmed land, it was reported that 79 % of sewage sludge from the UK was reused in agriculture. An additional 20 % was incinerated with a minimal quantity reaching landfill (OFWAT, 2015). In Italy however, landfill accounted for 48 % of disposals and another 4 % was incinerated. Overall, it met the EU average for agricultural reuse (Merzari et al., 2019). There are many places where sludge does not have

a beneficial use, such as China where only 3 % is recycled and 80 % is sent to landfill (Mateo-Sagasta et al., 2015). There are successful cases of repurposing sewage sludge, but it is still an energy intensive process. The material is required to be dewatered and dried, even for landfill.

Despite having valuable components such as organic carbon, it also contains many hazardous substances such as pathogens, heavy metals, and organic pollutants (Wang, Chang & Li, 2019). One of the greatest hurdles is the high ash content, which is a concerning characteristic in a fuel and activated carbon precursor. This could limit the functionality of the hydrochar product. The minerals are mainly made up of heavy metals and tend to include, but are not limited to, Al, Cd, Co, Cr, Cu, Fe, K, Li, Mn, Mg, Na, Ni, Pb, Si and Zn (Ahlberg et al., 2006), (Donatello, Tyrer & Cheeseman, 2010). As environmental regulations tighten, the water filtration must be more thorough before releasing to environment, thus producing more sludge (Fytili and Zabaniotou, 2008). The added impurities make it less applicable as a fertilizer. It poses risks to soil and groundwater when it is sent to landfill, where there is additional pressure due to a lack of available space. The practice can also trap biogas, causing unstable and unsafe conditions in the form of uncontrolled releases (O'Kelly, 2005). Incinerating the material directly is not efficient. It has a low energy density and because of impurities it releases harmful gases (Wu et al., 2014). However, it has been successfully trialled in co-firing with fossil coal (Parshetti et al., 2013). Ultimately, the potential in using this resource is minimal but due to the production volume, there is a need for a more efficient and environmentally friendly approach for sludge utilization.

The core processes of a wastewater treatment plant have remained consistent for a long time. The wastewater typically enters a screening process to remove large debris, like wood, which has been carried by the stream, to avoid blockages or damaging the plant. There is also apparatus to remove grit and grease. The primary treatment process relies on sedimentation in large clarifiers to separate out the solids. This tends to remove easily dewaterable components such as organic rich matter and other heavy materials. High concentrations of organic materials are still dissolved in the wastewater, so the secondary phase uses aeration. An aeration tank aids the growth of bacteria to breakdown the organic matter. This stage is biologically active and relies on waste-activated sludge to provide a culture of bacteria. The tertiary section follows, where chemicals are introduced. A coagulating agent or flocculant is mixed into the tank to reduce solubility and separate the organics out. They are easily collected from the surface as flocs or as sediment settled at the base (Canziani & Spinosa, 2019). Sewage sludge is the collective term for the solid component. When it is recovered it still has a high moisture content and contains pathogens. The collected sludge then undergoes processes of thickening, stabilization, dewatering and drying (Pradel, 2019).

The technology is old and simplistic which requires large areas of land and takes a long time to complete. The sludge can be directly treated by HTC, which offers a fast and low energy conversion compared to the traditional WWTP. Other processes such as gasification, pyrolysis and incineration are available; however, much of the energy released during these processes will be lost through drying the initial material. HTC accepts the material in the natural high moisture form. The post process does require drying, however after the HTC process the drying process is much simpler. Due to the destruction of hydrophilic functional groups, small negative surface charge and the removal of bound water, the

mechanical dewatering performance is much greater than the precursor, making the drying process easier (Wang, Chang & Li, 2019).

HTC has been applied to sewage sludge for the past decade to demonstrate the positive impacts. It is a well-documented process and a series of studies have tested a wide range of HTC parameters: adjusting residence time (15 minutes – 12 hours), temperature (180 – 300 °C), dry solids content (10 – 21 %), and total volume (0.08 – 19 L). (Ahn, Kim & Lee, 2020), (Escala et al., 2012), (He, Giannis & Wang, 2013), (Kim, Lee & Park, 2014), (Liu et al., 2016), (Marin-Batista et al., 2020), (Parshetti et al., 2013), (Peng et al., 2016), (Wilk et al., 2019), (Xu et al., 2020), (Zhai et al., 2020), (Zhao et al., 2014). The results tend to show a successful HTC process, but overall, the fixed carbon changes tend to be minor, and the energy density is rarely greater than 20 MJ/kg. Acid leaching has been found to be effective at removing ash and increasing the HHV. One study reported a loss of carbon to the liquid phase; however, the experiment limited the induced pressure. The major findings from the studies listed are summarised as follows:

- Calorific values of sewage sludge based hydrochars ranged from 11 - 23 MJ/kg.
- The ratio of fixed carbon to volatile matter can be increased tenfold through the process.
- The energy density, carbon content and dewaterability increased with increasing time and temperature. Temperature created the biggest effect. These results were seen in tests as short as 15 minutes.
- Recycling the aqueous phase through several cycles of HTC can increase HHV and hydrochar carbon content.
- Acid and alkaline conditions determine leaching of heavy metals between hydrochar and process water. In post processes, the hydrochars are more effective at preventing heavy metal leaching than in raw sewage sludge.
- The yield and properties became more stable as residence time was increased, plateauing after 6 hours.
- 200 °C was marked as the most efficient temperature for energy recovery, however 220 °C gave the greatest HHV.
- 90 % carbon can be recovered in the hydrochar. Nitrogen and sulphur contents were reduced by 60 % in hydrochar, which were released to the gas and liquid phases.

Ultimately a cleaner burning fuel was created. The high temperatures destroy pathogens which would otherwise render the waste toxic and there is evidence of HTC reducing the odour. A lot of studies tend to focus on a rapid treatment of the material in under an hour. From the broader collective of HTC studies on other materials, the method is suited to a longer residence time to allow reactions to progress. Pilot plants have inherently long residence times due to the time required to heat the mixture to the reaction temperature. It is proposed that a longer residence time is better suited for maximising fixed carbon content and a temperature of 200 °C is high enough to meet reaction targets whilst being energy efficient.

By operating at a fraction of the cost, reducing residence time, increasing dewaterability and creating a useful fuel substitute, HTC looks a valid technology to progress the WWT industry. With the increased carbon content, it could be more suitable as an activated carbon precursor. Many activation tests have been conducted on the raw sample. Chemical activation is the most popular option with examples of KOH, NaOH, $ZnCl_2$ and H_2SO_4

(Mu'azu et al., 2017). The highest surface area produced was 792 m^2/g by using $ZnCl_2$ (Kong et al., 2014). The examples of physical activation produce a much lower surface area. The most effective treatment agent was continually found to be steam, with the optimum reaching 226 m^2/g (Stüber et al., 2011). There are few examples of the physical method, and it was not properly optimised.

As a popular HTC precursor, some studies have conducted the combination of HTC and activation. Danso-Boateng et al. (2020) used HTC to treat sewage sludge and simulated faecal matter (180 °C, 5 L & 30 minutes) before using KOH chemical activation. The result improved the surface area of the starting material tenfold, however this was only 9 m^2/g. This showed potential for adsorbing organic pollutants from effluents. In a more direct attempt, Xin, Li & Son (2020) used H_2SO_4 for an activation agent but incorporated it before the HTC process to reduce the pH (180 °C, 9 %DS, 0.06 L and 12 hours). The activation was carried out as high temperature pyrolysis afterwards (900 °C, 3 hours). The micropore volume was increased resulting in a specific surface area of 134 m^2/g. The ash present was reported to improve mechanical strength. The potential of sewage sludge was shown by Saetea and Nakorn back in 2013. By using modest HTC conditions (200 °C, 20 %DS, 0.5 L and 1 hour) and aggressive steam activation conditions (900 °C, 1 hour, 20 cm^3/min steam) they produced commercially comparable AC, with a specific surface area of 595 m^2/g. This is an isolated case measuring the surface area four times greater than the nearest comparison. It was not stated whether this factored the ash content or a manipulation of the numbers to include only the carbon fraction.

Comparing the two activation routes, despite the different activation agents, a major differential is caused by the HTC residence time. Increasing from 30 minutes to 12 hours may have impacted the hydrochar structure to be a better AC precursor. The physical activation example from the work by Saetea and Nakorn had a low HTC residence period. Perhaps increasing the HTC residence time and following a similar activation pathway will maximise the potential of sewage sludge activated carbon.

3.4.3 Strawberry Pomace

Fruit pomace is the resulting waste from manufacturing juice, concentrate, nectar, essence, and puree, among other commercial products from fruit. It generally represents the skin, flesh, seeds, stems, and general pulp which have been pressed, sieved, and filtered off during the manufacturing process. It is a valuable industry and high quantities of agricultural wastes are produced each year through these methods. The bone-dry weight of a pomace is roughly 4 – 7 % mass of the raw product (Šaponjac et al., 2015). However, the actual quantity of waste recovered is between 25 – 35 % of the raw material mass input, as dewatering the material further is inefficient (Kruczek, Drygas & Habryka, 2016). This high moisture content provides a suitable base for HTC.

Table 3.8 Dry basis strawberry pomace composition (Nawirska & Uklańska, 2008)

Material	Cellulose	Hemicellulose	Lignin	Ash
Strawberry pomace	25 – 30 %	1 – 11 %	15 – 21 %	5 – 7 %

When strawberries undergo the juicing and maceration treatment, the end material is known as strawberry pomace. In 2016, 8 million tonnes of strawberries were produced worldwide (Cubero-Cardoso et al., 2020). Much of the produce is consumed as fresh fruit,

but a portion will go into the manufacture of jams etc. As seen in Table 3.8, there is a high organic content in strawberry pomace. A study by Xue et al. (2018) showed that a higher ratio of cellulose to lignin often produces a more mesoporous activated carbon. Whereas those with a greater lignin content tend to produce a greater microporous fraction. The ratio within strawberry favours a mesoporous activated carbon, but there is still a substantial lignin fraction which can contribute to microporosity. Much of the rest of the material is made up of fibre, antioxidants, and polyphenolic compounds, which can impact soil quality and aquatic ecosystems if sent to landfill. It has uses elsewhere as a biofuel, producing bioethanol or biogas from fermentation, as compost and animal feed. Further processing can remove pigments and nutrients for use as dyes or food flavouring. Ultimately it is another waste material which fits the HTC and activated carbon precursor requirements. Although the waste is not a huge issue alone, it will demonstrate the potential of fruit pomace in the process. Multiple forms of waste could be processed together for greater volumes.

There is little work done previously on strawberry pomace. Although, fruit pomace such as grape, orange, apple and olive have been successfully carbonized through HTC, with a maximum HHV of 31.14 MJ/kg (Erdogan et al., 2015), (Micali et al., 2019), (Zhang et al., 2018). They also showed significant reduction in moisture and ash content. There is concern that the high sugar content will require a higher temperature to react, however it was found that the temperature increase had little impact on the final yield. Strawberry pomace is an obscure precursor and has not had many HTC trials on it. Conditions and methods from other fruit pomace can be used as reference when planning the testing framework on strawberry. However, it should be noted that despite similarities between organic materials, slight differences in the precursor will elicit differing functionalities in the final product. This was demonstrated by Ciftyurek et al. (2018) when applying identical HTC and activation methods to blueberry and cherry pomace. Despite an initial similarity in glucose and other organic content, the resulting activated carbons had different surface area, porosity morphology and chemical characteristics.

One study by Yue et al. (2017) used rotten strawberries as a precursor, citing that the delicate nature of the material results in many being disposed of. The material underwent a thorough HTC pre-treatment (180 °C, 12 hours) and was chemically activated using a KOH method. Strawberry pomace will have a slightly different composition, but the rotten strawberry activated carbon product demonstrated the materials potential, with a highly microporous structure with surface areas exceeding 1500 m^2/g. Using the method of physical treatment would open a new direction for the activation of this material and can be compared to this study. It shows potential as a precursor material which could be optimized by HTC. The global food waste recorded in 2015 amounted to 1.3 billion tonnes (Kaza et al., 2018). So as a collective it needs to be explored further, and strawberry will act as a representation for this sector.

3.4.4 Summary

- Activated carbon is a highly sought-after material with a multitude of applications
- Transforming wet waste biomass to hydrochar creates a more desirable precursor for activation than the raw biomass, as it draws parallels to fossil coal, the standard AC precursor
- HTC reduces the drying costs and energy demand of wet waste disposal
- HTC is faster and more energy efficient than competing technology

- Physical activation with steam is the conventional way to mass produce ACs
- The concept of activating hydrochar is an emerging field, and few studies cover the selected materials
- Coffee grounds have not been physically activated > 700 °C before, which was established as the lower bound activation temperature
- Sewage sludge has been subject to many previous studies, but few examples of the physical activation are available. It is believed that these activation conditions have not been optimised. This work will build upon the knowledge from Saetea and Nakorn (2013) by altering the HTC conditions as well as reducing the activation temperature and optimising the approach
- Strawberry pomace has not been physically activated prior to this study. Similar waste products have proven there is a wide variation of components in fruit varieties, which impact the structure of the final product
- The combination of HTC pre-treatment and physical activation has not been applied to coffee grounds or strawberry pomace

4 Methodology

4.1 Sample Selection

The materials which have been selected for experimentation cover a broad spectrum of waste. They can be broken down into sectors representing outputs from industrial waste, commercial waste, and household waste. The common factor between the materials is a high moisture content which accompanies the material from the source. Wet wastes must go through drying processes before it is possible to be treated through applications such as pyrolysis. HTC is positioned as an emerging alternative technology that requires a high moisture content to operate. It has been identified that HTC is an ideal solution to treat high moisture waste. Dispensing of the need to dry a precursor is beneficial financially and environmentally. Listed in this section are some key details about the materials used and where they were sourced.

4.1.1 Strawberry Pomace (SP)

Strawberry was selected for its high cellulose content, which was found to be approximately one-third in Section 2.4.3. The ratio between cellulose and lignin is anticipated to yield a high mesoporous region carbon (Xue et al., 2018). The high moisture and organic content mean it is susceptible to quick degradation and would need to be processed through HTC soon after production or dried for other means. The waste was courtesy of Mainfrucht GmbH & Co. KG, Bavaria, Germany. Approximately 5 tonnes of strawberry waste were delivered to the Antaco HTC pilot plant in Kiel, Germany. The material was delivered in a dried form, to avoid issues of decomposition and additional weight during transportation. The material can be seen upon arrival in Figure 4.1. Water was added to the waste and mixed to create a slurry for processing. The known weight of SP was used to create a precursor with 12 % dry solids (DS).

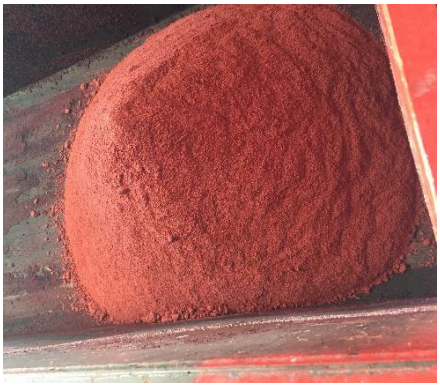

Figure 4.1 Dry SP feedstock for scaled HTC



Figure 4.2 Frozen raw SP for activation



Figure 4.3 Dried raw SP



Figure 4.4 Pelletized SP hydrochar

A separate batch of 10 kg was delivered to the laboratory at the University of Nottingham, UK, in a frozen form, seen in Figure 4.2. The waste contained 67 % moisture on average. A portion of the material was weighed, thawed, and dried in batches of approximately 300g in a drying oven for 24 hours. The dried raw strawberry before HTC can be seen in Figure 4.3. The dry mass was recorded afterwards and used to calculate the dry solids (DS) content and moisture content (MC), as seen in Equation 4.1 and 4.2 respectively. After the material was dried it was stored under refrigerated conditions in a sealed container to minimise contact with moisture. The image in Figure 4.4 shows the pelletized hydrochar samples produced from the HTC pilot plant. The pellets were uniform in shape and circumference but varied in length. Typically, 10 – 15 pellets would constitute a 5 g sample. This represents a generic household food waste, high in cellulose and available in small batches.

$$DS\ (\%) = 100(\frac{m_D}{m_W})$$

Equation 4.1

$$MC(\%) = 100 - DS$$

Equation 4.2

Where: m_D = Dry mass
m_W = Wet mass

4.1.2 Coffee Grounds (CG)

Coffee waste was selected for its high HHV potential and low ash content. The waste coffee grounds used in the experiment were courtesy of Lakeside Restaurant and Coffee Shop, Surrey, UK. The waste was selected from here for convenience and because a single brand of coffee is used here, 'Matthew Algie Tiki blend' espresso beans. This minimised variation between batches and decreased contamination from other beverages; to keep results consistent. The material was collected fresh from the store and still contained a high degree of moisture. The was recorded to contain an average of 52 % moisture, as expected (Gomez de la Cruz et al., 2015). Upon collection the material would be weighed and left in a drying oven for 24 hours. The dried powdered material can be seen below in Figure 4.5.



Figure 4.5 Dried raw CG



Figure 4.6 Dried HTC CG



Figure 4.7 Pelletized HTC CG

The DS and the MC were calculated using the same method as in Section 4.1.1. After the material was dried, it was stored under refrigerated conditions in a sealed container to minimise contact with moisture. This precursor was selected to represent a commercial waste from urban areas. A comparison of the material before and after HTC can be seen between Figures 4.5 and 4.6. In Figure 4.5 the material is a dark brown, and the contrast of the light coming from the top right shows the powder in a mound, with a shadow on the

front. After the HTC process, Figure 4.6, a finer powder with a much blacker appearance can be seen. Here no reflection of light can be seen, it is simply a deep black powder. Finally, the material was pelletized, as in Figure 4.7, as the material was too fine and was lost in the process. It also created a more similar starting product to the other materials, which had been pelletized onsite directly after HTC. In an industrial process the material would also be pelletized before use or further activation.

4.1.3 Sewage Sludge (SS)

The waste was courtesy of Abwasserverband Aarau und Umgebung (AVAU) and was processed on site at their wastewater treatment plant in Aarau, Switzerland. The plant currently serves a population equivalent of 125,000. Material was selected here due to a high percentage of fats, oils, and greases (FOGs) found when testing the raw material. This is attributed to dietary behaviours found in the region. FOGs mainly consist of lipids and fatty acids like triglyceride, with minor concentrations of carbohydrates and proteins. Sludges with a higher initial FOG content produce hydrochars with a greater heating value (Bhatt & Tao, 2020). The inlet had a high moisture content of 88 %, courtesy of Antaco Ltd UK. An image of the sample pellets can be seen in Figure 4.8, below. This precursor was selected to represent an industrial waste stream.



Figure 4.8 Pelletized HTC SS

4.1.4 Sample Key

The samples have been labelled to clearly define the treatment route. CG and SP are the only samples which were tested as 'raw' non-pre-treated samples for biosafety purposes. The naming convention template follows the trend [Material – Pre-treatment – Process – Temperature – Time] and the corresponding abbreviations can be found in the Appendix.

4.2 Hydrothermal Carbonization

4.2.1 The HTC Pilot Plant

The strawberry pomace and sewage sludge were processed at separate points in a continuous hydrothermal carbonization system. The plant is a pilot scale system to demonstrate the continuous HTC process. It is owned and operated by renewable energy start-up Antaco UK Ltd, Surrey, UK. The system was situated in Kiel, Germany where it was used to process various batches of waste materials, including the strawberry pomace. It is now operated in Aarau, northern Switzerland, attached to a WWTP, where the sewage sludge sample was collected from. The HTC unit is capable of processing 6 m^3/h of wet organic feedstock. It is one of the first commercially operated HTC plants in the world, among other competitors such as TerraNova Energy GMBH of Jining, China and Ingelia of Valencia, Spain. The strawberry pomace was processed April 2018 and the sewage sludge

was processed from July 2019 onwards. The technology is housed in a series of shipping containers for ease of movement when demonstrating the technology. Here is a brief description of the process.

The slurry was held in a continuously stirred mixing tank, seen in Figure 4.9, to keep it homogeneous. It was maintained at 12 % DS. The material was pulled from the mixing tank by a progressive cavity pump and pushed into the system. The system flowed at 2 m^3/h. A pressure was induced on the material by using a pump at the beginning and end of the system. The pump at the end of the system would provide resistance to the driving pump, allowing a pressure to be built, maintained, and controlled by the operator. It would also depressurize the outgoing hydrochar and establish the material residence time.



Figure 4.9 Stirred storage vessels for feed



Figure 4.10 Inside the continuous HTC process

Once the material was pumped into the system, it was heated up. It entered a heat exchanger where it raised the conditions to within the HTC window, using a thermal oil system. The reactor is a continuous piping system where the material is held at a constant temperature and pressure to undergo the HTC treatment. The residence time in this phase is 10 hours. The slurry was transported around the system at HTC conditions in a network of horizontal pipes which are trace heated and lagged. One of the vessels can be seen in Figure 4.10. As a new large-scale system undergoing testing, producing a large quantity of samples, the conditions used for the specific samples that were collected cannot be accurately pinpointed. However, it is known that the temperature was maintained between the range of 200 – 220 °C, while the sample was collected. During operation the pressure was kept relatively constant at a set point of 20 bar. The system was equipped with sensors in all key equipment, and was displayed on a screen, which is shown in Figure 4.11.



Figure 4.11 HMI control screen for pilot plant

After the HTC process was completed, the hydrochar passed through the heat exchanger once more to recuperate the heat, before being released by the depressurization pump. The outlet was recorded as 15 % DS, which can be seen in Figure 4.12. The material was sent to a filter press to increase the DS content. This resulted in the material seen in Figure 4.13. The material was stored in under shelter and dried further to 80 % DS before being pelletized. The cylindrical pellets that were collected ranged from 10 – 30 mm in height and 5 mm in diameter, which can be seen in Figure 4.14. Once pelletized, the samples were stored in an airtight container until use.



Figure 4.12 Wet hydrochar



Figure 4.13 Dry hydrochar



Figure 4.14 Pelletized hydrochar

4.2.2 The Laboratory Scale HTC Reactor

The coffee hydrochar was synthesised using a non-stirred high-pressure reactor. The body had a capacity of 1000 ml and, when operated, it replicated the conditions required for HTC. The experiment ran as individual batch reactions. The rig was assembled for this purpose. The vessel was purchased from Col-Int Tech, South Carolina, USA (model number: CIT-XHTC400-V1000B) and was modified for purpose, seen in Figure 4.15.

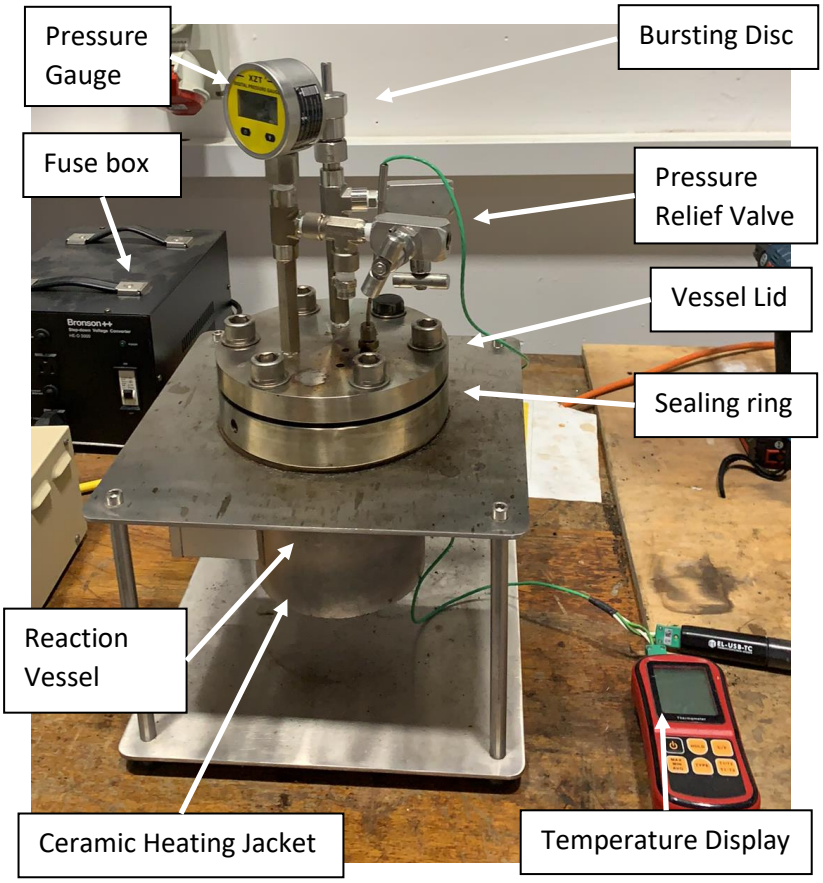

Figure 4.15 Lab scale batch HTC reactor

The vessel was affixed to a stainless-steel exterior support structure which caged the reaction chamber. Access to the reactor was gained through an opening at the top which was capped. This lid was held in place by 6 bolts. The structure around the body kept the reactor elevated and fixed in place while tightening and loosening the sealing bolts. Inside the reactor there was a PTFE sleeve to line the chamber walls. This would hold the slurry, so it was easier to remove and prevent it from sticking to the reactor walls. The temperature was controlled using a ceramic heating jacket which coiled around the rig.

The lid had 3 access points to allow peripherals to monitor the system during the reaction, consisting of a thermocouple, a pressure gauge, and a safety release line. They were fitted with Swagelok valves and wrapped in PTFE tape to create a seal. The thermocouple had a probe at the centre of the reactor to read the actual temperature. It was also attached to the ceramic heating jacket to form a feedback loop. With a single-phase electricity supply, the heating jacket was connected to the mains via a transformer to adjust the 220 V supply to the required 110 V. The safety release line had a T-junction valve which incorporated a pressure relief valve (PRV) and a bursting disc. The PRV was rated at 30 bar and a bursting disc was set to 60 bar. The vessel was enclosed behind a protective Perspex barrier during operation.

Feedstock was prepared using this method: The coffee was first dried to completeness in a fan oven at 90 °C for 24 hours to moisture free weight. Approximately 60 g of coffee grounds were weighed out and mixed with 540 g of deionised water in the PTFE sleeve. This ensured a consistent 10 % DS slurry. The vessel was only filled to 60 % capacity to

prevent over pressurisation. The moisture content was in line with the material entering the pilot plant and followed the successful methodology demonstrated by Afolabi et al. (2020), Cervera-Mata et al. (2021), and Zhang et al. (2018).

The mixture was lowered into the reactor. A graphite gasket was placed on top, and the lid was put in place to form a seal. It was secured with an electric torque wrench (> 130 N/m) to ensure it was tightened equally at all points. The system could be heat tested for leakage, which would confirm the system was closed. The ceramic heating jacket was programmed to heat and maintain a set point of 220 °C. The ramp rate was 2 °C /min. When the temperature set point was reached, the reaction would run at autogenic pressure, which would equate to 20 bar. The system was enclosed for safety, as the entire unit became hot during operation and provided a barricade for the bursting disc. Once the set point was reached, the experiment had a residence time of 5 hours at HTC conditions. At the end, the heating jacket was manually switched off at the mains and left to cool down. The process aimed to replicate similar conditions found in the plant. The only limitation was the time it could be run for, due to the operating hours of the laboratory. The method followed that which was reported by Crossley et al. (2019).

Before removing the lid, the temperature and pressure probes were checked to make sure they had sufficiently returned to an ambient range. Any additional pressure, caused by the evolution of gaseous by-products, was vented through the PRV prior to opening. The PTFE sleeve was removed, and the slurry was emptied. The hydrochar was filtered through vacuum filtration, using 11 µm filtration paper. The recovered solids were dried in an oven for 24h hours at 80 °C. The final material was a fine black powder and approximately 0.5 g was tablet pressed at 2 tonnes using a hydraulic pellet press, making a regular tablet with 6 mm height and 13 mm in diameter. Materials were stored in an airtight container under refrigerated conditions until further use.

4.3 Horizontal Tube Furnace

4.3.1 Activation Process

Sample activation was achieved through the physical activation method. The hydrochar output from the HTC systems arrived dried and pelletized (SP & SS: 10 – 30 mm H x 5 mm D, CG: 6 mm H x 13 mmm D). The activation was initiated with the sample in this form. Physical activation was selected because it is ideally suited for the samples; low moisture content chars which are targeted at creating GAC. The material has previously been carbonized during HTC, so it did not require an individual carbonization step. Instead, the removal of moisture and volatiles happened during the temperature ramp to the set point, in a ‘direct activation’ process. The other option was chemical activation, but introducing chemicals can have harmful environmental effects, increase operational costs, and include additional impregnation and washing phases. The pre-pelletised materials also did not suit this technique. Thus, the single step physical activation process was deemed to be more convenient, lower cost, more realistically scalable and better suited for producing GAC.

4.3.2 Activating Agent

Steam was selected as the activating agent for this experiment. Air was deemed too aggressive because the experimental plan was to allow a prolonged contact time between activating agent and char to allow the pores to develop sufficiently. During activation, oxygen from the activating agent reacts with the char to form gas products. It will also chemisorb to form surface oxygen complexes which offers surface stability and adsorption

qualities. The hydrogen introduced in steam activation can also chemisorb to the surface. The formation of C(H) inhibits the reaction rate of the gasification, which helps control the porosity development (Marsh & Rodriguez-Reinoso, 2006). The practice of using steam is more widely used in industrial direct-fired furnaces, which is a consideration with the long-term view of scaling the experimental process. The consensus is that there is a greater microporous development throughout samples created under the influence of CO_2. This creates more microporous materials due to the more endothermic reactions involved. Experiments have shown that CO_2 creates micropores whereas steam has more impact widening the micropores (Rodríguez-Reinoso, Molina-Sabio & González, 1995), (Pallarés, González-Cencerrado & Arauzo, 2018). Some results directly comparing CO_2 and steam can be conflicting. Experiments have shown steam to produce higher surface area and pore volume (Yang et al., 2016), (Zhang et al., 2020a), examples of increased surface burn off with CO_2 (Linares-Solano et al., 2000) and higher surface area from CO_2 but comparable mean pore widths on coffee endocarp samples (Nabais et al., 2008). This might be material or method specific, but steam can be a valid activating agent. The steam was injected with nitrogen as an inert carrier gas.

4.3.3 Activation Conditions

The activated carbons final form is strongly influenced by the activation conditions. The experimental design varied both to establish the optimum conditions for activation. Criteria for the optimum zone includes the total carbon loss, surface area, pore volume, pore size distribution and surface complexes formed. The trade-off which is focussed on is the competition between carbon yield and surface area found in the final product.

The two biggest factors affecting activation are the set temperature and time it is held for. The literature points towards a combination of a relatively low temperatures over a long period of time. Previous experiments activating hydrochar focus on a 1-hour activation: Aghababaei et al. (2021) steam activated at 850 °C for 1 hour, Congsomjit & Areeprasert (2020) steam activated between 700 – 900 °C for 1 hour, with the 200 °C HTC hydrochar performing best at dye removal and Mestre et al. (2015) steam activated at 800 °C for 1 hour, finding the highest carbon content in the steam activated ACs compared to CO_2 and pyrolysis experiments. The standard 1-hour timeframe has been halved and doubled to create the lowest timeframe and maximum timeframe, for comparison purposes and to study the morphology change over the timeframe. Identical times have previously been used on sewage sludge hydrochar at 900 °C. It is to be seen if the results can be matched using the pilot scale HTC production method and how temperature variation will impact the AC product (Saetea & Tippayawong, 2013).

The reaction required a minimum temperature of 700 °C, and the instrument was limited to 1000 °C, which set the constraints for temperature. Each interval was spaced at 50 °C to give a reasonable spread across the range. Chegini, Briens & Pjontek (2022) tested the range of 600 – 900 °C finding 800 °C for 2-hours to provide the highest surface area and adsorptive capacities. Congsomjit & Areeprasert (2020) stated that the 700 °C sample conditions were not high enough to cause activation, but studies such as Beri et al. (2021) have shown that a low 200 °C HTC process and 500 °C steam activation can yield positive results through the protection of surface functional groups and the benefit of lower energy consumption. Thus 700 °C remains the lowest temperature, expected to perform better over long duration and will compared to the highest temperature which is expected to perform better over short durations.

The experimental matrix decided upon is shown below in Table 4.1. In this scenario residence time refers to the time spent held at the set temperature while steam was injected, not the total time spent in the reactor.

Table 4.1 Basic testing matrix to vary the key parameters

	700 °C	750 °C	800 °C	850 °C	900 °C	950 °C
0.5 hours	-	-	-	-	-	-
1 hour	-	-	-	-	-	-
2 hours	-	-	-	-	-	-

A heating rate of 10 °C /min was selected. The consensus in the literature was that the heating rate has a low impact on the final surface area (Lua et al., 2004). An elevated heating rate reduces operation time and the energy input into the rig.

The system was under a constant flow of nitrogen to keep the atmosphere inert. Nitrogen was selected for its low cost and ease of availability. The nitrogen flow rate was kept constant at 1 L/min 1 bar, between experiments. This was standard across many experiments in the literature and was recommended by colleagues with experience using the horizontal tube furnace (Sterling, 2019).

Steam was injected into the system at a rate of 0.1L/hour. This kept the steam in excess to maximise interaction with the sample. This was continuously pumped for the duration that the equipment was held at the temperature setpoint. The peristaltic pump was set to this rate and was unable to be changed. However, it was concluded in the literature that an excess concentration of steam had no undue effects on the activation and overall had little effect. This kept the steam in excess at a partial pressure of 1 bar.

4.3.4 Apparatus

The experiment was conducted in a laboratory scale horizontal tube furnace, manufactured by Elite Thermal Systems Ltd, Leicestershire, UK (model no. THH 11/90/457). The apparatus can be seen in Figure 4.16. A thermocouple in the centre of the reactor provided an accurate reading of the operational temperature. The reactor was a cylindrical quartz tube, measuring 1000 mm length with a 60 mm internal diameter. The sample was held in a ceramic reaction crucible and was positioned at the centre of the furnace using a metal hook and sealed inside the tube. The tube was closed at both ends with rubber bungs holding inlet and outlet lines. This created a closed system with a boundary permeable to energy and only selected matter could enter the reactor through the inlet and exit through the outlet. This matter was intentionally introduced and recorded.

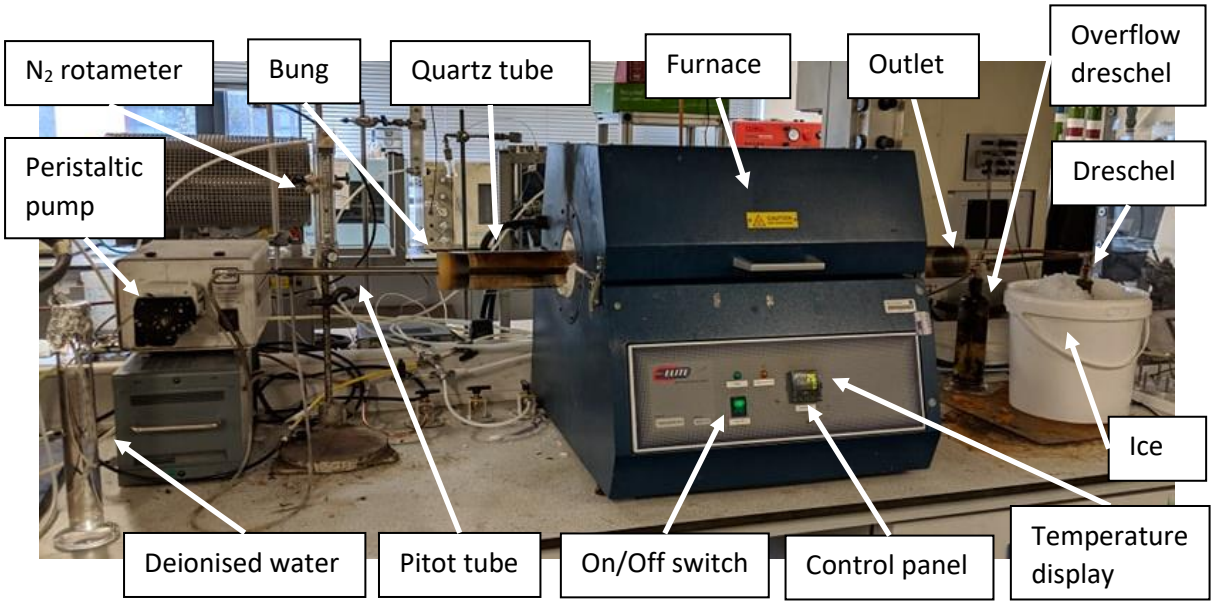

Figure 4.16 The experimental set-up which acts as a fixed bed reactor

The inlet pipe, designed like a pitot tube, allowed the simultaneous injection of nitrogen and steam. A schematic can be seen in Figure 4.17. The nitrogen flowed through the central tube and the water flowed through the outer rube in the space created between the two tubes. The rod stretched 450 mm into the quartz tube, so the liquid would vaporize as it was pumped closer to the outlet. The water was positioned here to maximise the heat exposure. Also, from a design perspective, it stopped mixing inside the tube as both inputs were regulated independently. The nitrogen rate was controlled by a flow meter and the water was controlled by a peristaltic positive displacement pump. Deionised water was stored in a 250 ml measuring cylinder to record the volume injected. When the peristaltic pump was switched on the water was ejected at the end of the rod as steam and elutriated through the system in the flow of nitrogen. A flanged end was used to aid the disbursement. The pressure inside the tube remained at 1 bar throughout the experiment. If the pressure was greater than this, then the bungs would pop out.

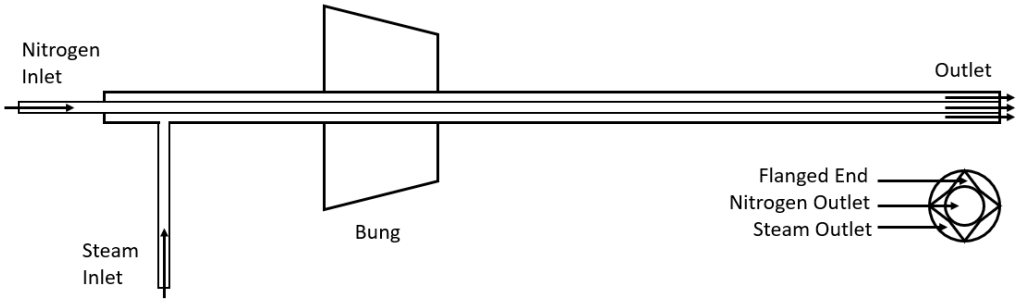

Figure 4.17 Pitot tube cross sectional schematic for the injection of the activating agent

Firstly, 5 g of sample was weighed out. This was a sufficient quantity to cover the base of the ceramic crucible without stacking pellets on top of one another. The system was closed with bungs and the nitrogen was switched on. The system was purged with nitrogen for 15 minutes prior to heating in order to remove the residing oxygen, preventing combustion and creating an inert atmosphere. During the heating/carbonization phase the nitrogen continued to flow to maintain the inert atmosphere. When the set point was reached the instrument was held isothermally for the desired residence time. The pump was switched

on to move deionised water through the injector rod. While the steam was injected, nitrogen flowed through the system throughout the activation to act as a carrier gas for the steam and a conduit for the reaction by-products. At the end of the allotted time, the pump and heating elements were switched off and the system was allowed to cool. This was aided by the continued flow of nitrogen which was only switched off when chamber at the end once the sample was removed. The sample was recovered once room temperature was achieved. A glass sample vial and cap were weighed. The sample was immediately put into the vial, sealed, and allowed to cool. The sample was weighed at room temperature to determine the activated carbon yield.

Safety measures were used when performing the activation. The outlet pipe was connected to a condenser; a dreschel bottle which was bathed in ice. This would cool down the outlet gas stream and collect tars and other liberated materials. This was connected to a secondary condenser and would be available in the event of an overflow. The gas line was fed into an extraction hood to remove any fumes. In case of a blockage or pressure build up there was a support for the injection rod so it would not pop out and smash the tube. There was also an automatic switch that would shut off the rig if the furnace was opened during operation.

4.3.5 Test Variations

4.3.5.1 Activation

The process can be separated into the carbonization and activation phases. The original testing sequence ran the activation to completion varying the temperature, time, and source material, as shown in Table 4.1. This produced the activated carbon from the HTC hydrochar. The experimental design was developed to provide an inert atmosphere for the pyrolysis step and then deliver the activating agent in excess during the activation step. The testing matrix was created to vary the key independent variables; time and temperature, which were controllable. These were altered in order to change the sample mass loss, which is hypothesised to increase the sample surface area and pore volume.

The lower bound temperature was chosen based on recommendations in the literature which indicated that 700 °C is the minimum temperature for physical activation. The upper bound temperature was limited by the horizonal tube furnace operating condition of 1000°C. The temperatures between were selected at equal increments of 50 °C to create a profile of how the temperature impacts the activation. This provided enough samples for comparison whilst reducing the number of experiments to allowed them all to be conducted within the research period. The duration of the experiment was selected at 30, 60, 90, and 120 minutes. This was to give an even profile when comparing the data. The 90-minute samples were initially intended to be included but had to be omitted due to unforeseen time constraints, such as failed runs and equipment damage. This has reduced the workable data, but it was the least detrimental duration for the study. The longest test period was selected so an experiment could be set up, run at 10 °C/min ramp rate, complete the activation and cool down so the sample could be collected within the lab opening hours. The testing plan set out to answer the hypothesis that commercial grade activated carbons could be produced from the HTC treated waste. The testing matrix was to develop further understanding of the parameters and selected the optimum activation conditions.

4.3.5.2 Pyrolysis

In order to dissect the process, the activation experiments were repeated except the activating agent was not injected. During these pyrolysis runs, the sample would only be subjected to heat for the prescribed period time with no additional input, other than nitrogen to keep the atmosphere inert. This determined the sample losses accounting for moisture and volatiles before the activation treatment. It also acts as a control to show the impact the activating agent has as well as the impact temperature alone has on the structure. It can be seen by the difference between Figure 4.18 and Figure 4.19, showing the visual impact of a pyrolysis run and an activation experiment. Without the oxidizing agent being present, the ceramic crucible was stained by the liberated carbon during the pyrolysis. In order to clean the ceramic boat, it was simply heated in a furnace with air present and the staining was removed and it returned to look like Figure 4.18. This is what the impact the oxidizing agent has during the activation. This showed the pyrolysis experiment was absent of oxygen and the activating agent was having a visable impact.



Figure 4.18 Hydrochar after pyrolysis



Figure 4.19 Hydrochar after physical activation

The testing procedure mirrored the activation testing plan and general method. It was repeated on strawberry pomace, coffee grounds and sewage sludge. This matrix is outlaid in Table 4.2. The conditions remain the same from the activation experiments for a direct comparison and are justified by the same reasoning.

Table 4.2 Testing matrix for pyrolysis experiments

	700 °C	750 °C	800 °C	850 °C	900 °C	950 °C
0.5 hours	-	-	-	-	-	-
1 hour	-	-	-	-	-	-
2 hours	-	-	-	-	-	-

4.3.5.3 Raw Activation

To test the hypothesis that pre-treating the sample with HTC has a positive impact on the activated carbon structure, the raw organic material was also tested. These samples, which had not undergone HTC treatment, were activated under the same conditions. Due to the high moisture content of the raw samples, they were dried at 105 °C for 24 hours before activation.

The conditions remain the same from the activation experiments for a direct comparison and are justified by the same reasoning. However, high losses were experienced in early trials, so 10 g of bone-dry sample was used. Additionally, due to the losses, the experiment was capped, and the highest temperature tested was 850 °C. Only raw strawberry pomace and raw coffee grounds were used due to the biologically unsafe nature of raw sewage sludge. This matrix is outlaid in Table 4.3.

Table 4.3 Testing matrix for raw experiments

	700 °C	750 °C	800 °C	850 °C
0.5 hours	-	-	-	-
1 hour	-	-	-	-
2 hours	-	-	-	-

4.4 Characterization Techniques

4.4.1 Textural Characterisation

Gas adsorption is a highly effective way of characterizing the textural properties of porous materials. The concept relies on the reversible phenomena of physical adsorption or physisorption. Gas molecules adsorb onto a solid surface under controlled conditions. This information is used to calculate the samples adsorption capacity as a function of the pressure recorded. Both nitrogen and carbon dioxide were used separately to ascertain the textural properties. High temperatures usually inhibit physical adsorption so the temperatures must be kept low. The nitrogen (N_2) isotherms were analysed in liquid nitrogen (-196 °C) from 0.01 to 0.99 relative pressure. These isotherms gave information on the microporous (> 0.8 nm) and mesoporous regions, as well as limited data on small macropores, below 100 nm. The CO_2 isotherms were analysed in ice/water (0 °C), testing relative pressures between 0.00002 and 0.03398. Due to the smaller, more linear shaped CO_2 molecules, this technique was able to give a more detailed analysis of the microporous region, mainly the ultra-microporous region (< 0.7 nm). Diffusion of CO_2 is much faster than N_2 at the operated temperature, so CO_2 can be adsorbed to ultra-micropores faster than N_2. A screening analysis was conducted on all samples using the N_2 method. A selection of 14 key samples were analysed with CO_2 which was combined with N_2 data. This will be discussed further in Section 5.

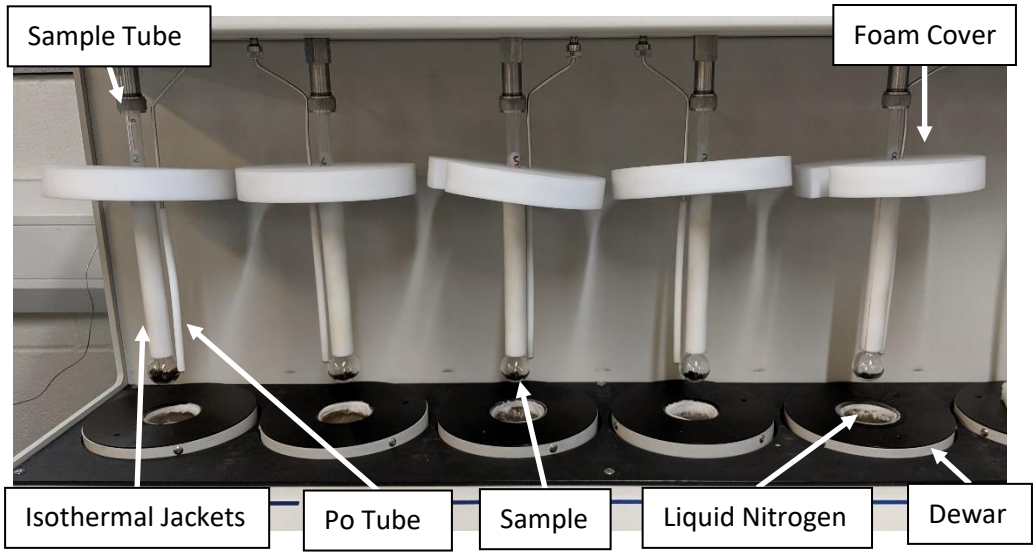

Figure 4.20 Micrometrics 2420 ASAP instrument used for textural characterisation

The analysis was performed using a Micrometrics 2420 accelerated surface area and porosity (ASAP) system (Micrometrics Ltd, Lincolnshire, UK). This can be seen in Figure 4.20. First the samples were prepared. Approximately 0.20 g was put inside a sample tube and closed with a sealed frit. More sample was added of materials with a low predicted surface area, up to 0.50 g. Filler rods were also inserted with these low porosity samples to increase the speed of the process, recommended for samples < 100 m^2/g. The tubes were

screwed into the degas ports and a heating mantle was placed around the chamber holding the sample. The samples were degassed under vacuum conditions (< 0.000013 bar) up to 120 °C for 12 hours to remove moisture and other constituents such as organic vapours. The tubes were then reweighed to determine the degassed or dry weight of the sample.

The dewar containers were filled with liquid nitrogen for the N_2 isotherms and ice/water for the CO_2 isotherms, to keep the analysis running at the desired temperature. The dewar containers were raised to a point where the sample tubes were submerged. Foam covers were used to maintain a constant temperature within and reduce boil off. They also protect the purity of liquid nitrogen and to steady the Po tube. The sequence was then run. Once the analysis was complete the dewar containers were lowered and the samples were removed. The method is non-destructive, so the sample was kept for future reference.

When the unit is in operation it measures the amount of gas adsorbed over time at various partial pressures. As the pressure is increased, the total adsorption increases. The desorption is also recorded when testing N_2 isotherms, by measuring the gas removed as the pressure is reduced. This creates an isotherm. Isotherms will differ depending on the pore structure and characteristics, but the trend can be linked to major isotherm type, shown in Figure 4.21, which can be used to categorise the internal features.

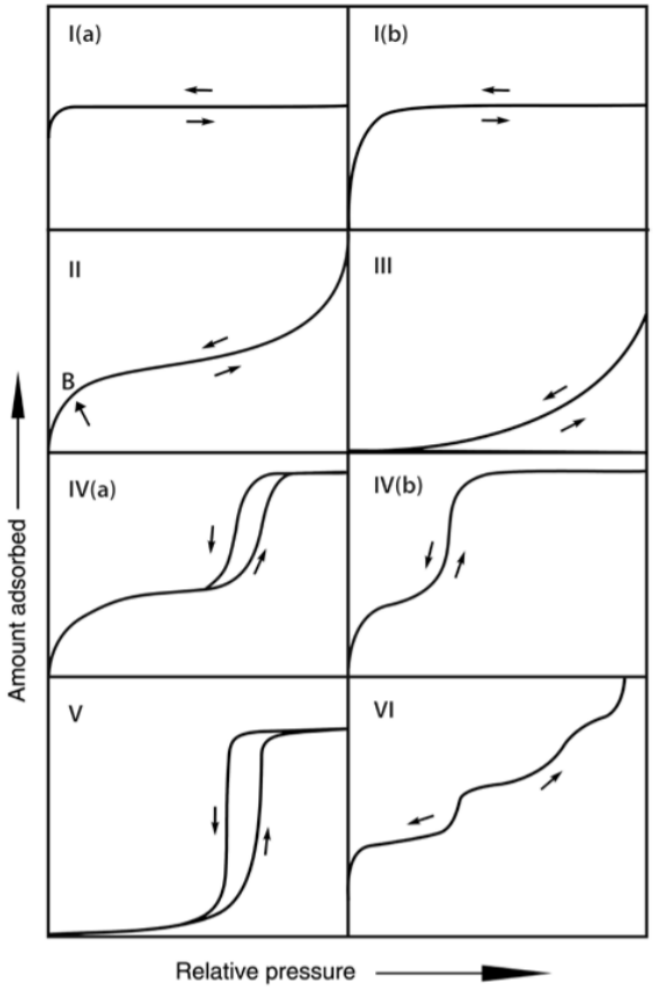

Figure 4.21 BET isotherm types (Thommes et al., 2015)

Type I: Samples displaying this shape are typically microporous. They possess a high internal surface area and a relatively low external surface area. There is a sharp uptake of adsorbate at a low partial pressure. Once a monolayer is formed there is little space for further adsorption, demonstrated by the horizontal plateau at higher partial pressures. The uptake is limited by the accessibility of the pore volume. This can be separated further into type I(a) and I(b). Type I(a) materials have narrow micropores, with widths < 1 nm, moving into the ultra-microporous region. Type I(b) materials cover a wider range of pore widths (< 2.5 nm) incorporating all size of micropores (Thommes et al., 2015).

Type II: This shape typically demonstrates low porosity or larger pore sizes, such as macropores. The first step, at point B in Figure 4.21, indicates that the first layer is complete. Multilayer adsorption is present and unrestricted by pore volume. This is demonstrated by the inflection after first monolayer adsorption plateau (Cychoz et al., 2016).

Type III: This isotherm is uncommon. It indicates the adsorbate-adsorbate interactions are greater than the adsorbate-adsorbent interactions. This happens when the heat of adsorption is less than the adsorbate heat of liquefaction. It is recognised by a convex curve. Without an asymptote, similar to point B on the Type II graph, a monolayer is unidentified, so it is not applicable for BET (Connelly, 2017).

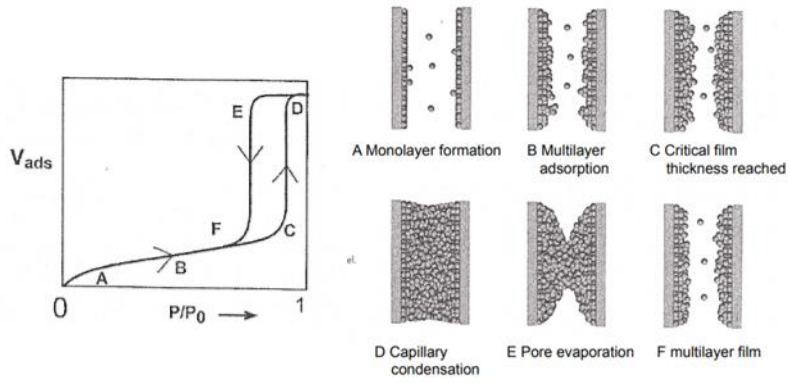

Figure 4.22 Capillary condensation phenomena complete process (Trunschke, 2013)

Type IV: This is typical of samples which are mesoporous. The isotherm is characterised by the hysteresis loop. The first half of the loop is the mono-multilayer adsorption, and the second half is the desorption of the adsorbate. At increased pressures there is a higher uptake of adsorbate as pores fill, suggesting capillary condensation in mesopores. When the multilayer thickness is great enough, capillary condensation occurs. The adsorbate will condense into a liquid phase at a pressure less than the standard saturation pressure. This phenomenon is ongoing during pore evaporation, which slows the rate of desorption, causing a delay in the desorption curve, thus explaining the hysteresis loop. This phenomenon occurs in porous materials with a wide range of pore sizes. The wider the pore size distribution the less steep the pore condensation step. The mechanism can be seen in Figure 4.22. Type IV can be classified further by the pore diameter present (Thommes et al., 2015). In Type IV(a) isotherms the pore width exceeds a critical width, leading to capillary condensation. However, when pore widths are smaller, Type IV(b) isotherms exist, which are completely reversible like the previously described isotherms (Types I – III).

Type V: In this isotherm the relationship between the adsorbent and adsorbate is similar to 'Type III' and is attributed to the same reasoning. There are weak adsorbent-adsorbate interactions. However, the addition of the hysteresis loop, like 'Type IV', shows the presence of meso/macropores. Thus, the material is also porous with a wide range of pore sizes.

Type VI: This type is characterised by stepwise multilayer adsorption. This is typically associated with a uniform surface, with little indication of porosity. The step height indicates a filled layer whereas the step sharpness is related to analysis conditions, such as temperature (Webb & Orr, 1997).

Hysteresis can be used as evidence of pore shielding or ink bottles, as well as detecting other types of pore geometry. It is a complex process which is attributed to capillary condensation but there are numerous structural features that can affect it. For example, if a large pore volume filled with condensate is only connected to the external surface by a narrow pore, such as an ink-bottle shaped pore, then the desorption will not occur in this region until the partial pressure is low enough to empty the narrow pore neck. The retention of adsorbate leads to hysteresis shaped isotherm (Thommes et al., 2015). The isotherm shapes can be seen in Figure 4.23.

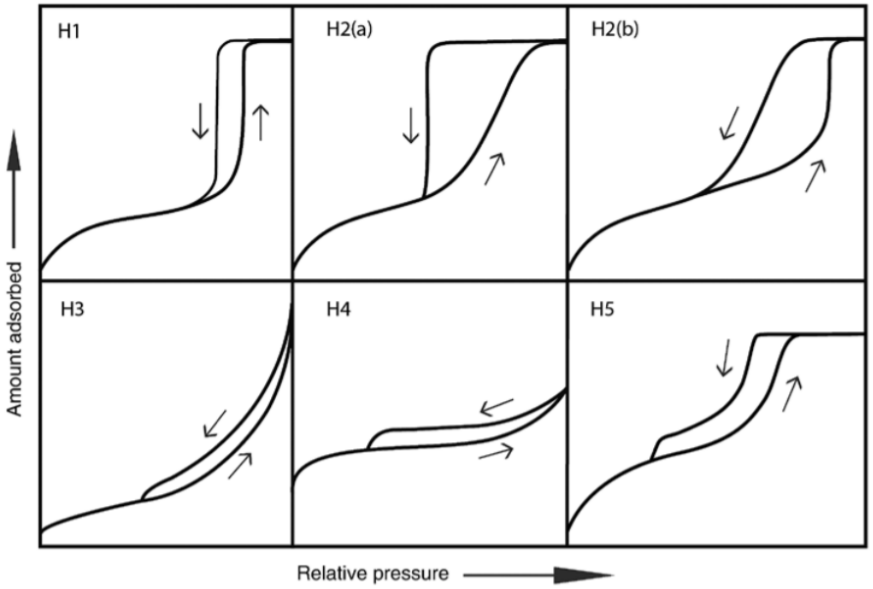

Figure 4.23 Classification of hysteresis loops (Thommes et al., 2015)

Type H1: These structures are well defined cylindrical pores with open channels. They display a narrow pore size distribution in the mesoporous range. The structure does not impede the desorption, thus the steep loop. Capillary condensation will occur in branching in the form of ink bottle pores (Trunschke, 2013).

Type H2: The are found in much more disordered structures where the network has a large impact on the transportation of adsorbate. Type H2(a) is attributed to pore blocking in a narrow range of pore necks. Type H2(b) is also due to pore blocking, but due to a wider range of pore necks, the retention of adsorbate is not as strong.

Type H3: These follow the principal shape of a Type II isotherm. There is no plateau before desorption, but it is more limited. The hysteresis is induced by a low degree of pore

curvature and a non-rigid structure. There is also indication of partially filled macropores which are subjected to capillary condensation (Sing & Williams, 2004).

Type H4: This is similar to Type H3, but the shape is more similar to Type I and II isotherms, with a greater uptake at a lower relative pressure showing the existence of micropores.

Type H5: this exhibits a distinctive shape, which is very specific to materials with mesopores which are open and partially blocked (Thommes et al., 2015). Based on this it is known that adsorption gives information relating to the pore size and the desorption relates to the pore neck size. The information provided by the isotherms can be used by certain models to work out the surface area, pore volume and pore size distribution.

Surface area: BET model

For working out the surface area, the BET equation is preferred to the Langmuir equation. The Langmuir theory only describes the surface area in microporous materials exhibiting type I isotherms. It assumes there is a fixed number of adsorption sites on a surface, of which only one molecule can occupy the space; ultimately assuming adsorption only occurs in a single monolayer. This is limiting when considering the range of pore sizes found in the activated carbons being tested. The BET theory builds upon the Langmuir theory. It first establishes the monolayer capacity, before accepting multilayer adsorption progresses and works out the specific surface area. However, the BET theory also has some limitations. When used on microporous and narrow mesoporous materials, pore filling can cause the calculation to overestimate the monolayer. Therefore, it only provides an apparent surface area (Cychoz et al., 2016). There is evidence that the discrepancies are due to intermolecular interactions between gas molecules, especially at high pressure, which BET ignores. BET is standard for surface area calculations and is the most widely used method which is good for comparisons with other studies.

The Brunauer-Emmett-Teller (BET) model is used for the calculation of specific surface area. The assumptions for the calculation are as follows:

- The surface is homogeneous
- Each site of adsorption has equivalent adsorption energy
- The top layer is in equilibrium with the adsorbate vapour
- Physical gas adsorption is infinite and is assumed so at $P/P_0 = 1$
- There are no lateral interactions between layers
- In each layer, except the first, the heat of condensation is equal to heat of adsorption

The BET equation can be expressed as:

$$\frac{1}{W\left(\left({}^{P_0}/_{P}\right)-1\right)} = \frac{1}{W_m C} + \frac{C-1}{W_m C}\left(\frac{P}{P_0}\right)$$

Equation 4.3

Where:

W = Amount of gas adsorbed (mmol/g)
P/P_0 = Relative pressure

W_m = Amount of adsorbed molecules in monolayer (mmol/g)
C = BET constant

BET needs a linear plot of [1/(W(P/P_0)-1)] against partial pressure. The slope, s, and intersection, i, can be combined to find the monolayer capacity, N_m.

$$s = \frac{C-1}{W_m C}$$

Equation 4.4

$$i = \frac{1}{W_m C}$$

Equation 4.5

$$W_m = \frac{1}{s+i}$$

Equation 4.6

The total surface area can then be worked out:

$$S_{BET} = \frac{W_m N \sigma}{M}$$

Equation 4.7

Where:

N = Avagadro constant (6.023×10^{23})
σ = Surface area covered by one molecule of adsorbate ($16.2 A^2$ for N_2 and $19.5 A^2$ for CO_2)
M = Molecular weight of adsorbate

From this, the specific surface area can be calculated:

$$S_s = \frac{S_{BET}}{m}$$

Equation 4.8

Where:

m = mass of sample measured

Pore size distribution model: NLDFT

The isotherms from CO_2 and N_2 analysis can be joined together to form a larger picture of the porosity. Models such as Kelvin equation, t-plot, BJH and Dubinin–Radushkevich (DR) are capable of this but are limited due a focus on a specific pore region. In this thesis the analysis was performed using non-local density functional theory (NLDFT). The NLDFT carbon slit pore model was used for plots because it can be applied across a wide range of pore sizes, and thus it was assumed that the activated carbon would have slit pores. Therefore, it can be used to determine the pore size distribution, assuming micropores < 2 nm, mesopores 2 nm – 50 nm and macropores > 50 nm. The pore width versus cumulative pore volume was used to obtain the values.

4.4.2 Thermogravimetric Analyser (TGA)

Thermogravimetric analysis was carried out to give the proximate analysis of the samples. This is useful for comparing the constituents of activated carbon samples created at different conditions. It is also useful when showing the change in carbon content from the base raw material to the hydrochar, and then again from the hydrochar to the activated carbon. The TGA is a thermal analysis tool whereby the mass of sample is continuously measured while it is subjected to temperature changes in a specific atmosphere.

The analysis was performed using a TA Q500 thermogravimetric analyser from TA Instruments inc., Philadelphia, USA. The samples were held in platinum pans. They were cleaned using water, acetone, and a flame torch before being tared. The sample was prepared using a pestle and mortar to grind the samples into a fine powder. This ensured the internal material was also being studied. Approximately 20 mg of sample was weighed and loaded onto a pan, providing it fully covered the base of the pan. The sequence was then run. The results were processed using the TA Universal Analysis 2000 software.

The TGA was used to determine the moisture content, volatile matter, fixed carbon, and ash content in the samples. The data was then manipulated to give the figures on a dry and ash free basis. The TGA would record the weight continuously and each section of the sequence would account for a different material loss. The sequence of the proximate analysis was as follows:

- Initial pan weight logged
- Nitrogen purge of 100 ml/min at 1 bar, for a stable nitrogen inert atmosphere
- Ramp the temperature at 5°C/min up to 110 °C
- Isothermal conditions 15 minutes to remove moisture content
- Ramp the temperature at 5°C/min up to 950 °C
- Isothermal conditions for 30 minutes to remove volatile matter
- Air introduced, 100 ml/min at 1 bar
- Isothermal conditions for 15 minutes to burn the fixed carbon
- Cool to room temperature
- Final pan weight logged belonging to the ash content

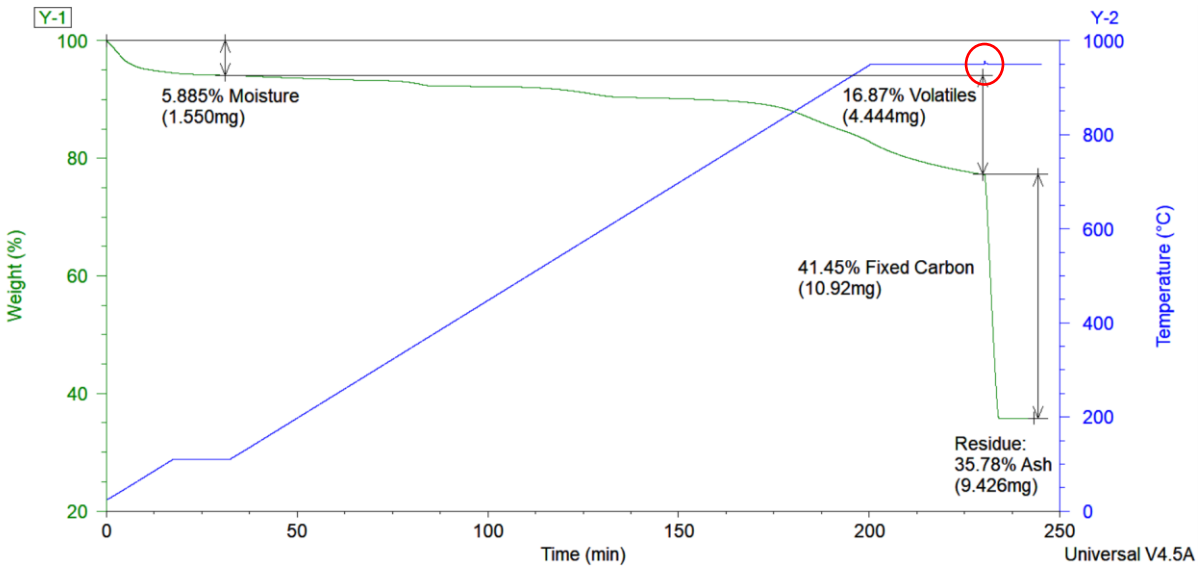

Figure 4.24 Standard TGA thermogram example

An example of the data received from a strawberry AC sample is shown above in Figure 4.24. The green line shows the weight percentage dropping over time as material is removed and the blue line shows the increasing temperature, according to the program outlined. The arrows indicate which material is being liberated at that stage. The red circle indicates the point at which the air is phased in. The temperature spikes momentarily from the exothermic combustion of the fixed carbon. The loaded sample can be seen in Figure 4.25. After the analysis, the remaining weight is taken to be the ash content, which can be seen in Figure 4.26 as residue on the plates.



Figure 4.25 Filled sample trays before analysis

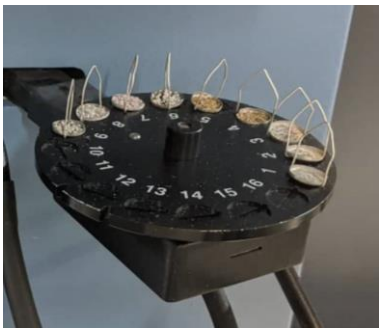

Figure 4.26 Residue after analysis with ash remaining

4.4.3 Elemental Analysis (EA)

Elemental analysis was carried out to assess the carbon, hydrogen, and nitrogen fractions for an ultimate analysis on the samples. This is useful for comparing the composition of biomass, hydrochar and activated carbon. The analysis was performed using a LECO CHN 628 elemental analyser, from LECO instruments UK Ltd, Cheshire, UK. Solid samples were prepared using a pestle and mortar. Samples were weighed in the range of 0.030 – 0.045 g for analysis and placed in tin capsules, which were folded to retain the contents.

Firstly, the analyser was calibrated through a series of 15 blank runs and then a predetermined standard sample was used for 6 runs. These samples were weighed out as 0.075 g and folded into the tin capsules. They were placed in the autosampler for analysis. The standard sample used was 2,5-(Bis(5-tert-butyl-2-benzo-oxazol-2-yl) thiophene (BBOT), the constituents can be seen in Table 4.4 below. The accuracy of the instrument could be determined by comparison and a sample drift feature would calibrate the instrument. The samples to be analysed were placed into the autosampler after the standards. Data from the TGA would determine the residue and moisture content which could be included in the data. This allowed the dry basis ultimate analysis to be worked out, subtracting the necessary hydrogen fraction included in the moisture. The sulphur data was collected from the literature.

Table 4.4 BBOT elemental composition

Sample	Carbon	Hydrogen	Nitrogen	Sulphur	Oxygen
BBOT	72.55 ± 0.43	6.13 ± 0.06	6.25 ± 0.06	7.49 ± 0.05	7.41 ± 0.05

4.4.4 Helium Pycnometry

The analysis was performed using an AccuPyc II 1340 Pycnometer, from Micrometrics Ltd, Lincolnshire, UK. The software used was the Micrometrics AccuPyc program. It was conducted to find the true density of the sample. The pycnometer determines the volume of the solid sample through gas displacement, measuring the pressure change of helium

within a known volume. From the known sample mass and volume, the true density can be determined. True density, also known as skeletal density, is the density of the material mass which excludes the volume of open and closed pores.

A 1 ml sample cup was filled two-thirds full of the selected sample, which measured approximately 100 mg. The cup was tapped so the sample became compact. Prior to analysis the samples were dried in a vacuum oven (< 0.03 bar, 120 °C) for 24 hours. This was done to remove moisture and obtain the true sample mass. The sample was cooled and reweighed. The sample cup was placed into the cell chamber and then sealed with the cell chamber cap. Then the analysis sequence was allowed to run. The fill pressure of helium was set to 1.35 bar. First the chamber was purged. 20 purges were run in order to further compact the sample, making sure no air remained in the sample cell. The equipment ran multiple cycles to achieve an average result. In this instance, 20 cycles were selected. Each cycle was complete when an equilibrium rate of ±0.00035 bar/min was achieved.

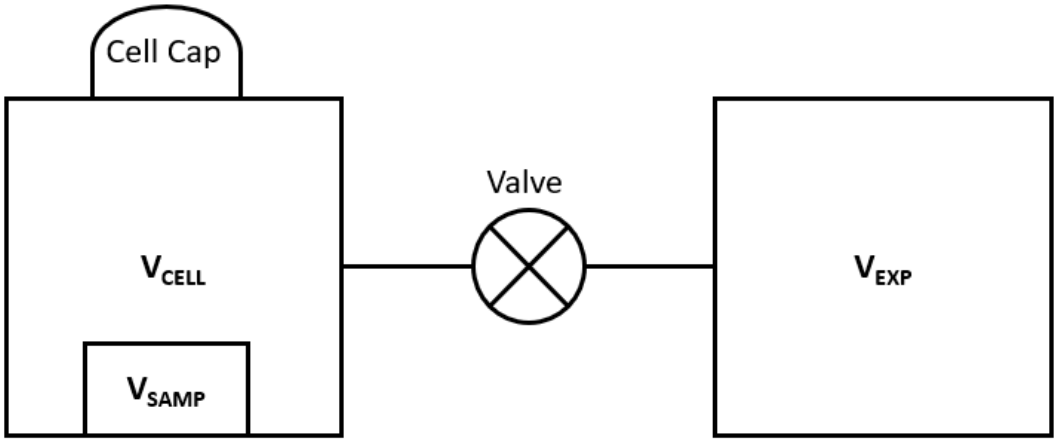

Figure 4.27 Helium pycnometer schematic

As in the diagram, Figure 4.27, the sample (V_{SAMP}) is placed in the cell chamber (V_{CELL}) which is connected to another chamber of equal size (V_{EXP}). Both chambers have a calibrated volume and are at ambient temperature (T_a) and pressure (P_a). The valve between the chambers was closed and cell chamber was filled with helium to the designated pressure (P_1), in this case 1.35 bar. The presence of the sample means a lower quantity of helium is required to reach the designated pressure.

Based on the ideal gas equation, the equation for the sample chamber goes as follows:

$$P_1 \, (V_{CELL} - V_{SAMP}) = n_C R T_a$$

Equation 4.9

Where n_C = moles of gas in V_{CELL} & R=ideal gas constant

The equation for the expansion chamber goes as follows:

$$P_a V_{EXP} = n_E R T_a$$

Equation 4.10

Where n_C = moles of gas in V_{EXP}

The valve was opened, and the pressure equilibrated between the chambers (P_2). The mass balance between the two chambers becomes:

$$P_2\ (V_{CELL} - V_{SAMP} + V_{EXP}) = n_C RT_a + n_E RT_a$$

Equation 4.11

Substituting Equation 4.9 and 4.10 into Equation 4.11 and rearranging gives:

$$V_{SAMP} = V_{CELL} - \frac{V_{EXP}}{\left(\frac{P_1 - P_a}{P_a - P_2}\right) - 1}$$

Equation 4.12

This is the working equation for the pycnometer, with consideration for the sample cup. The true density (ρ_T) was then worked out from:

$$\rho_T = {}^{V_{SAMP}}/_{m}$$

Equation 4.13

Where m = mass of sample

4.4.5 Mercury Intrusion Porosimetry (MIP)

Mercury intrusion porosimetry was conducted to find the bulk density of the sample and the pore size distribution through a deeper understanding of the macroporous region, it is the standard and most widely recognised method of assessing macroporous materials (Grobelak & Jaskulak, 2019). Bulk density considers the volume of the material mass, closed and open pores. Figure 4.28 below shows mercury in contact with a solid porous sample. MIP uses the surface tension, nonwetting and nonpenetrative characteristics of mercury to determine the size of an opening. A pressure, which is inversely proportional to the size of the pore, forces the mercury into the gap. Higher pressures will allow the mercury to enter smaller pores.

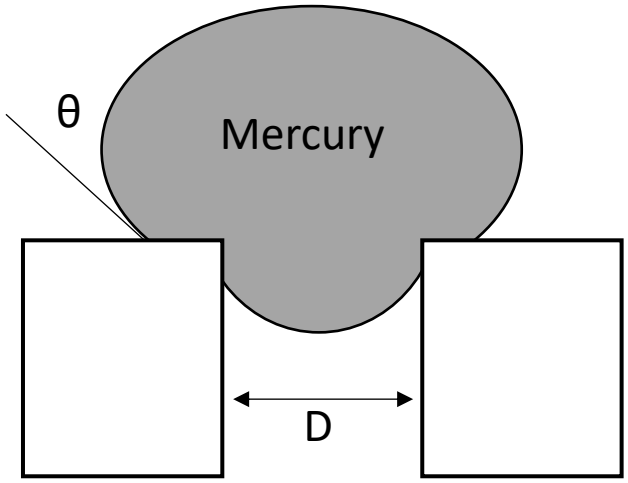

Figure 4.28 Mercury intrusion porosimetry process

The analysis was performed using Micrometrics Autopore IV instrument, from Micrometrics Ltd, Lincolnshire, UK. Prior to analysis the samples were dried in a vacuum

oven (< 0.03 bar, 120 °C) for 24 hours. Approximately 0.25 g of sample was weighed into a 5 ml powder penetrometer, 1.12 stem volume. The intrusion of mercury was recorded from 0 to 4137 bar. The volume of mercury entering the pores at a given pressure can be converted to pore volume and size using the Washburn equation for slit shaped pores, as seen below in Equation 4.14. A contact angle of 152.5^{o} for intrusion and extrusion of mercury and a surface tension of 475.5 mN/m for mercury intrusion in graphitic materials was used to provide a pore size distribution from approximately 231 µm to 2 nm (Thommes et al., 2015). Bulk density was determined at 0.04bar, the pressure that mercury envelopes the particles.

$$D = \frac{-2\gamma\, cos\theta}{P}$$

Equation 4.14 (Webb & Orr, 1997)

Where D = Average pore diameter
γ = mercury surface tension
θ = contact angle
P = pressure

4.4.6 X-Ray Photoelectron Spectroscopy

X-ray photoelectron spectroscopy (XPS) was carried out to analyse the chemical complexes formed on the activated carbon surface. This is useful for comparing surface chemistries formed between materials, conditions and attributing additional adsorption functionality. The analysis was performed using a Kratos AXIS ULTRA (Kratos Analytical Ltd, Lancashire, UK) with a mono-chromated Al kα X-ray source (1486.6eV) operated at 10 mA emission current and 12 kV anode potential (120 W). The spectra were acquired with the Krastos VISION II software.

Due to the sample size, they were lowered into a hollow sample bar to reduce their prominence above the bar while assessing the surface. Double sided tape was used to support the samples. XPS is conducted under vacuum conditions (< 5 x 10^{-9} mbar) to limit interference from the atmosphere. The equipment uses a focussed beam of X-rays to irradiate the surface of the sample material. When the kinetic energy level is sufficient to overcome the photon energy and binding energy, photoelectrons break away from surface elements. The emitted electrons are from the top layer of the surface only, approximately 1 nm deep. They are collected by an electron analyser which measures the kinetic energy of the electron. This is interpreted as peaks on a spectrum where the intensities are attributed to specific elements. It can identify the types of elements present on the surface, what they are bonded to and the proportional number of atoms. This allows the surface complexes to be determined.

For the analysis a charge neutralizer filament was used to prevent surface charging. Hybrid slot mode was used to measure a sample area of approximately 300 x 700 µm. Three areas per sample were analysed. Each consisted of a wide scan and a focused scan. The wide scan was performed at low resolution (Binding energy range 1400 eV to -5 eV, with pass energy 80 eV, step 0.5 eV, sweep time 20 minutes). Then a high-resolution spectra was performed for photoelectron peaks from the detected elements and these were used to model the chemical composition (pass energy 20 eV, step of 0.1 eV, and sweep times of 10 minutes). The spectra were charge corrected to the C 1s peak set to 284.5 eV. The data was recorded

using Kratos VISIONII software and exported into vms format for data processing with CASAXPS.

The sample analysis was conducted by Dr. Craig Stoppiello, at the University of Nottingham Nanoscale and Microscale Research Centre.

4.4.7 Scanning Electron Microscopy (SEM)

Scanning electron microscopy was used for images of the material topography throughout the development during activation. The SEM scans the surface with a focused beam of electrons. The interaction of electrons with the specimen initiates reactions inside the sample which creates signals with information about the sample morphology. This discharges secondary electrons, which gives information on surface topography. The secondary detectors convert the secondary electrons into a light signal, which is displayed as an image. The instrument has can generate high quality images, with a resolution of 1 µm and a magnification of 30,000x. For the sample preparation, the material had to be made conducting, as to avoid charge. The material was mounted on a specimen stub using conductive silver glue. The specimen surfaces were sputter coated with a thin film of gold. It was placed in a sample holder and viewed with a JEOL 6490 scanning electron microscope.

4.4.8 Transmission Electron Microscopy (TEM)

Transmission electron microscopy was used for images of the microporous features to distinguish how ordered and regular the structure was. The instrument fires an accelerated beam of electrons at a specific region on the sample and the transmitted beam is detected, which gives a magnified image of the surface. The images were acquired using a JEOL 2100F from JEOL Ltd., Hertfordshire, UK. The instruments operated at 200kV, equipped with a Gatan Orius CCD camera, from Gatan Inc, California, US. The best activated carbon sample derived from each material was selected for this process. The samples were dried in a vacuum oven (< 0.03 bar, 120 °C) for 24 hours. They were then grinded with a pestle and mortar and then sieved to collect particles of 50 µg and below. Samples were deposited from suspension onto graphene oxide on 'holey carbon support films' purchased from EM Resolutions, Yorkshire, UK, which was laid on a grid. Each grid held < 0.005 g of sample. Images were captured from 10,000x to 500,000x magnification. A tilt series was acquired at 5° steps and aligned within a digital micrograph to better comprehend the porosity.

The sample analysis was conducted by Dr. Michael Fay, at the University of Nottingham Nanoscale and Microscale Research Centre.

4.4.9 Adsorption of Organic Material from HTC Process Water with AC

The filtration experiment was to test the application of the successfully activated hydrochars. Only key activated hydrochars from spent coffee grounds and strawberry pulp were selected for this. Batch sorption studies were conducted on commercial granular activated carbon, experimentally activated hydrochars, and the basic hydrochar for the removal of colour and total organic carbon (TOC) from HTC process water. The process water used was collected from the batch HTC coffee experiments described in Section 4.2.2.

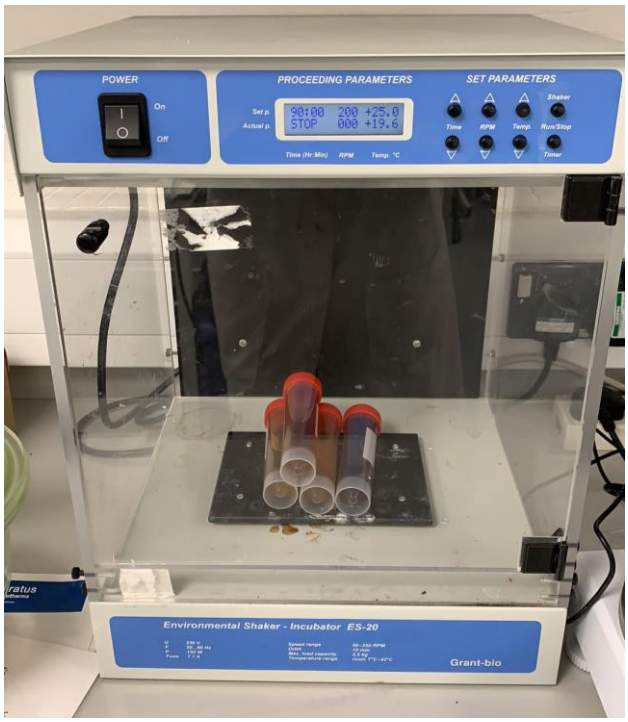

Figure 4.29 Loaded samples being agitated

The desired loading was attained by adding the calculated mass, approximately 0.5 g of adsorbent, to a known volume of process water, 10 ml. The mixtures were incubated and shaken for 72 hours at 25 °C, as in Figure 4.29. The resulting mixture was centrifuged, and the supernatant was filtered through a 0.22 µm syringe filter. The filtered process water was then analysed for TOC content and absorbance over the visible spectrum. TOC was measured using a VarioTOC Select (Elementar UK Ltd, Cheshire, UK) and the light absorbance was measured with an Evolution 201 UV-Visible Spectrophotometer (Thermo Fisher Scientific, Massachusetts, US). The wavelength (470 nm) was chosen as the visible light absorbance of undiluted HTC process water became saturated at lower wavelengths.

The sample analysis was conducted by Dr. Bethany Campbell, at the University of Surrey, Chemical Engineering Department.

4.4.10 Bomb Calorimeter

Bomb calorimetry was used to determine the heating value of the hydrochar. It is useful when comparing the raw biomass to the HTC product. The analysis was performed using an IKA C5003 bomb calorimeter (IKA England Ltd., Oxford, UK). First it was turned on ensuring there was sufficient water, an oxygen flow and a fan switched on. A calibration test was run with a known sample of benzoic acid. The HHV of this sample was 26465 MJ/kg.

The sample was prepared using a manual hydraulic press. 1 g of sample was weighed out and placed between two metal disks in a dye. Pressure was induced on the dye by manually working a lever. The samples were pressed to 1 tonne of pressure. A cotton thread was tied to the ignition coil and directed into the crucible. The sample was placed on top of this and suspended inside a reaction vessel. This was sealed with a screw cap. It was secured in the bomb calorimeter.

$$H = \frac{c\,\Delta T - Q_F}{m}$$

Equation 4.15 (Gravalos et al., 2018)

Where H= Gross calorific value (J/g)
c = Heat capacity of calorimeter (J/K)
ΔT = temperature change (K)
Q_F = energy from ignition and combustion of cotton thread (J)
m = mass (g)



Figure 4.30 Decompression vessel, showing inner crucible and cotton fuse

The vessel, seen in Figure 4.30, was lowered, and the surrounding area was filled with water. The decomposition vessel was filled with pure oxygen to 30 bar. The gross calorific value is calculated by the known weight of sample and the temperature increase in the surrounding water.

5 Results & Discussion

5.1 Strawberry pomace

5.1.1 SP HTC Pre-Treatment

The raw strawberry pomace was processed through an industrial HTC unit. Based on the recorded conditions it was subjected to, it is expected that the material underwent a thermochemical transformation. The first evidence of this can be seen in Table 5.1. The calorific values were recorded from a sample before and after HTC process to understand any changes. The values were recorded from bone dry samples, given in the dry HHV column. The wet HHV has been calculated based on the original sample moisture content.

Table 5.1 The calorific value before and after the HTC treatment of SP

Sample Name	Wet HHV	Dry HHV
	MJ/kg	MJ/kg
SP-RAW	7,400	22,400
SP-HTC	23,000	24,100

The results show that the HTC pre-treatment process has improved the HHV of the material, from the raw variant to the hydrochar variant. It is clear that the material has undergone a change which has improved the calorific fuel value, which synonymous with a hydrothermal carbonization reaction. There is a significant increase when compared on a wet, as received basis. Despite the threefold increase between the pre and post HTC samples, it must be taken into consideration that the HTC process includes a dewatering section which would concentrate the energy content and the raw strawberry pomace could not be combusted in its high moisture state.

For a more direct comparison of the base components, moisture can be eliminated from the discussion. Consistent with the wet HHV data, when moisture is not taken into consideration, the dry HHV results still shows an increase in the thermal value. Although the increase does not appear as dramatic here. In reality, the improved dewaterability of the hydrochar would make the net energy greater in the HTC sample. Based on the improvement, the HTC process is considered to show a successful transformation of waste into a higher value product, which in this case could be used as a fuel.

To analyse how the material constituents were altered, a proximate analysis was conducted on the two samples. However, the material did not return the expected results. Based on the trends found in the literature in Section 3.2.7, it was anticipated that HTC would decrease volatile and ash contents, whilst increasing fixed carbon.

Table 5.2 Dry basis proximate analysis on raw and hydrochar variations of SP

Sample Name	Volatiles	Fixed Carbon	Ash
	%	%	%
SP-RAW	70.7	26.5	2.8
SP-HTC	74.6	22.9	2.5

According to the results in Table 5.2 only the ash content followed the predicted trend. After the HTC process, the volatiles increased slightly while the fixed carbon fell. The fundamental reason to carry out a carbonisation method is to increase the fixed carbon

fraction, so losses of this nature are undesirable. The problem could be feedstock specific or expose some of the frailties in using proximate analysis. Another consideration is that there could have been bound moisture within the sample, which was not liberated during the drying process, but instead removed during the volatile phase and recorded as such. The improvement in the previous calorific tests may have been due to the increased volatile content.

Table 5.3 Dry basis ultimate analysis on raw and hydrochar varieties of SP

Sample	Carbon	Hydrogen	Nitrogen	Oxygen	Ash	H/C	O/C
	Wt %	Wt %	Wt %	Wt % BD	Wt %	Atomic Ratio	Atomic Ratio
SP-RAW	56.7	5.8	2.8	32.0	2.8	1.22	0.42
SP-HTC	61.3	6.0	2.0	28.3	2.5	1.17	0.35

Oxygen wt % by difference (BD)

An ultimate analysis was conducted to gain a better understanding of the elemental constituents. Based on Table 5.3, there is a minor growth in the elemental carbon fraction. So, the pre-treatment process made a slight difference, but this will be a combination of both the volatile and fixed carbon content. The atomic ratios of H/C and O/C both decrease as anticipated. The O/C ratio decreases proportionally more than the H/C so the reaction conditions may have favoured the liberation of carbon dioxide over water. However, the oxygen fraction was calculated by difference and may not be entirely accurate. Additionally, the hydrogen (wt%) increases after the HTC treatment. This counters what is expected during carbonization. The H/C ratio only decreases because the carbon fraction increases more proportionally.

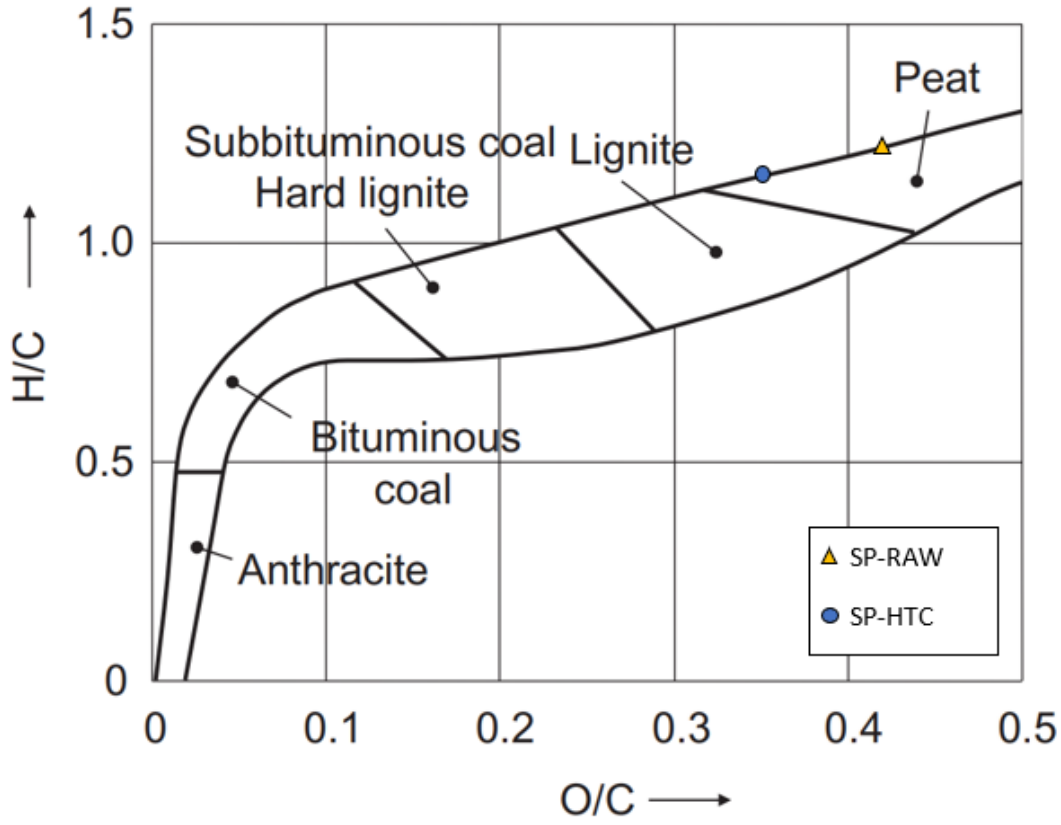

Figure 5.1 Van Krevelen diagram of solid fuel atomic ratios (Agraniotis et al., 2017)

The results may be presented in Van Krevelen diagrams. Figure 5.1 displays the degree of carbonization a material has been subjected to using the atomic ratios H/C against O/C. In the chart, the values of the strawberry pomace raw material and the hydrochar have been included for direct comparison and to show the change through the pre-treatment. The diagram also provides context amongst other solid fuels and standardised grades of coal. Lower degrees of carbonisation are represented in the upper right corner, where the ratios of hydrogen and oxygen to carbon are higher. During the pre-treatment there is a reduction in both the H/C and O/C ratios. However, the change is minimal and the atomic ratios of both are comparable to that of peat, a low grade of solid fuel with minimal carbonization. This does not align with the findings from the calorific tests, which suggests the O/C ratio should be < 0.3 and the H/C ratio should be < 1.0.

The unusual results indicate that the carbonization conditions in the HTC industrial scale reaction may not be sufficient to complete the HTC reactions. The thermal treatment has degraded the biomass sufficiently to increase the thermal value and improve the carbon fraction, but the increased volatile fraction and increased hydrogen fraction are not in line with what is expected from HTC. Rather than a traditional hydrochar, the process has formed an upgraded biomass material with features more in line with a hydrochar. But without the sufficient completion of the carbonization mechanisms, the material cannot be considered to have undergone HTC. By observing the experiment, these remarks can be made: Ultimately the process has changed the fundamental appearance and texture of the strawberry pomace. Before it entered the HTC system it began as a deep red mulch. Features from the strawberry precursor such as the seeds, stalks, and flesh could be recognized. The aroma would also identify it as a strawberry product. Upon removal from the treatment, the immediate difference is the colour. It is now a deep brown. The material appears more homogeneous but upon closer inspection, there are still seeds present within the pellets. The pellets are strong and did not require any additional binders to hold. Overall, it appears the pre-treamment process has been successful in providing a higher quality product. Although the proximate analysis does not provide evidence for a full HTC reaction, the material will be referenced as hydrochar throughout.

5.1.2 SP Independent Pyrolysis Tests

The pyrolysis experiments replicated the carbonization stage of activation. Carbonization losses are an unavoidable consequence of heating the biocoal in an inert atmosphere. The experiments also show the effect that the conditions have on the material in the absence of the activating agent, steam. ‘Pyrolysis’ will be used from here onwards to represent the carbonization phase, to separate it from the pre-treatment which is also considered a carbonization. Table 5.4 shows the total losses experienced by the materials under these conditions. These initial losses account for the removal of moisture and volatiles. It can be seen that the losses are very similar in all of the samples and curtail at 66 – 73 %, hitting an upper bound of how much material can be removed in an inert atmosphere. As the temperature used is increased, the losses increase. There is a slight correlation that indicates more loss as time is increased, but this could be a function of being subjected to the heat for longer. The range between the losses is tight enough to validate the method; the ramp rate and residence time provide an adequate period for the carbonization process to proceed.

Table 5.4 Dry basis proximate analysis of SP hydrochar after pyrolysis phase

Sample Name	Loss	Volatiles	Fixed Carbon	Ash
	%	Product Dry Basis Weight %		
SP-HTC-PYR-700-0.5	67.5	9.7	84.0	6.3
SP-HTC-PYR-750-0.5	69.6	10.5	82.5	7.0
SP-HTC-PYR-800-0.5	68.9	10.2	82.3	7.5
SP-HTC-PYR-850-0.5	69.5	9.3	83.6	7.1
SP-HTC-PYR-900-0.5	70.0	7.2	85.6	7.2
SP-HTC-PYR-950-0.5	70.0	9.0	83.6	7.4
SP-HTC-PYR-700-1	66.1	12.0	81.3	6.6
SP-HTC-PYR-750-1	69.5	11.8	80.4	7.9
SP-HTC-PYR-800-1	69.4	8.8	83.4	7.8
SP-HTC-PYR-850-1	68.0	6.8	86.0	7.1
SP-HTC-PYR-700-2	68.0	12.4	81.0	6.6
SP-HTC-PYR-750-2	69.0	8.6	84.9	6.5
SP-HTC-PYR-800-2	72.3	9.0	82.5	8.5
Standard Error (±)	1.3	0.5	1.4	1.2

Standard error from Table 9.4 & Table 9.7 (Appendix)

Additional pyrolysis runs were conducted for an extended period of 6 hours at 750 °C and 850 °C to test more extreme time periods. The loss calculated here was 69.1 % for 750 °C, which falls within the range of 69.0 % to 69.6 % found in the lower time periods. A loss of 70.4 % was found in the 850 °C sample, which creates an upward trend that loss over time could continue to creep, but the pyrolysis losses are mainly influenced by the temperature used.

The differences in removed mass will also be impacted by a varying moisture content in the pellet. Another idea, stemming from the notion that a higher set temperature increases the loss, could signal that the mass loss is from materials which require a higher heat to be removed. Ultimately this would make little difference to the final product. A more troublesome issue would be if the constituents of the material can vary between batches of biomass. The samples were collected at a similar time, but it cannot be ruled out that constituents between batches could differ by 6 %.

Based on an average of the losses recorded, a working figure of 69.5 % of the original sample mass is anticipated to have already been lost from a SP-HTC sample before activation commences. So, based on this and the similarity shown across the samples, increasing the conditions during the carbonization phase a minor effect. There is effectively a cap on the losses which can be achieved.

The material produced from the pyrolysis run is the starting point for the activation. Some experimental set ups separate the carbonization and activation phases (Okada et al., 2003), (de Fatima Salgado et al, 2018). The material would be allowed to cool down before the activation would begin, sometimes in a different chamber (Heidarinejad et al., 2020). The activation experiment design in this work allows the two phases to be combined, reducing energy consumption between the cool down and second heating phase for the activation.

In Table 5.4 it can also be seen that, after the pyrolysis treatment, the weight content of the ash has increased. The larger presence of ash is because of the losses to other elements, while the ash is not removed during the process. The volatile content has dropped significantly. The volatile organics have been liberated by the increased temperature and is the main source of loss in the pyrolysis experiment. This impacts the fixed carbon by increasing the percentage. The fraction of carbon which remains represents approximately the same mass which the sample began with, as fixed carbon should not be lost in this phase. This has been demonstrated using one of the longer tests, SP-HTC-PYR-800-2. The fixed carbon content of the initial hydrochar sample, SP-HTC, and the final pyrolysis product, SP-HTC-PYR-800-2, have been compared in Table 5.5. In this example there is no measurable change in fixed carbon during the pyrolysis, preserving the fixed carbon for the activation stage. So maximum fixed carbon yield can be retained during the carbonization phase.

Table 5.5 Mass of retained carbon after the pyrolysis step

Sample name	Sample Mass	Fixed Carbon	Carbon Mass
	g	%	g
SP-HTC	4.99	22.9	1.14
SP-HTC-PYR-800-2	1.39	82.5	1.14

5.1.3 SP Activation Tests

The SP hydrochar was activated over a range of conditions to determine the weight loss encountered in the process. The matrix which was set out in Section 4.3.3 was initially conducted. However, during the experimental plan, the highest temperatures combined with the longer timespans were found to drastically reduce yield, leaving only ash. The revised model can be seen in Table 5.6, where all (✓) marked samples were conducted successfully, all (⦸) marked samples were conducted but only returned ash and all (-) samples were not performed due to the unsuccessful attempt resulting from previous experimental condition. Any experiments which did not produce tangible and analysable samples have been omitted from the data beyond this point. The results from the experimental procedure in full can be seen in the Appendix.

Table 5.6 Modified testing program based on sample feedback

Conditions	700 °C	750 °C	800 °C	850 °C	900 °C	950 °C
0.5 hours	✓	✓	✓	✓	✓	✓
1 hour	✓	✓	✓	✓	⦸	-
2 hours	✓	✓	✓	⦸	-	-

In this section the activating agent is introduced, which is the only parameter which has changed in the experimental set up from the results in Section 5.1.2. As a visual aid, Figure 5.2 is included to show the difference in mass loss between samples with and without the presence of steam as the activating agent. For this, results from the 0.5-hour experiments have been used as an example. The average pyrolysis loss, 69.5 %, has been included as a dashed red line, for appreciation of losses in the samples not displayed in the chart. This demonstrates the to the consistency between the pyrolysis samples in the chart, as well as tests conducted for a longer time which are omitted.

The grey bars represent the pyrolysis phase, and as the temperature increases, there is a trend showing a slight increase to the mass loss each time. Note that the pyrolysis samples reach a higher bound which it does not pass beyond. The black bars represent the same conditions when the steam activating agent is introduced. It can be clearly seen that the mass loss is higher at each temperature point compared to the pyrolysis experiment. This demonstrates the activating agent is the factor causing this. As fixed carbon is the largest remaining fraction, seen in Table 5.4, the activation will mainly impact this region. Higher temperatures correlate with a greater mass loss. This is seen more explicitly in the activation experiments. The losses associated with the inclusion of the activating agent increase approximately 5 % overall for every increase of 50 °C. Any increases above 950 °C would most likely result in only ash remaining. Analysis on the activation conditions will be covered further in Section 5.1.7.

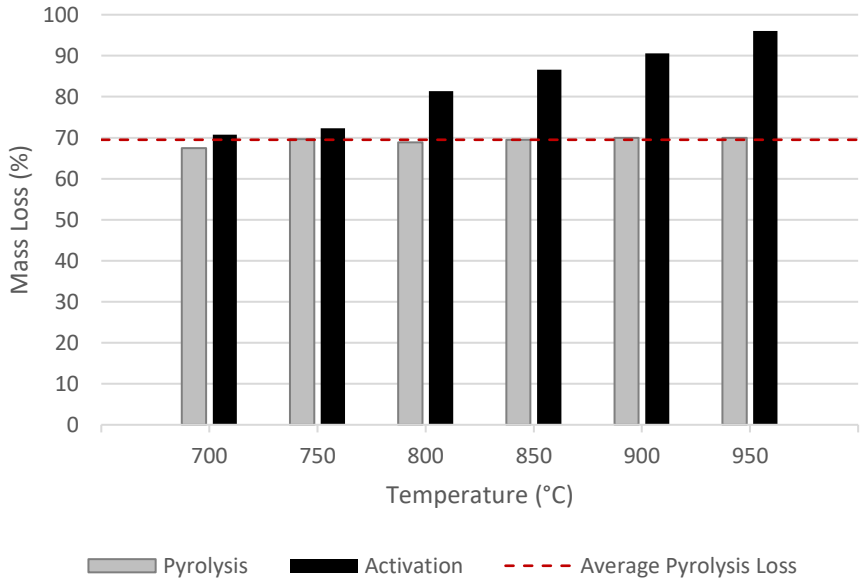

Figure 5.2 Comparison of mass loss encountered in the independent pyrolysis and the complete activation reaction of HTC strawberry pomace, during 0.5-hour runs

5.1.4 SP Activation Yield

The weights of the samples were recorded before and after to attain the yield, which can be seen in Table 5.7. Mass losses are necessary to create activated carbon, but this is countered by a desire for a large yield. High losses contribute to reducing the yield, so it is a balance between the quantity and quality. In the central column, the activated hydrochar yield ranges from 3 % – 29 % which represents a significant loss from the starting material. From the literature review in Section 2.1.7.2, it was established that an activated carbon yield of 15 % is standard. Based on this, much of the losses can be justified by being within the expected range. However, the highest temperature conditions in each timeframe may return too little yield to justify the process.

Table 5.7 Activated hydrochar and carbon yield achieved from activated SP hydrochar

Sample Name	Activated Hydrochar Yield	Carbon Yield
	%	%
SP-HTC-ACT-700-0.5	29.3	105.6
SP-HTC-ACT-750-0.5	27.7	97.6
SP-HTC-ACT-800-0.5	18.6	64.9
SP-HTC-ACT-850-0.5	13.4	42.4
SP-HTC-ACT-900-0.5	9.4	28.0
SP-HTC-ACT-950-0.5	3.9	12.3
SP-HTC-ACT-700-1	27.4	97.9
SP-HTC-ACT-750-1	22.5	78.3
SP-HTC-ACT-800-1	12.0	51.8
SP-HTC-ACT-850-1	2.9	7.8
SP-HTC-ACT-700-2	25.6	92.6
SP-HTC-ACT-750-2	18.3	62.4
SP-HTC-ACT-800-2	5.3	12.7
SP-HTC-ACT-700-4	21.5	75.4
Standard Error (±)	1.3	5.4

Standard error from Table 9.4 (Appendix)

The general trend of the carbon yield is to decrease as temperature increases. This is also relevant for timespan, as the carbon yield decreases as the time is increased. In the samples subjected to 700 °C, the activated hydrochar yield shows a large loss, but the carbon yield is still high. This loss will account for the moisture and volatiles which are removed before the carbon. It also suggests that this temperature is not high enough to cause a strong activation and relies on the timespan to make a greater impact. The anomalous result of 105.6 % can be attributed to the variations between samples and inaccuracies of using the data from the analysis of one sample to predict the starting quantity of another. A high carbon retention is aimed for, but at the same time, carbon must be removed to create the porosity. The porosity of each sample will be presented later, and the discussion will decide whether the yield is acceptable for the level of porosity achieved.

From the pyrolysis tests, the fixed carbon is the biggest fraction going into the activation stage. As predicted, most of the mass loss experienced during the activation step is from the fixed carbon fraction. The proximate analysis in Table 5.8 gives more evidence of the carbon losses. The general trend is that the harsher the activation, the more the fixed carbon content drops. For example, SP-HTC-ACT-700-0.5 has a similar profile to a pyrolyzed sample. The conditions have caused a slight increase in loss than the average carbonization loss, 70.8 % compared to 69.5 %. As the temperature is increased, the fixed carbon losses are increased, to create a profile like SP-HTC-ACT-950-0.5. Regardless of this, the fixed carbon remains as the bulk of the material, thus defining it as an activated carbon. The ash proportion increases in all samples. It is more prevalent in experiments with a higher temperature and a longer duration. The ash content was low before the activation process, measuring 2.45 %, but as the process liberates material around it, the proportion becomes greater until it occupies > 20 % in some samples. Overall, the actual mass of ash will remain relatively unchanged and reside within the sample. Without a pre-process treatment such

as acid leaching, the presence of ash is unavoidable. Finally, the volatile content loses considerable mass from the initial SP-HTC sample, established in Table 5.4. This removal occurs primarily during the pyrolysis stage. Between the pyrolyzed sample and the activated hydrochar sample, a reasonably stable proportion of volatiles are retained, measuring between 8.0 – 17.0 % compared to the pyrolysis sample, between 7.2 – 12.4 %.

Table 5.8 Dry basis proximate analysis of activated SP hydrochar

Sample Name	Volatiles	Fixed Carbon	Ash
	% Dry Basis		
SP-HTC	74.6	22.9	2.5
SP-HTC-ACT-700-0.5	10.1	82.7	7.2
SP-HTC-ACT-750-0.5	11.5	80.6	7.8
SP-HTC-ACT-800-0.5	8.9	79.8	11.3
SP-HTC-ACT-850-0.5	14.8	72.6	12.6
SP-HTC-ACT-900-0.5	12.4	68.0	19.7
SP-HTC-ACT-950-0.5	11.2	71.6	17.2
SP-HTC-ACT-700-1	11.0	82.0	7.0
SP-HTC-ACT-750-1	11.2	79.6	9.2
SP-HTC-ACT-800-1	9.09	73.0	17.9
SP-HTC-ACT-850-1	15.2	61.7	23.1
SP-HTC-ACT-700-2	8.0	83.0	9.1
SP-HTC-ACT-750-2	10.9	78.2	10.9
SP-HTC-ACT-800-2	17.0	54.7	28.3
SP-HTC-ACT-700-4	8.7	80.1	11.2
Standard Error (±)	0.5	1.4	1.2

Standard error from Table 9.7 (Appendix)

Figures 5.3-5.5 show the mass of constituents left within the activated hydrochar sample under each condition. The columns are ordered from left to right in order of increasing temperatures. Each chart collates a single residence time. The figures have been manipulated as if each precursor started as exactly 5 g, for ease of comparability. Within each bar, there is the relative amounts of each component of the activated carbon. All three charts show that as temperature increases, the mass remaining decreases. The graphs clearly display that the fixed carbon bracket is the most impacted by the activation conditions. Section 5.1.3. proved the activating agent to be having an effect on the loss, and this section shows the losses are happening in the desired place. It is anticipated that the removal of fixed carbon will increase the porosity, providing the removal has happened in the correct places. In selecting the best samples, a balance between yield and quality needs to be reached. It will most likely be found in the central bars, where loss has occurred but not to the detriment of an acceptable yield.

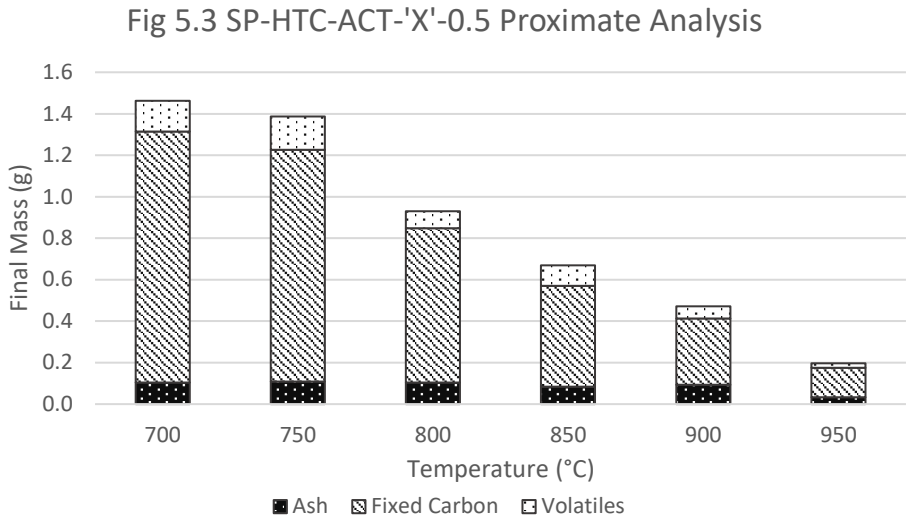

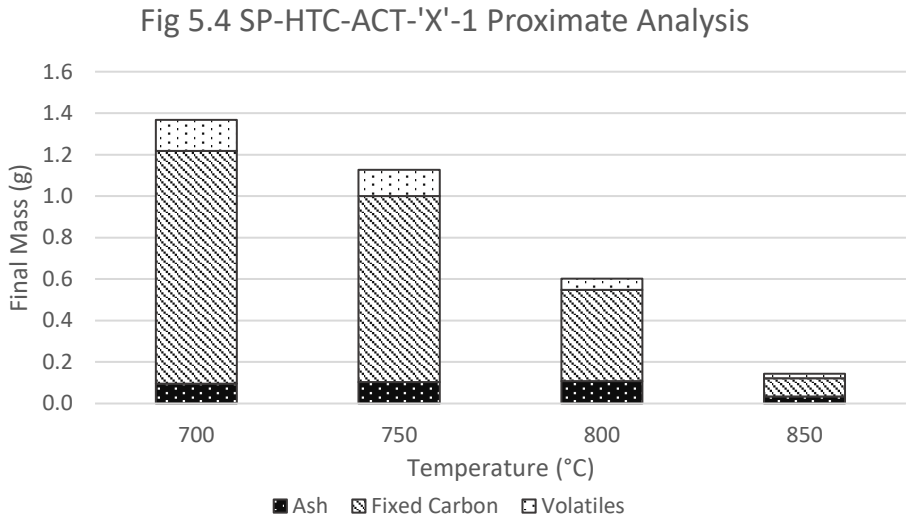

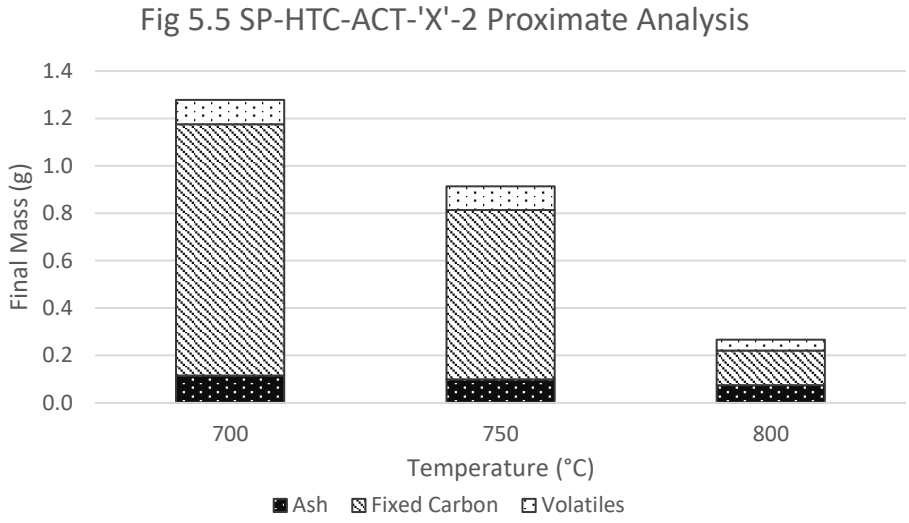

Figures 5.3 – 5.5 The mass of the major constituents in activated carbons derived from 5 g of strawberry pomace hydrochar and treated at incremental temperatures. The figures are separated by residence time

The behaviour of ash can be observed easily in this format, where it occupies the base of each bar, seen in black. The ash fraction is even across most samples, except the highest temperature experiment in each chart. Here there may have been difficulty in collecting the sample due to extreme losses, including some ash which was no longer within the retrieved pellets. Despite this, the fraction which ash occupies is highest in these low yield samples, shown in Table 5.8. The set conditions which produce these samples would not be ideal due to the low yield and high ash proportion. Fewer experiments are present in the graphs depicting higher timeframes because they resulted in unusable samples. An example of this happening can be seen in Figure 5.6. A few small dark pellets can be seen, which is the remainder of the activated carbon, but most of the carbon has been removed leaving only the sand-like ash behind. This reiterates the need for a steady balance between the set temperature and the residence time.



Figure 5.6 A collected sample which was made primarily of ash

The same results have been interpreted based on time, which is shown in Figure 5.7. Each trend line connects studies carried out at the same temperature but with residence times increasing from left to right. The brackets of samples increase in temperature from left to right. This demonstrates the residence time also has an impact on reducing the yield. As the time is increased, the final mass reduces. Including every sample in one graph helps gain an appreciation for how much mass is retained between each experiment, and how quickly this drops between the temperature brackets. The incline of the trend line increases at higher temperatures showing temperature has a greater immediate effect on the activated carbon yield within the range tested. It was anticipated that time and temperature would display a similar pattern, but that temperature would have a more severe effect, which has been proven to be correct.

There are only a few samples to work with in each temperature band, but trend lines appear quite linear. This could be used to anticipate the impact elongated residence times would have at a given temperature. The 700 and 750 °C bracket could most likely double in duration, providing the loss remained relatively linear. These additional experiments fall outside the scope of this study, but it could be an area of further work to pursue. This could be bolstered with more trials in between the 50 °C increments to solidify the trend.

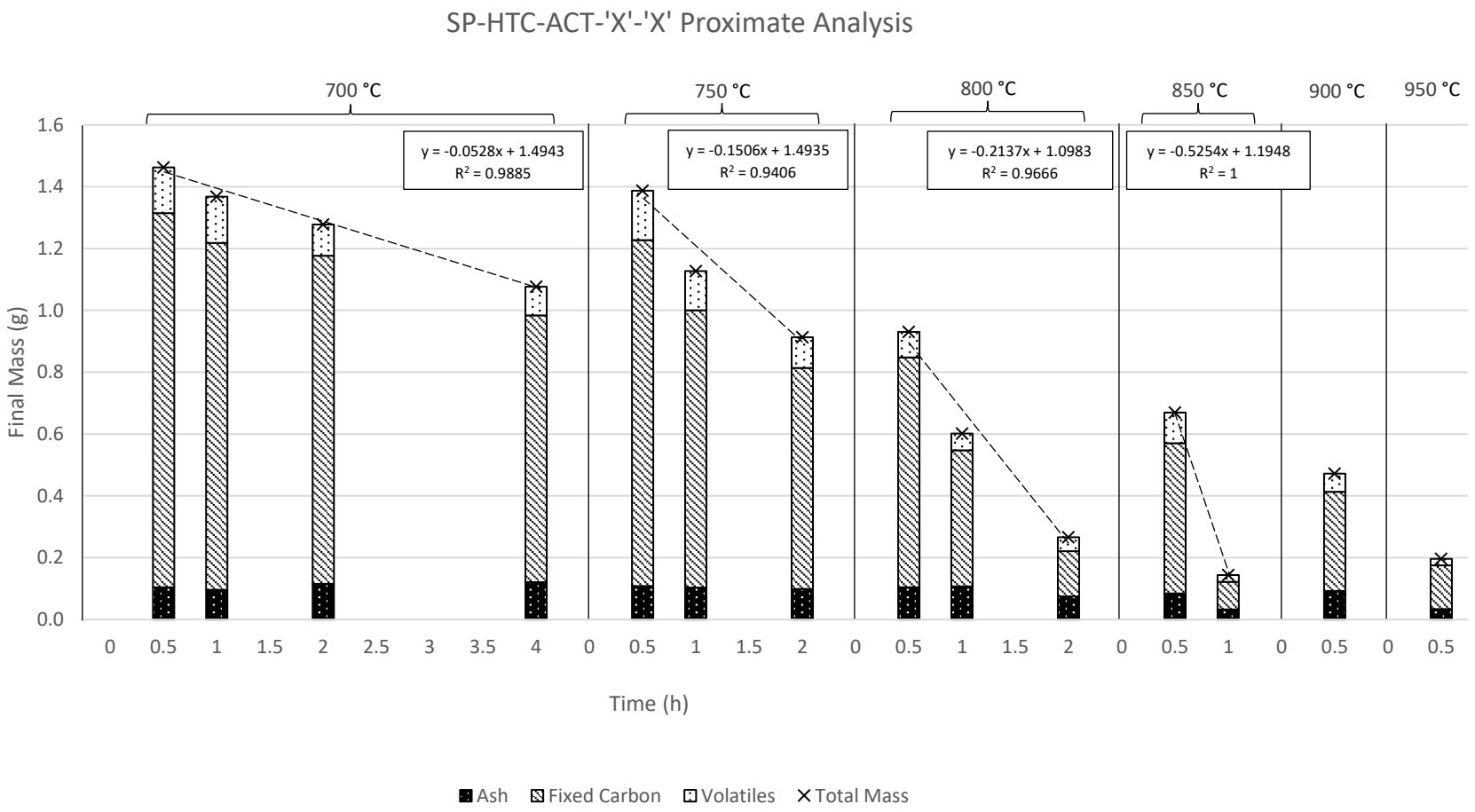

Figure 5.7 The mass of the major constituents in activated carbons derived from 5 g of strawberry pomace hydrochar based on residence time and spaced proportionally. The samples are grouped in terms of treatment temperature which can be seen across the top.

Theoretically, if the losses derived from the pyrolysis phase step are excluded, the resulting yield would display the losses during activation only. This has been termed activation yield and can be seen in Table 5.9, compared alongside the activated hydrochar yield and carbon yield. Limiting the calculation only from the available mass for activation gives a more accurate view of the effect from this stage. Within the activation yield the ineffective materials, like ash, which are retained are taken into account. So, another column has been collated for the consideration of the carbon yield only, which shows the retention of carbon from the original SP-HTC. Carbon yield and activation yield show a similar pattern, as the activation yield has a high proportion of fixed carbon, showing that the activating agent used is primarily reacting with carbon. When compared side by side with the overall hydrochar yield, the quantity of mass retained appears more reasonable. For example, SP-HTC-ACT-850-0.5 has an activated hydrochar yield of 13.4 % which is established to be a close to the standard value for product yield, which corresponds to an 86.6 % % mass loss. However, the carbon and activation yields signal that around 60% of the available mass has been lost in the process. The carbon yield and activation yield are also better at comparing the conditions and separating how severe the treatment process is. Focussing on SP-HTC-ACT-700-2 and SP-HTC-ACT-750-2, the activated hydrochar yield shows a difference of 7.3 %, but the activation yield is actually 20.8 % and the carbon yield difference is much greater, at 30.2 %. By discounting the unusable fractions, the perspective allows the losses to be separated further. Therefore, the activation yield should be considered when comparing losses faced.

Table 5.9 Activation yield compared to overall hydrochar yield

Sample name	Carbon Yield	Activated Hydrochar Yield	Activation Yield
	%	%	%
SP-HTC-ACT-700-0.5	105.6	29.3	89.9
SP-HTC-ACT-750-0.5	97.6	27.7	91.3
SP-HTC-ACT-800-0.5	64.9	18.6	59.8
SP-HTC-ACT-850-0.5	42.4	13.4	43.9
SP-HTC-ACT-900-0.5	28.0	9.4	31.5
SP-HTC-ACT-950-0.5	12.3	3.9	13.1
SP-HTC-ACT-700-1	97.9	27.4	80.6
SP-HTC-ACT-750-1	78.3	22.5	73.8
SP-HTC-ACT-800-1	38.7	12.0	51.6
SP-HTC-ACT-850-1	7.8	2.9	9.0
SP-HTC-ACT-700-2	92.6	25.6	79.8
SP-HTC-ACT-750-2	62.4	18.3	59.0
SP-HTC-ACT-800-2	12.7	5.3	19.2
Standard Error (±)	5.4	1.3	4.8

Standard errors from Table 9.4 (Appendix)

5.1.5 SP Chemical Composition

Ultimate analysis was conducted on the samples for further assessment of the constituents. Table 5.10 shows a study between 3 stages of the activation during the experimental conditions of 800 °C for 1 hour. The analysis will focus on the journey of each element and how the change impacts the other elements. Carbon begins and ends as the

largest fraction. The fraction peaks during the pyrolysis step, after which none of the fixed carbon has been removed, and it remains the majority of the sample. In the activation step, the activating agent reacts with the carbon and removes atoms from the sample. This reduces the amount of carbon in the sample, but it continues to occupy the largest fraction. This pattern was anticipated and is typical for an activation process.

Table 5.10 Ultimate analysis of activated hydrochar derived from SP during three key points of the activation reaction

Sample	Carbon	Hydrogen	Nitrogen	Oxygen	Ash	H/C	O/C
	Wt.%	Wt.%	Wt.%	Wt.% BD	Wt.%	Atomic Ratio	Atomic Ratio
SP-HTC	61.3	6.0	2.0	28.3	2.5	1.17	0.35
SP-HTC-PYR-800-1	91.4	0.4	2.9	0.0	7.8	0.05	0.00
SP-HTC-ACT-800-1	71.9	0.8	1.3	7.5	18.5	0.13	0.08

Most of the hydrogen fraction is contained within volatile compounds. During the pyrolysis phase, much of the volatiles are liberated, from 74.6 % to 8.8 % as per Tables 5.2 & 5.4. This explains the removal of most of the hydrogen. When the steam activation is introduced, the presence of hydrogen gives opportunity for chemisorption to the surface. This appears non-existent in the final product as hydrogen is reduced to a trace. This is highly possible, as the weight fraction of hydrogen does increase. When this is adjusted for the mass available, the actual mass of hydrogen drops from 6 mg to 5 mg. This breakdown can be seen in Table 5.11. The drop in mass could be due to removal of trapped or longer chain volatiles. Using data which has been previously presented, it can be calculated that the volatile content in both the pyrolysis sample and the activated sample is roughly 9 %, showing the volatiles continue to be removed proportionally during the activation step. The percentage loss of hydrogen during the pyrolysis phase correlates closely with the volatile mass loss across the same time, at 98 % compared to 96 %. It would be assumed that this relationship would continue in the activation phase where the volatile mass drops further. However, during the activation, there is a 17 % mass loss of hydrogen as opposed to a 55 % mass loss of volatiles. This discrepancy could be attributed to the types of volatiles remaining or the introduction of hydrogen in the activating agent. There could be a proportional 55 % a loss of hydrogen and then a gain of chemisorbed hydrogen onto the activated hydrochar surface. It does end as the lowest weight fraction, but that must be considered against its low atomic weight.

Table 5.11 The change of volatile and hydrogen mass between reaction steps

Sample	Volatile Mass mg	Loss	Hydrogen Mass mg	Loss
SP-HTC	3,722		298	
		96 %		**98 %**
SP-HTC-PYR-800-1	135		6	
		55 %		**17 %**
SP-HTC-ACT-800-1	61		5	

Similarly, the oxygen was anticipated to chemisorb to the surface. At the beginning oxygen is the second largest weight fraction. After the pyrolysis phase the oxygen content has been depleted completely. Oxygen from the sample would be the only oxidising agent in the otherwise inert atmosphere and combined with the presence of heat, would combust in a controlled manor, with oxygen acting as the limiting factor. At the end of the activation, the weight fraction of oxygen has recovered considerably to 7.5 % from being non-existent. It can be certain that this oxygen is from the activating agent, which has chemisorbed and formed surface complexes on the activated hydrochar.

The nitrogen content shows a trend of mass reduction throughout the process. The weight percent peaks after the pyrolysis step, but that impact is because of the other material losses in the sample. In the pyrolysis step 55 % of the nitrogen mass is lost and in the subsequent activation, 81 % of the remaining nitrogen is removed. The continued removal of the nitrogen could show it requires a longer time to be removed. Additionally, despite being in a nitrogen rich environment, the purge gas appears to remain inert and not affect the product.

A similar trend is seen in the ash content. The fraction it occupies increases each time as none of the ash is removed. The mass does show a very slight drop, a negligible 1 mg from start to finish, and this could be attributed to variations between the sample or ash dropping from the main pellets in the reaction boats and not being recovered. The final ash content makes it the second largest constituent in the activated hydrochar, a fraction which is undesirable.

The sample comparison in Table 5.10 gives a general trend for the activation. The complete results for the ultimate analysis can be seen in Table 5.12. The complete results show a high proportion of carbon across the samples. The top entry is the pre-treated sample, SP-HTC, which has the lowest carbon weight. The carbon content has increased in all activated samples. It was established in Section 2.1.2.1 that activated carbons are anticipated to have an approximate carbon content of 85 – 95 %. Few samples reach these values, but those which do are from the low temperature experiments, between 700 – 750 °C. The trend shows that, as the temperature increases, the carbon content is reduced. So, the more aggressive treatments remove carbon more rapidly. Looking at the expected trends, it seems the samples treated at 800 °C for 0.5 and 1 h durations have a lower carbon fraction than would be expected compared to the temperatures either side of them. Interestingly the carbon fraction peaks in all the 750 °C samples, potentially from the reduction in oxygen, nitrogen and hydrogen compared to the 700 °C samples. Or it might be the case that 750 °C is an optimum temperature for the preparation of high carbon weighted activated carbons from strawberry pomace, this will be considered in the balance of quality against quantity.

In terms of hydrogen content, it was established in the previous example that chemisorption from the steam activation is a possibility. The results in Table 5.12 tend to agree, showing similar weightages, with some even larger. There is a slight preference toward the longer timeframe samples, allowing more exposure to the activating agent. This could indicate that increasing the contact time with the activating agent increases the chemisorption of hydrogen. However, the frequent 0.0 g values indicate issues with the validity of working out the dry hydrogen weight by using a moisture value derived from proximate analysis. The TGA is a destructive method of analysis, so the exact sample was

not tested in both instruments. Although the TGA sample is from the same batch, it may not accurately represent the sample used in the ultimate analysis. For instance, it may have absorbed additional moisture while awaiting testing on the autosampler tray. Either way, there is no pattern to the appearance of a blank. The blank samples have a remaining volatile fraction which would contain hydrogen, invalidating the values.

The same critique can be applied to the oxygen column. The oxygen content often shows a 0.0 g value. The oxygen content was expected to be low, but not entirely absent. This is especially true when some samples show a large fraction of oxygen. The value was based on the remaining fraction of unaccounted mass. The difference calculation included values from two instruments which added to the inaccuracy. The values are sporadic and may not be representative of the ultimate analysis sample. This is despite best practice to effectively calibrate the instrument after every 10 samples. Despite this, the samples which are reported to contain oxygen would prove the chemisorption of oxygen to the surface, since all pyrolysis samples were completely devoid of the initial oxygen content.

Compared to the starting sample, the H/C and O/C ratios are reduced dramatically. Most of the associated hydrogen and oxygen is removed during the pyrolysis phase, as demonstrated in Table 5.10. In the final sample, both hydrogen and oxygen fractions are very low. In contrast the carbon is the highest weight percentage recorded. It is to be seen whether the remaining fractions have created useful functional groups as a result of chemisorbing to the activated hydrochar. This will be investigated further in Section 5.2.8.3 with more precise characterisation.

The nitrogen content stayed relatively stable throughout. There is a correlation between a lower nitrogen fraction at higher temperatures. When comparing SP-HTC-ACT-700-0.5 and SP-HTC-ACT-950-0.5, the higher temperature method shows a > 50 % reduction in nitrogen. This pattern is replicated in other residence times. Compared to the precursor, the fraction generally increases in the lower temperature samples and then drops below the initial fraction at temperatures greater than 800 °C. This hints that higher temperatures will remove more nitrogen. In terms of the ash content, this increases throughout the experiment as it is not removed in the reaction. This has been covered in Section 5.1.4. Finally, it is assumed that there is no sulphur in the final material. Research states there is a low trace of sulphur in the initial material, 0.1 – 0.15 % (Gondek et al., 2020), and this should reduce similar to the nitrogen content.

Table 5.12 Ultimate analysis of activated SP hydrochar

Sample	Carbon	Hydrogen	Nitrogen	Oxygen	Ash	H/C	O/C
	Wt.%	Wt.%	Wt.%	Wt.% BD	Wt.%	Atomic Ratio	Atomic Ratio
SP-HTC	61.26	5.97	1.97	28.26	2.54	1.17	0.35
SP-HTC-ACT-700-0.5	86.89	1.14	2.65	2.17	7.16	0.16	0.02
SP-HTC-ACT-750-0.5	89.92	0.61	2.47	0.00	7.84	0.08	0.00
SP-HTC-ACT-800-0.5	80.35	0.00	1.79	6.60	11.26	0.00	0.06
SP-HTC-ACT-850-0.5	82.15	0.00	1.36	3.88	12.61	0.00	0.04
SP-HTC-ACT-900-0.5	84.89	0.00	1.44	0.00	19.70	0.00	0.00
SP-HTC-ACT-950-0.5	69.88	0.25	1.17	11.50	17.21	0.04	0.12
SP-HTC-ACT-700-1	87.55	0.86	2.41	2.17	7.01	0.12	0.02
SP-HTC-ACT-750-1	87.88	0.59	2.24	0.09	9.21	0.08	0.00
SP-HTC-ACT-800-1	71.9	0.8	1.3	7.5	18.5	0.13	0.08
SP-HTC-ACT-850-1	79.63	0.65	1.45	0.00	23.06	0.10	0.00
SP-HTC-ACT-700-2	85.35	1.13	2.36	2.09	9.06	0.16	0.02
SP-HTC-ACT-750-2	83.12	0.00	2.02	0.00	10.86	0.00	0.00
SP-HTC-ACT-800-2	79.35	0.27	1.36	0.00	28.26	0.04	0.00
SP-HTC-ACT-700-4	79.45	1.40	1.77	6.16	11.21	0.21	0.06
Standard Error (±)	3.01	0.14	0.06	2.59	1.19	0.13	0.09

Ash content from proximate analysis, moisture content from proximate analysis used for dry hydrogen weight, oxygen calculated by difference (BD). Standard errors from Table 9.8 (Appendix)

An additional test was completed at 700 °C for 4 hours, to understand the impact of a longer duration. The temperature was selected because it produced the lowest losses during shorter runs, which gave more assurance that 4 hours at 700 °C would return a sizable yield. The values from the ultimate analysis have been converted into mass by using the final sample weights recorded and are presented in Table 5.13.

Table 5.13 Ultimate analysis of activated hydrochar derived from SP converted to mass

	Carbon mg	**Hydrogen** mg	**Nitrogen** mg	**Oxygen** mg	**Ash** mg
Hydrochar Precursor	3056.6	298.0	98.5	1410.3	126.7
Post-Pyrolysis	1482.8	10.4	46.7	0.0	122.0
0.5 h Activation	1281.4	16.8	39.1	32.0	105.6
1 h Activation	1197.9	11.8	32.9	29.6	96.0
2 h Activation	1102.4	14.6	30.5	27.0	117.0
4 h Activation	867.6	15.3	19.4	67.3	122.4

During the activation, the carbon is continuously removed by the activating agent. Using the mass values, a removal rate can be calculated. In the first 30 minutes, the carbon is removed at a rate of 6.7 mg/min. This could include some additional volatile matter which would inflate the figure. In the subsequent 30 minutes, the removal rate subsides to 2.8 mg/min. In the following hour, this value drops again to 1.6 mg/min. Finally, in the last 2 hours, the rate has increases to 1.95 mg/min. Generally, there appears to be a rapid removal on the initial introduction of the activating agent. This figure then dampens and settles at a rate below 2 mg/min. this figure could be used to predict further losses at longer durations and cap the losses at what is considered an acceptable yield.

The hydrogen values generally agree with the idea that the chemisorption is happening. Other than the outlier at 0.5 h, the trend shows a large reduction with the removal of volatiles, before the mass steadily increases, slowing after the first 2 h period. This works out around 5 μg/min. The oxygen values also agree that chemisorption has taken place, as oxygen is present after that total removal during the pyrolysis step. Although there is no visible trend between the oxygen uptake, the longest activation period shows the most sizable gain in oxygen. It is possible that the oxygen initially binds to the surface and then mass plateaus until the pores are wide enough to go deeper. At that point the oxygen enters the pores, where there are more active sites are available for the oxygen to bind to. Hydrogen is smaller and does not face this same issue.

Mass of nitrogen is constantly reducing. In the first 30 minutes, the nitrogen is removed at a rate of 255 μg/min, dropping to 204 μg/min in the subsequent 30 minutes. In the following hour there is a large drop off to 40 μg/min, before increasing again to 93 μg/min. This could be due to the same issue as the oxygen but in reverse, trapped inside the pores until they are large enough to release the nitrogen.

Figure 5.8 visualises the changes recorded across the 4 hours of activation, beginning with the values after the pyrolysis phase. The final carbon fraction was 79.5 %. The activation reduces the carbon fraction at a slow and relatively even rate throughout the duration. The smaller fractions are similar in value, so a larger graph is provided to the right in which to focus on the trends. The nitrogen, diamond, is depleted throughout. Oxygen, triangle, and hydrogen, square, both drop initially during the pyrolysis phase, and then the fractions both increase due to the removal of carbon and nitrogen as well as the chemisorption in practice. Ash, cross, grows throughout. This happens initially due to the removal of hydrogen and oxygen, and then continues steadily through the continued removal of carbon and nitrogen.

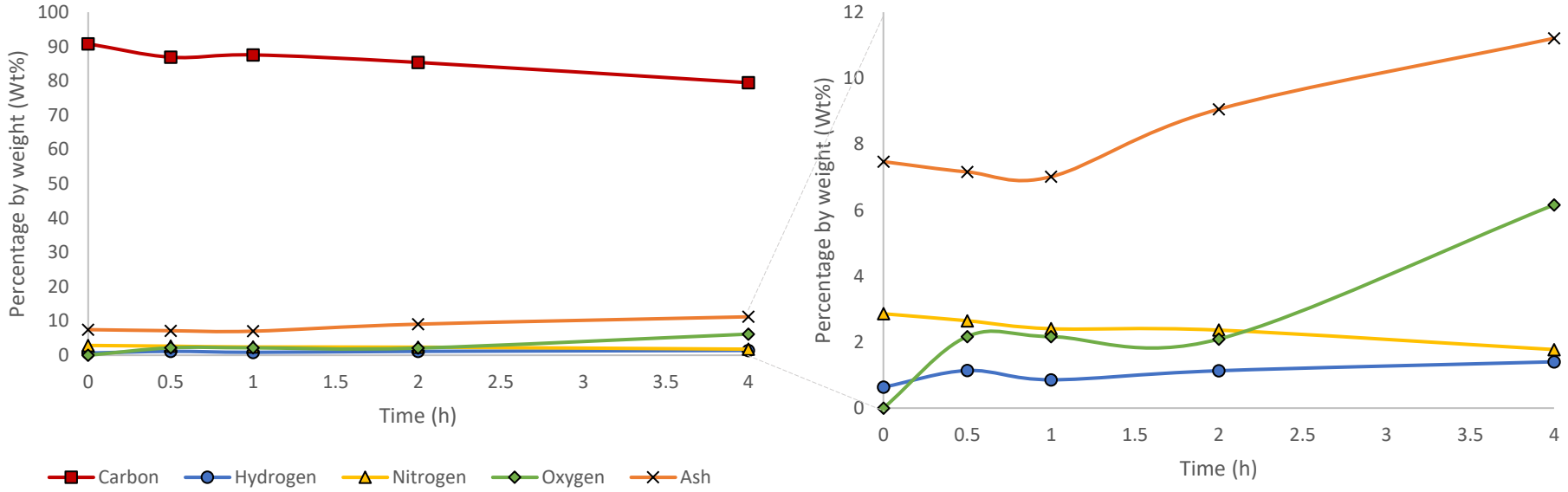

Figure 5.8 A timeline of elemental weight during the activation of strawberry pomace hydrochar at 700 °C. 0-hours uses the weightages found in the pyrolysis samples. Data from ultimate analysis.

5.1.6 SP Textural Properties

This section will present the findings from the textural analysis. The samples were evaluated by N_2 adsorption to characterize the surface area and pores. The results for the activated hydrochar can be viewed in Table 5.14. In all but one of the tested conditions, the surface area and pore volume has increased from the initial hydrochar sample. This indicates that pores have been created and widened, demonstrating that the removed material was liberated from within the sample as well as from the exterior surface. The conditions in SP-HTC-ACT-700-0.5 were not high enough to cause any serious change to the material. In comparison to the initial sample, the surface area has more than doubled and the microporous region is larger, showing micropore formation, but not to a degree where it significantly impacts the surface area. This could signify the pore formation process beginning, but at such an early stage the pores are only developing on the external surface. All other treatment conditions tested have resulted in a large growth in surface area.

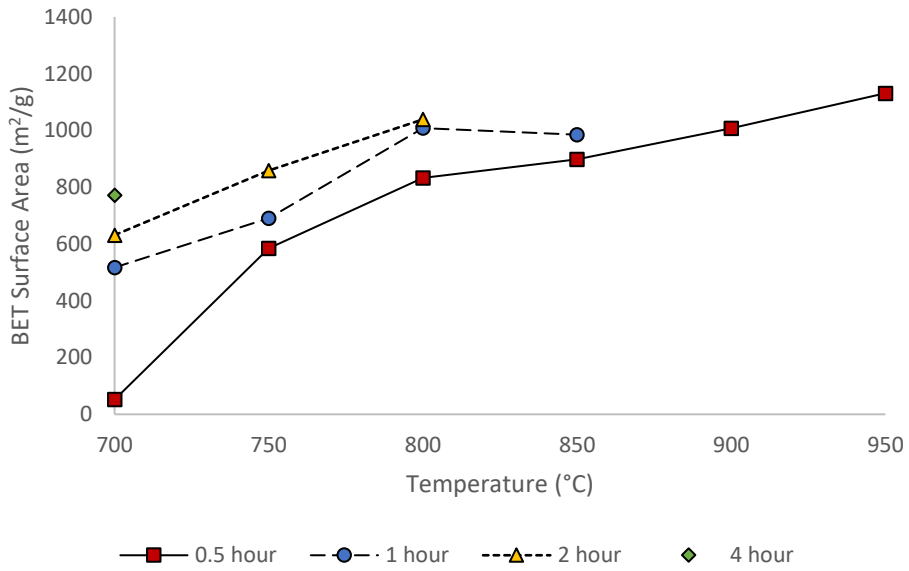

Figure 5.9 Activated strawberry pomace hydrochar surface area produced from the activation conditions

Figure 5.9 demonstrates how the surface area was affected with respect to the activation conditions. Based on this graph it can be said that as the experimental temperature was increased, the resultant surface area also increased. This is a success for the method as a high surface area is a key characteristic of an activated carbon. The highest surface area achieved was 1,131 m^2/g in sample SP-HTC-ACT-950-0.5, which was at the highest temperature that was tested. In Section 5.1.3 it was established that higher temperatures resulted in more sample loss. In terms of the surface area potential, the losses here are viewed positively. On the other hand, losses indicate excessive burn off resulting in pore collapse and overall surface area loss, as the sample returned 13.1 % activation yield, as per Table 5.9. It can be noted here that increasing the time duration was also seen to be effective at increasing the surface area. The triangles representing the 2-hour batch have higher surface areas than the corresponding temperatures at lower durations and the single value at 4-hours is the highest among the 700 °C samples. It is to be noted that the 800 °C sample at 1-hour achieves a surface area close to the 2-hour sample, with much higher yield.

The activation has a significant impact at increasing the surface area at lower temperatures, compared to the precursor. As the temperature is increased, the surface

area continues to increase, but the impact of each 50 °C increment has less significant gain each time, shown by the general curve in the trend lines. The 1-hour trend line has a shape which begins to drop slightly after 800 °C, which could indicate the highest value is achieved in this temperature region for a 1-hour run. The 0.5-hour sample collection begins to show a shape which rounds, until 850 °C, but then the results go on to show higher surface areas. This continuation could be explained by the losses faced in the higher temperature samples. Due to the low yields of SP-HTC-900-0.5 and SP-HTC-950-0.5, there were not many remaining pellets at the end of a run to collect. Some pellets were completely reduced to ash and other pellets had dropped small granules of ash from the surface as the size reduced. When selecting the sample for BET, the granule selected would not include the ash around it, and which may falsely inflate the surface area per gram, as a good portion of the mass remaining was ash. The trajectory of the 2-hour samples does not curve, which would indicate greater surface areas could be attained at higher temperatures. But it is thought that reaction conditions slightly over 800 °C for 2-hours would reduce the yield too low. The test operated at 850 °C returned only ash, as displayed in Table 5.6. Additionally, SP-HTC-ACT-800-2 had a low yield, 5.3 %, and could have benefitted from the same selective sample testing as the 0.5-hour samples at 900 and 950 °C.

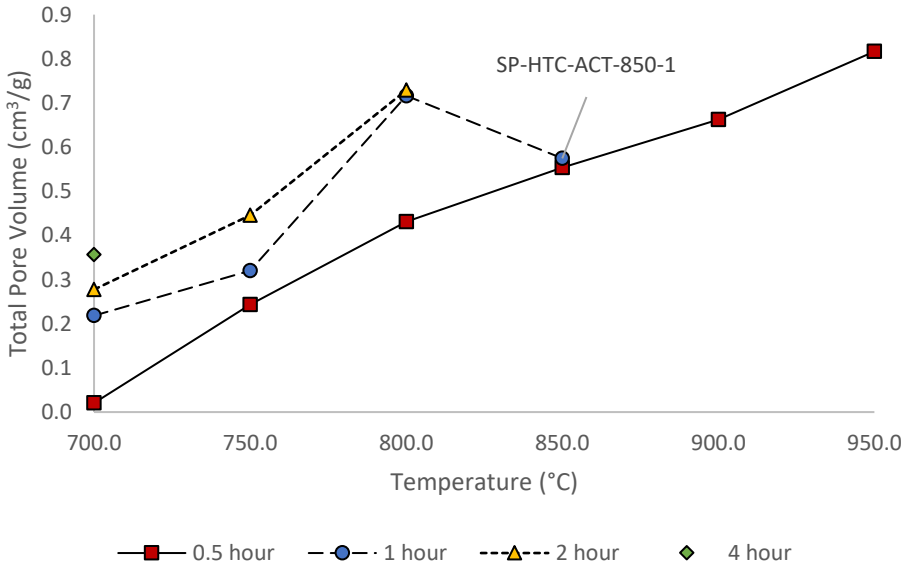

Figure 5.10 Activated strawberry pomace hydrochar pore volume produced from the activation conditions

The pore volume also follows a similar pattern to surface area, which is displayed in Figure 5.10. This graph demonstrates how the total pore volume was affected with respect to the activation conditions. Based on this graph it can be said that as the experimental temperature was increased, the total pore volume generally increased. The exception to the rule is SP-HTC-ACT-850-1. Between the 800 – 850 °C tests at 1-hour marks a tipping point for the pore volume recorded. Above this point the temperature appears to have a detrimental effect on the pore volume. SP-HTC-ACT-850-1, identified in Figure 5.10, is the only sample where the surface area, mesopore volume and total volume is below the lower temperature sample which preceded it, in this case SP-HTC-ACT-800-1. Additionally, in Table 5.14, the micropore volume remains almost the same, most likely indicating new pores are still being developed, as they transition into mesopores. But there is a large drop

off in mesoporous volume showing pores are being destroyed. In these conditions the mesopores have continued to widen and eventually transition into macropores, explaining the drop in mesopore volume. In the transition from 800 – 850 °C at 1-hour, the surface area decreases slightly, which is further evidence for pore walls breaking down and macropores developing. This sample succumbs to the highest loss recorded and these losses are having a detrimental effect on the quality of product produced. In the 2-hour samples, increased temperature leads to an increased pore volume. This leads to the creation of the most mesoporous sample in SP-HTC-ACT-800-2.

Focusing on the pore structure in Table 5.14, micropores appear to be created first because the microporosity is highest in the lower temperature and shorter duration reaction conditions i.e., SP-HTC-ACT-700-0.5. For the 0.5-hour samples, the lower temperature tests show prominently microporous pore volume growth. Conversely, at the higher temperature conditions, the mesoporous volume is increasing at a faster rate than the micropore volume. As the temperature is increased, the mesoporous fraction is increased until the mesoporosity and microporosity are reasonably even, which occurs between 850 – 900 °C. This demonstrates that the micropores are widening, joining, and becoming mesopores which increases the total pore volume. For the 2-hour samples, a similar trend occurs. The lower temperatures produce the most microporous samples, but the proportion is not as high as the 0.5-hour samples because there is a longer duration for them to grow and develop into mesopores. The 1-hour samples begin in the same manor but peak in the 800 °C sample. The change beyond here shows additional degradation of the sample, which has been explained above.

When comparing time durations at a fixed temperature in Table 5.14, it can be said that as time increases, micropore volume increases. The only outlier is between 1-hour and 2-hours at 850 °C, which could show the maximum microporosity is achieved close to 1-hour at this temperature. Additionally, as time increases, so does the mesopore volume. The balance of microporosity and microporosity also follows a trend. As time increases, microporosity increases, but microporosity decreases. The only outlier here is between 0.5-hours and 1-hour at 850 °C, which can be attributed to the tipping point explained previously. The drop off at the harshest conditions show that these trends have an upper bound where they succumb to excessive degradation, but not all of the experimental conditions have not pinpointed this tipping point yet. It should be noted that time has a less aggressive effect on the activation than the temperature.

$$Average\ Pore\ Diameter\ (nm) = \frac{\left[\frac{4\,V_{Total}}{SA}\right]}{1000}$$

Equation 5.1

The widening of pores is also demonstrated by the average pore diameter column in Table 5.14. This was calculated using Equation 5.1, above. This information is important in distinguishing the pore classification range. The figures prove that micropores were developed first and then widened through the process. The raw hydrochar sample, SP-HTC, was mesoporous and was measured to have few micropores. When the activating agent was added in the least severe conditions, the average pore size was within the micropore limits. As the temperature and time are increased, the average pore size increases. When the average measures above 2 nm, the classification changes to the larger size range, which

is the mesoporous region. Despite this, the micropore volume continues to increase, showing micropores continue to be created throughout the process.

Table 5.15 shows the results of textual analysis on the pyrolysis samples. It shows that pores are created during the pyrolysis phase. During this phase the micropores are also created first, possibly by the removal of moisture or volatiles which leave voids. Across the tests the mesopore volume remains constant or drops from the initial sample. The total volume is increased at low temperatures and during longer durations, which is replicated in the surface area also. Despite this observation, the pore volume is minor compared to the activated samples. There are some samples with increased surface areas. The highest was 465 m^2/g which happened in SP-HTC-PYR-800-2, but there is little correlation between the duration and the surface area. The relationship with temperature is different at high and low durations. For < 1-hour tests, the higher the temperature, the lower the surface area. The surface area peaks at the lowest temperature value, surpassing the initial precursor. As the temperature increases the surface area declines until it is below the precursor. Whereas at 2-hours, the material generally has a good increase in surface area, with no correlation to the temperature. This is linked with an increase in microporous volume. To check if the micropores continued to develop, sample SP-HTC-PYR-750-6 was tested for 6 hours, the longest duration, which produced the lowest surface area recorded. So, lengthening the time indefinitely does not continue to increase the surface area or lead to more micropore development. The growth of the micropore region at 2-hours may have been growth of ultra-micropores which were not detected before, as the average pore diameter has reduced to < 2 nm, whereas the 1-hour samples were in the mesoporous region.

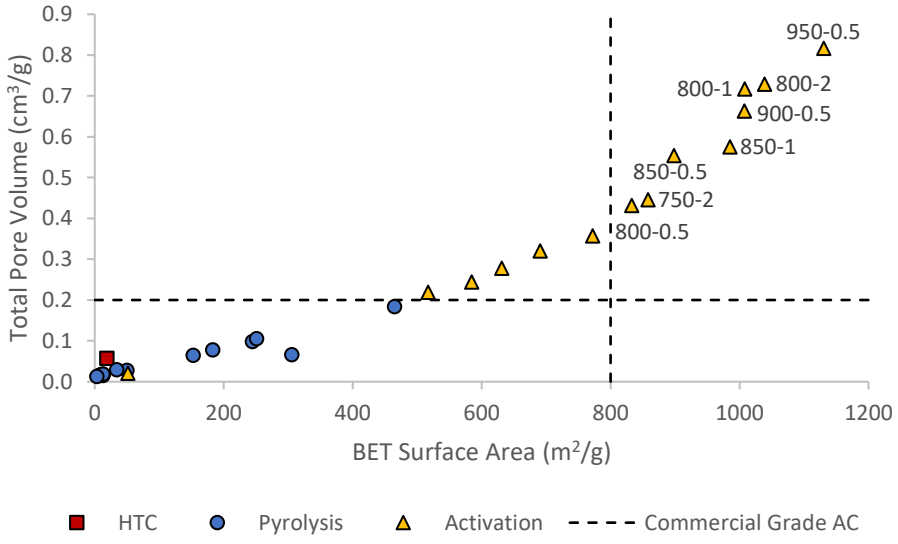

Figure 5.11 Comparison chart of all strawberry pomace samples textual properties, separated by stages of the process

The pore volume growth is very minimal, except in the low temperature samples and the 2-hour samples. It appears there can be pore development without an activating agent present, but progress is slow and inconsistent. The pyrolysis samples are primarily fixed carbon, and those with growth in surface area and pore volume are bordering on being activated carbons without the need of an activating agent. Figure 5.11 compares all the samples in terms of total pore volume and surface area. The dashed line represents the

boundary to be considered a commercial grade AC. This was established in Section 3.1.1 to be a surface area greater than 800 m^2/g and a total pore volume greater than 0.2 m^3/g. Markers Above the horizonal line and to the right of the vertical line meet these criteria. None of the pyrolysis are considered commercial grade. All but one outlying activation sample, are superior in quality compared to the pyrolysis and HTC samples in terms of total pore volume and surface area. The HTC sample has a greater pore volume than some of the tests.

Apart from the lowest test condition, all other activation samples have total pore volumes expected of commercial activated carbons. A total of eight samples are considered commercial grade overall due to the surface area. The conditions have been listed alongside the markers. They correlate with the more aggressive test conditions.

Table 5.14 S*urface area, pore volume and pore size distribution of activated SP hydrochar*

Sample	BET Surface Area	Microporous Volume	Mesoporous Volume	Total Volume	Average Pore Diameter	Microporosity	Mesoporosity
	m^2/g	cm^3/g	cm^3/g	cm^3/g	nm	%	%
SP-HTC	19	0.001	0.052	0.057	11.83	2	91
SP-HTC-ACT-700-0.5	52	0.019	0.001	0.020	1.58	94	6
SP-HTC-ACT-750-0.5	585	0.205	0.037	0.243	1.67	84	15
SP-HTC-ACT-800-0.5	833	0.276	0.149	0.431	2.07	64	34
SP-HTC-ACT-850-0.5	898	0.285	0.262	0.553	2.46	52	47
SP-HTC-ACT-900-0.5	1008	0.322	0.333	0.663	2.63	49	50
SP-HTC-ACT-950-0.5	1131	0.363	0.443	0.817	2.89	44	54
SP-HTC-ACT-700-1	517	0.186	0.031	0.218	1.69	85	14
SP-HTC-ACT-750-1	691	0.235	0.083	0.320	1.85	73	26
SP-HTC-ACT-800-1	1008	0.317	0.390	0.716	2.83	45	54
SP-HTC-ACT-850-1	985	0.319	0.248	0.574	2.33	56	43
SP-HTC-ACT-700-2	631	0.232	0.044	0.277	1.76	83	16
SP-HTC-ACT-750-2	858	0.286	0.156	0.445	2.08	64	35
SP-HTC-ACT-800-2	1039	0.317	0.402	0.729	2.81	44	55

SP-HTC-ACT-700-4	772	0.261	0.093	0.357	1.85	73	26
Standard Error (±)	23	0.007	0.037	0.044	0.11	2	2

Standard errors from Table 9.9 (Appendix)

Table 5.15 Surface area, pore volume and pore size distribution of pyrolyzed SP hydrochar

Sample	BET Surface Area	Microporous Volume	Mesoporous Volume	Total Volume	Average Pore Diameter	Microporosity	Mesoporosity
	m^2/g	cm^3/g	cm^3/g	cm^3/g	nm	%	%
SP-HTC	19	0.001	0.052	0.057	11.83	2	91
SP-HTC-PYR-700-0.5	306	0.050	0.013	0.066	0.86	77	20
SP-HTC-PYR-750-0.5	183	0.061	0.014	0.078	1.69	79	18
SP-HTC-PYR-800-0.5	13	0.004	0.012	0.018	5.50	20	66
SP-HTC-PYR-850-0.5	13	0.004	0.009	0.015	4.63	27	60
SP-HTC-PYR-900-0.5	8	0.002	0.010	0.015	7.60	15	68
SP-HTC-PYR-950-0.5	8	0.002	0.011	0.016	7.50	14	68
SP-HTC-PYR-700-1	245	0.085	0.011	0.098	1.60	87	11
SP-HTC-PYR-750-1	50	0.016	0.010	0.027	2.17	57	35
SP-HTC-PYR-800-1	34	0.010	0.014	0.029	3.35	37	48
SP-HTC-PYR-850-1	9	0.003	0.011	0.016	6.90	17	70

SP-HTC-PYR-700-2	251	0.086	0.018	0.105	1.68	81	17
SP-HTC-PYR-750-2	153	0.051	0.008	0.064	1.67	80	13
SP-HTC-PYR-800-2	465	0.167	0.014	0.183	1.58	91	8
SP-HTC-PYR-750-6	3	0.001	0.010	0.012	14.29	6	78

5.1.7 SP Raw Activation Tests

This section presents the results from the trials on raw, untreated strawberry pomace. The samples were activated under the same conditions to the hydrochar. Although 10 g of sample was used compared to 5 g and the flowrate of carrier gas was reduced. A selected group of samples has been included for analysis. Based on the results of Table 5.16, the material has been successfully activated, demonstrated by the high surface areas and pore volumes. Across the samples there is a good range of surface areas. The highest surface area attained was SP-RAW-ACT-850-0.5, at 812 m^2/g. The highest pore volume was also found in this sample. This shows strawberry pomace does not need HTC in order to be activated and reach the criteria for commercial grade AC. The trend witnessed in the hydrochar activation tests remain; as temperature and residence time are increased, so too does the loss, surface area and pore volume.

Table 5.16 Key features upon activation of raw SP

Sample Name	Yield	BET SA	V tot
	%	m^2/g	cm^3/g
SP-RAW-ACT-750-0.5	21.6	639	0.330
SP-RAW-ACT-800-0.5	13.2	743	0.393
SP-RAW-ACT-850-0.5	6.6	812	0.581
SP-RAW-ACT-900-0.5	2.8	-	-
SP-RAW-ACT-750-1	16.5	678	0.335
SP-RAW-ACT-800-1	4.2	678	0.539
SP-RAW-ACT-850-1	3.9	437	0.363
SP-RAW-ACT-700-2	20.6	567	0.260
SP-RAW-ACT-750-2	13.2	755	0.438
SP-RAW-ACT-800-2	2.0	-	-
Standard Error (±)	1.31	23	0.044

Standard errors from Table 9.5 & Table 9.9 (Appendix)

Considering the results, it appears that without the HTC treatment, the material is more susceptible to the activation conditions. Sample SP-RAW-ACT-800-2 returned a lower yield compared to the hydrochar sample which retained 5.3 %. SP-HTC-ACT-800-2 produced the largest recorded surface area in the hydrochar tests, so the same conditions were anticipated to produce a good comparison. The conditions have had an overwhelming effect on the raw strawberry pomace and the raw activation sample was primarily ash and unusable for textural analysis. A similar scenario happened to SP-RAW-ACT-900-0.5,

returning 2.8 % compared to the hydrochar yield of 9.4 %. The start of excessive burn off can be seen in SP-RAW-ACT-850-1. The surface area and pore volume both decrease from the previous sample, SP-RAW-ACT-800-1. This trend was also experienced in the hydrochar tests. Perhaps 850 °C is too high to treat the material for a 1-hour duration. In all 3 examples, the highest temperature tested has created the most loss, but this loss is seen to be negatively impacting the AC characteristics.

Another point to reiterate, which was stated in Section 4.3.5.3, is that the quantity of material in the raw experiments was doubled from the activation experiments. In the first raw trials, such little product was returned because the material was so susceptible to loss. To create enough sample for analysis, it was decided to double the starting quantity. It is thought that the additional sample within the same sized ceramic boats may have had an influence on the activation, but the activating agent remained in excess and the yield is still a valid comparison. The consequences may be negligible, but it is an observation from the experimental procedure.

The main textural characteristics of the hydrochar and raw samples are directly compared in Table 5.17. The characteristics are more equal than anticipated. In some instances, the raw activation sample looks to have better characteristics, such as at 750 °C for 0.5-hours, with a higher surface area, microporous volume and mesoporous. At lower timeframes and temperatures, the raw activation samples generally have a higher pore volume. However, to achieve the quality parameters required of a commercial ACs, higher treatment conditions are warranted. As the timeframes become larger, the hydrochar samples return higher pore volumes compared to the raw counterpart. But they are not vastly superior and remain relatively close. The surface area is higher in the activated hydrochar samples, except in the lowest conditions tested. The difference in surface area becomes more apparent at higher temperature tests. As raw strawberry appears to be affected more by the reaction conditions, potentially less time is needed to produce a comparable result. It can also be seen that the hydrochar sample always has a lower average pore diameter, pointing towards greater microporosity from the HTC pre-treated materials.

The most important area to note from the raw tests is the yield value. Similar to the hydrochar samples, many of values are below the target yield of 15 %. But there is only one example where the raw activation yield is greater than the hydrochar activation yield. The condition of 850 °C for 1 hour has been discussed previously and it appears too harsh for both samples, as it has too much loss associated. In the preluding test, at 800 °C for 1 hour, the activated hydrochar has a much superior yield, creating 3 times more product by including the HTC pre-treatment step. On top of this, the surface area and pore volume are also much improved. All other samples create at least 25 % extra product by undergoing HTC. Along with a greater yield, the HTC samples produce greater surface areas at comparable conditions. There are instances where lower severity conditions for hydrochar activation create higher surface areas than more severe raw activations, despite the more severe conditions positively impacting the raw sample. For example, the 750 °C for 1-hour hydrochar sample produces a greater surface area than the 800 °C for 1-hour raw sample. So, the HTC pre-treatment could create catalysis effect where lower conditions are required. Despite undertaking the same activation treatment as the hydrochar, the raw sample is more susceptible to mass loss. Not only was the yield poorer but none of the raw samples reached the quality of the hydrochar samples. The consequences of the pre-treatment process and whether this is justified will be covered in Section 5.5.

Table 5.17 Raw activation against HTC pre-treatment activation comparison

Sample	Yield	BET Surface Area	Microporous Volume	Mesoporous Volume	Total Volume	Average Pore Diameter	Microporosity	Mesoporosity
	%	m^2/g	cm^3/g	cm^3/g	cm^3/g	nm	%	%
SP-RAW-ACT-750-0.5	21.6	639	0.232	0.095	0.330	2.06	70	29
SP-HTC-ACT-750-0.5	27.7	585	0.205	0.037	0.243	1.67	84	15
SP-RAW-ACT-800-0.5	13.2	743	0.243	0.147	0.393	2.11	62	37
SP-HTC-ACT-800-0.5	18.6	833	0.276	0.149	0.431	2.07	64	34
SP-RAW-ACT-850-0.5	6.6	812	0.253	0.315	0.581	2.86	43	54
SP-HTC-ACT-850-0.5	13.4	898	0.285	0.262	0.553	2.46	52	47
SP-RAW-ACT-750-1	16.5	678	0.224	0.109	0.335	1.98	67	33
SP-HTC-ACT-750-1	22.5	691	0.235	0.083	0.320	1.85	73	26
SP-RAW-ACT-800-1	4.2	678	0.209	0.316	0.539	3.18	39	59
SP-HTC-ACT-800-1	12.0	1008	0.317	0.390	0.716	2.83	45	54
SP-RAW-ACT-850-1	3.9	437	0.133	0.217	0.363	3.32	37	60
SP-HTC-ACT-850-1	2.9	985	0.319	0.248	0.574	2.33	56	43
SP-RAW-ACT-700-2	20.6	567	0.197	0.061	0.260	1.83	76	24
SP-HTC-ACT-700-2	25.6	631	0.232	0.044	0.277	1.76	83	16
SP-RAW-ACT-750-2	13.2	755	0.243	0.192	0.438	2.32	55	44
SP-HTC-ACT-750-2	18.3	858	0.286	0.156	0.445	2.08	64	35
Standard Error (±)	1.3	23	0.007	0.037	0.044	0.113	2.06	2.00

Related to the problem of low yield, the remaining ash in the samples causes a separate issue. Table 5.18 displays the proximate analysis of some raw samples. The proportion of ash to fixed carbon is high. In some cases, the ash content surpasses that of the carbon. At this point it is no longer an AC. The table is bookended 18 % ash content value, similar results were found in activated SP hydrochars. However, these samples also produced surface areas greater than 1000 m^2/g. Although the fraction which remains as carbon was able to reach respectable surface areas, a large proportion of the sample is waste. This may not have been picked up by the gas adsorption tests due to the samples being cherry picked.

Table 5.18 Dry basis proximate analysis of activated raw SP

Sample Name	Volatiles	Fixed Carbon	Ash
		%	
SP-RAW-ACT-800-0.5	13.9	67.2	18.9
SP-RAW-ACT-850-0.5	18.0	44.0	38.0
SP-RAW-ACT-800-1	17.3	36.9	45.8
SP-RAW-ACT-850-1	16.7	30.5	52.8
SP-RAW-ACT-750-2	13.5	67.8	18.7
Standard Error (±)	0.5	1.4	1.2

Standard error from Table 9.7 (Appendix)

5.1.8 SP Key Samples Detailed Characterization

Six strawberry pomace samples were selected for additional testing due to interesting characteristics and comparability.

- SP-RAW was chosen because this is the initial material which all samples are derived from and can be compared against
- SP-HTC was chosen because it is the hydrochar precursor, and the precursor for all activated hydrochars produced. The sample will explore the pre-treatment pathway.
- SP-HTC-ACT-750-2 was chosen because it recorded a commercial AC comparative surface area, contains the highest carbon content of SP samples, and has a yield > 15 %. This material is microporous.
- SP-HTC-ACT-800-1 was chosen because it produced one of the highest surface areas recorded for SP and is a mesoporous AC. It also returned similar textural properties to SP-HTC-800-2 with a greater yield, despite the reduced time. It appears close to the optimum temperature for a 1-hour activation sample.
- SP-HTC-PYR-800-1 was selected as a step in the transition of SP-HTC-ACT-800-1 to an activated hydrochar, to understand more about the transition undertaken during the process
- SP-RAW-ACT-800-1 was chosen because it is produced under same conditions as SP-HTC-ACT-800-1 without an HTC pre-treatment, offering a comparison for answering the initial hypothesis

The initial nitrogen adsorption tests were used for screening the samples. Due to the high microporosity found, further detailed textural analysis has been carried out on the selected key samples. Using CO_2 analysis at 273 K is considered the best way of understanding the true micropore surface area, with linear molecules that can access to pores as small as 0.35 nm. The surface area calculated from N_2 BET surface area can differ from the true surface area by a margin of 20 % (Rouquerol, 1999). The cumulative curve formed from the results of CO_2 adsorption and longer N_2 adsorption studies will give more accurate results and an in-depth profile of the micropore and mesopore regions. The isotherms will be important in understanding the classification and the longer N_2 studies will show the desorption phase which can indicate structural features.

Density analysis has been carried out for an additional method of attaining the mesopore volume, as well as understanding the microporous region and the true porosity of the samples. This was carried out my MIP and helium pycnometry. XPS analysis is included to explore the surface complexes found on the materials and to gather if there is a different chemical composition on the surface compared to the bulk, which might explain the adsorption patterns. TEM & SEM images are included discussion of the transformation and proof of activation features appearing.

5.1.8.1 SP Adsorption / Desorption Isotherms & Micropore Analysis

The results of the further textural analysis have been compiled into Table 5.19. In terms of surface area, from highest to lowest: SP-HTC-ACT-800-1 > SP-HTC-ACT-750-2 > SP-RAW-ACT-800-1 > SP-HTC > SP-HTC-PYR-800-1 > SP-RAW. It is seen that the steam activation samples possess the highest surface area, with the HTC pre-treated samples surpassing the sample without a pre-treatment phase. The other samples have very minor surface areas, but it can be seen that through the process, the value is increased from SP-RAW through HTC, and then reduced during pyrolysis. The surface areas produced through this more accurate method are all slightly lower than the results presented in Section 5.1.6. The HTC-ACT samples are within 1% showing consistency between samples. SP-RAW-ACT-800-1 is just a fraction outside what can be considered machine error, but there will be a slight variation between samples, due to waste being the source. The samples with low surface area values are out by a wider margin relatively. The largest fluctuation is seen in SP-HTC-PYR-800-1 which is 10 % of the previously reported value. This may be due to the mesopore volume reporting 0.000 cm^3/g in this set of results, but previously reported 0.014 cm^3/g in the short nitrogen adsorption test.

Table 5.19 Textural data determined from CO_2 & long N_2 gas adsorption tests on key SP samples

Sample	BET Surface Area	Vultra	Vsuper	Vmicro	Vmeso	Vtot	Av. Pore Diameter
	m^2/g	cm^3/g	cm^3/g	cm^3/g	cm^3/g	cm^3/g	nm
SP-RAW	1	0.001	0.000	0.001	0.001	0.002	7.80
SP-HTC	12	0.001	0.000	0.001	0.050	0.057	19.69
SP-HTC-ACT-750-2	850	0.190	0.091	0.281	0.166	0.451	2.12
SP-HTC-ACT-800-1	996	0.106	0.214	0.320	0.410	0.742	2.98
SP-HTC-PYR-800-1	3	0.011	0.000	0.011	0.000	0.011	17.15
SP-RAW-ACT-800-1	650	0.100	0.103	0.203	0.284	0.499	3.07
Standard Error (±)	23	-	-	0.007	0.044	0.113	2.00

Standard errors from Table 9.9 (Appendix)

The CO_2 analysis allows for a more accurate depiction of the smallest micropore region, Vultra. Only the activation samples report any significant presence in this column, with the HTC pre-treated samples showing the largest figures. The sample conducted at 750 °C for 2-hours has almost double the sample formed at 800 °C for 1-hour. The lower temperature appears to develop more ultra-micropores and nurture a slower pore development so the micropores remain narrow. This more gradual development is effectively demonstrated by difference in pore diameter, which is 50 % wider in the higher temperature sample. The ultra-micropore volume between the activated hydrochar and raw activation sample is very similar, showing a consistent pore formation in the identical reaction conditions. The difference between the samples can be seen in the super-micropore and mesopore regions, where the HTC pre-treated sample is over 0.1 cm^3/g greater in both columns. SP-HTC-ACT-800-1 was able to create new pores and develop them into larger pores, creating a more gradual growth. Whereas the losses sustained by SP-RAW-ACT-800-1, 95.8 % compared to 88.0 % in SP-HTC-ACT-800-1, indicates that the pore widening led to more a rapid burn-off and the same pore volume could not be achieved. The super-micropore values equal zero for the non-activated samples. SP-HTC-ACT-750-2 has a super-micropore volume lower than both higher temperature samples. Vsuper is about half that of the Vultra in SP-HTC-ACT-750-2, showing narrower micropores are favoured at this condition. Overall, the micropore volumes are within 0.006 cm^3/g of the original textural properties analysis, but the weightage between Vultra and Vsuper is better understood.

The mesopore volumes are again seen to be superior in the activation samples. This time both samples activated at 800 °C for 1-hour show the largest volume. The higher temperature induces more loss, which results in larger pores. The raw sample shows a lower mesopore volume, which is consistent with the loss found that would assume more mesopores have grown into macropores. In SP-HTC-ACT-800-1 the balance between microporosity and mesoporosity remains similar, 43 % and 55 % respectively. The pore diameter is also close to the original result and reiterates that the sample is slightly more mesoporous. The raw sample is slightly more microporous and slightly less mesoporous than first thought, 41 % and 57 % respectively. This means the mesoporosity and microporosity in the raw sample are very similar to the pre-treated sample, as is the pore diameter. The characteristic separating them is a greater volume in the pre-treated sample, which is combined with a higher surface area. SP-HTC-ACT-750-2 has a lower mesopore volume to SP-HTC-ACT-800-1, due to the less aggressive conditions. This test has increased the measured mesopore volume by using the long N_2 method. This has changed the balance in the sample, but it remains a microporous sample, at 62 % microporosity. The mesoporous region is the majority volume in SP-HTC making it a mesoporous sample, showing a growth from the SP-RAW which has a more equal split, in favour of mesopores. The concerning result comes from SP-HTC-PYR-800-1, as mentioned previously, omits any data for the mesopore volume, despite measuring a value previously. The average pore diameter implies that it is not a microporous sample, despite the analysed values stating that it is. It is proposed that the surface area, mesopore volume and total volume be used from the short N_2 samples for comparison purposes. The remaining pore diameters show all the samples to be mesoporous, except SP-HTC-ACT-750-2 which is on the borderline.

With the micropore and mesopore volume known, we arrive at the total pore volume. In terms of total pore volume in descending order: SP-HTC-ACT-800-1 > SP-RAW-ACT-800-1 > SP-HTC-ACT-750-2 > SP-HTC > SP-HTC-PYR-800-1 > SP-RAW. The activated samples give the largest values, like the surface area findings. SP-HTC-ACT-800-1 is found again to be the

highest value, followed by the same conditions on the raw sample, mainly due the contribution of the mesopore volumes to the total pore volume. SP-HTC remains the same value as the earlier textural property tests, whilst the activated hydrochars show a minor increase within the machine error range. SP-RAW-ACT-800-1 drops by 12.5 % which could show a greater variation between samples. Finally, SP-HTC-PYR-800-1 would vary greatly but the original value will be assumed. The results of Table 5.19 have been extrapolated into isotherms below.

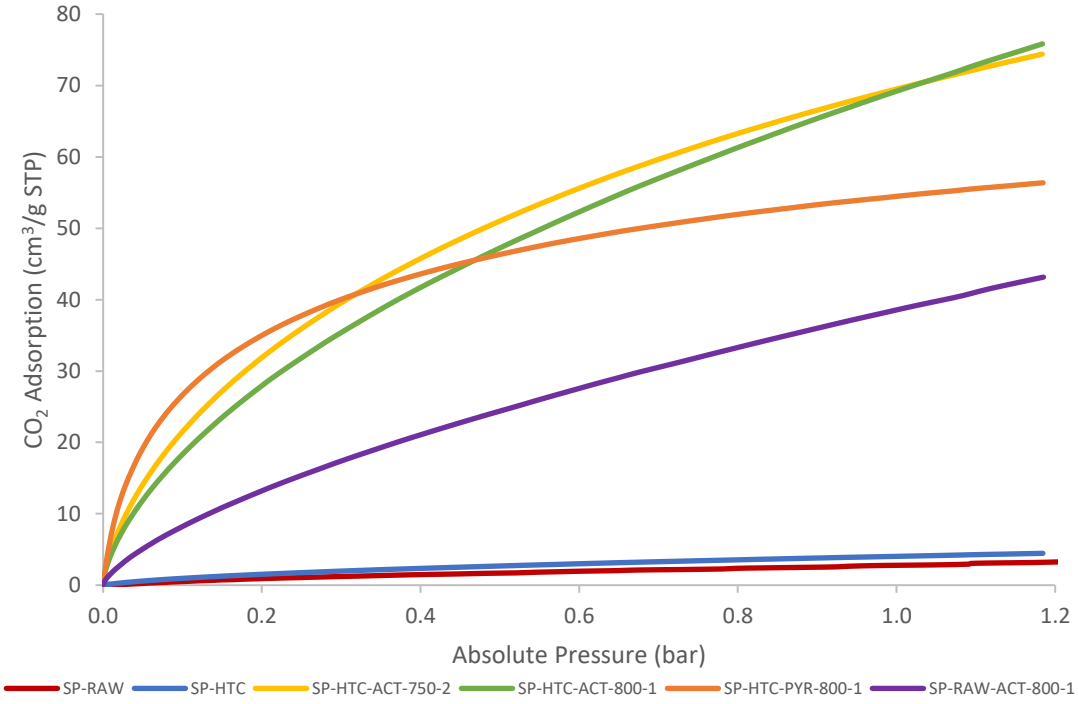

Figure 5.12 CO_2 adsorption isotherms of key SP samples

The isotherms from the low-pressure CO_2 analysis can be seen in Figure 5.12. Across the base of the graph, the adsorption for the base samples can be seen. The HTC sample has the capacity to adsorb more than the RAW sample, despite the identical micropore volume values in Table 5.19. The HTC process appears to adsorb in the microporous region slightly but neither sample shows a high micropore presence. SP-HTC has a higher total pore volume, but the majority is found in the mesopore region. SP-HTC is also known to have a higher surface area which may improve adsorption. In general, there is a factor of error across the machine and may be at play here, and both samples are close to one another. The raw sample was delivered as a 10 kg sample and the HTC batch was conducted in the scale of tons. If enough repeats were taken to be representative of the batch it is assumed to be within the standard deviation. The remaining samples present Type 1 isotherms confirming the presence of micropores. The two highest adsorption capacities come from the green and yellow lines which represent SP-HTC-ACT-800-1 and SP-HTC-ACT-750-2 respectively. The hydrochar activation samples lines overlap, with yellow showing a steeper initial adsorption at lower pressure, indicating narrower micropores, which is verified with the highest Vultra value and comparatively lower average pore diameter. It was also established that the sample shows the highest microporosity. The rate of adsorption then drops off in the yellow line and the green line surpasses it with the highest CO_2 adsorption value, which corresponds to the largest micropore volume. Neither line levels off, representing isotherms closer to Type 1b, showing the porosity is not limited to micropores

and there is further porosity at wider pore diameters. The raw activation sample, in purple, also shows a Type 1b shape. The CO_2 adsorption is much lower in this example, without the aid of the HTC pre-treatment, it shows half the capacity of the green line. The pyrolysis sample, seen in orange, provides a Type 1a isotherm, with a rise and then the trend begins to plateau. There is a sharp incline at the beginning demonstrating more ultra-microporosity, but in Table 5.19 total micropore volume is lower. Despite this, the sample may contain lots of narrow micropores. The material is representative of sample at the point before the activating agent is introduced, as the pyrolysis experiments are subjected to less aggressive conditions. These narrow micropores are enlarged into larger micropores and beyond with the introduction of the activating agent, as seen in the yellow and green lines, where the micropores have shifted slightly to the right, requiring a higher pressure for adsorption. The surface area value is derived from the nitrogen experiments, perhaps the pores are too narrow to be counted here, thus the value could be higher than 3, but not recorded through this method.

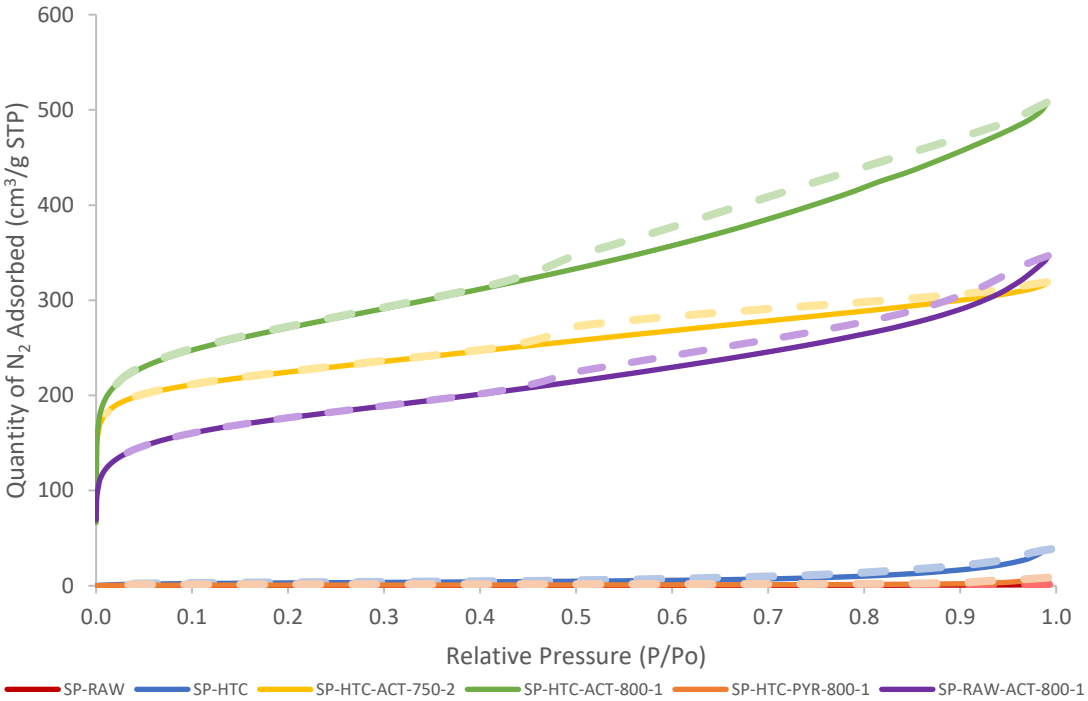

Figure 5.13 N_2 adsorption isotherms of key SP samples

The long N_2 adsorption was conducted for a more accurate depiction of the adsorption and the desorption pattern, which can be seen in Figure 5.13. It can be seen that the root samples have little adsorption compared to the activation samples. SP-RAW lays flat against the baseline and shows no adsorption. SP-HTC has a limited increase at relative pressures greater than 0.7. This indicates larger mesopores are present and the potential existence of macropores beyond the experimental range. In this chart, the pyrolysis sample (orange) also lays flat to the baseline. This correlates with the results indicating no mesoporous volume but it is a departure from the high CO_2 adsorption isotherm previously. The three activation samples (green, yellow & purple) show there is a mesoporous fraction as well as the microporous zone as the lines do not plateau after 0.1 relative pressure, which is considered the boundary of micropores. The lines display a hybrid of Type 1 adsorption isotherms at low relative pressures and the trend of Type 2 adsorption isotherms at high relative pressure. This is common in carbons with micropores

and mesopores / small macropores. The lines are seen exhibit a Type 4a isotherm shape, with the dotted line representing the desorption phase. The hysteresis loop indicates the presence of porosity in larger pores. The sharp uptake at the low relative pressure (< 0.1 P/Po) indicates the existence of micropores, which matches the order found in the CO_2 adsorption. At low relative pressures largest the N_2 adsorption capacities are SP-HTC-ACT-800-1 > SP-HTC-ACT-750-2 > SP-RAW-ACT-800-1. The samples continue the uptake of N_2 as the relative pressure is increased, showing the wide pore size distribution in the mesopore region. SP-HTC-ACT-750-2 remains at a steady incline up until the saturation point, showing fewer large mesopores and lower probability of a large macropore region, due to the activation conditions. However, the two samples activated at 800 °C for 1-hour both show an ascent beyond 0.9 relative pressure, indicating a large macropore volume is possible. Approximately 0.95 – 1 relative pressure is approaching the macropore range. The saturation pressure of nitrogen at 196 k is 1 bar, so there is also a lot of instability at this point, which is another explanation for the inflection. Above 0.9 relative pressure, the N_2 adsorption capacity of SP-RAW-ACT-800-1 surpasses that of SP-HTC-ACT-750-2, corresponding to the higher Vmeso value. The highest N_2 adsorption is found in SP-HTC-ACT-800-1, represented by the green line. This correlates with the material showing the highest mesopore volume and it is considered a mesoporous carbon. When the desorption line does not match the adsorption line, it indicates hysteresis is present, which can give information on the pore geometry and connectivity. Hysteresis is present in each of the activation samples and the shape of the hysteresis loops indicate pore shielding to different degrees. The desorption lines follow a similar trend on the purple and green lines, showing a Type H4 hysteresis curve. The desorption follows the adsorption line in parallel and then connects at around 0.45 relative pressure. This suggests some of the mesopores are close ended pores contained behind smaller micropores. These micropores, or pore necks, assuming slit shaped pores, are a funnel to the larger cavity which limits the desorption. The yellow hysteresis line appears more horizontal, and the distance between the adsorption and desorption line increases as the relative pressure drops. This indicates greater pore shielding. The necks must be emptied before the trapped N_2 volume can leave via the opening. All three desorption lines re-join the adsorption line at 0.45 relative pressure, as expected of a Type H4. This is the point where cavitation occurs and the N_2 exits the pore as a gas. A value of 0.4 relative pressure corresponds to approximately 4 nm on the NLDFT method. This means the necks are around 4 nm or below (Li et al., 2021). Without a thorough pore size distribution, the necks could be mesoporous or microporous.

Figure 5.14 shows the differential pore volume chart, for the three activated samples. There is a range of mesopores between 2.5 – 4 nm which could represent the narrow mesopore necks leading to larger mesopores behind, explaining the hysteresis. Notice the yellow line of SP-HTC-ACT-750-2 is the lowest in the mesopore volume (> 2 nm). It is likely the pore shielding here is impacted by the micropore range, some of the pore necks may be narrower than 4 nm. The micropore trends are typically repeated between the lines. The yellow line has a peak at approximately 0.3 nm and again between 0.4 – 0.8 nm, which will encompass the large ultra-micropore volume. These two peaks seem to be reiterated by the green line of SP-HTC-ACT-800-1 slightly to the right of the yellow counterpart. This could demonstrate the additional pore widening from the increased temperature. The samples have two distinct peaks for the super-micropore range, in between 1 – 1.5 nm and between 1.5 – 2 nm. The difference between the purple line and the green line, which were the raw and HTC samples activated at identical conditions, demonstrates pore volume

gained by subjecting the sample to an HTC pre-treatment. The purple line is also slightly offset to the right, as it is more impacted by the activation conditions causing the pre diameters to be wider. The data in Figure 5.14 is useful for ascribing the common pore sizes in the material, which can offer insights into what applications it would be most suitable based on the selectivity of adsorbents at certain pore sizes. This information can also be useful for tuning the pore size. For instance, if the microporous peak was desired to be at 0.9 nm, it could be suggested that 775 °C would be a good activation temperature to achieve this value, due to 0.9 nm being positioned between the yellow and green peaks, and the temperature is in between the two sample conditions.

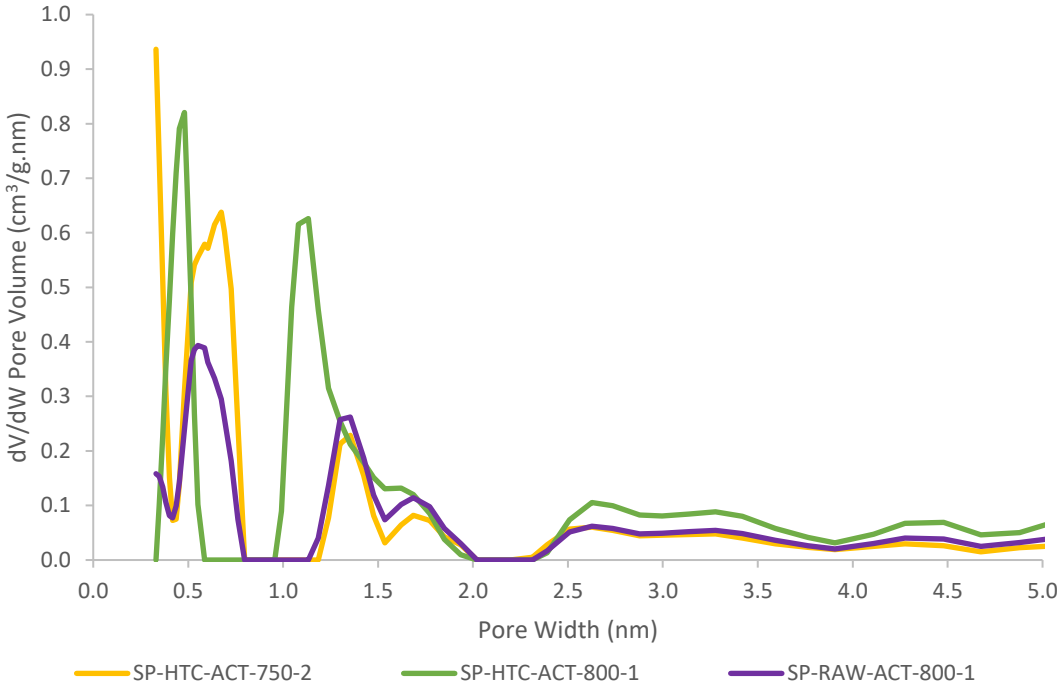

Figure 5.14 Differential pore volume of key SP activated samples

The cumulative pore volume chart is shown in Figure 5.15. The ranges are specified as micropore (< 2 nm), broken down further into ultra-micropore (< 0.7 nm) and super-micropore (0.7 – 2 nm), mesopore (2 – 50 nm) and macropore (50 – 100 nm). SP-RAW is seen as the lowest value, the red horizontal line across the base, exhibiting a marginal pore volume. The orange line, slightly above, rises early at a low pore width, during the micropore range, and then remains flat. Above that is the blue line representing SP-HTC. There is a negligible increase during the micropore range, then a gradual increase across the mesopore range from 5 nm onwards. There is some growth in the macropore range, but it settles at pore widths upwards of 60 nm. The three aforementioned samples have the highest average pore diameters due to this grouping of pore sizes. The other 3 have average pore sizes closer to the micropore range because of the sharp rises at the beginning. The yellow line, denoting SP-HTC-ACT-750-2, has the sharpest initial increase, due the high ultra-micropore presence. There is a smaller super-micropore presence where the curve begins. Compared to the other two activation samples, the mesopore volume is low so the curve drops away and flattens. The yellow line is subsequently surpassed by the purple line, SP-RAW-ACT-800-1. The mesopores in SP-HTC-ACT-750-2 are extensively held below 20 nm. The line plateaus beyond this point. For SP-RAW-ACT-800-1, the initial gradient is not as sharp, with the lowest Vmicro value for the activation samples. The momentum continues into the mesopore region, which begins to curve off, but continues

right until 50 nm, showing a broad mesoporous pore size distribution. There is slight growth at the beginning of the macroporous region and again an inflection at the end, indicating larger pores. SP-HTC-ACT-800-1 shows the same trends through the mesoporous and macroporous zones as the raw sample. However, the vastly superior microporous volume value, combined with the highest mesopore volume, sets it as the highest total pore volume by a good distance. The varied pore size distribution in the 800 °C for 1-hour samples shows the material has good transportation throughout the material.

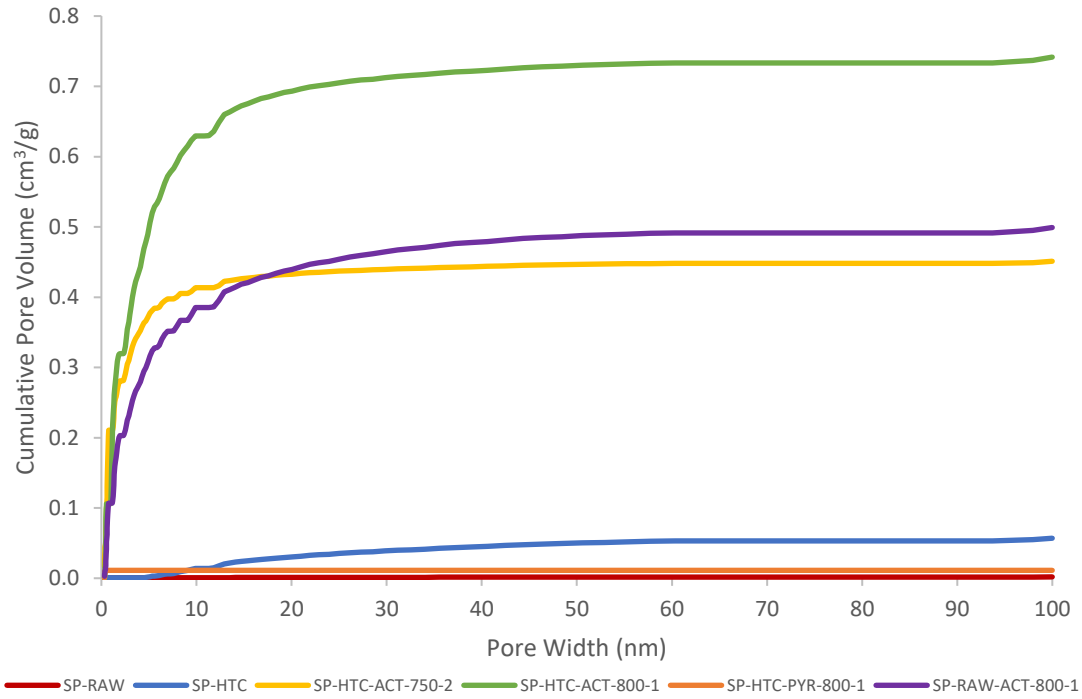

Figure 5.15 Cumulative pore size distribution of key SP samples

The existence of pore shielding, and cavitation is possible due to the wide pore size distribution and the existence of both micropores and mesopores. SP samples have varied pore sizes which is good for the transportation of adsorbate around the adsorbent. Materials which are predominantly carbon tend to be microporous. While it is true there are micropores, the activated SP samples have significant mesoporous region as well, so there are larger pores which have been developed, and the inflections at the end of the lines in Figures 5.13 & 5.15 allude to a macroporous presence. MIP will test to what extent macropores exist.

5.1.8.2 SP Density, Porosity & Macropore Analysis

The results of the density tests can be viewed in Table 5.20. The total volume does not include Vinter. This value represents the interparticulate space around the material which is essentially the volume found between the samples. The Vinter value often accounts for a large fraction of the total volume and would skew the results of all samples. The interparticulate data records pore sizes up to 230,000 nm and would inflate Vtot and the average diameter values. Vmeso is recorded from 2 – 50 nm. The lower bound is the smallest size that mercury can intrude, and the range has been established as mesoporous. Vmacro is recorded from 50 – 6100 nm. The lower bound is the crossover between mesopore to macropore and 6100 nm is the lower bound for the interparticulate void volume.

The Vtot values in Table 5.20 are all higher than the Vtot calculated in Section 5.1.8.1, as the MIP measuring range mentioned previously is above the detection range through N_2 adsorption and the macropores contribute a large fraction to the total. The volume is lowest in the raw sample and highest in the activated hydrochar samples, specifically the higher temperature treatment sample SP-HTC-ACT-800-1. The HTC sample is greater than the raw sample, showing the porous volume is developed through the pre-treatment. The result for SP-HTC is similar, but slightly higher than the pyrolysis sample, showing pyrolysis does not have a positive impact on the development of larger pores.

Table 5.20 Structural data determined by MIP & helium pycnometry on key SP samples

Sample	Pore Area	Vinter	Vmacro	Vmeso	Vtot*	Av. Diameter	Bulk Density	Skeletal Density	Porosity
	m^2/g	cm^3/g	cm^3/g	cm^3/g	cm^3/g	nm	g/cm^3	g/cm^3	%
SP-RAW	14	1.325	0.142	0.056	0.197	441	0.43	1.32	67
SP-HTC	30	0.436	0.439	0.105	0.544	131	0.58	1.34	57
SP-HTC-ACT-750-2	73	0.606	0.840	0.152	0.992	88	0.29	1.95	85
SP-HTC-ACT-800-1	172	0.976	1.172	0.410	1.583	59	0.29	2.06	86
SP-HTC-PYR-800-1	6	0.368	0.511	0.020	0.531	639	0.63	1.89	67

Vtot is the sum of Vmacro & Vmeso, disregarding Vinter. Inter.

The Vmacro column shows there is a macroporous presence in each sample. The macropore volume grows across the sample treatment process. HTC causes a rise in macropore volume from the raw sample. The pyrolysis phase, seen in SP-HTC-PYR-800-1, creates more microporosity, possibly from the removal of volatiles. As the activating agent is introduced there is a markable increase in macropore volume. This progresses again from SP-HTC-ACT-750-2 to the higher temperature sample SP-HTC-ACT-800-1, as pores widen, and more loss is incurred. SP-HTC-ACT-800-1 has the highest macroporous volume, as well as the highest micropore volume, mesopore volume and surface area, from Section 5.1.8.1. The macropore volumes > 0.436 cm^3/g match the inflections seen at the end of the nitrogen adsorption isotherms in Figure 5.13.

The Vmeso value largely shows growth in the same way. Except in the pyrolysis sample, which shows a large drop in mesopore volume compared the source sample, SP-HTC. This is in agreement with the low valuation seen in the long N_2 sample. The difference in Vmeso between the two activated hydrochar samples is high, with SP-HTC-ACT-750-2 being known to have more microporosity and SP-HTC-ACT-800-1 having more mesoporosity. SP-HTC-ACT-750-2 has a lower Vmeso value recorded in MIP then in N_2 adsorption, by 0.014 cm^3/g. This denotes a small value relative to the total pore volume but enough to contribute to the hysteresis. This backs the thought that some mesopore volume is trapped behind narrow necks, and some of those necks may be too narrow for mercury to intrude (< 2 nm). The mesopore volume from MIP and N_2 adsorption for SP-HTC-ACT-800-1 is in agreement, with both forms of analysis showing 0.410 cm^3/g. In this sample, the pore necks leading to the larger closed pores are most likely all narrow mesopores, around 4 nm, which the mercury is able to intrude and account for all of the mesopore volume in the sample. The higher temperature used on this sample has widened the necks above 2 nm, unlike in the 750 °C sample. The base samples of SP-RAW & SP-HTC have a higher mesoporous volume calculated through the MIP method. These samples have not previously been considered to have any considerable volume in the mesopore range. It is possible, that since these samples have not been exposed to a treatment method known to improve porosity, that there are closed pores within the material. At high pressure during the MIP analysis, samples with closed pores can be compressed. This is a known limitation of the MIP method (Westermarck, 2000). The effects show themselves as an overestimation in the small and medium sized pores, ergo the inflated mesoporous volume. This could also account for the higher Vmeso value for SP-HTC-PYR-800-1 through MIP, which happens to a lesser extent. Otherwise, the presence of mesopores in the precursors are an explanation for the highly mesoporous products created, as the precursor structure is an important parameter in influencing the final structure (Franklin, 1951). The average pore diameter is majorly impacted by the mesopore volume. A high mesopore volume correlates with a lower pore diameter in this MIP trial, even if there is also a large macroporous presence. This is due to mesopores having a narrower size range (2 – 50 nm) than the macropores (≥ 50 nm). The average diameter is smallest in the activated hydrochar samples. They are highest in the pyrolysis due to the low detection of mesopores combined with the significant presence of macropores.

The chart in Figure 5.16 shows the MIP results interpreted as cumulative intrusion. The graph is a useful reflection of connectivity within a sample. The first signs of macropore volume begins at a pore width region just upwards of 5000 nm. SP-RAW, red, has some large macropores, with a lot coming between 500 – 1000 nm. This rise accounts for half of the intrusion volume. There is another increase between 50 – 75 nm showing smaller

macropores, accounting for another quarter of the intrusion volume. This increase continues into the mesopores which contributes the remaining quarter. SP-HTC, blue, has macropores across the entire range studied, contributing 80 % of the intrusion volume. The mesopores are found between 20 – 50 nm and below 8 nm. The largest rise is seen between 6 – 8 nm which accounts for 10 %. The HTC process has caused an increase in the pores found below 10 nm. The pyrolysis sample, orange, follows the HTC macropore trend. The difference being that the treatment has created larger macropores, offset slightly to the left and above relative to the chart, to show a larger cumulative intrusion and pore width. The similarities stop in the mesopore region (< 50 nm). The orange line plateaus with little mesoporosity. Due to the mesopore peak below 10 nm in the HTC sample, the blue line surpasses the orange liner here and ends with a higher cumulative intrusion volume. The loss of mesopore volume due to the pyrolysis is proving difficult to explain. This could be due to the losses featured in the pyrolysis phase. The removal of macromolecules, such as volatiles, would increase the macroporosity. This may widen pre-existing mesopores, break down walls between mesopores or connect mesopores with larger macropores (Achaw, 2012). The activated hydrochars show similar patterns. SP-HTC-ACT-750-2, yellow, has some large macropores > 200 nm, accounting for 5 % of the intrusion volume. The is another spike of macropores between 100 – 225 nm which accounts for 70 % of the volume. There remains steady appearance of macropores from 50 – 100 nm and continued presence of mesopores below 50 nm. The increasing gradient shows that the mesopores are weighted more towards the smaller diameters. SP-HTC-ACT-800-1, green, displays the largest cumulative intrusion volume. The shape mimics the yellow trend but offset to the left accounting for the higher temperature causing the pores to increase in size. The mesopore region is also has a larger presence. SP-HTC-ACT-750-2 is known to be more microporous than mesoporous, which is not accounted for in this chart. The higher temperature of SP-HTC-ACT-800-1 may have converted a sum of those micropores into mesopores, as the mesopore range increases steeply, and results in a much higher cumulative intrusion value.

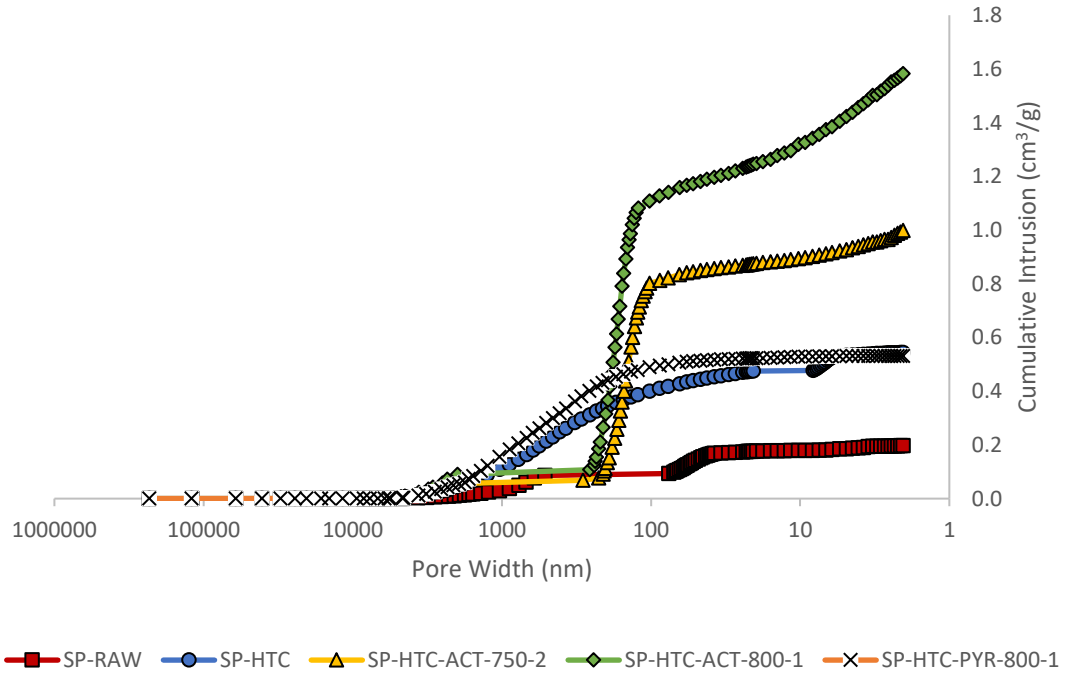

Figure 5.16 Mercury intrusion porosimetry of strawberry pomace excluding interparticulate void space

In the activated hydrochars, the largest macropores can be considered diffusional pores. The mesopores can be considered mass transport channels, creating a network leading to the micropores, although they can be useful for adsorbing larger molecules. The micropores are where most of the energetic adsorption sites are present. The wide range of pores available in SP samples show it has a good network. It would be an effective material for water treatment or gas adsorption. Due to the large volumes of macropores, which are non-energetic sites, the material would not be useful for applications like carbon capture. When comparing the pore area of the activated hydrochars to the N_2 tests, the area shows a sharp decline. SP-HTC-ACT-750-2 falls from 850 m^2/g to 73 m^2/g and SP-HTC-ACT-800-1 falls from 996 m^2/g to 172 m^2/g. The fall is prevalent in samples found to have a large microporous zone. This proves that the micropores offer the bulk of the surface area, which is important for adsorption. The surface area of the base and transitionary samples increases, due to the materials predisposition to be more macroporous. SP-RAW increases from 1 m^2/g to 14 m^2/g, SP-HTC increases from 12 m^2/g to 30 m^2/g and SP-HTC-PYR-800-1 increases from 3 m^2/g to 6 m^2/g. The surface areas listed are low, due to the existence of large pores and minimal microporous region, which benefits pore volume greater than it does surface area.

The porosity shows the fractional volume considered void space in a material. The degree of porosity is an important parameter in assessing an AC. Porosity was calculated by Equation 5.2.

$$Porosity = [1 - Bulk\ Density/Skeletal\ Density]\ x\ 100$$

Equation 5.2

The values can be seen in Table 5.20. The materials bulk density is determined by surrounding the sample and measuring the sample mass and the pores together. At the point on Figure 5.16 where the lines begin to rise is the point of intrusion, and the bulk density value is calculated at this point. The skeletal density demonstrates the space taken up by the mass alone and discards the pores, except those closed to the surface, which is accounted for as part of the material. This was found by helium pycnometry. The bulk density is increased through carbonisation process and drops with the activation. The skeletal density increases throughout the treatment process. Biomass by nature is a low-density material. This is reflected in SP-RAW, confirmed by the lowest skeletal density recorded and a bulk density of 0.43, despite showing the lowest total pore volume. The starting porosity is 67 %, albeit with a low pore volume and surface area. The HTC process and pyrolysis both increase the bulk and skeletal density. Although the HTC process does not improve the skeletal density much, perhaps due to the HTC not reaching completion. The HTC process should densify the material through the carbonization mechanisms. Despite a growth in pore volume, the densification of the bulk is sufficient to drop the porosity to 57 %. Pyrolysis can densify the material through shrinkage, and the sample releases close to 70 % of the mass, which leaves voids and increases the porosity back to 67 %. The introduction of steam removes amorphous carbon, leaving the dense crystalline structures and graphitic carbons. This increases the skeletal density massively. The pore development in all pore size regions, and particularly in the mesoporous region, causes the bulk density to drop rapidly, culminating in porosities of 85 % and 86 %. SP-HTC-ACT-800-1 has the highest value, which correlates with the superior pore volume in each region when compared with SP-HTC-ACT-750-2.

5.1.8.3 SP Surface & Bulk Chemistry

XPS analysis was performed on each of the base and activated samples in the key sample groups. Repeats were taken in different areas of the same sample for consistency. The use of XPS was anticipated to observe the surface chemistry compared to the bulk, particularly focussed on the oxygen functional groups formed on the surface. Unfortunately, the physical properties of the solids were ill equipped for the apparatus. The material was considered to be too friable, so the solids broke apart and would not stick to the sample bar. Instead, granules of sample were taken and pressed down onto the bar. This provided information of the internal but gives no indication of whether this differs from external surface properties.

The comparison between internal and external was achieved with one sample: SP-HTC-ACT-800-1. The atomic concentrations can be seen in Table 5.21 and the spectra of the oxygen peak can be seen in Figure 5.17. Both indicate that the surface oxygen content is much greater than the bulk. The spectra representing the surface is above and has a much greater peak. The split between peaks is seen as 97 % organic bonds, red, and 3 % carbonyl groups, blue. The bulk spectra, below, has a more equal split of 51 % organic bonds, yellow, and 49 % carbonyl bonds, green. This influx in organic bonds is most likely be proof of chemisorption on the external surface.

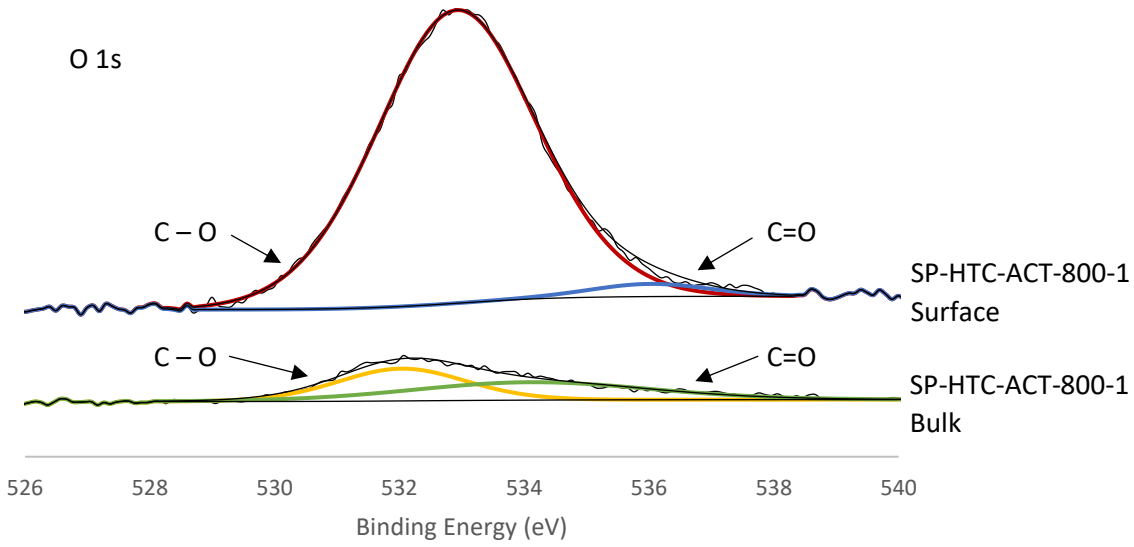

Figure 5.17 XPS Spectra of the oxygen identified on the surface and in the bulk of SP-HTC-ACT-800-1

The results of the additional samples can be seen in Table 5.22. Each sample detected the expected cornerstone elements of carbon, oxygen, and nitrogen. In addition to the these, the characterization by XPS demonstrates the presence of calcium, phosphorous, magnesium, potassium, iron, silicon, chlorine, boron, fluorine. These elements have been detected in varying quantities in different forms of entities. It is anticipated that these elements are the largest components in the ash. This is because ash materials are more prominent in the activated samples, where the ash content is higher, so a bigger proportion of the material is available to be detected.

Table 5.21 Internal and external surface XPS results of major heteroatoms identified in SP-HTC-ACT-800-1

Sample	C	O	N	Ca	P	Mg	K	Fe
	%	%	%	%	%	%	%	%
SP-HTC-ACT-800-1 Internal	91.56	6.73	0.20	0.36	0.81	0.23	0.12	0.00
SP-HTC-ACT-800-1 External	77.29	14.09	0.45	2.98	2.53	1.58	1.1	0.01

Calculated by atomic concentration %. Full list of repeats in Appendix.

Table 5.22 External surface XPS results of major heteroatoms identified in key SP samples

Sample	C	O	N	Ca	P	Mg	Si	F	B	Cl
	%	%	%	%	%	%	%	%	%	%
SP-RAW	74.51	21.88	0.67	-	0.07	-	2.88	-	-	-
SP-HTC	80.25	18.54	1.12	0.11	-	-	-	-	-	-
SP-HTC-ACT-750-2	92.31	7.56	0.24	-	-	-	-	-	-	-
SP-RAW-ACT-800-1	69.72	13.42	-	2.90	2.72	2.64	2.57	0.32	4.88	0.81

5.1.8.4 SP Surface Topography & Features

SEM images were taken of SP at four intervals of a physical activation using steam at 750 °C. Figure 5.18, below, displays the scanning electron micrographs of the surface morphology of SP-HTC after pyrolysis, and at the steam activation durations of 0.5, 1 and 2-hours.

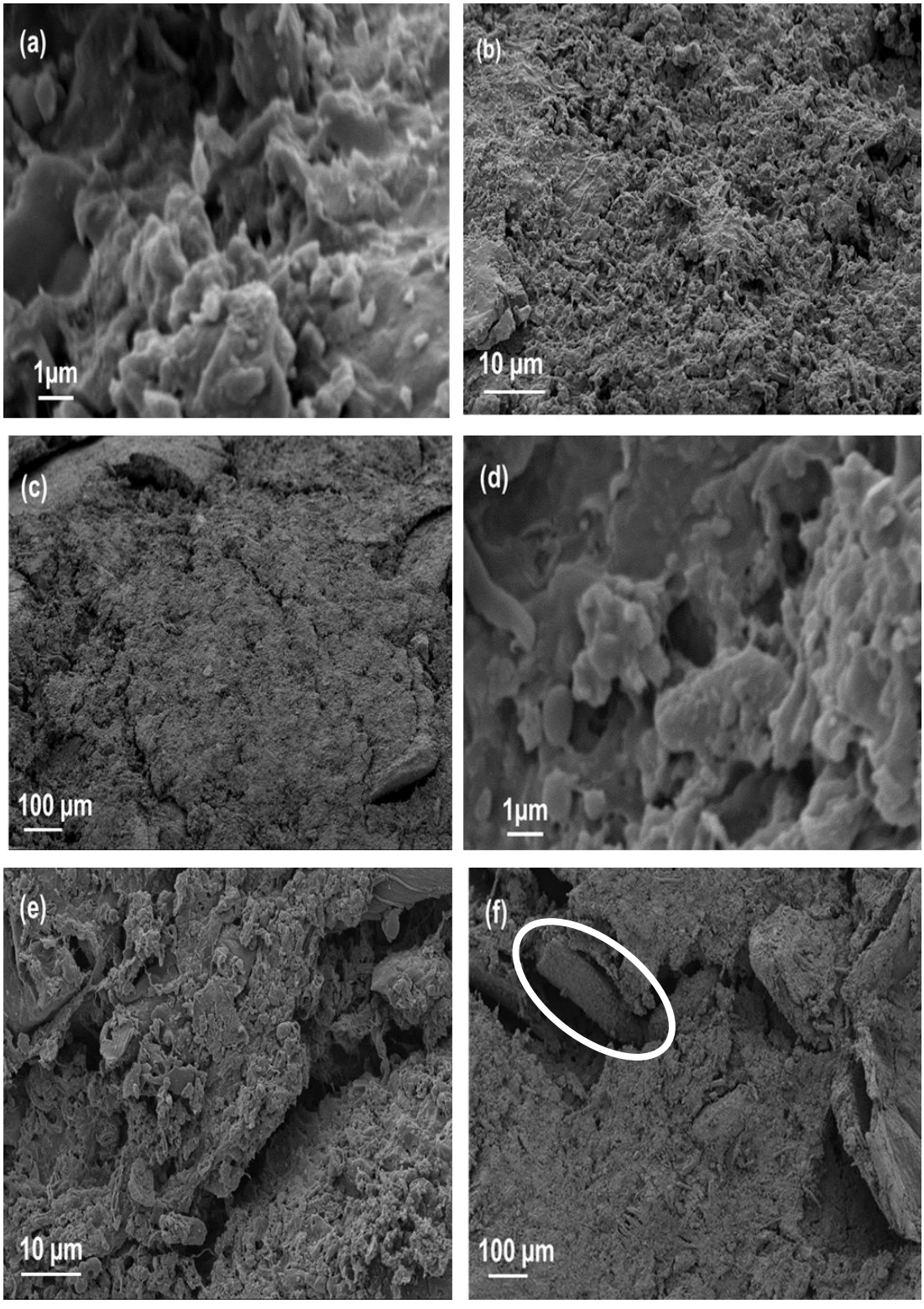

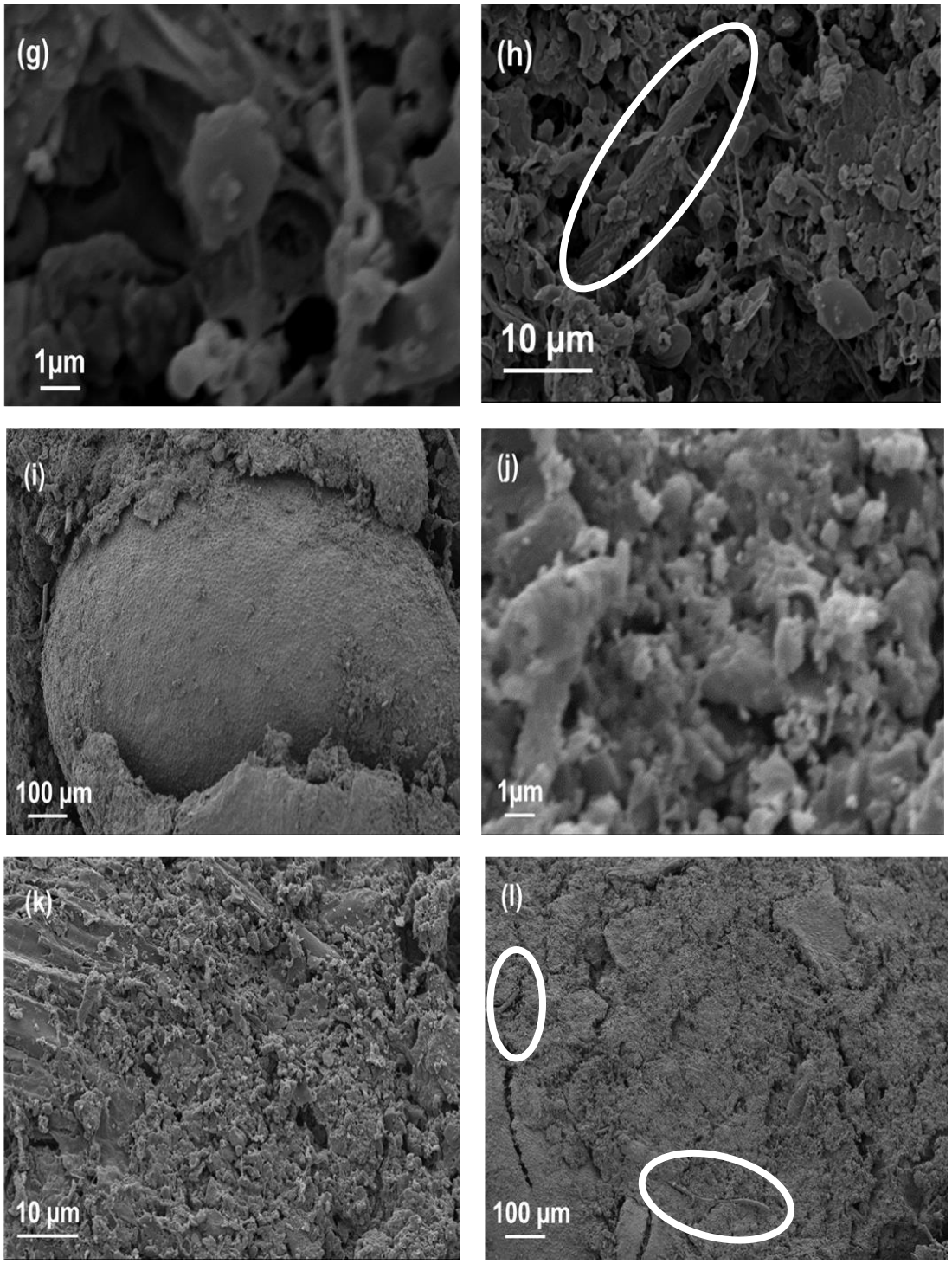

Figure 5.18 (a-l) low and high magnification SEM images of SP activated at 750 °C
(a, b, c) SP-HTC-PYR-750-0.5, (d, e, f) SP-HTC-ACT-750-0.5, (g, h, i) SP-HTC-ACT-750-1, (j, k, l) SP-HTC-ACT-750-2

Generally, the images show that all the carbon samples display a highly developed porous structure in the carbon matrix with widely distributed regular cavities. The initial images (a-c) show the surface to be quite dense and without a great deal of porosity, except some cracks, which would match with the low surface area and pore volume found in the pyrolysis samples. After the introduction of steam activation, the activated hydrochars appear to have a smooth and less rigid amorphous texture (Figures d-l), presumably due to the activation treatment. The surface is loose with many cracks and crevices. Images d and g present the onset of wider transitional pores. Image j, the longest duration sample still

has evidence of pores, but the image appears more cluttered. This sample has the highest ash content of the samples viewed, which may be collecting on the surface, as found in Section 5.1.8.3. However, despite the time exposed to the activating agent increasing, there is little to distinguish the development from one sample to the next. It was seen that time is a less influential factor than temperature, which may be the case here.

In images f, h, and l, areas of interest are circled. These appear to show nonhomogeneous features which are found in the strawberry pomace waste, such as the stem, fruit truss or calyx. The materials are formed of lignin which would not undergo HTC at 200 °C, which these samples would be treated at. In image i, the rounded structure appears to show an achene. The seeds were noticeably still present in the final material and was not impacted by the pre-treatment or activation. One of the risks of converting from waste is that the source may not always be pure. The waste SP Mainfrucht GmbH & Co. contains any leftover material which is filtered out from the food manufacturing process.

TEM was used to observe the internal structure. SP-HTC-ACT-800-1 was selected as the highest surface area and micropore volume of the SP key samples. Despite the general trend of mesoporosity in SP hydrochars, the main feature in Figure 5.19 is the display of micropores. The carbon is disordered and shows a highly three-dimensional interconnected network; the red circles highlight these areas of interest.

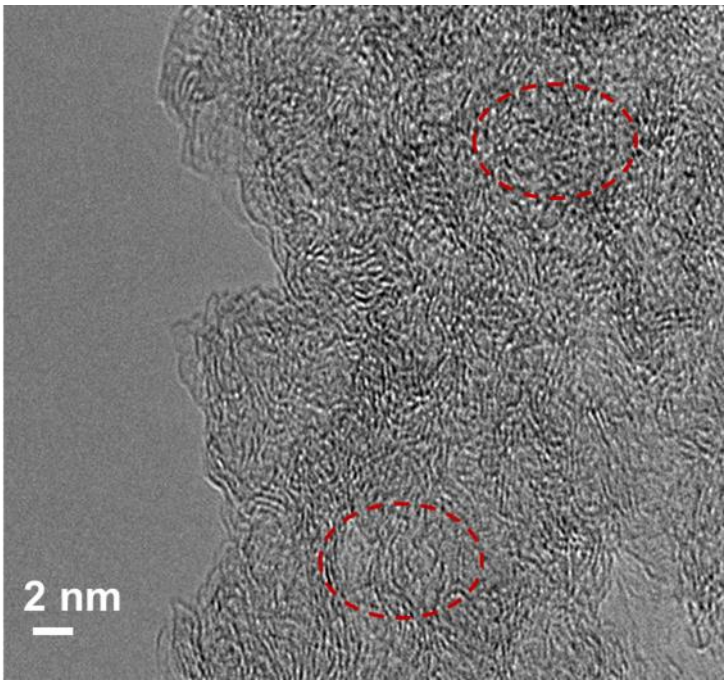

Figure 5.19 TEM image of SP-HTC-ACT-800-1

5.1.9 Summary

Activated carbon derived from strawberry pomace was previously an untrialled pathway. The method has proven to be successful in creating AC products from SP, with features comparable to commercial grade ACs. This demonstrates SP to be a good precursor for AC and the process works as a disposal route for the waste, creating a higher value product. The experiments were able to produce solids with surface areas greater than 1000 m^2/g and pore volumes exceeding 0.7 cm^3/g. The product struck a balance between microporosity and mesoporosity, with both present in the product. Samples created with lower activation conditions favoured microporous carbons and the higher activation

conditions produced more mesoporous carbons. The combination imposed some challenges, including pore shielding and cavitation during desorption. Overall, the samples contain porosities ~ 85 % with a wide pore size distribution in each region. Based on the results, ACs made from SP hydrochar would be recommended for wastewater treatment.

Samples which underwent a pre-treatment were able to produce higher activation yields than those which did not. Despite the starting products of SP-RAW and SP-HTC being subjected to the same time and temperature during activation, the more dense and carbonaceous nature of the hydrochar, was able to withstand the conditions better than the raw untreated sample, resulting in a more controlled burn off. The more gradual removal of mass generally resulted in samples with a higher surface area, in the range of 10 – 20 %. The faster burn off in the raw samples created larger pores, so the pore volumes were often found to be higher in the raw samples, confirmed by a larger average pore diameter. The raw samples followed similar trends to the pre-treated samples, only on an accelerated trajectory. Although the highest values achieved were vastly superior in the hydrochar samples, with SP-HTC-ACT-950-0.5 producing 0.817 cm^3/g and 1131 m^2/g, compared to SP-HTC-ACT-850-0.5 producing 0.581 cm^3/g and 812 m^2/g. Only this raw sample met the threshold to be considered a commercial grade AC, however the yield was 7 %. Finally, producing raw ACs was not a straightforward process, the method had to be modified to combat the losses, so a sample remained to be analysed, which included an increased batch size and reduced carrier gas flowrate. The raw sample would react faster with the activating agent, returning 20 % less product at lower temperatures and > 50 % at high temperatures. It can be argued that greater surface areas could be achieved under faster and less severe conditions using the raw precursor, but the desired quality would not be generated.

The activation conditions were key to producing the ACs. Temperature had by far the most profound effect on the activation. Higher temperatures resulted in reducing yields, but the loss was accounted for within the structural characteristics, with larger surface areas and pore volumes. On one occasion the tipping point was located for when a higher temperature reduced the surface area. The other instances resulted in no sample returned at all. This curtailed the testing matrix. Time also influenced these features, but it had less of an individual impact. The residence time subjected the material to a longer exposure to the activating agent, but the severity of reaction was due to the temperature. It has been established that the range of 750 – 800 °C for between 1-2 hours is the optimum range when accounting for pore development and yield. At 750 °C for 2 hours, the sample reaches 850 m^2/g and 0.451 cm^3/g, with a strong microporosity, favouring narrow pore widths. The sample returns 18 % of the starting mass, of which 73 % is fixed carbon. At the higher temperature of 800 °C for the shorter duration of 1 hour, the higher temperature develops a mesoporous carbon, despite retaining a similar micropore volume, boosting the textural properties to 996 m^2/g and 0.742 cm^3/g. The higher temperature incurs a lower yield of 12 % but it improves the surface chemistry with 4 % oxygen and 1 % hydrogen detected, after being absent in prior transitionary stages. The research can be used to finetune the desired product. A balance between these key samples' characteristics would begin to optimise the materials potential.

The pre-treatment conditions themselves proved to be unsuccessful at hydrothermally carbonising SP into a traditional hydrochar. The volatile content was found to increase from the treatment, contradictory to what would be expected. There were also inconsistencies

arising from the transformation, including an increased hydrogen fraction and a reduction in fixed carbon, although the elemental carbon increased. However, the Van Krevelen diagram showed the material had still been upgraded through the process. Through the pre-treatment, a more suitable precursor is made. The results are evident from the quality and quantity of product produced, compared to the direct route. Without this step, the material is susceptible to the activation conditions leading to rapid burn off. Perhaps there is more potential in the material if a full HTC treatment is completed. In addition to this, the pre-treatment has upgraded the material to a better fuel stock, which is comparable with sub-bituminous coal based on HHV, if a coal alternative was desired.

Most samples achieved at least 80 % carbon in the final product, which is an acceptable value for AC. The material has some issues with ash content, which begins at 2.5 %. The losses sustained increases this to between 10 – 20 % of the final product, which would be a concern for product retailing. The losses must be constrained to avoid maximising the ash fraction. The pre-treatment reduces the ash content slightly and a more effective HTC process may remove more. The process shows chemisorption the activating agent in the form of oxygen and hydrogen, with greater success at higher temperatures.

Through the sample analysis and comparison of processes, it can be stated that a pre-treatment process is necessary to produce ACs from SP which are in line with consumer grade products. Generally, SP AC exhibits mesoporous characteristics.

5.2 Coffee Grounds

5.2.1 CG HTC Pre-Treatment

The raw coffee grounds were processed through a lab scale pressurized reactor under HTC conditions (220 °C, 5 hours). The data in Table 5.23, shows the calorific value of coffee grounds before and after the process. The samples were tested at the bone-dry weight, seen in the dry HHV column. The calorific value was greatly improved in CG-HTC, compared to the precursor CG-RAW, from undergoing the process. The wet HHV value was calculated using the original sample moisture content. There is a clear and noteworthy improvement by undertaking the HTC process.

Table 5.23 Calorific value before and after HTC of CG

Sample Name	Wet HHV	Dry HHV
	MJ/kg	MJ/kg
CG-RAW	10,900	22,700
CG-HTC	27,400	28,200

The results indicate an effective thermochemical conversion has taken place. CG-HTC is on par with high-volatile bituminous coal (Engineering ToolBox, 2010). The heating value and equivalent coal comparison shows that CG-HTC would be a highly effective fuel. The raw precursor also shows potential but with a 52 % moisture content, the drying and energy costs would be discouraging. This enhancement through the HTC process demonstrates a positive use for the waste material, as a higher value product and adhering to the notion of energy from waste.

Table 5.24 Dry basis proximate analysis on raw and hydrochar variations of CG

Sample Name	Volatiles	Fixed Carbon	Ash
	%	%	%
CG-RAW	80.8	17.7	1.6
CG-HTC	72.0	27.8	0.2

Table 5.24 shows the results of proximate analysis on the two samples. The results portray that a carbonization process has been undertaken to a degree consistent with the carbonization process. The material begins with a high level of volatiles, which drops through the process to form CG-HTC. The key area is the fixed carbon content. This increases through HTC, demonstrating an effective carbonization. Another valuable part of the HTC process is the leaching of ash. The ash content begins low and drops further during the process. Mineral mater in CG ash must be highly soluble or affected by the water in a solvent state. This is beneficial to the hydrochar, no matter the application as it is purer. For combustion there will be less ash remaining after combustion to cause slagging and fouling, a common feature from combusting biomass. The low ash content makes the sample especially attractive as a precursor to AC because the ash will have a lower presence in the final product in proportion to the loss. Overall, the transition follows what is expected of a HTC reaction, backing up the process.

Table 5.25 Dry basis ultimate analysis on raw and hydrochar varieties of CG

Sample	Carbon	Hydrogen	Nitrogen	Oxygen	Ash	H/C	O/C
	Wt %	Wt %	Wt %	Wt % By difference	Wt %	Atomic Ratio	Atomic Ratio
CG-RAW	59.3	5.7	2.6	30.9	1.6	1.15	0.39
CG-HTC	70.6	6.8	2.9	19.5	0.2	1.15	0.21

Ultimate analysis was carried out on the samples, shown in Table 5.25. The carbon column reiterates how the content increases during HTC. The hydrogen fraction increases somewhat, contrary to what was expected. The growth remains proportional to the carbon growth, which is demonstrated by the H/C ratio, which remains constant between the two materials. HTC seems to primarily remove oxygen and ash from the material. The Van Krevelin diagram, pictured in Figure 5.20, presents this data in comparison to a range of solid fuels. The raw precursor begins in the range expected of peat. The O/C ratio after HTC takes the material to the level of subbituminous coal. The identical H/C ratio means the hydrochar is parallel with the raw sample and has a higher H/C ratio than expected of a subbituminous coal. Based on the results in Table 5.23, it would be anticipated that the O/C and H/C ratio would be lower, placing CG-HTC between the bracket of bituminous coal and anthracite.

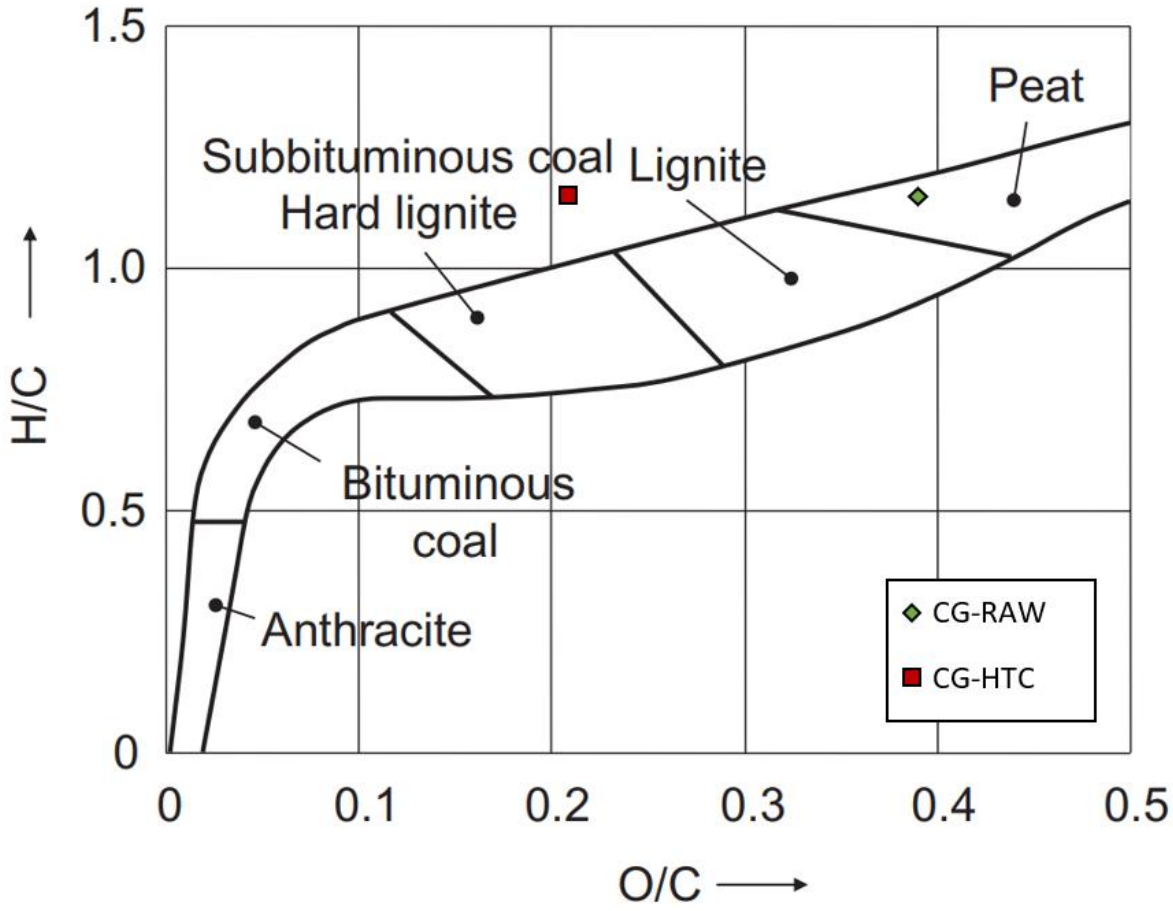

Figure 5.20 Van Krevelen diagram of solid fuel atomic ratios (Agraniotis et al., 2017)

The lab scale HTC process was conducted in batches. This approach gave greater control over the independent variables and allowed more precise verification of the input and outputs compared to the continuous pilot scale rig. The solid and liquid mass were recorded at the start and end of each run to formulate a mass balance. The results have been presented in Table 5.26 and 5.27. *Results in these tables were collected and calculated by Dr. Bethany Campbell, at the University of Surrey. All data used with their permission (Campbell, 2022).* The carbon content was analysed by total organic carbon (TOC) analysis. The output carbon mass accounts for 99.9 % of the input value. The critical values generated from the analysis is the total carbon (TC) in the precursor compared to the carbon in the hydrochar. Through the HTC process 82.4 % of the carbon has remains in the hydrochar. This retention contributes to a 55.7 % overall solids yield. Both figures are within the anticipated range for HTC, which appears to show the thermochemical process has been achieved. Additionally, the liquid yield has surpassed 100 % demonstrating the presence of dehydration reactions. It is to be noted that the values for CG-RAW and GC-HTC differ to the results presented earlier in this section, this will be discussed later.

Table 5.26 Carbon mass balance across HTC

			Value	Error (±)
Inlet	Spent Coffee Grounds (CG-RAW)	Mass (g)	60	1.0
		TC (%)	53.6	0.9
		C (g)	**32.2**	**0.8**
	Total	**Carbon (g)**	**32.2**	**0.8**
Outlet	Char (CG-HTC)	Mass (g)	33.4	1.1
		Carbon %	79.2	2.7
		Solid C (g)	**26.5**	**1.3**
	Liquid	Mass (kg)	0.55	0.0
		TC (g/L)	9.83	0.44
		C (g)	**5.4**	**0.2**
	Gas	RHP (bar)	2.8	0.7
		Head vol (ml)	200	20
		CO_2 (mol)	0.023	0.006
		C (g)	**0.276**	**0.006**
	Total	**Carbon (g)**	**32.1**	**1.3**

10 wt% DS of CG. Residual Head Pressure (RHP).

Table 5.27 Yields for HTC char and process water at 10 wt% DS of CG

	Value	Error (±)
Solid Yield (%)	55.7	2.1
Liquid Yield (%)	101.9	-
Liquid density (kg/L)	1.003	-
Carbon Yield to Char (%)	82.4	4.4
Carbon Yield to Liquid (%)	16.7	0.9

5.2.2 CG Independent Pyrolysis Tests

The powdered CG-HTC was pelletized for the pyrolysis and activation experiments. Each experiment tested ten 0.5 g pellets. Based on knowledge from the SP pyrolysis experiments, it is known that there is an approximate upper limit in how much material can be removed during the pyrolysis step, within the time and temperature limits introduced. These results were consistent across all samples tested and showed a limit to the pattern of loss. This has been found to be true with the CG samples also. The average upper limit value loss in CG during pyrolysis is 64.7 %. Following on from the findings in the SP results, a small selection of the CG pyrolysis samples have been displayed in Table 5.28. The columns offer little in the way of trends, with the columns presenting similar figures. The greatest losses are seen in the highest temperatures and longest times, although they only deviate by 2.5 %. In terms of the constituents, most of the material is fixed carbon. All samples report > 90 % carbon content. This highly carbonaceous material can be a promising precursor for activation, with a high fixed carbon presence for the activating agent to react with. The volatile weight has dropped considerably from CG-HTC, seen in Table 5.24. The highest volatile content is found at the lowest temperature point. There is a growth in ash during the pyrolysis, but this presence remains minimal, with all samples reporting < 1 %, so the ash will require large factor of material loss to become a major component.

Overall, a release of volatiles has concentrated the carbon fraction, for the benefit of the sample, as well as concentrating the ash fraction. However, the ash fraction is still relatively low. This can be considered a success and the material is primed for the activation step.

Table 5.28 Dry basis proximate analysis of CG hydrochar after the pyrolysis phase

Sample	Loss	Volatiles	Fixed Carbon	Ash
	%	Product Dry Basis Weight %		
CG-HTC-PYR-900-0.5	65.1	4.4	94.9	0.7
CG-HTC-PYR-700-1	64.4	7.5	91.9	0.6
CG-HTC-PYR-750-1	64.9	4.8	94.6	0.7
CG-HTC-PYR-800-1	63.4	5.6	93.7	0.8
CG-HTC-PYR-850-1	65.2	6.7	92.7	0.6
CG-HTC-PYR-800-2	65.8	5.4	94.1	0.5
Standard Error (±)	1.7	0.4	0.7	0.2

Standard error from Table 9.11 & Table 9.14 (Appendix)

5.2.3 CG Activation Yield

The activation experiments introduced the steam activating agent. The same framework of experimental conditions was conducted in the same manner as the SP samples, using the same tested conditions. Given the results, the coffee samples could potentially have been tested at even higher temperatures and durations, due to the slower burn off and lower ash fractions. The framework was based on feedback from the strawberry tests which anticipated a higher rate of burn off.

Looking at Table 5.29, it appears the losses sustained in the activation of coffee grounds are manageable. There are only two examples, CG-HTC-ACT-900-0.5 & CG-HTC-ACT-950-0.5, where the material dips below the 15 % expected return. The material seems most

susceptible to loss at high temperatures, as demonstrated in the aforementioned samples. Across all timeframes tested, it is seen that as temperature is increased, the yield decreases. The same pattern is noted for increasing time. As the time duration increases, the yield decreases.

Table 5.29 Activated hydrochar and carbon yield achieved from activated CG hydrochar

Sample Name	Activated Hydrochar Yield	Carbon Yield
	%	%
CG-HTC-ACT-700-0.5	34.5	115.1
CG-HTC-ACT-750-0.5	33.1	111.6
CG-HTC-ACT-800-0.5	29.0	99.6
CG-HTC-ACT-850-0.5	22.8	76.3
CG-HTC-ACT-900-0.5	13.6	45.5
CG-HTC-ACT-950-0.5	5.5	18.4
CG-HTC-ACT-700-1	33.2	109.2
CG-HTC-ACT-750-1	31.4	106.2
CG-HTC-ACT-800-1	25.2	82.9
CG-HTC-ACT-850-1	16.9	56.5
CG-HTC-ACT-700-2	31.3	102.8
CG-HTC-ACT-750-2	25.5	84.4
CG-HTC-ACT-800-2	17.2	56.4
CG-HTC-ACT-700-4	31.1	104.3
Standard Error (±)	1.7	5.7

Standard errors from Table 9.11

In the right-hand column, the carbon yield across the activation is shown. The trend of the carbon yield mirrors the activation yield. Where lower yields are presented, the carbon yield also drops accordingly, showing the mass removal is impacting the fixed carbon. Many samples show a carbon yield above 100 %, which is implausible. The carbon content cannot grow during the activation, as no carbon-based materials are introduced in the activation. It is likely that the starting value of CG-HTC is not consistent with the activated samples, as multiple batches were produced, and is not representative of the starting carbon content. Another explanation could be due to the carbon from the liberated volatiles. The volatiles are assumed to be vapourised during the temperature ramp and elutriated by the nitrogen. CH-HTC is pelletised with 2 tonnes of pressure for the activation, the tightly bound tablet could trap volatiles within in the pellet, which form part of the structure. The carbon is then accounted for in the subsequent tests.

Focusing on the low temperature samples, in the 700 °C bracket, very little loss has been demonstrated during the activation step. The base activation yield, working backwards from the information in Section 5.3.3, is 35.3 %. This means CG-HTC-ACT-700-0.5 has only lost 0.8 % of the sample weight, 0.04 g. This is assumed to be from the fixed carbon, although the inflated carbon yield denies this information. Other materials at the lower temperatures, such as CG-HTC-ACT-750-0.5 or CG-HTC-ACT-700-4, have also not shifted far away from the pyrolysis loss value. This could indicate that not much activation is taking place at low temperatures. Oppositely, the material could have a slow, controlled removal and boast a high yield.

Figure 5.21 shows difference in loss encountered in the pyrolysis phase alone compared to the full activation process. The grey bars, representing the pyrolysis losses, remain at a similar level, despite the advancing conditions. The red line shows the 64.7 % average loss, which is considered the threshold of how much loss is encountered in this phase, during the conditions tested. It also takes into account the samples which are not present in the chart, which further states how equal the losses are found to be during pyrolysis. The black bars, representing the activation losses, are always higher than the grey bars. The losses in these experiments are influenced by the conditions and the losses increase as the temperature increases.

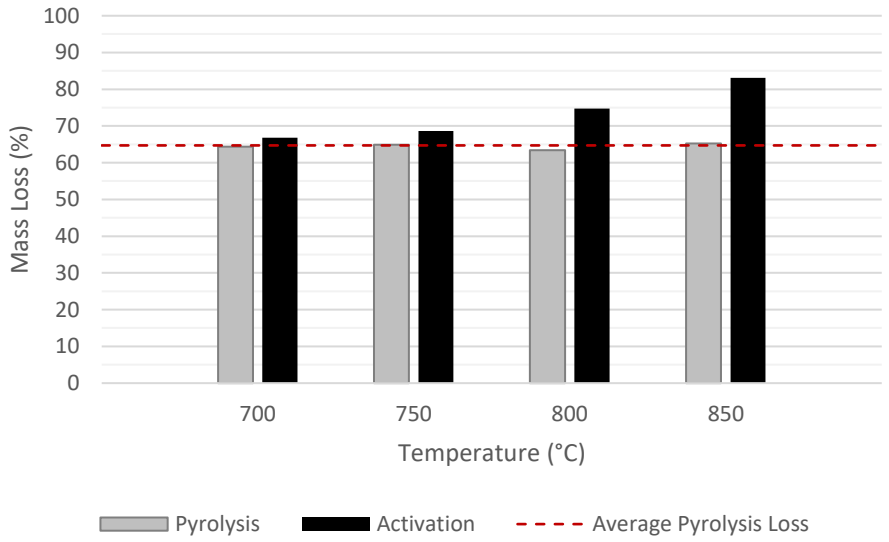

Figure 5.21 Comparison of mass loss encountered in the independent pyrolysis and the complete activation reaction of HTC coffee grounds, during 1-hour runs

Table 5.30 presents the proximate analysis of the activated hydrochars. It was noted previously that the CG-HTC sample may not be entirely accurate, but it is listed at the top for comparison purposes. Despite the samples representing the final product which has undergone a thermal degradation which has amounted to sample loss, all of the fixed carbon contents remain > 90 % of the sample mass. The fixed carbon bracket has been become the main fraction through the pyrolysis phase, and then the site of reaction for the activating agent in the activation phase. There is a slight drop from the ~ 95 % starting region, but in all cases, the mass is mainly removed from the fixed carbon. The emergence of fixed carbon as the main feature is through the large loss of volatiles, which can be seen by comparing the GC-HTC value in the left-hand column to any of the activated hydrochar values. In general, the volatile component is elevated slightly from that in the mid-way pyrolysis step. Although some volatile mass has been removed during the activation alone, it is minimal, amounting to < 0.01 g in most cases. So, the volatile weight % increases, due to the larger removal of fixed carbon. The ash also increases, but it is still a minimal part of the final product, and the smallest value in each test. The highest values correlate with the highest temperature tests and those which had the greatest loss, baring a few inconsistencies. This shows the ash is remaining in the sample is being concentrated. But due to the small starting fraction and sustainable losses recorded, it is not as prevalent in the final product.

Table 5.30 Dry basis proximate analysis of activated CG hydrochar

Sample Name	Volatiles	Fixed Carbon	Ash
	% Dry Basis		
CG-HTC	72.0	27.8	0.2
CG-HTC-ACT-700-0.5	6.5	92.9	0.6
CG-HTC-ACT-750-0.5	5.5	93.8	0.7
CG-HTC-ACT-800-0.5	3.7	95.5	0.7
CG-HTC-ACT-850-0.5	6.1	92.9	1.0
CG-HTC-ACT-900-0.5	5.6	93.0	1.4
CG-HTC-ACT-950-0.5	5.6	92.2	2.3
CG-HTC-ACT-700-1	8.0	91.4	0.6
CG-HTC-ACT-750-1	5.1	94.1	0.8
CG-HTC-ACT-800-1	7.4	91.4	1.3
CG-HTC-ACT-850-1	5.3	93.3	1.4
CG-HTC-ACT-700-2	8.0	91.4	0.7
CG-HTC-ACT-750-2	6.7	91.9	1.4
CG-HTC-ACT-800-2	6.4	91.1	2.5
CG-HTC-ACT-700-4	6.0	93.2	0.8
Standard Error (±)	0.4	0.7	0.2

Standard errors from Table 9.14

Figures 5.22 – 5.24 visually represent the proximate analysis. The figures have been manipulated as if each precursor started as exactly 5 g, for ease of comparability. The charts are separated by time intervals, denoted in the headings. The columns are ordered from left to right in order of increasing temperatures. The major component in all the samples is the remaining fixed carbon, which shows the activated hydrochar has a high carbon purity. From left to right, the increased mass loss can be seen in each chart. The fixed carbon region is particularly reduced, showing the activation is having an impact on this component the most. The volatile mass drops from left to right. The mass of ash is at the base of each sample column in black. The bar representing ash is difficult to see, as the quantity is so minor. However, the presence does remain at the foot of each sample. The samples in Figure 5.22 show the lowest final mass at the highest temperature tested. All the charts show a smooth drop in mass between intervals. From the Y axis it can be seen that a larger mass of sample was collected from in the lower duration tests.

The influence of time is best demonstrated in Figure 5.25. The results are presented in groupings of the activation temperature and separated in proportion to the time. The 750, 800 and 850 °C samples show the anticipated trend of final mass reducing as time is increased, with a smooth drop between samples. The 700 °C tests also show this, but the loss between 2 hours and 4 hours appears to plateau as opposed to dropping in the same manner. This could show that duration has a weak effect on the losses. Comparing all samples together shows the high fixed carbon content present in activated CG hydrochar as well as the consistency of components between activation conditions. Based on the trends seen, and the 4-hour sample showing a plateau, it is proposed that even longer durations than those initially tested would return acceptable yields.

Fig. 5.22 CG-HTC-ACT-'X'-0.5 Proximate Analysis

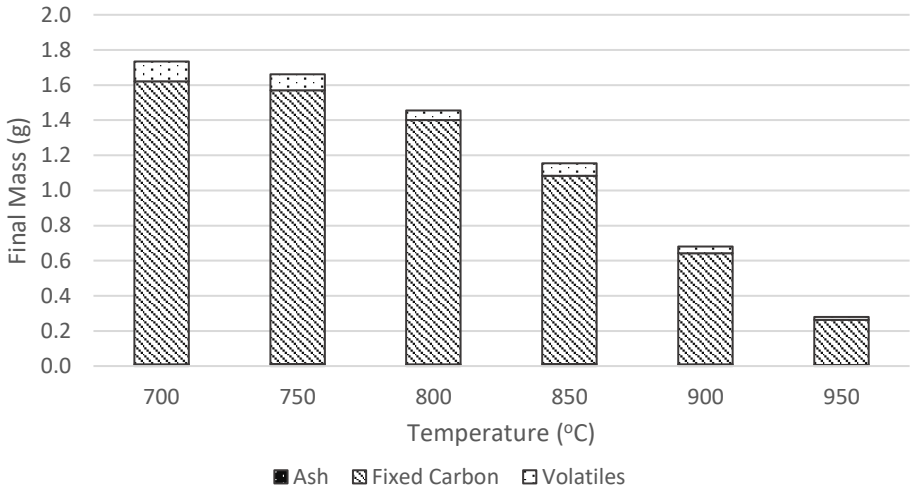

Fig 5.23 CG-HTC-ACT-'X'-1 Proximate Analysis

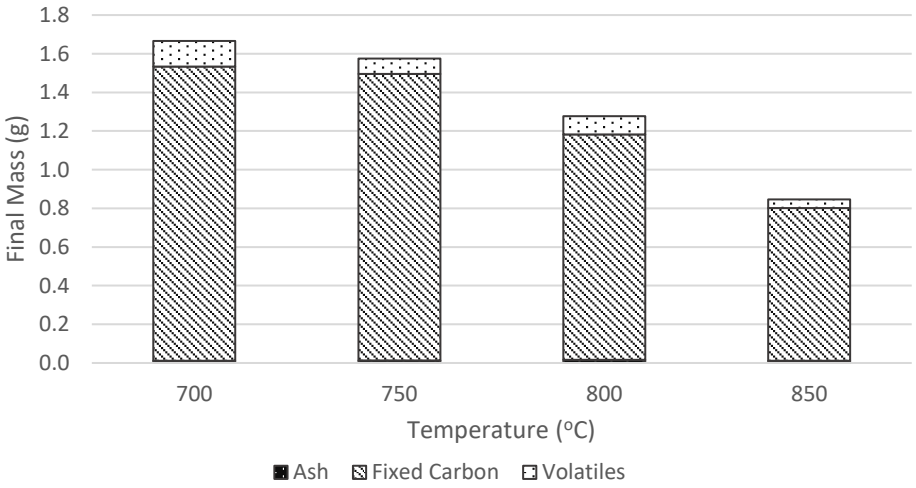

Fig 5.24 CG-HTC-ACT-'X'-2 Proximate Analysis

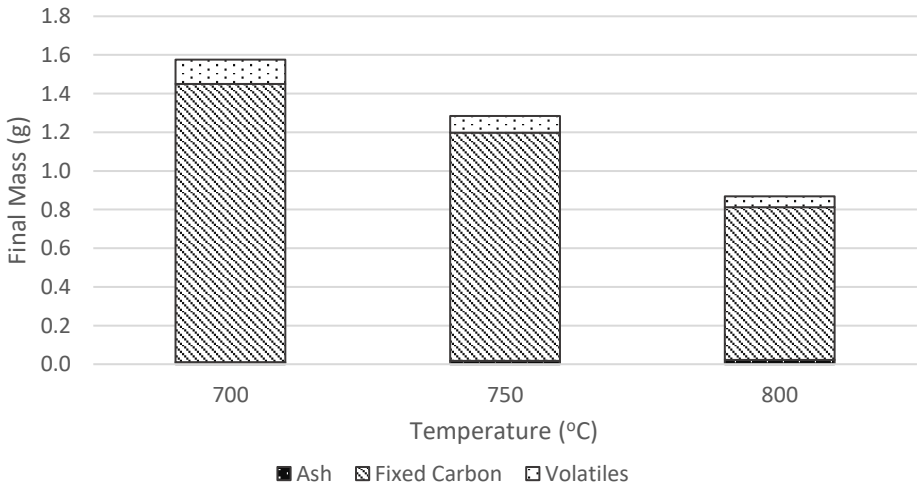

Figures 5.22 – 5.24 The mass of the major constituents in activated carbons derived from 5 g of coffee ground hydrochar and treated at incremental temperatures. The figures are separated by residence time

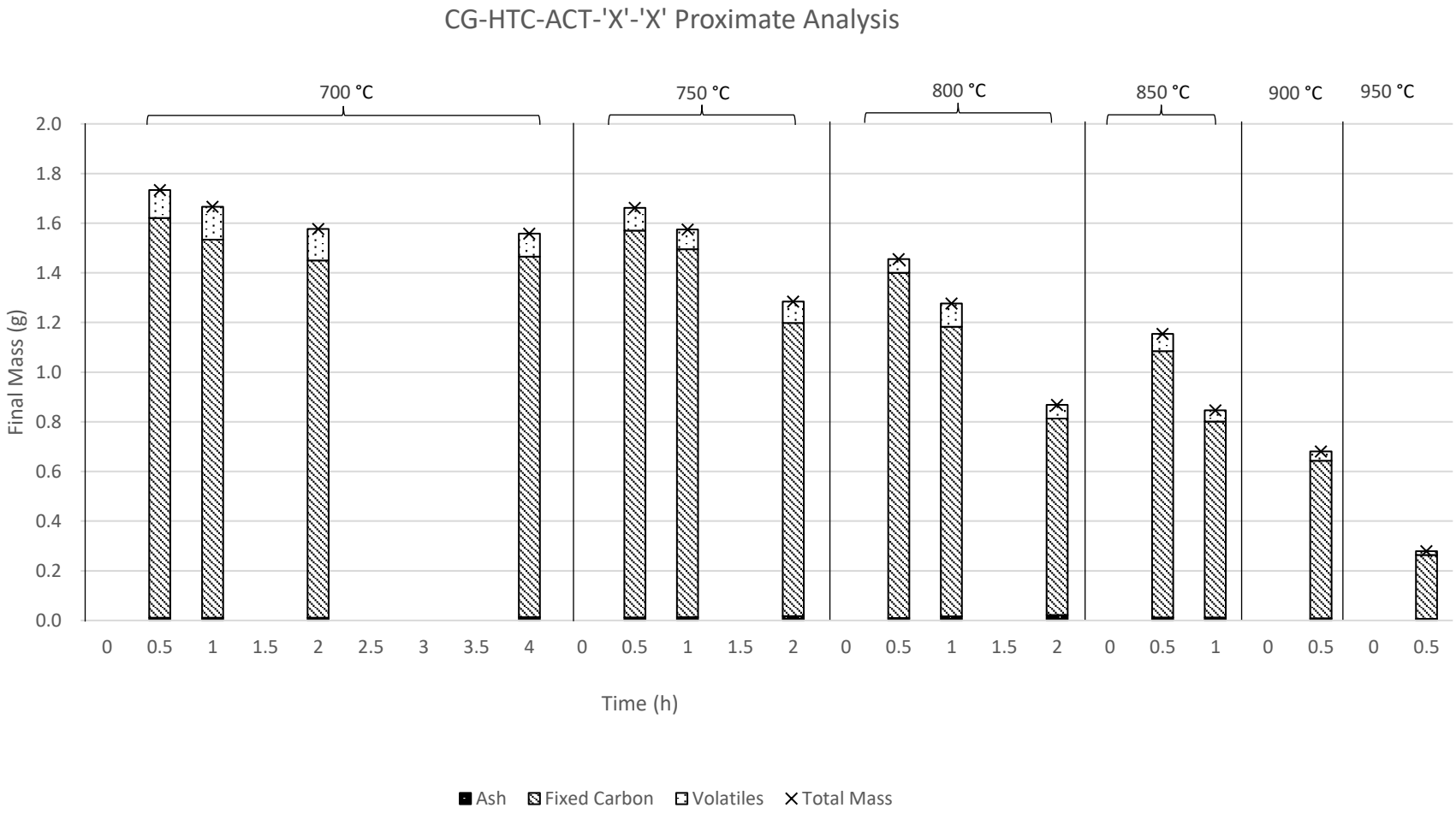

Figure 5.25 The mass of the major constituents in activated carbons derived from 5 g of coffee ground hydrochar based on residence time and spaced proportionally. The samples are grouped in terms of treatment temperature which can be seen across the top.

5.2.4 CG Chemical Composition

Ultimate analysis was used to establish the elemental composition of the samples. Table 5.31 introduces the sample constituents at the start of the experiment, mid-way through after the pyrolysis stage is complete and the final sample after activation. The carbon content increases through the pyrolysis, as expected and similar to the proximate analysis results in the previous section which recorded a 93.3 % fixed carbon content. The remaining carbon may be found in the volatile organic compounds. In the activation, the carbon content increases again, which is not to be expected, as this is intended to be the target of the activating agent and the site of the largest loss. In mass terms, the carbon drops by 0.55 g, 11 % of the starting sample mass. This shows the activation process impacting the carbon content. So, the increased carbon concentration results from the loss of other materials. Although the total mass loss of the other constituents during the activation step adds up to a tenth of the carbon losses, the mass losses are significant to the presence of both hydrogen and oxygen, which appear as trace amounts in the final product. Hydrogen is lost considerably during the pyrolysis step, in the volatile removal. The remaining presence is minor, around 8 mg. The remainder of the hydrogen is lost during the activation, potentially with further loss of volatiles. There is no evidence that hydrogen chemisorbs to the surface, as it is introduced in the steam. A similar unexpected outcome takes place in the oxygen contingent. The oxygen content drops heavily during the pyrolysis. But it is not all removed, which is questionable, as oxygen under the conditions would be expected to react and the quantity to be depleted. Based on this result, there is oxygen present as the activation begins. However, with the introduction of steam, it was expected that the oxygen would chemisorb, and the quantity would increase. This is not the case, however, the total oxygen in the final sample is nil. From this it is obvious that the H/C and O/C ratios have been calculated as 0.0 in both cases.

Nitrogen experiences losses in the pyrolysis phase, removing approximately half of the mass and the weight fraction increases. Similar levels of losses are experienced during the activation, again losing just over half of the mass. Even with the removal of hydrogen and oxygen, the fraction decreases. The ash fraction increases throughout as expected. But with regard to the mass remaining, there are some losses. These are difficult to explain as the pellets remained in shape throughout the activation. Perhaps they were fine enough to be elutriated from the system or remained in the ceramic boat. Despite this, the content and losses are negligible.

Table 5.31 Ultimate analysis of activated hydrochar derived from CG during three key points of the activation reaction

Sample	Carbon	Hydrogen	Nitrogen	Oxygen	Ash	H/C	O/C
	Wt.%	Wt.%	Wt.%	Wt.% by difference	Wt.%	Atomic Ratio	Atomic Ratio
CG-HTC	70.6	6.8	2.9	19.5	0.2	1.15	0.21
CG-HTC-PYR-850-1	94.4	0.5	4.3	0.2	0.6	0.06	0.00
CG-HTC-ACT-850-1	95.86	0.0	2.7	0.0	0.7	0.00	0.00

Overall, it seems that each component tested is continually impacted by losses in each step. This is a success for the activated hydrochar due to the impact on the carbon fraction. The carbon experiences losses, which is hoped to improve porosity of the char, but the other losses experienced by other elements allow the active hydrochar to remain 96 % pure with carbon, despite the removal of carbon. The lack of surface reactivity with heteroatoms is a curious development. Table 5.32 is available below for the full list of ultimate analysis results. The precursor material CG-HTC is at the top of the chart for comparison. All products contain a high carbon content, > 90 %, which has improved from the initial sample. The 1-hour samples are the only group which produces a consistent trend. In these results, as the temperature is increased, the carbon content increases. The 0.5-hour samples fluctuate between 92 – 96 % with no true trend. It appears at the 950 °C sample, more degradation has been felt as the carbon content drops off slightly, there is a presence of all other elements, which is not the case for the previous tests 800, 850 & 900 °C. Additionally, the ash content has shown the biggest presence of any CG sample. This matches with the loss data as it is the sample with the lowest yield returned, at 5.6 %. The high temperature may be too aggressive for the sample, even in the short duration. The 2-hour samples all return a similar carbon content.

The oxygen and hydrogen profiles offer an interesting behaviour. Both are introduced to the experiment in excess through the steam activating agent. Yet the amount remaining drops considerably in each condition tested. Both materials are only present in low temperature samples. The shorter duration also boasts a greater quantity. As CG-HTC-ACT-800-0.5 does contain hydrogen, however longer timeframes at that temperature do not, and CG-HTC-ACT-750-1 contains hydrogen, yet the longer timeframe does not. The hydrogen and oxygen present in the samples could be because of the activating agent, which has bonded to the char during the activation. It is more likely, however, that it is residual material from the starting material which has not yet been removed, due to being treated at the less extreme conditions. The ash trend is consistent. As the temperature increases, the ash content also increases. This too is seen across the timeframes, as the time is increased the ash content increases. The fraction has jumped from the initial CG-HTC sample, but the results remain small, with most samples containing < 1 %. As reported in Section 5.2.1, the raw material contained 1.6 % ash, so through the HTC pre-treatment and activation, only two samples have surpassed the starting material ash content. Nitrogen shows continual losses. Despite an initial peak, owing to the losses of neighbouring elements, the nitrogen succumbs to greater losses as the temperature is increased. More nitrogen is lost at longer timeframes also.

Combining data may lead to issues in elements only present in trace amounts. The accuracy is potentially not there to trace heteroatoms on the surface. Many samples may have the hydrogen and oxygen present but overlooked in the analysis. Many samples which were recorded could be consumed by the standard error. Hydrogen was detected in all samples in the unprocessed, wet basis result. The dry basis calculation accounted for all of the hydrogen in some samples. In others the hydrogen was in a deficit and produced an impossible negative figure. A similar issue was faced with the oxygen. The weight by difference often left the figure in a negative space. H/C and O/C ratios have been set to 0.0 where trace amounts, we're present outside of the significant figures. But blank entries are for those samples that did not return any hydrogen/oxygen traces or were calculated as a negative figure.

The results from X-ray photoelectron spectroscopy, shown in Appendix Table 9.21, find oxygen present on samples such as CG-HTC-ACT-850-1, which highlights the frailties of calculating the oxygen content by weight difference. It also puts into perspective that a lot of the samples with no oxygen observed in Table 5.32 may have an oxygen fraction. This would highlight that activated CG hydrochars also engage in chemisorption with oxygen. Additionally, it shows the presence of phosphorus in the sample. The only trace metal in the ash is magnesium.

Table 5.32 Ultimate analysis of activated CG hydrochar

Sample	Carbon	Hydrogen	Nitrogen	Oxygen	Ash	H/C	O/C
	Wt.%	Wt.%	Wt.%	Wt.% BD	Wt.%	Atomic Ratio	Atomic Ratio
CG-HTC	70.6	6.8	2.9	19.5	0.2	1.15	0.21
CG-HTC-ACT-700-0.5	93.4	1.7	4.2	0.1	0.6	0.22	0.00
CG-HTC-ACT-750-0.5	92.8	1.1	4.0	1.4	0.7	0.15	0.01
CG-HTC-ACT-800-0.5	94.9	0.6	3.8	0.0	0.7	0.08	-
CG-HTC-ACT-850-0.5	96.8	0.0	2.2	0.0	1.0	-	-
CG-HTC-ACT-900-0.5	96.3	0.0	2.3	0.0	1.4	0.01	-
CG-HTC-ACT-950-0.5	93.5	0.6	1.8	1.8	2.3	0.08	0.02
CG-HTC-ACT-700-1	93.5	1.0	4.2	0.7	0.6	0.13	0.01
CG-HTC-ACT-750-1	94.3	0.9	4.0	0.0	0.8	0.12	-
CG-HTC-ACT-800-1	95.2	0.0	3.5	0.0	1.3	-	-
CG-HTC-ACT-850-1	95.9	0.0	2.7	0.0	1.4	-	-
CG-HTC-ACT-700-2	94.6	0.7	4.0	0.0	0.7	0.09	-
CG-HTC-ACT-750-2	95.2	0.0	3.4	0.0	1.4	-	-
CG-HTC-ACT-800-2	94.6	0.0	2.9	0.0	2.5	-	-
Standard Error (±)	2.02	0.12	0.07	2.18	0.40	0.01	0.03

Ash content from proximate analysis, moisture content from proximate analysis used for dry hydrogen weight, oxygen calculated by difference (BD). Standard errors from Table 9.15

5.2.5 CG Textural Properties

This part will deliver the adsorption test results and provide an assessment on the products textural properties. The characterization was achieved through N_2 adsorption, and the values were calculated using the BET method, described in Section 4.4.1. The complete set of results can be viewed in Table 5.33. In all CG tests, the samples have increased in specific surface area from the precursor sample. The growth can be used as justification of the losses, as the activation has been successful, and it has resulted in a greater surface area and a more porous material. The highest recorded figure was 1675 m^2/g, during the in highest temperature run, using sample CG-HTC-ACT-950-0.5. This was the sample noted before as having the lowest sample yield. But as further proof, an additional 5 samples returned values above 1000 m^2/g, which are all comparable to commercial activated carbons. These were all achieved under more intensive activation conditions. Based on the results, the surface area per unit mass available increases as temperature is increased. This trend can be seen in Figure 5.26, which denotes how the activation conditions impacted the surface area.

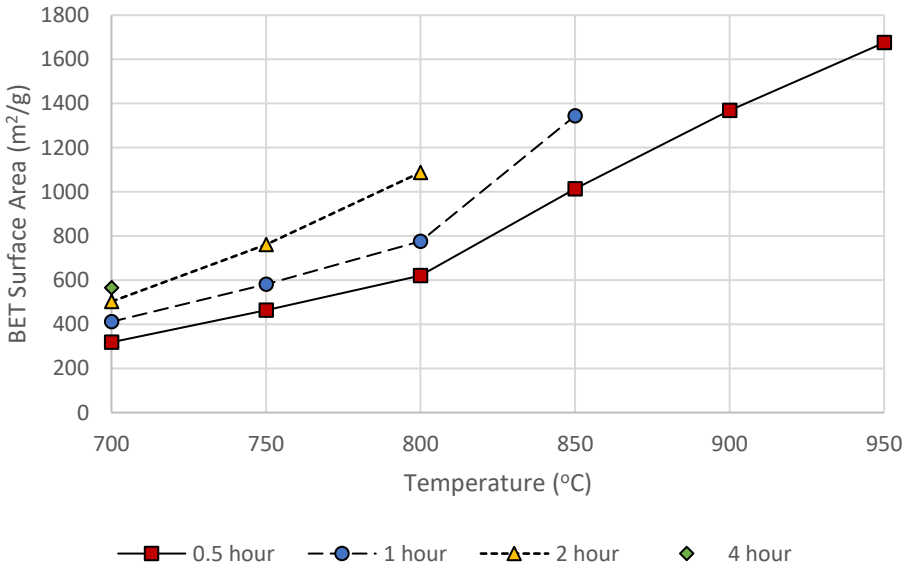

Figure 5.26 Activated coffee ground hydrochar surface area produced from the activation conditions

The upward curve between 700 – 850 °C shows the surface area growth is larger in each elevated temperature interval. This is present for all timeframes. In the region between 800 and 850 °C, there is a kink in the trend and the incline increases. This can be read as a greater increase in surface area between these experiments. In the 0.5-hour samples, this development is the largest incremental increase, all the following temperatures growth is not as high and begins to drop away. It is as if the activating agent is more effective at creating pores at temperatures above 800 °C. An increase in surface area is also witnessed as the experimental duration is increased. Longer timeframes, combined with the higher temperatures, increase the difference between the highest and lowest result at a given temperature. The range in surface areas between the 0.5-hour and 2-hour samples is 184 m^2/g at 700 °C but 468 m^2/g at 800 °C, showing an important balance of both parameters are needed to maximise the potential surface area. Based on this graph alone, it appears if samples of 1-hour and above were tested at higher temperatures, the surface areas would surpass that of CG-HTC-ACT-950-0.5. The high surface area is linked to the microporosity

demonstrated by all products. Table 5.33 shows that every sample has an average pore diameter < 2 nm, the threshold between micropores and mesopores. The substantial formation of micropores capitalises on the material available and produces surface areas superior to larger pore sizes.

Figure 5.27 displays the total pore volume measured in samples, and how that was affected by the activation conditions. The graph presents a similar image to the surface area graph. But the trend lines each show a smoother curve in Figure 5.27, with a consistent upward trajectory between temperature intervals. There is still an increased pore volume growth between 800 and 850 °C. Using the 0.5-hour figures, the growth is three times more than between the 750 – 800 °C samples. However, the subsequent pore volume growth is greater at 900 and 950 °C. This is likely as the pores grow larger at higher temperatures and amount to a higher total pore volume. So, increasing the experimental temperature results in an increased total pore volume. Likewise, the increased time amounts to an increased total pore volume. The highest pore volume is found in CG-HTC-ACT-950-0.5, at 0.77 cm3/g. This value is correlated with the greatest sample losses. This total pore volume result, combined with the high surface area result, could be exaggerated. The conditions would not be selected again for future use because the yield produced is too low, when compared to the other conditions. Despite the measurement units in m2/g and cm3/g, this flatters the sample as there was not close to a gram remaining. The minor sample mass remaining may have been highly porous, but being logical, the yield has to be considered.

The 2 and 4-hour results at 700 °C are close. Although they still obey the trend, the impact of the longer duration at the lower temperature seems to cause less pore growth. Like the surface area analysis before, the combination of longer timeframes and higher temperatures cause the gap between results to widen more.

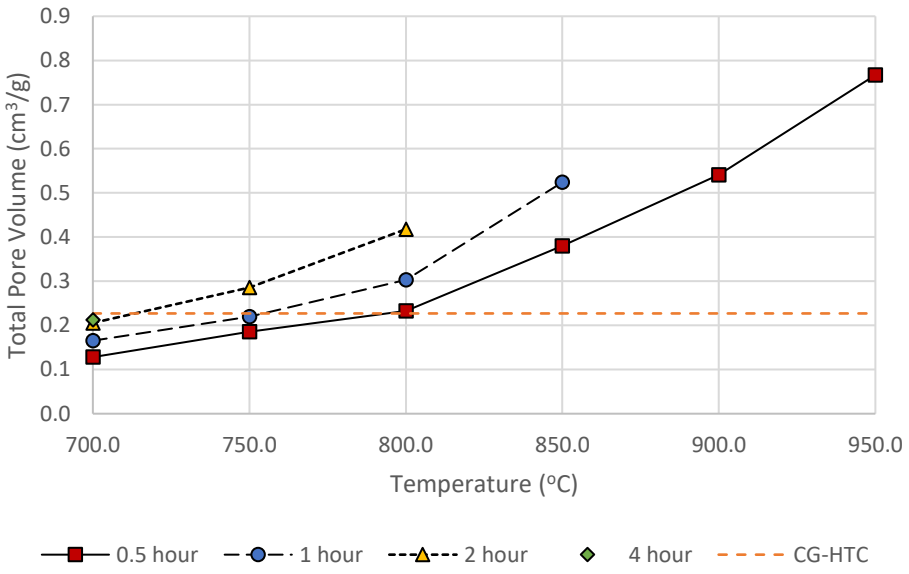

Figure 5.27 Activated coffee ground hydrochar pore volume produced from the activation conditions

It cannot be stated that all reaction conditions lead to a greater total pore volume. The pore volume of the starting sample is represented in the chart as a dashed line. Many of less aggressive conditions drop from the starting value. CG-HTC begins the process as a mesoporous carbon with the presence of a large mesopore volume. As mesopores are larger than micropores, a greater volume is occupied. The mesopore volume here accounts

for the majority of the total volume in the precursor sample. Potentially the way the powder has been pelletized has impacted this region. The products, by contrast, are more microporous. The micropores maximise the surface area which has more restraint on the total pore volume, as the pores are smaller.

Returning to Table 5.33, the microporosity can be seen the micropore volume and microporosity columns. All samples report a higher microporous volume compared to the start. CG-HTC begins with little trace of micropores. Instead, it has a substantial mesoporous volume, and it would be considered a mesoporous material. The major growth of new micropores reverses this characteristic and all products become highly microporous carbons, displayed against the mesoporosity on the right in terms of percentage. Most samples present a microporous contingent of ~ 90 %. The only exception would be CG-HTC-ACT-950-0.5. Under these intense conditions some micropores have transitioned into mesopores. This does not impact the surface area or pore volume as there is still additional growth in the micropore volume. There is no loss from the mesopores as collectively the micropore and mesopore portion accounts for 98 % of the total pore volume. This is a tricky sample to judge based on the losses experienced and may not be wholly reliable.

The micropore volume grows as the temperature increases and as time increases, independently. The mesopore volume is less straight forward. The mesopore volume in the lowest temperature samples is usually around 0.015 m^3/ g. This value drops further when it is treated at the next interval, to as low as 0.010 m^3/ g. Beyond this, at even higher temperatures, the mesopore volume starts to increase, but it never returns to the level of the precursor. An explanation into this trend is that the mesopore volume seen in lower temperature samples may well be present from the initial starting material. As the structure changes through the activation process, the mesopore volume reduces. When the activation conditions are great enough to cause micropores to grow into new mesopores, the mesopore volume begins to increase again.

It can be seen in Table 5.34, which presents the textural data of the pyrolysis samples, that the mesopore volume is reduced during the pyrolysis experiments. All of these conditions show values below 0.015 m^3/ g, the average mesopore volume for the 700 °C samples. As all of the pyrolysis experiments return a similar starting product for activation and all precede the activation data, the theory of the mesopore volume remaining from CG-HTC would be dispelled. The mesopore volume is only around 5 % of the total in these highly microporous materials, and the formation of mesopores in this material not of high concern.

The pyrolysis results generally show a drop in surface area from CG-HTC. Across the results longer durations and higher temperature correlate to further reducing the surface area. The drop in surface area correlates with an insignificant increase in the microporous volume, and a major drop from the starting mesoporous volume. This culminates in a small total pore volume. The lack of microporous growth means the samples remain majority mesoporous, but not as concentrated as the initial sample. The average pore diameter agrees with this, placing the average size within the mesopore category. Most of the results are so minor, it can be said that the pyrolysis has had a negligible effect on the surface area and pore volume. The exception is the 900 °C sample. Temperature was a major factor of surface area growth in the activation samples, so perhaps this maximises the potential surface area for the pyrolysis samples as well. The surface area doubles from the starting sample, and this increase relates to a growth in the sample micropore volume. The

average pore diameter is just within the range for micropores, and the microporosity proportionally higher in the material. It is interesting that a fast run at a high temperature can induce some porosity into the sample. Despite the growth and the high carbon content, it is not a useful activated carbon and there is a magnitude of difference when compared with the samples activated with steam, as shown in Figure 5.28. The pyrolysis samples are clustered in the bottom left corner, displaying little porosity. CG-HTC begins above the pore volume threshold for a commercial grade AC but is lacking severely in surface area. The activated samples display a straight trend of surface area and total pore volume increasing together and a reasonably consistent ratio. The triangles above the trend represent the more mesoporous materials, such as those activated at 700 °C and samples which have succumbed to greater losses. The CG samples as a sample group produced a high yield, which was hailed as a positive, but this has come at the expense of pore development. Only five samples qualify as commercial grade ACs. Each of them is labelled in the chart, it is noticed that these all came in the highest temperatures tested in each timeframe. It is thought that permitting more loss, by using more extreme conditions would produce greater results. The porosity growth in CG seems to respond slower to the activation or requires temperatures of 800 °C and above, where a sharp increase in the pore development was noticed.

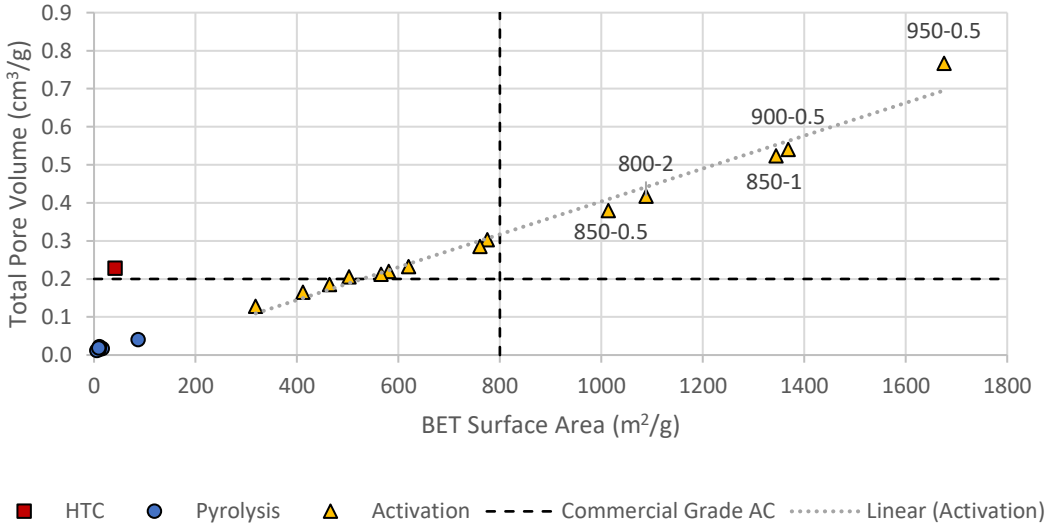

Figure 5.28 Comparison chart of all coffee ground samples textual properties, separated by stages of the process

Table 5.33 Surface area, pore volume and pore size distribution of activated CG hydrochar

Sample	BET Surface Area	Microporous Volume	Mesoporous Volume	Total Volume	Average Pore Diameter	Microporosity	Mesoporosity
	m^2/g	cm^3/g	cm^3/g	cm^3/g	nm	%	%
CG-HTC	42	0.000	0.214	0.227	21.81	0	94
CG-HTC-ACT-700-0.5	319	0.110	0.015	0.128	1.61	86	11
CG-HTC-ACT-750-0.5	464	0.165	0.015	0.186	1.60	89	8
CG-HTC-ACT-800-0.5	620	0.218	0.012	0.233	1.50	94	5
CG-HTC-ACT-850-0.5	1014	0.358	0.016	0.380	1.50	94	4
CG-HTC-ACT-900-0.5	1369	0.495	0.037	0.541	1.58	91	7
CG-HTC-ACT-950-0.5	1675	0.600	0.155	0.767	1.83	78	20
CG-HTC-ACT-700-1	412	0.148	0.014	0.165	1.61	90	8
CG-HTC-ACT-750-1	581	0.203	0.010	0.220	1.52	92	5
CG-HTC-ACT-800-1	775	0.279	0.015	0.303	1.56	92	5
CG-HTC-ACT-850-1	1344	0.490	0.027	0.524	1.56	94	5
CG-HTC-ACT-700-2	503	0.183	0.016	0.206	1.64	89	8
CG-HTC-ACT-750-2	760	0.266	0.011	0.286	1.50	93	4
CG-HTC-ACT-800-2	1088	0.389	0.021	0.418	1.54	93	5

CG-HTC-ACT-750-4	565	0.199	0.010	0.212	1.50	94	5
Standard Error (±)	54	0.020	0.014	0.034	0.03	1.36	1.37

Standard errors from Table 9.16 (Appendix)

Table 5.34 Surface area, pore volume and pore size distribution of pyrolyzed CG hydrochar

Sample	**BET Surface Area**	**Microporous Volume**	**Mesoporous Volume**	**Total Volume**	**Average Pore Diameter**	**Microporosity**	**Mesoporosity**
	m^2/g	cm^3/g	cm^3/g	cm^3/g	nm	%	%
CG-HTC	42	0.000	0.214	0.227	21.81	0	94
CG-HTC-PYR-900-0.5	87	0.024	0.013	0.041	1.89	59	32
CG-HTC-PYR-700-1	16	0.005	0.010	0.017	4.32	28	59
CG-HTC-PYR-750-1	10	0.003	0.009	0.014	5.89	20	61
CG-HTC-PYR-800-1	11	0.003	0.012	0.022	8.32	15	56
CG-HTC-PYR-850-1	5	0.001	0.008	0.012	9.03	13	66
CG-HTC-PYR-800-2	9	0.003	0.011	0.019	8.16	15	56

5.2.6 CG Raw Activation Tests

The raw activation tests were carried out on the sample material defined CG-RAW. This is the dried spent coffee grounds that were used as the precursor for HTC in the batch reactions to form the hydrochar, defined as CG-HTC. The tests were conducted as a control for the activated hydrochar samples to understand the impact of HTC pre-treatment. The raw sample was dried, pelletized, and activated in an identical manner to the active hydrochar samples. However, the experimental procedure did not run to plan. The material seemed extremely sensitive to the activation conditions on the initial runs. The experiments would routinely deliver zero product. Unusually there was no trace of ash remaining in the reaction crucible after the experiment, which served as evidence that the cause of loss was different. After multiple failed experiments through the apparatus bursting, it seemed the material was being elutriated by the carrier gas. The powder would build up in the outlet tube, eventually leading to a blockage. This would cause a pressure spike, which would burst the outlet bung. The remaining sample was exposed to air and would combust immediately.

CG-RAW was pelletized in the same manner, under the same pressure, but it was not compacting and binding as CG-HTC was. CG-HTC pellets were visibly shiny and had a smooth texture. They were solid and had strength to withstand being squeezed. CG-RAW pellets were brittle and dusty. They would crumble under the introduction of force. The powder appeared to have trouble forming and maintaining the pellet shape. This may have led to the pellets crumbling in the reaction and the powder would be fine enough to be carried with the N_2 gas. In an attempt to curtail losses experienced with the raw material samples, a series of trials were developed as a solution which introduced a binder. Molasses and starch were selected and tested as independent organic binders. The molasses was a viscous liquid, and the starch was in powdered form. The materials were purchased from Sigma Aldrich. The hypothesis was they would maintain the pellet shape without hindering the pore development, and this would reduce the loss encountered in the CG-RAW experiments. The binders were tested first on CG-HTC samples to understand the impact the binder had on the final structure. The conditions for CG-HTC-ACT-750-1 were selected for these tests. Binders were introduced during the sample preparation. The binders were mixed with the powdered CG and pelletized in the same way as the hydrochar activation tests. An approximate total of 50 g of each variation was mixed and then pelletized. The powdered starch was mixed with water to create a 10 % concentration solution (Hong et al., 2018), (Jezowski & Kowalczewski, 2019). Only the mass of material and starch was taken into account when measuring the concentration introduced to the hydrochar. The molasses was already in a liquid phase, mixed with 10 % phosphoric acid to assist with curing, which was believed to occur at 300 °C. This was mixed at 10 wt% with CG-HTC. The materials were tested at 750 °C for 1 hour in 5 g batches. The textural properties of the samples are shown below in Table 5.35. The column values are relatively close. The original sample remained highest for surface area and total volume. The molasses sample is similar to the original and is within the error range of the original sample. Molasses is seen not to impede the pore development. The starch sample has the poorest results. The values deviate the furthest from the original, outside of the error range. The 10 wt% occupied by the binder could have impacted the sample results, as it was only 90 wt% CG-HTC subjected to the same external factors. Based on the ease of production and the negligible effect on the pore development, the molasses was used as a binder for CG-RAW.

Table 5.35 Textural analysis of activated CG hydrochar with binders

Sample	BET Surface Area	Total Volume	Average Pore Diameter
	m^2/g	cm^3/g	nm
CG-HTC-ACT-750-1	581	0.220	1.52
CG-HTC-ACT-750-1-M	556	0.208	1.51
CG-HTC-ACT-750-1-S	492	0.198	1.54
Standard Error (±)	54	0.034	0.03

CG-HTC-ACT-750-1 represents the original, CG-HTC-ACT-750-1-M represents 10 wt% molasses and CG-HTC-ACT-750-1-S represents 10 wt% starch. Standard errors from Table 9.16 (Appendix).

A range of ratios of molasses to CG-RAW were tested to understand the minimum required concentration. The dataset has been omitted; the tests showed that 2 & 5 wt% molasses resulted in failure due to catastrophic losses. 10, 15 & 20 % returned similar yields and produced a useable, more robust pellet that without the molasses. So, 10 % molasses was used as the standard concentration in the raw activation tests. In addition to the binder, the experiments had some other minor changes to facilitate the results. The N_2 gas flowrate was reduced from 1 l/min to 0.5 l/min. This was the minimum flowrate which could be consistently held by the apparatus. The sample size also increased from 5 g to 10 g to increase the product mass available for further tests. The testing matrix was also capped on duration and temperature basis due to the susceptibility of CG-RAW to the conditions.

Despite the specialist measures, the continuous narrative of unsustainable losses is the takeaway from this section. The yield of the raw samples has been displayed in Table 5.36, side by side with the yield from the HTC pre-treated sample, activated for the same time and temperature. The raw activation yield is significantly lower under each tested condition. CG-RAW has suffered greater losses and can be said to be more sensitive to the activation conditions than CG-HTC. The HTC pre-treatment has improved the yield achieved during activation. Only the lowest temperature and timeframe has returned a sample over the 15 % yield expectation of an activated carbon. It was found in Section 3.1.6.2 that this condition is least conducive to forming porosity. It has been found that temperature is the most impactful parameter on loss in the activated hydrochar samples. Although the material has higher losses at high temperatures, it is particularly impacted by time. Not a single 2-hour sample returned any yield. Perhaps the binder effect of molasses wore out as it was degraded itself. And in a longer duration there was more opportunity the CG to be removed by the carrier gas.

Table 5.36 Yield comparison between raw CG and hydrochar CG activation

Sample Name	Raw Activation Yield	Activated Hydrochar Yield
	%	%
CG-RAW-ACT-700-0.5	18.9	34.4
CG-RAW-ACT-750-0.5	2.7	33.1
CG-RAW-ACT-800-0.5	12.8	29.0
CG-RAW-ACT-850-0.5	11.2	22.8
CG-RAW-ACT-900-0.5	4.2	13.6
CG-RAW-ACT-700-1	12.1	33.2
CG-RAW-ACT-750-1	1.1	31.4
CG-RAW-ACT-800-1	3.4	25.2
Standard Error (±)	1.7	1.7

Standard errors from Table 9.13 (Appendix).

It is worth noting that all samples are expected to contain a high ash content. Unacceptable levels of ash will be in the samples with the lowest yields. The sample ash is 1.6 % of the starting mass and is not removed in the experiment. So, the single figure results are expected to be majority or all ash. The higher value yields also have a larger presence of ash compared to the activated hydrochar counterparts, which would impact an AC performance. CG-HTC started the activation process with a lower ash content due to ash losses in the HTC process, demonstrated in Table 5.37. In addition, the HTC samples can sustain treatment at higher temperature and time intervals, which produced the highest textural results.

The raw activation yield has no associated calculable error. The trials developed an irregular pattern of whether mass remained at the end or not, so consistent repeats could not be undertaken. This is particularly notable in CG-RAW-ACT-750-0.5, which would be anticipated to have a higher yield to fit between 12.8 – 18.9 % and create the loss trend experienced in all other experimental runs. Despite no other apparent change of conditions and the introduction of a binder, this was the highest yield recorded. Therefore, the raw activation sample error is high and inconsistent due to the unreproducible nature of the experiment. For that reason, it can be concluded that spent coffee grounds cannot be effectively activated without the introduction of a pre-treatment phase.

The material produced from the raw activation samples is still of interest. CG-RAW-ACT-850-0.5 has been selected as it has one of the closest yields to the activation sample both by difference and proportionally. Additionally, the conditions performed well during the hydrochar activation experiments. Higher surface areas were attributed to high temperatures, this is the highest temperature with a useable sample, and the duration is

the lowest, due to the assessed impact of that on the raw CG. In Table 5.37, the proximate analysis of the raw sample is grouped with that of the raw precursor, the activated hydrochar produced under the same conditions and its HTC precursor. Through the activation, the volatile content of the raw sample shows a huge reduction. However, the volatiles are twice as concentrated in the raw activation sample, despite the thermal conditions during the ramp up, which were found to reduce the volatile fraction to ~ 6 % during pyrolysis testing. The volatile fraction is lower in the HTC contingents because it was reduced by the HTC process. The higher volatile content appears to be carried through into the raw AC. The concentrated volatiles are unlikely to be due to the higher loss, because the volatile content remained stable in the hydrochar activation samples, no matter the yield. The fixed carbon has increased four times of that in the raw sample through the activation. The heat up phase is the first carbonization treatment the sample is subjected to, causing a large proportional increase. The HTC sample only increases three times from the hydrochar sample. However, this is the second carbonization treatment this material has received. So, the overall fixed carbon is still bigger in the activated hydrochar. Due to the ash reduction through HTC and the higher yield during the activation, CG-HTC-ACT-850-0.5 has a substantially smaller ash content than the raw counterpart. The ash content is lower than the original raw sample. A low ash content is more fitting for a commercially viable activated carbon.

Table 5.37 Dry basis proximate analysis comparison of CG raw and HTC activation pathways

Sample Name	Volatiles	Fixed Carbon	Ash
	%	%	%
CG-RAW	80.8	17.7	1.6
CG-RAW-ACT-850-0.5	14.0	72.0	14.0
CG-HTC	72.0	27.8	0.2
CG-HTC-ACT-850-0.5	6.1	92.9	1.0

In Table 5.38, the ultimate analysis gives a breakdown of the elemental components. The higher volatiles content in CG-RAW-ACT-850-0.5 is represented by the presence of hydrogen. This is reflected again in the H/C ratio greater than zero. The oxygen is completely depleted in both samples. This would be caused during the pyrolysis phase and does not recover in the activation phase. This suggests oxygen from the activating agent does not react with the char to form surface complexes. Finally, the carbon content is the highest fraction in both materials, which correlates with the fixed carbon in the previous table. The activated hydrochar remains higher and a purer AC, due to the differing ash fractions.

Table 5.38 Dry basis ultimate analysis comparison CG raw and HTC activation pathways

Sample	Carbon	Hydrogen	Nitrogen	Oxygen	Ash	H/C	O/C
	Wt.%	Wt.%	Wt.%	Wt.% by difference	Wt.%	Atomic Ratio	Atomic Ratio
CG-RAW-ACT-850-0.5	83.7	0.3	2.1	0	14.0	0.04	0.0
CG-HTC-ACT-850-0.5	96.8	0	2.2	0	1.0	0.0	0.0

5.2.7 HTC Pre-Treatment Temperature Alteration

An additional sample has been produced for the detailed characterization section: CG-HTC-ACT-850-0.5 R200. The 200 °C HTC conditions used to create SP hydrochar is under question, so a CG sample has been produced using the HTC batch reactor, keeping all other constraints the same, but reducing the temperature from 220 °C to 200 °C. The sample characterization for CG-HTC-ACT-850-0.5 R200 is laid out below, in Tables 5.39 – 5.42, with comparison to the original sample, CG-HTC-ACT-850-0.5.

Table 5.39 Yield comparison

Sample Name	Activated Hydrochar Yield	Carbon Yield
	%	%
CG-HTC-ACT-850-0.5	23.7	79.4
CG-HTC-ACT-850-0.5-R200	14.9	47.6

Table 5.40 Dry basis proximate analysis comparison

Sample Name	Volatiles	Fixed Carbon	Ash
	%	%	%
CG-HTC-ACT-850-0.5	6.0	93.1	0.9
CG-HTC-ACT-850-0.5-R200	7.1	89.1	3.8

It can be seen that the lower pre-treatment temperature has created a weaker AC candidate. The mass loss is greater, and the carbon retention is lower across the activation, Table 5.39. The greater loss shows that the material is more affected by the activation conditions. In terms of the constituents, the volatile content is increased, fixed carbon is reduced, and ash content is increased, which are all negative traits, Table 5.40. This is also reflected in the ultimate analysis, Table 5.41, where the carbon fraction drops. They are equally non receptive to hydrogen chemisorption. However, the lower temperature pre-treatment sample has a higher oxygen content, meaning chemisorption has occurred during this activation, unlike the original. Table 5.42 demonstrates the biggest factor separating the materials structurally. The greater loss has improved the surface area and pore volume in the material. The micropore volume is slightly larger, but the biggest change is in the form of mesopores. The mesoporosity of the original sample was 4 % but the new sample has increased to 26 %. This has greatly influenced the total pore volume.

Table 5.41 Ultimate analysis comparison

Sample	Carbon	Hydrogen	Nitrogen	Oxygen	Ash	H/C	O/C
	Wt.%	Wt.%	Wt.%	Wt.% BD	Wt.%	Atomic Ratio	Atomic Ratio
CG-HTC-ACT-850-0.5	96.8	0.0	2.2	0.0	1.0	0.0	0.0
CG-HTC-ACT-850-0.5-R200	80.5	0.0	1.6	14.4	3.5	0	0.13

Table 5.42 N_2 adsorption comparison

Sample	BET SA	V micro	V meso	V tot	PD	Microporosity	Mesoporosity
	m^2/g	cm^3/g	cm^3/g	cm^3/g	nm	%	%
CG-HTC-ACT-850-0.5	981	0.342	0.015	0.363	1.48	94	4
CG-HTC-ACT-850-0.5-R200	1174	0.402	0.143	0.549	1.87	73	26

The lack of a complete HTC pre-treatment creates a sample which is less resistant to the activation conditions. This causes greater losses, which in this case, has improved the surface area and pore volume, but decreased the overall yield. The final sample also contains more impurities, with a higher volatile and ash content. However, there does appear to be an increase in the chemisorbed oxygen.

5.2.8 CG Key Sample Detailed Characterization

Six coffee ground samples were selected for additional testing due to interesting characteristics and comparability.

- CG-RAW was chosen because this is the initial material which all samples are derived from and can be compared against.
- CG-HTC was chosen because it is the hydrochar precursor, and the precursor for all activated hydrochars produced. The sample will explore the pre-treatment pathway.
- CG-HTC-ACT-850-1 was selected as it produced one of the highest surface areas found for CG while simultaneously keeping a yield greater than the 15 % yield target. There is a high microporous volume and the ratio of microporosity is equal highest. Based on these factors it appears close to the optimum temperature for a 1-hour activation sample.
- CG-HTC-PYR-850-1 was selected as a step in the transition of CG-HTC-ACT-850-1 to an activated hydrochar, to understand more about the transition undertaken during the process.
- CG-RAW-850-0.5 was chosen because it is activated under same conditions as CG-HTC-ACT-850-0.5 without an HTC pre-treatment, offering a comparison for answering the initial hypothesis.
- CG-HTC-ACT-850-0.5 R200 has been selected for an understanding of the impact of HTC pre-treatment conditions.

5.2.8.1 CG Adsorption / Desorption Isotherms & Micropore Analysis

The results of the further textural analysis have been compiled into Table 5.43. Looking at each of the columns, there is a significant divide between the samples that were physically activated and those which weren't. The activation causes vast improvements in surface area and pore volume, whilst significantly reducing the average pore diameter. In terms of surface area, from highest to lowest: CG-HTC-ACT-850-1 > CG-HTC-ACT-850-0.5 R200 > CG-RAW-ACT-850-0.5 > CG-HTC > CG-HTC-PYR-850-1 > CG-RAW. The activated hydrochar samples produce the highest surface area, followed by the raw activation sample, grouping the steam activated samples together. There is then a significant drop to the base and transitionary samples, which offer very little in the way of surface area. Most samples return a very similar value compared to the initial tests, with slightly lower returns. CG-HTC-ACT-850-0.5 R200 has a wider degree of variance, losing 79 m^2/g, a 7 % drop.

Table 5.43 Textural data determined from CO_2 & long N_2 gas adsorption tests on key CG samples

Sample	BET Surface Area	Vultra	Vsuper	Vmicro	Vmeso	Vtot	Av. Pore Diameter
	m^2/g	cm^3/g	cm^3/g	cm^3/g	cm^3/g	cm^3/g	nm
CG-RAW	2	0.000	0.000	0.000	0.003	0.004	7.92
CG-HTC	39	0.000	0.000	0.000	0.179	0.188	19.19
CG-HTC-ACT-850-0.5 R200	1095	0.224	0.161	0.385	0.126	0.514	1.88
CG-HTC-ACT-850-1	1331	0.220	0.265	0.485	0.040	0.529	1.59
CG-HTC-PYR-850-1	4	0.012	0.000	0.012	0.012	0.013	12.53
CG-RAW-ACT-850-0.5	961	0.179	0.157	0.336	0.133	0.471	1.96
Standard Error (±)	54	0.020	0.014	0.034	0.03	1.36	1.37

Standard errors from Table 9.16 (Appendix)

The micropore volume is highest in CG-HTC-ACT-850-1. It consists of both ultra-micropores and super-micropores, with a larger volumetric contribution from the supermicropore category, which is the highest Vsuper value listed also. The closest micropore volume value is 20 % lower and is attributed to CG-HTC-ACT-850-0.5 R200. The difference between the two samples can be seen by the weightage in subcategories of the micropores. CG-HTC-ACT-850-0.5 R200, the shorter duration sample, has the highest Vultra result, and the ratio between ultra-micropores and super micropores is 4:6.

However, CG-HTC-ACT-850-1 has a ratio of 5:6 in favour of supermicropores. The additional 30 minutes has created larger micropores from those created during the first 30-minute spell. The difference in Vultra between the two samples is very minor, showing new ultra-micropores continue to be created at a similar rate in the 1-hour experiment. CG-RAW-ACT-850-0.5 has the third highest value. Despite being activated at identical conditions as CG-HTC-ACT-850-0.5 R200, the Vmicro is 10 % lower, due to the lack of pre-treatment. The ratio remains in favour of Vultra, although it has shifted a little towards Vsuper. The Vsuper values are very similar between the two, but the Vultra values are further apart, showing the ability of the HTC pre-treated sample to create more narrow pores during activation. The micropore volume appears non-existent in the raw sample or the HTC sample. It is worth noting both samples were tested as powders. The pelletization may have impacted the porosity in the sample and affected all of the tested parameters in this section. Ultra-micropores are recognised in the pyrolysis sample but are very low. The lack of ultra-micropore volume in CG-RAW and CG-HTC, and the understanding that pyrolysis does not promote the growth of new pores, leads to the belief that this may be an anomalous detection. The Vmicro volume matches Vmeso, and the combination is higher than the total detected. This sample is more likely to have mesopores than micropores, as shown in the initial analysis in Section 5.2.5. It seems the CO_2 test could have accounted for the mesopores as ultra-micropores. Perhaps there are ultra-micropores formed on the surface of mesopores, and each analysis method has quantified the pore size differently.

In terms of the mesopore volume, the HTC sample shows the highest value. This is born out of the HTC process, as the raw sample has a negligible mesopore volume. The process continues into the pyrolysis phase, where the detection of mesopores is low once more. The two samples conducted at 850 °C for 0.5-hours can be seen to show a very similar mesopore volume. Continuing from the findings that the micropore volume in CG-RAW-ACT-850-0.5 is leaning towards the larger micropores, favouring the creation of larger pores is to be expected. These mesopores are not present in CG-RAW so they would be created through excessive burn off. On the other hand, the appearance of mesopores can be attributed to the altered pre-treatment. The other activated hydrochar sample, CG-HTC-ACT-850-1, has a lower mesopore value, despite the longer treatment process. The lower HTC pre-treatment conditions appear to create a material which, when activated, has the surface area and narrow microporous features of CG-HTC-ACT-850-1, but the lower yield and higher mesoporous volume of CG-RAW-ACT-850-0.5. The increased losses sustained by the lower HTC conditions, seen earlier in Table 5.43, suggests material has undergone a more radical activation process. CG-HTC-ACT-850-0.5 R200 remains microporous but also has a high mesoporosity which may help with transportation. Based on the average pore diameter, the mesopores detected are mainly in the transitionary area. The average pore diameter is heavily swung by the appearance of micropores. Those samples which were activated are considered highly microporous, and thus the average pore size falls within the micropore range, specifically the super-micropore range. Those which were not introduced to an activating agent have wider pore volumes which fall under the mesopore range.

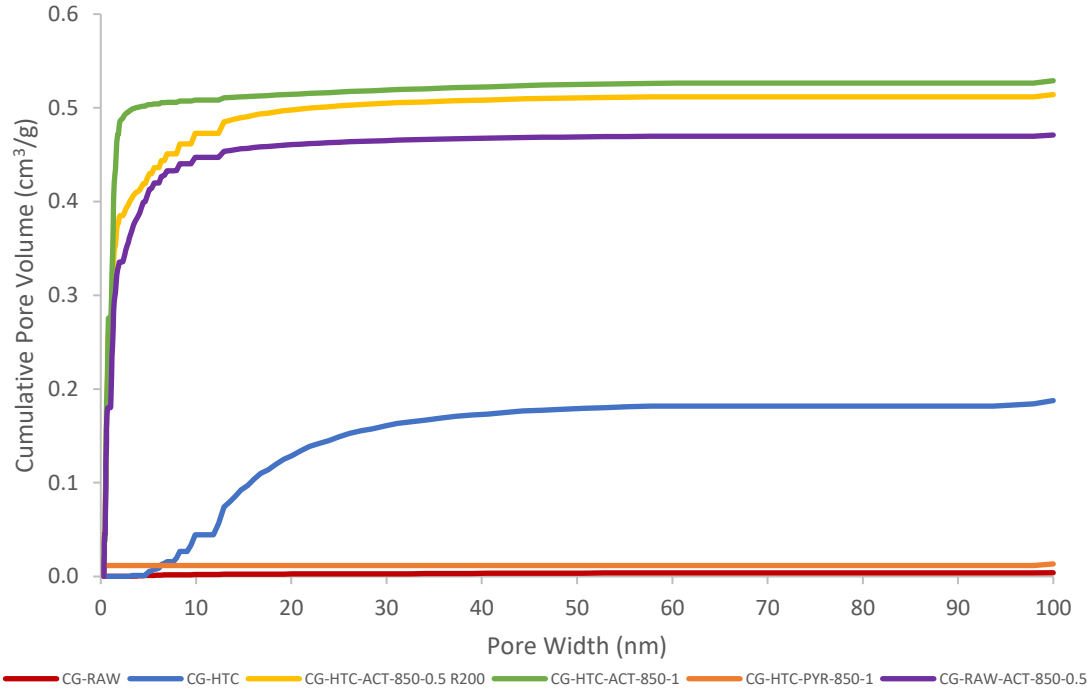

Figure 5.29 Cumulative pore size distribution of key CG samples

The total pore volume results are highly affected by the presence of micropores, which have been formed as a result of activation. This can be seen in Figure 5.29 by the sharp initial rises in samples reporting the highest pore volumes. The results in descending order go as follows: CG-HTC-ACT-850-1 > CG-HTC-ACT-850-0.5 R200 > CG-RAW-ACT-850-0.5 > CG-HTC > CG-HTC-PYR-850-1 > CG-RAW. The highest value is the activated hydrochar sample with the higher temperature pre-treatment, seen in green, which also has the highest surface area, micropore volume and the smallest average pore diameter. The sample remains within 1 % of the original textural analysis results. The additional capture of mesopore volume in CG-HTC-ACT-850-1 has dropped the microporosity from 94 % to 92 %, although it remains highly microporous. The pyrolysis sample also remains consistent with the previous result. CG-HTC-PYR-850-1 can be seen along the base in orange, with an initial rise in the ultra-microporous region, and plateaus across the other pore sizes. CG-RAW is also present at the bottom, in red, which reports very little pore volume. CG-HTC can be seen in the graph as the blue line. The Vtotal for the sample has reduced by 0.029 cm^3/g from the initial tests, due to a reduced mesopore detection. The graph shows the mesopores begin from 5 nm and have a major increase between 10 – 30 nm. Beyond that there is a minor flick at the end which pre-empts a macroporous zone. A lower recorded volume in both the micropore and mesopore regions has caused CG-HTC-ACT-850-0.5 R200 to reduce by 0.035 cm^3/g from the original test. The detection of ultra-micropores through CO_2 adsorption can be seen by the sharp rise of the yellow line at the beginning of the chart. The large Vmeso values of the 850 °C for 0.5-hour samples compared to the 850 °C for 1-hour sample can be seen by the more rounded curves of the yellow and purple lines, which gets closer to the green line as the pore widths increase > 2 nm. The green shows a sharp vertical increase then a sharp horizontal plateau, showing less of a curve and a more compact pore size distribution.

Figure 5.30 shows the isotherms from the low-pressure CO_2 analysis. CG-RAW is represented by the red line which is flat across the base. With little porosity detected, any

rise is attributed to instrument error, and is within the standard deviation. CG-HTC is mainly mesoporous, so despite the Vtotal being around half that of CG-HTC-ACT-850-0.5 R200, the blue line is unable to thrive in the CO_2 adsorption test. The remaining samples all exhibit Type 1a isotherms and are all within the micropore region. CG-HTC-PYR-850-1, seen in orange, shows the truest Type 1a isotherm. It peaks early, with the detected ultra-microporous volume, and then plateaus. The adsorption is strikingly high compared to the measured surface area and pore volume. The activated hydrochar samples show very similar trends and essentially match one another. The yellow line, representing the lower timeframe, rises higher at the beginning, with the higher ultra-micropore ratio, but is overtaken by the green line, which has a similar ultra-micropore volume but a greater overall micropore volume due to the super-micropores. The raw sample, purple, has lost some of the narrowest micropores and created larger ones, shifting the line below and to the right.

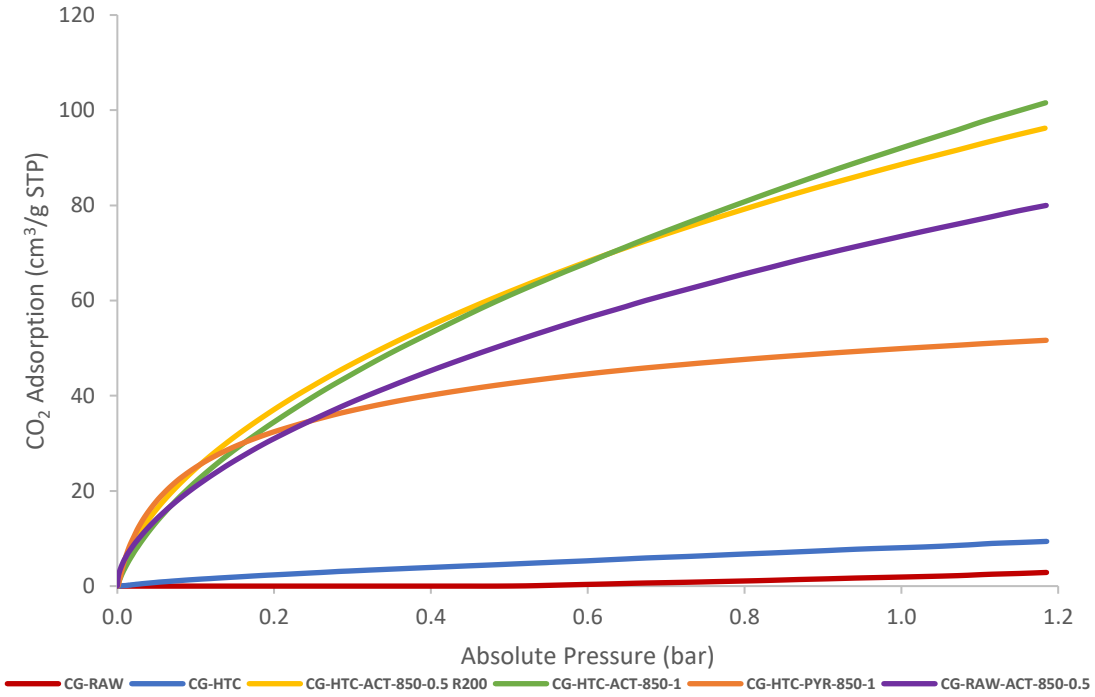

Figure 5.30 CO_2 adsorption isotherms of key CG samples

Figure 5.31 shows the long N_2 adsorption, which also displayed the desorption trend, represented by the dotted lines. Similar to the previous figure, CG-RAW is found at the base of the chart with no nitrogen adsorption. It is accompanied by the orange line, representing the pyrolysis sample. In comparison to the previous chart, there is a large departure in adsorption. The sample potentially has ultra-micropores with no mesopores and an affinity for CO_2 but not for N_2. CG-HTC, blue, steadily increases as the relative pressure increases. The adsorption rises at higher relative pressures, showing no presence of micropores but the onset of larger mesopores and macropores beyond the measurement. The trend is most fitting to a Type 5 isotherm, where the adsorbent-adsorbate relationship is weak. The hysteresis loop indicates the pore size distribution among the pores are wide, offering some shielding.

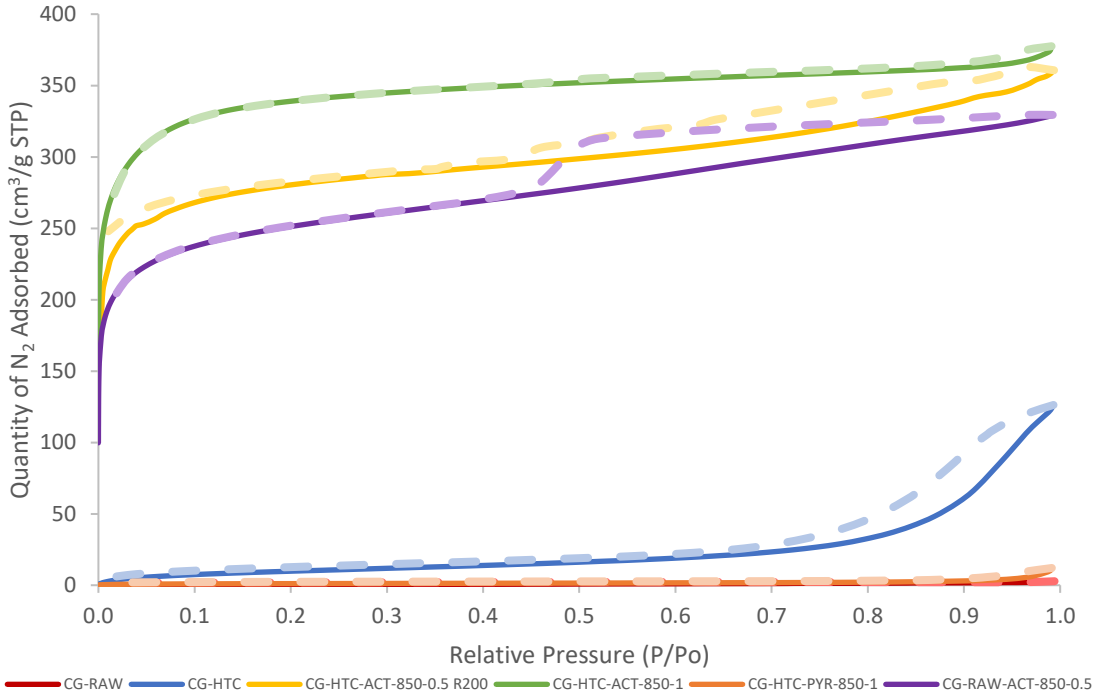

Figure 5.31 N_2 adsorption isotherms of key CG samples

CG-HTC-ACT-850-1, green, shows a small and steady growth after the surge of micropores at the lower relative pressures. The line essentially plateaus, remaining a Type 1a isotherm. A minor inflection is seen at the end insinuating the potential for macropores but is more likely instability at the saturation pressure of the N_2 adsorbate. The hysteresis is negligible, due tight pore size range. Any hysteresis has dropped in line with the adsorption line at 0.9 relative pressure, which represents a pore neck of approximately 30 nm. This sample has the highest adsorption capacity of all. CG-HTC-ACT-850-0.5 R200, yellow, also shows a surge at the beginning due to the micropore presence, albeit lower than the green line. It remains in parallel with the green line until approximately 0.5 relative pressure, where it begins to curve upwards, which does not let up until the end, showing larger mesopores are present. The isotherm is more typical of Type 4. There is an initial single layer adsorption, and multilayer begins in the larger pores, due to the additional mesopores present. The hysteresis curve has multiple gradient changes, which can signify a wide range of pore necks. These appear at 0.9 and 0.7 relative pressure, before cavitation occurs at 0.45 relative pressure. The desorption curve deviates from the adsorption curve at low relative pressure, also retaining adsorbate. This could signify pore shielding in micropores. The raw activation sample, purple, competes with the activated hydrochar created under the same conditions. The adsorption capacity is unable to surpass that of the sample which has been pre-treated, due to the higher intial rise in the micropore adsorption range. The large presence of mesopores leads the formation of a hysterisis loop. The desoprtion resembles a Type H2a hysterisis loop, which remains flat and then cavitition occurs a 0.45 relative pressure. This indicates massive pore shielding, from pore necks of approximately 4 nm and below (Li et al., 2021). The sample is developing mesopores deep within the channels, potetnially from pore wall collape and micropores joining.

5.2.8.2 CG Density, Porosity & Macropore Analysis

Findings from the density tests are reported in Table 5.44. Vtot has been calculated without Vinter, as it does not serve to display this information. Vinter is the interparticulate void volume and powder consolidation from the recorded samples, which offers no information on the samples internal volume. It can be seen in the table that Vinter would be a substantial contribution to Vtot, which is sometimes greater than Vtot. The measurements for Vmeso were recorded from 2 – 50 nm. The lower bound is the smallest size that mercury can intrude, and the range has been established as mesoporous. Vmacro is recorded from 50 – 6100 nm. The lower bound is the crossover between mesopore to macropore and 6100 nm is the lower bound for the interparticulate void volume. The Vinter records pore sizes up to from 6100 – 230,000 nm. The high Vinter of CG-RAW and CG-HTC is due being tested as a powder.

The total volume values are all higher than the total volumes calculated in Section 5.2.7.1, as the MIP measuring range is above the detection range on N_2 adsorption and the macropores contribute a large fraction to the total. The volume is lowest in the raw sample and highest in the activated hydrochar samples, specifically the lower temperature pre-treatment sample CG-HTC-ACT-850-0.5 R200. This is followed by CG-HTC-ACT-850-1 with a slightly lower value. The HTC sample ranks third, above samples CG-RAW-ACT-850-0.5 and CG-HTC-PYR-850-1 which have been heat treated. The pyrolysis sample only drops slightly from the HTC sample, although it does indicate that the pyrolysis phase has no impact on the development of larger pores.

Table 5.44 Structural data determined by MIP & helium pycnometry on key CG samples

Sample	Pore Area	Vinter	Vmacro	Vmeso	Vtot*	Av. Diameter	Bulk Density	Skeletal Density	Porosity
	m^2/g	cm^3/g	cm^3/g	cm^3/g	cm^3/g	nm	g/cm^3	g/cm^3	%
CG-RAW	11	1.760	0.022	0.044	0.066	646	0.36	1.31	72
CG-HTC	28	2.641	0.779	0.198	0.978	507	0.21	1.23	83
CG-HTC-ACT-850-0.5 R200	75	0.366	0.934	0.173	1.474	78	0.40	1.86	79
CG-HTC-ACT-850-1	54	0.110	1.085	0.141	1.226	94	0.42	1.96	78
CG-HTC-PYR-850-1	9	0.226	0.779	0.035	0.814	455	0.59	1.92	69
CG-RAW-ACT-850-0.5	86	3.172	0.228	0.268	0.496	169	0.19	2.04	91

Vtot is the sum of Vmacro & Vmeso, disregarding Vinter.

The macropore volume is the biggest contributor of the total volume from MIP. The smallest Vmacro is in the raw sample. The macropore volume increases significantly through the HTC process and during pyrolysis remains constant. The largest Vmacro values are presented by the activated hydrochar samples. CG-HTC-ACT-850-1 has the largest value, followed closely by CG-HTC-ACT-850-0.5 R200. The influxes of adsorption seen at the end of the nitrogen adsorption isotherms indicated a large macropore volume, which has been proven. The activating agent has a large influence on the macroporosity. Although CG-HTC-ACT-850-0.5 has a surprisingly small macroporous region. With the loss sustained and the high mesoporous region in the nitrogen adsorption, which continued to rise until saturation pressure appeared to indicate there would be a large macroporous presence. Perhaps the conditions are so extreme that the macropores have grown wider than the accepted limits. The Vinter column proves this, with the largest value by far, despite being in pellet form.

The mesopore volumes fluctuate greatly from the initial values listed in Section 5.2.5. The mesopore volume is found to be lowest in the pyrolysis sample, despite a proportionally large 0.023 cm^3/g increase on the previous result. The lack of mesoporous and microporous volume from these samples shows that the activating agent is the main cause of porosity. Incidentally, the porosity for this sample is also seen to be the lowest, stripped of volatiles, it leaves a dense fixed carbon structure with a minor accessible pore volume. CG-RAW has a similarly low mesopore volume. A large mesoporous volume is formed through the HTC process. Combined with the macropore and the non-existent micropore regions, this would be seen as providing the AC precursor with many large pores as sites for the activating agent to react. However, this is wiped out during the ramp up through volatile removal. The mesopore volume has decreased from the previous total by 0.016 cm^3/g, which will go some way to explaining the large hysteresis loop. Due to the lack of micropores, it is more likely due to condensate in the large pores. Both activated hydrochar samples increased in mesopore value from the previous tests. However, they both rank lower than the initial mesopore value in CG-HTC, the precursor. CG-HTC-ACT-850-0.5 R200 increases by 0.03 cm^3/g, providing a large developed mesopore volume, although it still remains microporous. The value is higher than that of CG-HTC-ACT-850-1, as confirmed by the original tests, but the initial N_2 adsorption results with either very conservative or the MIP measured volume is incorrect, as it increases by the substantial denomination of 0.114 cm^3/g. The increases in pore volume from the initial sample shows there is little pore shielding. The additional recorded values could be small macropores which are trapped behind mesoporous necks. These pores are then recorded as mesopores due to the pressure applied, making it only an approximate pore size distribution (Ma & Li, 2013). MIP is understood to compress the samples at higher pressures, could account for the increase in mesopore volume as detecting the micropore volume through compression (Brown & Lard, 1974). Finally, the highest mesopore value is attributed to CG-RAW-ACT-850-0.5 which has a higher Vmeso than Vmacro. This stems from the large mass removal and the growth of micropores due to the susceptibility of the material.

The values are plotted in Figure 5.32 as a porosity spectrum. For the raw sample, red, a third of the pore volume is found at approximately 100 nm, the remaining is in the mesoporous range of 10 – 15 nm. For the HTC, blue, sample there is a rise in the macroporous region between 2000 – 5000 nm, but the majority comes as a spike between 50 – 100 nm. The intrusion curtails here, and plateaus at 20 nm, demonstrating the mesopores are at the wider end of the scale, which is my they culminate into a large

mesopore volume. With the introduction of heat in the pyrolysis phase, seen by the orange line, the intrusion drops with the decreased pore volume. But the shape of the trend line has dropped down and to the left, relative to the chart. This has turned mesopores to macropores and widened the macropore distribution, creating pores across the entire recordable range. The largest intrusion is conducted on CG-HTC-850-1, in green. This has a steady group of macropores up to 500 nm. Above this a large portion of the intrusion happens until 350 nm. The curve settles into a steady incline, showing the wide range of mesopores. There is an inflection from 3 nm onwards, implying some of the micropores have widened enough to become mesopores and allow intrusion. CG-HTC-ACT-850-0.5 R200 is seen to mimic the pattern of CG-HTC-850-1, offset below and to the left due to the materials susceptibility. The yellow line can be seen to pick up at a higher pore width, about 1000 nm, before a smoother curve, due to the logarithmic graph, positions the line parallel to the green line. They separate more around 25nm, showing CG-HTC-850-1 has more pores in this area. Then the incline begins much sooner, at 7 nm, which shows the pores which have been widened from micropores. This section accounts for half the mesopore intrusion in the sample. Finally, the purple line shows CG-HTC-PYR-850-1, the pyrolysis sample. Here it mimics the predecessor, CG-HTC and the sample before that CG-RAW, in the middle between them. The first rise is down and to the right of the blue line, relative to the graph, at 1500 nm. It plateaus, as the others do, until a sharp upturn between 15 – 20 nm, which is slightly higher than the growth in CG-RAW. Beyond 15 nm the intrusion continues which contributes to the largest mesopore volume recorded. The ACs each have a wide pore size distribution, with peaks in each region and continuous growth throughout which is anticipated to be translated as a strong network of porous tunnels.

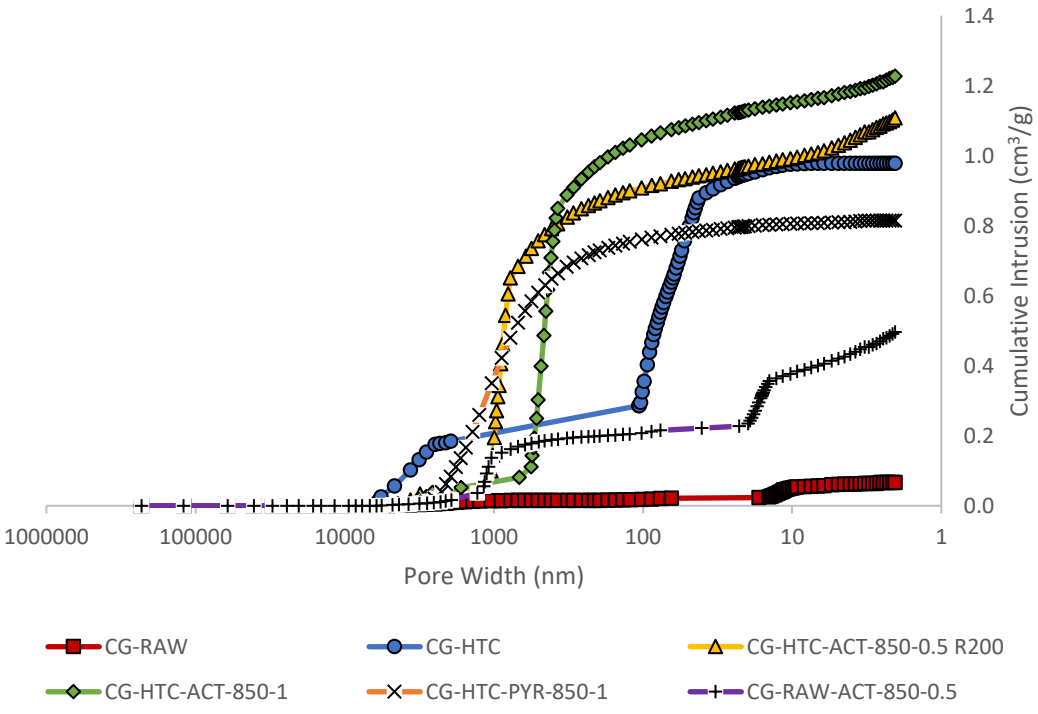

Figure 5.32 Mercury intrusion porosimetry of coffee grounds excluding interparticulate void space

The initial porosity of the raw sample is 72 %. This is due to the lack of in the biomass product itself, as the high porosity value is present despite the lack of pore volume within

the material. The sample has a lot more porosity after the carbonisation. Despite the anticipated densification, the skeletal density drops from the precursor. This will be related to the high Vmacro and Vmeso values, as well as the high volatile content in the solid fraction which is not highly dense. The porosity drops off to the lowest recorded value after the pyrolysis. Very little pore volume was recorded in any of the porous zones, combined with the material not being extremely dense, has resulted in a lower porosity. This leaves a good template to create pores using the activating agent. The densities of the activated hydrochars are similar due to the similar pore volumes in each region. The porosity is slightly higher in CG-HTC-ACT-850-0.5 R200, which could be attributed to the greater mesoporosity. The raw sample is very porous, despite recording lower total volume through MIP than the other activated hydrochars. It seems so much of the material has been eroded, yet there was surface area and pore volume still present for analysis, causing a low bulk density value. This may also be influenced by the high ash content, which was recorded at 14 %, which would cause the highest skeletal density value.

The density tests have proven the activated hydrochars from CG have a strong basis of interconnectivity, despite the high proportion of microporosity. When the MIP Vmeso is compared with the Vmeso extrapolated from the long N_2 runs, the samples are found to have more mesoporosity, which removes the possibility of pore shielding. This is found to be different in the lower HTC treatment sample which experiences issues with pore shielding. The adsorption and desorption cycles in the other CG samples would be effective due to the lack of pore shielding. The wide range of pore sizes aid the transportation of adsorbate around the adsorbent, allowing for rapid adsorption.

5.2.8.3 CG TEM images

The more microporous features of the CG samples are suited to the use of TEM. Figure 5.33 (a-b) presents TEM images of CG-HTC-ACT-850-1. This sample displays the peak surface area and micropore volume of the key CG samples. The material exhibits a disordered structure. The red circles highlight the three-dimensional interconnected microporous structure found in activated CG hydrochars.

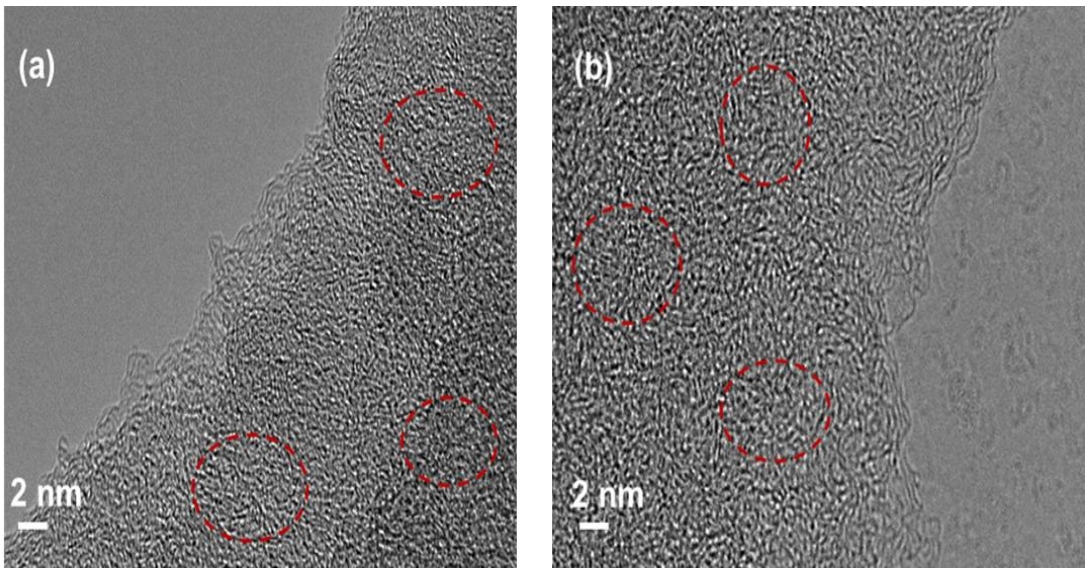

Figure 5.33 (a-b) TEM image of CG-ACT-850-1

5.2.9 Summary

Prior to this paper, CG hydrochar had not been physically activated with steam. Applying this method has produced a highly microporous AC, with surface areas and pore volumes comparable to commercially available ACs. By adopting this practice, the surface areas produced were upwards of 1300 m^2/g and pore volumes of 0.5 cm^3/g. The materials were of a high carbon content and low in impurities. This signifies CG is a highly effective precursor for AC. The results have surpassed those of, Castro et al. (2011) and Alves et al. (2019), who undertook the activation of CG without prior treatment. Using the pre-treatment method and higher activation temperatures, the method has increased the surface area above their findings of 400 and 620 m^2/g. The materials in this study also have higher carbon purities and has improved the microporous region, for the ACs in the referenced studies were found to be mesoporous. The concentration of smaller pores reduced the appearance pore shielding in the material.

The pre-treatment process framework can be seen as a success. The sample went through HTC and produced a solid yield of 55 % and a carbon yield of 82 %. Batch producing the hydrochar as 10 % DS at 220 °C for 5 hours is adequate to hydrothermally carbonize CG. Analysis of the constituents showed a markable increase in carbon and a reduction in oxygen and volatile content. The process was very effective at reducing the material ash content which was seen to reduce by 88 %. This was integral to the AC purity. The hydrogen content was seen as an outlier, although the mass was reduced, the ratio with carbon remained constant after the transformation. Despite this, CG-HTC was good precursor. The test at a lower HTC temperature, which produced CG-HTC-ACT-850-0.5 R200, gave an insight into the pre-treatment requirements. HTC at 200 °C produced a far weaker precursor which negatively impacted the key characteristics of CG AC. In addition to a lower carbon yield there was an increased ash and volatile content in the final product. In the trial at 850 °C for 0.5-hours, the hydrochar yields were reduced from ~ 22 % to ~ 14 %, with a lower fixed carbon fraction when the lower HTC conditions were used. The accelerated loss trend retained the micropores and produced more mesopores, to the advantage of surface area and pore volume. This insight can be used to tune the pre-treatment to make a more microporous or mesoporous AC. The increased mesoporous fraction resulted in pore necks which caused pore shielding and altered the desorption isotherm. The resulting hydrochar has superior characteristics as a fuel source, with the HTC pre-treatment upgrading the material to a tier similar to a hard coal, such as anthracite.

A feature of the CG samples was the relatively high yields that were generated. The measurement was aided by a lower volatile fraction in CG-HTC, due to the pre-treatment. This resulted in less material loss during the pyrolysis treatment, and more fixed carbon for the activating agent to react with. The final product had a high purity of carbon, with the tested conditions ranging from 92 – 97 wt% of the final product. The low starting ash fraction meant ash in the final product was restricted, with most samples had < 1 %, with the highest reaching 2.3 %. This is remarkable for an AC derived from waste. The chemisorption of oxygen and hydrogen was rarely detected in the samples, which may impact surface functionality.

The raw trials were able to produce ACs but was let down by the reliability of the sample. The method could not continuously reproduce the same results as the losses sustained would often be ruinous to the experiment. The losses could cause equipment blockages

and lead to breakage. Multiple adaptive measures had to be introduced, such as the mixing 10 wt% molasses as a binder. This could be deemed an alternative pre-treatment step to HTC, which was not as effective. In reality, this would require additional material to be sourced and equipment to manage. The raw sample was more susceptible to the conditions causing a greater burn off. One raw AC sample created a respectable surface area of 961 m^2/g and still created a high micropore volume, only 10 – 30 % lower than the activated hydrochars. The additional mass loss was represented in the mesoporous region. In this particular example, the yield was 49 % lower than the activated hydrochar counterpart, but in some samples, this increased to 70 %. Samples which underwent HTC prior to activation produced a higher yield of greater quality product. The results signify a successful testing framework and underline the need for a pre-treatment process to activate this material.

The conditions of temperature and time were varied to optimise the sample. Temperature had the greatest impact, on both loss and the material structure. Higher temperatures induced more rapid losses which culminated in higher surface areas and pore volumes. The time influenced in a similar way, but with less impact. Given the yield results, and the materials porosity of ~ 78 %, there is potential to expand beyond the conditions already tested to understand if a greater pore structure can be achieved by activating over a longer duration. The study concluded that a temperature in the remit of ~ 850 °C for 0.5 – 1 hour is the optimum range for producing ACs for CG hydrochar. Between the samples CG-HTC-ACT-850-0.5 and CG-HTC-ACT-850-0.5, the surface areas recorded were 1014 – 1331 m^2/g, with a pore volume of 0.38 - 0.53 cm^3/g which highly favoured microporous development and a yield between 16.9 – 22.8 %. A balance between these key sample characteristics would begin to optimise the materials potential.

In this experiment the objectives have been met and the methodology can be used to create a microporous AC from CG. The losses and unreliability experienced with the raw sample makes a certain argument for the use of a pre-treatment phase to carbonize the material prior to activation. CG hydrochar is an ideal precursor for AC, with the products exhibiting low ash content and high carbon purity. The relatively high solids yields show promise for CG AC, which exhibits a high microporosity.

5.3 Sewage Sludge

5.3.1 The Context for Sewage Sludge Research

Solid wastewater sludge was selected because regardless of the whether it is reused or disposed in landfill, the biological content requires treatment, as mentioned in section 2.4.2. However, there is concern with the total ash content and potential for variation between batches. (Fan et al., 2020) There are many benefits to selecting sewage sludge as a precursor, such as the infrastructure connecting sewage systems is already in place meaning tonnes of waste can be directed towards a specified location. The waste is abundant and with an increasing global population, the amount of wastewater requiring treatment will increase. SS featured as a significant part in the creation of this project. Antaco Ltd., project sponsor, consider the wastewater industry to be the most prominent application for HTC and the best function to test the pilot plant continuously. The plan was to create a higher value product from sewage sludge hydrochar, for additional revenue streams. The literature presented activation as a strong prospect. In addition, the idea to create a 'circular economy' effect was attractive by using the AC product for process wastewater treatment. This provided an inhouse use for the product and reduced procurement costs.

Planned testing of the pilot plant began with water to practice plant operation, test the functionalities, calibrate sensors, and check the conditions operating range. This progressed to hot water testing to bring the thermal oil system online. Batches of waste materials were introduced for slurry testing. This saw the introduction of strawberry pomace, as well as other materials such as brewers' grains. The strawberry sample was collected to create the testing framework for activation. The success of the initial trials generated interest for its own research plan. At this point, sewage sludge hydrochar was not being processed in the pilot plant due to factors outside the control of this project. Upon completing the strawberry research plan, coffee grounds became a joint venture with two PhD students at the University of Surrey who were also sponsored by Antaco. Their work centred on HTC process water. So together we created batches, which created products for both sets of research.

When the sewage sludge samples were ready, they were tested in the pre-developed testing matrix. Unfortunately, the results were poor, which thrust the SP and CG samples as the focus of the research. Here is a summary of the sewage sludge results.

5.3.2 SS HTC Pre-Treatment

The raw sewage sludge was processed through an industrial HTC unit. Based on the recorded conditions it was subjected to, it is expected that the material underwent a thermochemical transformation. The calorific value was recorded from a post HTC process to show the benefit as a fuel stock, which is shown in Table 5.45. Due to the biological nature of raw sewage sludge and the hazards associated, it was not possible to perform the test on the raw sample. The material HHV is within the range expected from the literature and is comparable to sub-bituminous coal. The value is the lowest of the three materials.

Table 5.45 The calorific value of HTC treated SS

Sample Name	Wet HHV	Dry HHV
	MJ/kg	MJ/kg
SS-HTC	18,300	19,100

The lack of raw comparison poses issues when validating the HTC process conditions. The conditions used closely replicated the SP-HTC test. In retrospect, these conditions were found to upgrade the biomass to a higher value product but not complete the HTC process as anticipated. The treatment of SS may have met the same fate, however without the raw comparison, this cannot be confirmed. Although, this is a different material, with a different structure, and previous studies have considered 180 – 200 °C sufficient for HTC in sewage sludge (Danso-Boateng et al., 2020), (Xin, Li & Son, 2020), (Saetea and Nakorn, 2013).

5.3.3 SS Activation Analysis

The pyrolysis and activation phase were tested separately. The pyrolysis tests showed that the lowest loss during pyrolysis was 71.3 % and the maximum was 75.8 %, in SS-HTC-ACT-950-1, full results in Appendix Table 9.17. In this material, more losses were experienced at higher pyrolysis temperatures. The timeframe made a minor difference to the increase in losses incurred. So, with the understanding that higher temperatures can remove more mass, no upper loss value has been predicted for this sample.

The proximate analysis tests, Table 5.46, show the composition of a few selected sampled. The transition of SS-HTC, the precursor, to SS-HTC-PYR-800-0.5, the pyrolysis sample, shows the anticipated drop in volatiles and the increase in fixed carbon as well as ash. SS-HTC right away shows the primary reason why this source of SS is not ideal for AC; the ash content is bigger than the fixed carbon content. The ash content is expected to and does continue to grow through the treatment. From the inescapable pyrolysis losses alone, the ash becomes the largest constituent in the sample. From there, the introduction of the activating agent further removes both the fixed carbon and the volatiles. This drives the ash content further until most of the sample is ash. In terms of the remaining fixed carbon, it is a minor fraction. In a typical AC, the values of ash and fixed carbon would be expected to be the other way around. The initial volatile content in SS-HTC is the highest of the three materials tested, with that of CG-HTC at 72.0 %, which did undergo HTC, and SP-HTC at 74.6 %, was only upgraded. This would put SS-HTC more in line with SP-HTC, which would imply a semblance of HTC was achieved but not completed. However, it is impossible to say without the raw data, and the ratio between the volatile content to the other components is much changed compared to SP-HTC and SP-CG.

Table 5.46 Dry basis proximate analysis on SS samples

Sample Name	Volatiles	Fixed Carbon	Ash
	%	%	%
SS-HTC	77.2	6.8	16.0
SS-HTC-PYR-800-0.5	18.0	24.2	57.8
SS-HTC-ACT-800-0.5	6.6	14.0	79.5
SS-HTC-ACT-750-1	19.4	5.3	75.4
SS-HTC-ACT-800-1	17.1	6.6	76.3

The pyrolysis yield and the activated hydrochar yield can be seen side by side in Table 5.47. With the largest volatile fraction created in this study, the pyrolysis yield is the lowest of all. All samples retain < 30 % mass with some dipping below 25 %. When compared to the activated hydrochar yield, it comes as no surprise that the values are so close, with the revelation that the material begins the process with 16 % ash. With that in mind, there are some samples which dip below 16 %, which are anticipated to be purely ash. When put into the context of activation yield, introduced in Section 5.1.4, the samples remain relatively high. In the SP experiments, many of the highest scoring surface areas and pore volumes were found in materials with 50 % or less, which lead to greater porosity, such as SP-HTC-ACT-850-0.5.

Table 5.47 Activated hydrochar and pyrolysis yield achieved from SS hydrochar

Sample Name	Equivalent Pyrolysis Yield	Activated Hydrochar Yield	Activation Yield
	%	%	%
SS-HTC-ACT-700-0.5	28.3	25.5	90.3%
SS-HTC-ACT-750-0.5	26.8	22.7	84.8%
SS-HTC-ACT-800-0.5	26.4	20.2	76.6%
SS-HTC-ACT-850-0.5	25.5	16.8	65.7%
SS-HTC-ACT-900-0.5	26.7	14.9	55.9%
SS-HTC-ACT-950-0.5	24.9	15.2	61.0%
SS-HTC-ACT-700-1	28.7	23.5	81.8%
SS-HTC-ACT-750-1	26.6	21.0	78.8%
SS-HTC-ACT-800-1	26.3	18.2	69.2%
SS-HTC-ACT-850-1	26.4	14.9	56.5%
SS-HTC-ACT-900-1	25.0	15.0	60.3%
SS-HTC-ACT-700-2	26.7	21.0	78.7%
SS-HTC-ACT-750-2	26.0	18.0	69.2%
SS-HTC-ACT-800-2	26.1	15.8	60.4%
SS-HTC-ACT-850-2	25.6	15.2	59.6%

The samples underwent ultimate analysis to gain a deeper understanding of the constituents. The results are presented in Table 5.48. The carbon fraction is highest on the lowest temperature samples, treated at 700 °C. This is also true for the time fraction, the lower the time, the higher the carbon content. With so little carbon to work with from in the precursor, it is quickly removed. Each timeframe shows an example of a sample returning zero carbon content. Those samples with < 16 % activated hydrochar yield, are primarily ash. The hydrogen content is better detected in the lower temperature and lower timeframe samples. The oxygen content is more sporadic, and due to the calculation by difference, will suffer from inaccuracies based on the samples which did not undergo proximate analysis, and instead have calculated ash content, based on the knowledge that a sample would begin with approximately 16 % ash content, as per SS-HTC in Table 5.46. Oxygen was calculated to be present in the three samples which undertook proximate analysis, which gave accurate ash values. The presence of oxygen on the three accurate samples, and not on the pyrolysis sample, shows the action of chemisorption working during the activation. The oxygen values are better represented in low temperature and low duration samples. Regardless, the H/C and O/C values are quite irrelevant since the carbon content it too minimal for the material to be considered an activated carbon.

Table 5.48 Ultimate analysis of activated sewage sludge hydrochar

Sample	Carbon	Hydrogen	Nitrogen	Oxygen	Ash	H/C	O/C
	Wt.%	Wt.%	Wt.%	Wt.% BD	Wt.%	Atomic Ratio	Atomic Ratio
SS-HTC-ACT-700-0.5	36.7	0.5	1.8	2.2	58.8	0.01	0.06
SS-HTC-ACT-750-0.5	27.3	0.1	1.2	4.8	66.6	0.00	0.18
SS-HTC-PYR-800-0.5	*41.7*	*0.4*	*1.5*	*0.0*	***56.4***	*0.01*	*0.00*
SS-HTC-ACT-800-0.5	19.2	0.5	0.7	0.1	**79.5**	0.03	0.00
SS-HTC-ACT-850-0.5	3.8	0.0	0.3	6.0	89.9	0.00	1.55
SS-HTC-ACT-900-0.5	0.0	0.0	0.3	0.0	99.7	0.00	0.00
SS-HTC-ACT-950-0.5	0.0	0.0	0.1	0.0	99.8	0.00	0.00
SS-HTC-ACT-700-1	28.6	0.2	1.5	6.2	63.5	0.01	0.22
SS-HTC-ACT-750-1	19.4	0.0	0.9	6.5	**73.1**	0.00	0.34
SS-HTC-ACT-800-1	10.2	0.0	0.5	9.8	**79.5**	0.00	0.96
SS-HTC-ACT-850-1	0.0	0.0	0.2	0.0	99.8	0.00	0.00
SS-HTC-ACT-900-1	0.0	0.0	0.3	0.0	99.7	0.00	0.00
SS-HTC-ACT-700-2	24.1	0.1	1.2	1.8	72.8	0.00	0.08
SS-HTC-ACT-750-2	12.3	0.0	0.6	2.6	84.4	0.00	0.21
SS-HTC-ACT-800-2	2.5	0.0	0.2	0.0	97.3	0.00	0.00

SS-HTC-ACT-850-2	0.0	0.0	0.3	0.0	99.7	0.00	0.00
SS-HTC-ACT-700-4	18.3	0.7	0.8	0.0	80.1	0.04	0.00
Standard Error (±)	3.01	0.14	0.06	2.59	1.19	0.13	0.09

Ash content from proximate analysis in bold, other ash content calculated from SS-HTC starting ash content, average moisture content from proximate analysis used to calculate dry hydrogen weight, oxygen calculated by difference (BD). Single pyrolysis sample SS-HTC-PYR-800-0.5 included in italics. Standard errors from Table 9.15

5.3.4 SS Textural Analysis

The samples underwent characterization through nitrogen adsorption. The full set of figures can be seen in Table 5.49 and Table 5.50. Beginning with the activated hydrochar surface area, it can be seen in the 0.5-hour samples, the surface area increases with temperature until it peaks and falls after 800 °C. In the other time frames, it peaks at the lowest temperature and drops from there to a negligible value. It seems the peak is reached early in the activation, due to there being little carbon available, and the activating agent is in excess. The highest surface area seen in SS-HTC-ACT-700-1 closely followed by SS-HTC-ACT-800-0.5.

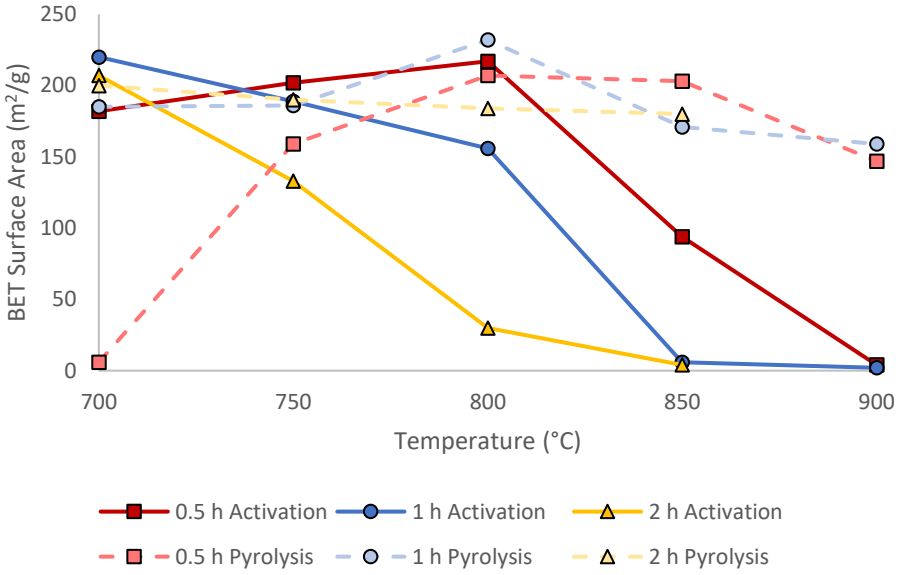

Figure 5.34 Sewage sludge hydrochar surface areas after pyrolysis or activation, produced at the listed conditions

In Figure 5.34, the activation samples have been compared to the pyrolysis counterpart, which was also assessed through nitrogen adsorption. The bold coloured lines represent the activation and the faint dotted lines of the same colour represent the matching pyrolysis results. Surprisingly the samples do not deviate far from the initial surface area before the activating agent is added. As the temperature is increased, the pyrolysis samples begin to drop also, but not as severely and they become the highest surface area at temperatures greater than 800 °C. The most unexpected result is that of SS-HTC-PYR-800-1, which produces the highest surface area of all at 232 m^2/g. These surface areas do not meet the measures that were aimed for. Also, the closeness between all samples shows there is not much room for optimisation for improvement, as all trends go down. As demonstrated by Figure 5.35, the activation and pyrolysis samples are within the same range, and the pyrolysis samples withstand the higher heat treatments without an oxidising agent present.

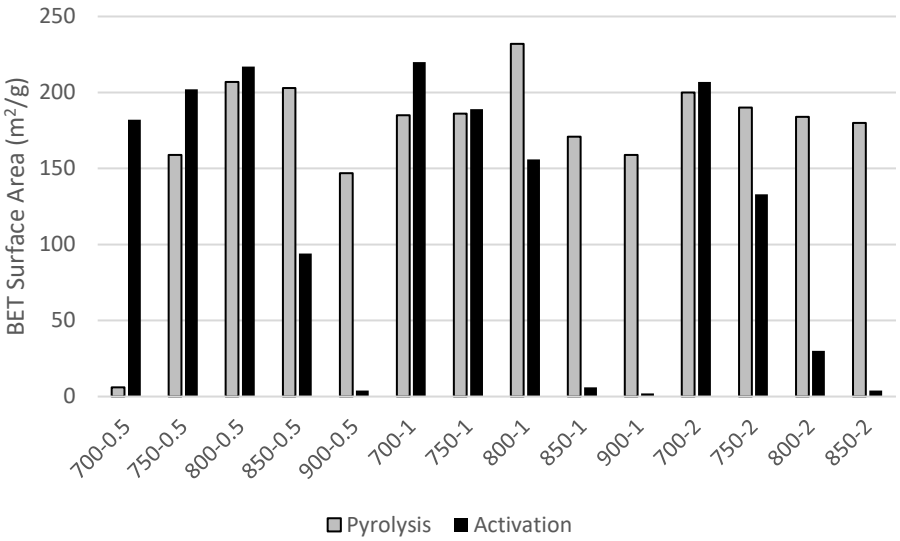

Figure 5.35 Comparison of sewage sludge hydrochar pyrolysis and activation surface areas

The pore volume was also recorded during the testing and the total pore volumes of both activation and pyrolysis tests are displayed in Figure 5.36. The 0.5-hour and 1-hour samples increase in pore volume with increasing temperature, up to 800 °C, where it proceeds to drop. The shorter timeframe drops of gradually whereas the more extreme condition drops suddenly, most likely indicating a huge loss of material between 800 – 850 °C. The 2-hour sample plateaus to 750 °C and then drops. The pyrolysis samples show a more consistent trend, averaging around 0.1 cm^3/g throughout. They show a vague order from largest to smallest: 2-hour > 1-hour > 0.5-hour. However, the difference between them is minor. SS-HTC-ACT-700-0.5 appears to be an incorrect reading because the pyrolysis reaction was a success, confirmed by the drop in volatile content. However, the surface area and pore volume are more in line with what would be expected from SS-HTC.

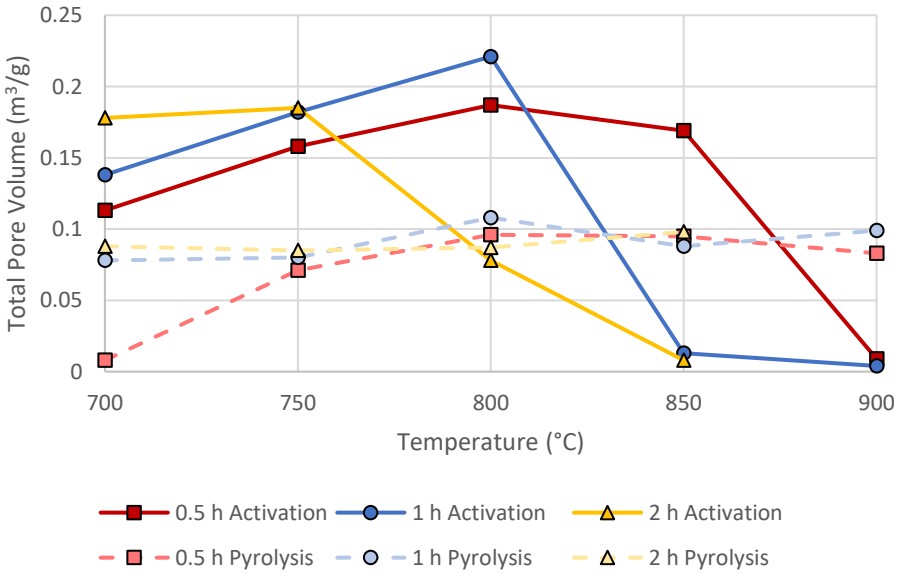

Figure 5.36 Sewage sludge hydrochar total pore volume after pyrolysis or activation, produced at the listed conditions

Only one sample reaches the commercial grade of 0.2 cm^3/g, in SS-HTC-ACT-800-1, but it is most likely due to the presence of mesopores or even macropores. The combination of the higher pore volumes and lower surface areas in the activation samples than the pyrolysis samples show the activated samples most likely have much larger pores due to the reaction with the activating agent. In the pyrolysis samples, the pre-existing structure and the naturally formed voids from the liberation of the volatiles creates a smaller pore volume with an equal or greater surface area, signalling the existence of smaller pores. This is confirmed by the average pore diameter which is consistently < 2 nm for the pyrolysis but spreads sporadically around the lower mesopore region in the activation samples. The pyrolysis samples are microporous materials while the activated samples are firmly mesoporous.

Given the need for additional apparatus to provide the activating agent and energy to prolong the treatment, the expenditure can be curtailed after the pyrolysis phase. There is no real benefit to the introduction of the activating agent, even at the optimum points, unless there is a particular need for a low surface area mesoporous carbon. Due to the performance of the pyrolyzed samples, it is proposed to take forward SS-HTC-PYR-800-0.5 and the activation equivalent of SS-HTC-ACT-800-0.5. They have similar surface areas, both ranking second in their categories, both samples rank comparatively highly in total pore volume. However, the pyrolysis sample portrays microporous traits whereas the activation sample has progressed the voids to larger mesopores. Both samples retain a quantity of both pore sizes. Together they appear a good representation of the sample's potential.

Table 5.49 S*urface area, pore volume and pore size distribution of activated SS hydrochar*

Sample	BET Surface Area	Microporous Volume	Mesoporous Volume	Total Volume	Average Pore Diameter	Microporosity	Mesoporosity
	m^2/g	cm^3/g	cm^3/g	cm^3/g	nm	%	%
SS-HTC-ACT-700-0.5	182	0.058	0.053	0.113	2.49	52	46
SS-HTC-ACT-750-0.5	202	0.059	0.098	0.158	3.14	37	62
SS-HTC-ACT-800-0.5	217	0.063	0.121	0.187	3.46	34	65
SS-HTC-ACT-850-0.5	94	0.024	0.134	0.169	7.16	14	79
SS-HTC-ACT-900-0.5	4	0.001	0.007	0.009	7.94	6	84
SS-HTC-ACT-950-0.5	1	0.000	0.009	0.010	27.53	0	85
SS-HTC-ACT-700-1	220	0.070	0.066	0.138	2.50	51	48
SS-HTC-ACT-750-1	189	0.057	0.123	0.182	3.86	31	67
SS-HTC-ACT-800-1	156	0.043	0.168	0.221	5.67	19	76
SS-HTC-ACT-850-1	6	0.001	0.011	0.013	8.96	5	83
SS-HTC-ACT-900-1	2	0.000	0.003	0.004	7.61	3	80
SS-HTC-ACT-700-2	207	0.066	0.106	0.178	3.45	37	60
SS-HTC-ACT-750-2	133	0.035	0.140	0.185	5.56	19	76
SS-HTC-ACT-800-2	30	0.005	0.065	0.078	10.25	6	84

SS-HTC-ACT-850-2	4	0.001	0.007	0.008	8.05	7	80
SS-HTC-ACT-700-4	191	0.059	0.117	0.187	3.92	31	63
Standard Error (±)	23	0.007	0.037	0.044	0.113	2.06	2.00

Standard errors from Table 9.16 (Appendix)

Table 5.50 Surface area, pore volume and pore size distribution of pyrolyzed SS hydrochar

Sample	**BET Surface Area**	**Microporous Volume**	**Mesoporous Volume**	**Total Volume**	**Average Pore Diameter**	**Microporosity**	**Mesoporosity**
	m^2/g	cm^3/g	cm^3/g	cm^3/g	nm	%	%
SS-HTC-PYR-700-0.5	6	0.002	0.006	0.008	5.14	18	72
SS-HTC-PYR-750-0.5	159	0.054	0.015	0.071	1.78	77	21
SS-HTC-PYR-800-0.5	207	0.072	0.023	0.096	1.86	75	24
SS-HTC-PYR-850-0.5	203	0.070	0.024	0.095	1.87	74	25
SS-HTC-PYR-900-0.5	147	0.048	0.033	0.083	2.26	58	40
SS-HTC-PYR-700-1	185	0.064	0.013	0.078	1.69	82	17
SS-HTC-PYR-750-1	186	0.064	0.015	0.080	1.73	80	19
SS-HTC-PYR-800-1	232	0.081	0.026	0.108	1.87	75	24
SS-HTC-PYR-850-1	171	0.059	0.028	0.088	2.06	67	32
SS-HTC-PYR-900-1	159	0.051	0.046	0.099	2.50	52	47

SS-HTC-PYR-700-2	200	0.069	0.018	0.088	1.77	78	21
SS-HTC-PYR-750-2	190	0.066	0.018	0.085	1.80	78	21
SS-HTC-PYR-800-2	184	0.063	0.023	0.087	1.90	73	26
SS-HTC-PYR-850-2	180	0.060	0.036	0.098	2.17	62	37
Standard Error (±)	23	0.007	0.037	0.044	0.113	2.06	2.00

Standard errors from Table 9.16 (Appendix)

Table 5.51 Textural data determined from CO_2 & long N_2 gas adsorption tests on key SS samples

Sample	**BET Surface Area**	**Vultra**	**Vsuper**	**Vmicro**	**Vmeso**	**Vtot**	**Av. Pore Diameter**
	m^2/g	cm^3/g	cm^3/g	cm^3/g	cm^3/g	cm^3/g	nm
SS-HTC-PYR-800-0.5	155	0.0379	0.0161	0.0540	0.0235	0.0785	2.03
SS-HTC-ACT-800-0.5	192	0.0352	0.0199	0.0551	0.1564	0.2157	4.49

Table 5.52 Structural data determined by MIP & helium pycnometry on key SS samples

Sample	**Pore Area**	**Vinter**	**Vmacro**	**Vmeso**	**Vtot***	**Av. Diameter**	**Bulk Density**	**Skeletal Density**	**Porosity**
	m^2/g	cm^3/g	cm^3/g	cm^3/g	cm^3/g	nm	g/cm^3	g/cm^3	%
SS-HTC-PYR-800-0.5	2	0.184	0.187	0.008	0.194	737	1.08	2.45	56
SS-HTC-ACT-800-0.5	62	0.238	0.183	0.153	0.335	37	0.92	2.72	66

Vtot is the sum of Vmacro & Vmeso, disregarding Vinter.

5.3.5 SS Detailed Characterization

The results from the in-depth adsorption tests can be seen in Table 5.51 above. The BET surface area of both samples has dropped from the initial tests. The microporous volumes have both dropped, however the pyrolysis sample has dropped more, making them even. The pyrolysis sample has a higher ultra-micropore volume. The CO_2 adsorption isotherms of the two samples can be seen in Figure 5.37. Both display Type 1 isotherms, displaying the presence of micropores in both. The pyrolysis sample is superior in this category, the higher ultra-micropore volume causes the red line to rise sharply. Despite the blue line having a larger Vsuper and Vmeso, it remains below the red line, offering half the adsorption capacity. The red line offers slightly less capacity than the competing SP and CG pyrolysis samples. However, it is dwarfed by the activation samples representing the other materials.

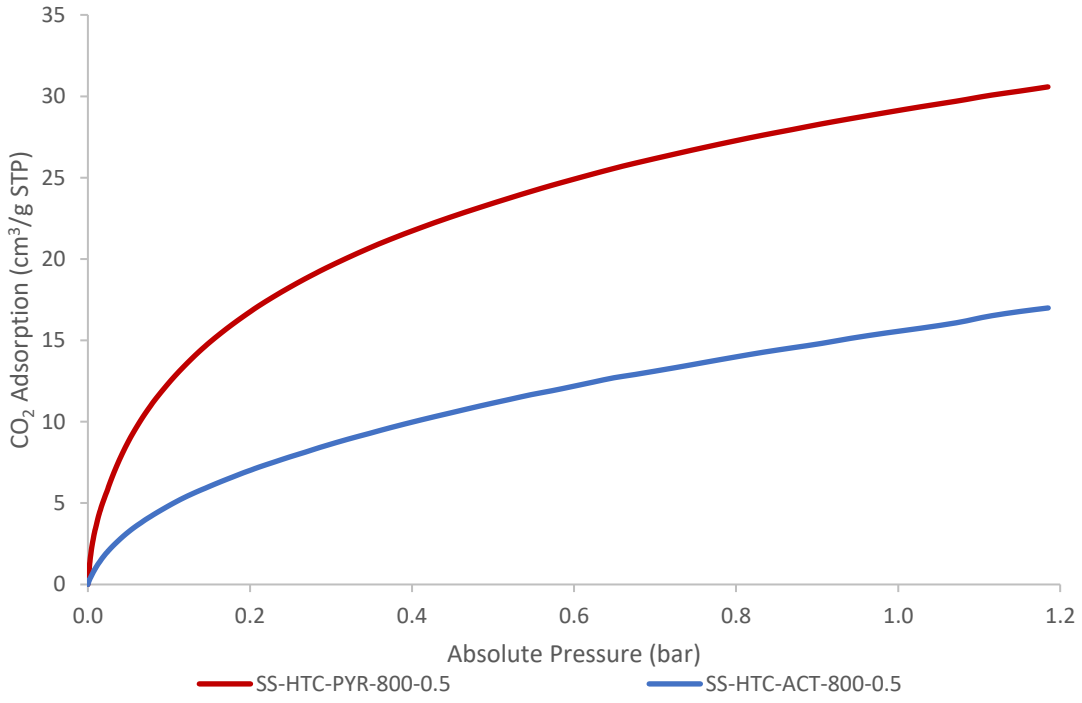

Figure 5.37 CO_2 adsorption isotherms of key SS samples

The mesopore volume of each sample has reduced through this test, and thus the total pore volumes have reduced as well. The average pore diameters have increased, pushing the pyrolysis sample over 2 nm. The nitrogen isotherms are shown in Figure 5.38. Here the activation sample performs better due to the much greater mesopore value. It displays a typical Type 4 isotherm, which grows continuously within the mesopore range and accelerates at the end showing large mesopores and the onset of macropores. The hysteresis loop is reminiscent of a Type H5. This would indicate mesopores which are open and partially blocked. The structure will be controlled by the presence of ash which may be a part of some pore walls and blocking others. The adsorbate cavitates at 0.45 relative pressure. The red line remains a Type 1a isotherm, mainly microporous, but a small presence of mesopores. The hysteresis loop remains horizontal and cavitates at 0.45 relative pressure. This could illustrate pore shielding, and mesopores pre-existing within the sample, as there is no activating agent to widen the pores. It is displaying Type H4 hysteresis, which will be impacted by the non-ridged structure of the ash.

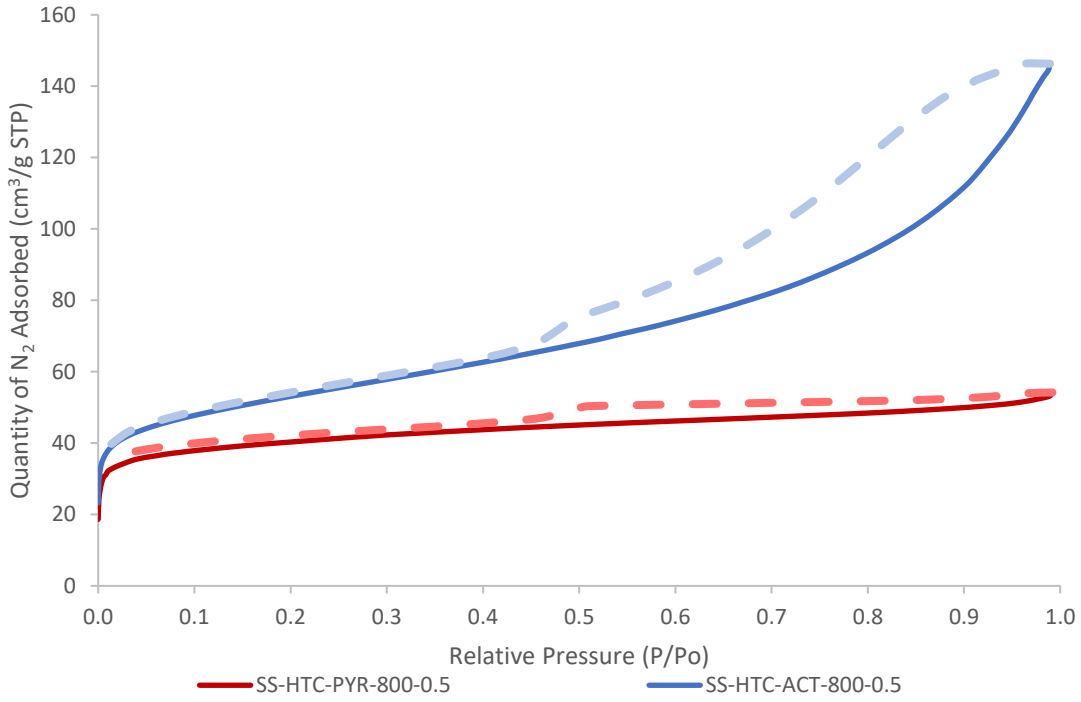

Figure 5.38 N_2 adsorption isotherms of key SS samples

The results from MIP and helium pycnometry are seen in Table 5.52. The Vinter value has been excluded from the total volume. The macropore volume is very similar, which is displayed on the cumulative intrusion chart in Figure 5.39. The pyrolysis sample, red, has a smooth curve between at 50 – 5000 nm which encapsulates the macropore region. This characteristic is carried through into the activation sample, with the same rounded shape repeated in the same position. This shows the macropore structure seems unaffected by the activation. Potentially it is influence by the structure of the ash, allowing it to be so consistent between samples. Below the macropore range, the pyrolysis sample plateaus and has very little movement in the mesoporous range. Whereas the activation sample rises at 20 nm. The increased total pore volume is found here, which adds an extra 75 % total pore volume on to the activation sample compared to the pyrolysis sample. This growth is from the pyrolysis micropores seen in Figure 5.37 growing into mesopores with the aid of the activating agent. This may explain the why the blue line is below the red line in the CO_2 adsorption chart. The mesopore volume for the pyrolysis sample is so low, compared to the nitrogen adsorption. This suggests pore shielding within the material. Neither sample is particularly porous, however the activation has succeeded in improving the porosity, through the increased pore volume present. The density will be impacted by the low pore volumes and high ash content. The high skeletal density is most likely influenced by the high ash content in each sample.

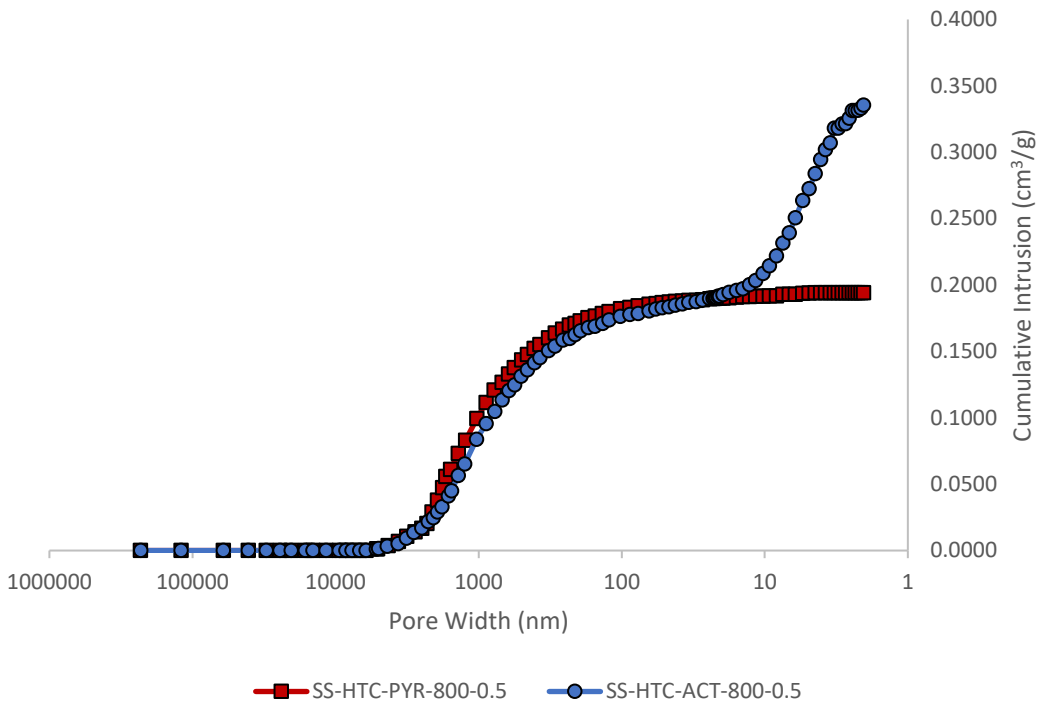

Figure 5.39 Cumulative intrusion from MIP of SS samples excluding interparticulate void space

5.3.6 SS Summary

This study has shown that although sewage sludge can be activated, there a few benefits of introducing the activating agent. The pyrolysis phase alone produces the highest surface area and has a narrower micropore range. Activating the sample causes a widening of the pores, causing growth in the mesopore range, and the creation of new micropores. The root cause of this is loss from the fixed carbon composition. However, the carbon fraction in the hydrochar is low, so once the losses are accounted for, only a small amount of AC is created. The central column in Table 5.53 shows the carbon mass in the activated hydrochar as a fraction of the sample starting mass. The range is all within single figures, with some demonstrating that no carbon remained. The carbon yield column shows that all samples had > 70 % carbon removal from the activating agent, however the surface areas and pore volumes produced do not meet the expectation of a commercial activated carbon.

Table 5.53 Carbon mass remaining post activation from 5 g SS-HTC samples

Sample Name	Activated Hydrochar Carbon Mass	Carbon Retained from SS-HTC (5 g)	Carbon Yield
	g	%	%
SS-HTC-ACT-700-0.5	0.47	9.4	28.8
SS-HTC-ACT-750-0.5	0.31	6.2	19.2
SS-HTC-ACT-800-0.5	0.20	3.9	12.0
SS-HTC-ACT-850-0.5	0.03	0.6	2.0
SS-HTC-ACT-900-0.5	0.00	0.0	0.0
SS-HTC-ACT-950-0.5	0.00	0.0	0.0
SS-HTC-ACT-700-1	0.34	6.7	20.5
SS-HTC-ACT-750-1	0.21	4.1	12.5

SS-HTC-ACT-800-1	0.09	1.9	5.7
SS-HTC-ACT-850-1	0.00	0.0	0.0
SS-HTC-ACT-900-1	0.00	0.0	0.0
SS-HTC-ACT-700-2	0.25	5.1	15.9
SS-HTC-ACT-750-2	0.11	2.2	6.9
SS-HTC-ACT-800-2	0.02	0.4	1.2
SS-HTC-ACT-850-2	0.00	0.0	0.0
SS-HTC-ACT-700-4	0.18	3.6	11.1

The highest carbon content proportionally is seen after the pyrolysis phase. This sample has a greater surface area and higher microporosity. In terms of the yield, there is more product available. The sample is still plagued by a large ash content. The material is predisposition to fail as an AC due to the large ash content. There is potential for leaching and adding an additional pre-treatment process, but for the fraction of carbon available, the practice would create more steps for little gain. Figure 5.40 shows the ash sample of SS, central vial, compared to the ash sample from SP, left vial. The SP ash is much finer and sandier. SS retains the initial pellet shape from the strength of the ash. There is a stark difference in colour, showing the difference in constituents that make up each ash sample. The vial on the right shows an activated SS hydrochar. The colour is not as bright as the purely ash sample.



Figure 5.40 Left, SP ash, centre, SS ash, right, SS activated hydrochar

The study collected by Saetea and Nakorn (2013) shows surface areas approaching 600 m^2/g at steam activation conditions of 900 °C. In this thesis, the results were attempted to be replicated. So, this experiment also followed the 30-, 60- and 90-minute timeframes set out by Saetea and Nakorn, as well as testing more temperature set points to optimise the process. This experiment has found that lower temperature is more effective for activating SS. The study by Saetea and Nakorn shows 40 % ash content is in the equivalent sample to SS-HTC. The losses faced by a SS sample at 900 °C for any timeframe returned no carbon carbon in this testing set up, and the highest recorded surface area is 220 m^2/g. The only conceivable way the reported results make sense, especially as the starting ash content is higher than in this experiment, is if the ash content is particularly porous (such as silica) and contributed surface area, or the results have been manipulated to exclude the presence of ash. With that in mind, Table 5.54 presents the results for this experiment if the surface area is attributed to the non-ash fraction. Based on the final column, the value can be greatly inflated compared to the measured value. The low temperature samples are on par with the study by Saetea and Nakorn, but the highest ash content samples attribute the

surface area to a tiny mass fraction creating unrealistic surface areas. These values cannot be used to characterize the material.

Table 5.54 Manipulated surface area to exclude ash

Sample Name	Activated Hydrochar Ash Fraction	BET Surface Area of Total Sample	Ash Free Surface Area
	%	m^2/g	m^2/g
SS-HTC-ACT-700-0.5	58.8	182	442
SS-HTC-ACT-750-0.5	66.6	202	605
SS-HTC-ACT-800-0.5	79.5	217	1057
SS-HTC-ACT-850-0.5	89.9	94	932
SS-HTC-ACT-900-0.5	99.7	4	1487
SS-HTC-ACT-950-0.5	99.8	1	749
SS-HTC-ACT-700-1	63.5	220	603
SS-HTC-ACT-750-1	73.1	189	701
SS-HTC-ACT-800-1	79.5	156	762
SS-HTC-ACT-850-1	99.8	6	2884
SS-HTC-ACT-900-1	99.7	2	741
SS-HTC-ACT-700-2	72.8	207	761
SS-HTC-ACT-750-2	84.4	133	854
SS-HTC-ACT-800-2	97.3	30	1122
SS-HTC-ACT-850-2	99.7	4	1377
SS-HTC-ACT-700-4	80.1	191	958

Ultimately, the target of 585 m^2/g was not met or surpassed. No sample produced a commercial grade AC. The carbon yield is seen to be too low, and the ash content is too high. The pyrolysis sample arguably creates a similar material, with a different emphasis on the microporosity and microporosity. Even then it is most likely not worth the expenditure of the pyrolysis process unless the sample is gasified to collect the volatiles. The sample is better purposed as a fuel stock. Under the activation conditions used, the sample has not created a successful activated carbon from sewage sludge hydrochar. However, the HTC process is still able to continuously treat sewage sludge to produce a low-grade fuel.

5.4 Application Test: Adsorption of Organic Material from HTC Process Water with Activated Hydrochars

AC is known for its ability to remove organic matter from wastewater, this test will trial a range of materials produced in this study. It has been noted that despite identical activation methods, the variations in the starting material are enough to separate SP and CG AC. Firstly GC AC is a highly microporous material. It has shown to produce a higher yield with a lower ash proportion. The material is thought to be suitable for gas adsorption applications. SP on the other hand is a much more mesoporous carbon. In that respect, the surface area is not as great as CG, but it can be useful for different applications. The materials are hypothesized to be suitable for wastewater treatment and the removal of large organic materials.

To test this theory, batch sorption studies were conducted for the removal of colour and organic matter from HTC process water. The tests used hydrochars, activated hydrochars and a consumer grade AC. The samples were tested on HTC process water collected from the CG pre-treatment method which produced CG-HTC. This section introduces a commercial AC comparison material, which has been labelled 'GAC'. The material was purchased from APC Pure and is derived from charcoal. GAC was ground between 150 µm – 1 mm using a manual coffee grinder and sieved to the correct fraction. The assessed capacities of GAC are listed below in Table 5.55. The material offers a legitimacy control for commercial competitors, and it meets the threshold of a commercial AC that this study has been working to.

Table 5.55 'Charcoal activated granular' or 'GAC' specifications

Sample	BET Surface Area	Micropore Volume	Mesopore Volume	Total Volume	Average Pore Diameter	Microporosity	Mesoporosity
	m^2/g	cm^3/g	cm^3/g	cm^3/g	nm	%	%
GAC	841	0.309	0.036	0.349	1.23	89	10

Analysis performed on Micrometrics 2420 ASAP. Relative density: 1.8 - 2.1 g/cm³. Material CAS number: 7440-44-0. EINECS number: 231-153-3. Product code: GPC8059

Desired loadings were attained by adding 0.5 g of each sample to 10 ml of untreated HTC process water. For these results, the absorbance was measured undiluted. The values at 470 nm are reported, as this was the wavelength corresponding to the highest unsaturated absorbance in untreated HTC process water. The process water results were recorded as a control and labelled as 'initial'. The results can be seen in Figure 5.41.

The hydrochar samples SP-HTC and CG-HTC had little impact on TOC, due the low porosities, 19 m^2/g and 39 m^2/g respectively but were able to remove about half of the coloured material absorbing at 470 nm. The TOC in SP-HTC measured higher than the initial batch, which may indicate the hydrochars can introduce more pollutants into the effluent. The activation has improved the adsorption in all the hydrochars. SP-HTC-ACT-700-2 demonstrated the least improvement, particularly with the removal of coloured material. This may be owing to the low activation temperature which may not have developed the material enough. This sample had the lowest surface area of the ACs trialled and the lowest micropore and mesopore volume of the SP hydrochars tested.

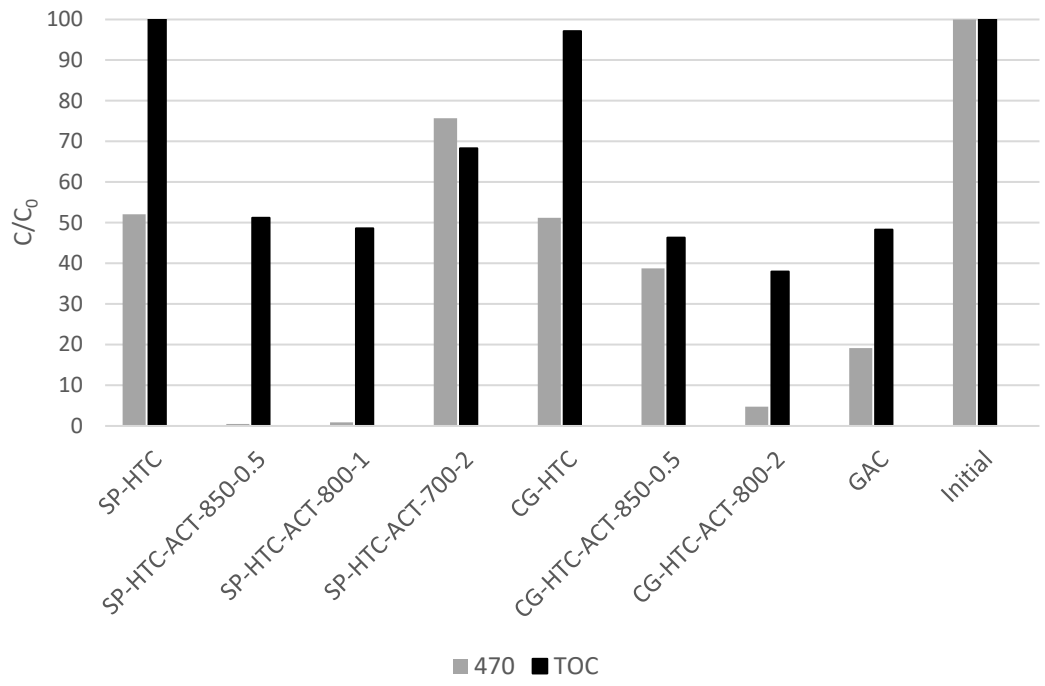

Figure 5.41 TOC and absorbance at 470 nm for HTC process water after batch adsorption at 50 mg / ml

The remaining results show a strong performance from the synthesized materials. The TOC removal of the remaining samples equalled or surpassed the performance of GAC. SP-HTC-ACT-850-0.5, SP-HTC-ACT-800-1 and CG-HTC-ACT-800-2 all exceeded the removal of coloured material by GAC. The best removal of coloured material came from these two SP samples, with both removing > 99 %. Both had similarly high surface areas and high pore volumes which had relatively equal split between micropore and mesopore volume. Comparing the coffee samples, the largest difference between the structures was found to be the mesopore volume also. The sample which performed better had a far superior mesopore volume. The weakest performing samples are lacking a developed mesopores, which appears integral to success in this test. It is predicted that SP-HTC-ACT-850-0.5 R200, the lower temperature HTC sample, would produce superior results to the SP-HTC-ACT-850-0.5 sample which was tested. GAC itself was found to have a strong micropore value but lacked a defined mesoporous fraction. The material may not be suited to this exact application.

The study presents a brief trial of a real-world application. This proposes the possibility of using the SP samples to treat organics in wastewater, but further investigation should be undertaken to better understand the logistics of this and its efficiency. The CG samples perform well, but water treatment may not be the ideal supplication for the highly microporous material. There may also be complications which prevent a material from treating its own process water.

5.5 Discussion

In this study it has been found that the materials tested benefitted from the introduction of a pre-treatment phase before physical activation. It could be claimed that it is necessary to treat the waste materials with HTC before activating. In the case of SP, the raw material was stable enough to produce surface areas > 700 m^2/g with mesoporous tendencies. However, without the pre-treatment the pellets were more susceptible to losses at identical activation conditions, producing far lower yields. The AC produced could not contend with the activated hydrochar in terms of key performance measurements. A major issue was the ash component, which became a leading presence in the material due to the rapid burn off. Despite the successful production of both raw AC and activated hydrochar, the latter material was a superior product. For CG experiments, the use of an HTC pre-treatment is more clearcut. Activating raw CG under the methodology proved unpredictable. The experiment would routinely return no product, through a combination of burn off, elutriation, and sample fragility. Samples which had been treated were much more resistant to loss, allowing a controlled reaction which developed a highly microporous structure. In terms of SS, the material was not trialled without HTC, but the process treats a biologically active waste into a useable product, but activation is not a suitable use.

Throughout the study, the pre-treated materials have been referred to as hydrochars. While the materials were placed in reactors and treated within the accepted HTC range, there is an argument that the biomass did not undergo HTC during the pre-treatment. Rather, the material produced is simply an upgraded biomass, instead of a traditional hydrochar. Both SP and SS were subjected to and held at a temperature between 200 – 220 °C. Due to the nature of the large-scale continuous unit, the exact parameters cannot be pinpointed at the time of production. But it is guaranteed to have operated at 200 °C as a minimum standard. There is less data for the SP HTC pre-treatment process. So, the slurry DS content was measured on the inlet as 12%, but the outlet was not measured so a mass balance cannot be performed to shaw up the claim, and the process water was not studied.

As part of the project, the aim was to be the first to produce ACs from a large-scale HTC plant. Despite best efforts, including personal operation of the pilot plant, some things are out of the control of a research project, such as tailoring the operational conditions of a pilot plant to the needs of this thesis. Therefore, this was the only way to collect an industrially processed sample. Studies have shown cellulose will decompose at 200 °C in subcritical water. The reaction will not run to completion, but the duration has an impact (Gagic et al., 2018). This reaction was allowed to continue for 10 hours, so it should meet some specifications of an HTC reaction. Additionally due to the design of the unit, pressure was not autogenic and could be increased manually, which can impact the product. A study using decoupled temperature and pressure hydrothermal reactions at 200 °C were able to replicate the product of a typical HTC autogenous reaction conducted at 230 °C (Yu et al., 2023). Considering the pre-treatment conditions, and the compositional changes recognised in SP-HTC, the material has undergone an HTC treatment, but it is ceded that it has not been run to completion. Although this may be the case, the results prove that the pre-treatment method used has caused a major improvement to the materials ability to be converted into activated carbon. This step has upgraded the material, and there is potentially more efficiency to be found by optimising the pre-treatment step. 220 °C been shown to be the most economical temperature for HTC (Kim, Lee & Park, 2016). It is a

consideration for future work to vary the conditions of the HTC process and potentially make a higher quality AC from the waste. Conversely, an increased temperature would incur increased energy usage and production cost. This would have to be justified by the production of a more robust material, which is less susceptible to losses in the activation step and retain a similar, or better, internal structure. Taking this into account, this study can be considered the first foray into activating hydrochars produced from industrial HTC equipment which can be a first step towards activating directly from HTC plants.

As CG was unable to be processed in the large continuous unit, the conditions were replicated in the small-scale batch process as a mimic of the large-scale production. The greater control over a small-scale batch reactor allowed the parameters to be controlled and dictated easier, hence why 220 °C was used as the reaction condition. Based on the chemical makeup of the coffee grounds, the material would have been subjected to the mechanisms of HTC. Studies conducted by Crossley et al. (2020) and Campbell et al. (2021), were research projects in parallel with this project, under the umbrella of Antaco Ltd. They focussed their attention on the process water, from the coffee grounds HTC batch rig. From their analysis of the process water, it shows key components were present in the process water, which are synonymous with the HTC reaction taking place. The results of 56 % char yield and 82 % carbon yield follows the trend HTC reactions. Based on this, there is confidence that CG underwent an effective HTC pre-treatment, meaning that this thesis has physically activated CG hydrochar under these conditions for the first time.

It has been alluded to above, that the CG products were very microporous, whereas the SP hydrochars were more balanced between mesopores and micropores, with many forming a more mesoporous material. Throughout the study it has been attributed as an inherent feature of the materials to form this structure. However, the characteristic might not be intrinsically linked to the material itself. This trait may be a product of the HTC pre-treatment conditions. In Section 5.2.7 the shortcomings of the SP pre-treatment conditions were addressed, and CG was pre-treated at 200 °C in the batch reactor and then activated. Compared to CG prepared at 220 °C, it created a much weaker precursor. The results showed a material which was more immediately impacted by the activation conditions. This resulted in a 37 % drop in yield. The additional losses formed a greater surface area and pore volume, upgrading the AC by around 200 m^2/g and 0.2 cm^3/g respectively. The materials response towards the activation conditions were more like the properties found in the SP experiments This raised questions over whether the AC characteristics were a product of the material or the method. Table 5.56 shows a comparison of SP and CG pre-treated and activated at the same conditions, as well as the higher temperature HTC CG sample, activated under the same conditions.

Table 5.56 Yield comparison at 850 °C for 30-minutes

	CG-HTC-ACT-850-0.5	CG-HTC-ACT-850-0.5 R200	SP-HTC-ACT-850-0.5
Hydrochar Yield %	23.7	14.9	13.4
Carbon Yield %	79.4	47.6	42.2
Carbon Content %	95	81	82
Oxygen Content %	0	14	4
Ash Content %	1	4	13
Surface Area m^2/g	981	1174	898

Micropore Volume cm^3/g	0.34	0.40	0.29
Mesopore Volume cm^3/g	0.02	0.14	0.26
Total Pore Volume cm^3/g	0.36	0.55	0.55
Microporosity %	94	73	52

There are many similarities between CG-HTC-ACT-850-0.5 R200 and SP-HTC-ACT-850-0.5. Both the hydrochar yield and carbon yield are close together. The materials carbon contents are comparable, and the total pore volume is identical. There is a shared trend of an increased ash content and a greater ability to chemisorb oxygen. However, these attributes are mostly in favour of the GC sample. It is recognised that the type of HTC apparatus may also have an impact, which cannot be disproven. The similarities between the samples end as the surface area is much larger in the CG sample. Although the ash trends were in line, the ash content in strawberry is much more prominent. These are products of the initial material, as CG starts with less ash and more fixed carbon, so there is a greater body of fixed carbon to activate. Also, despite matching the pore volumes, the breakdown tells a different story. The coffee continues to exude a highly microporous volume, explaining the high surface area, whereas the strawberry eclipses both CG samples with the mesopore volume. Yet there is growth in the mesopore volume in CG-HTC-ACT-850-0.5 R200 compared to the original sample. This shows the characteristics of the char meet somewhere in the middle, as per the microporosity row, offering features from both materials. An interesting development from the desorption isotherms showed that the regularly microporous CG samples had a smooth desorption curve which matched the adsorption. However, the introduction of the larger mesopore bracket in CG-HTC-ACT-850-0.5 R200 created pore shielding from a range of neck widths. This is more in line with the SP tests, which all showed symptoms of hysteresis.

The analysis shows the answer is not as contrasting as 'one or the other'. The pre-treatment conditions impact the activation trends of the material, but the arrangement of the precursor sets the precedent for the materials potential. The coffee hydrochar would be deemed a higher quality AC, and CG is considered the better suited material for activation overall. It can be concluded that CG is predisposition to produce more microporous carbons, whereas SP is more suited to creating more mesoporous carbon. This is not seen as a negative trait and should be considered on the contrary. As observed in the application test in Section 5.4, only the samples with a suitably wide pore size were able to treat the process water, and the most effective samples at removal of coloured material. The pre-treatment conditions will have a bearing on the materials final form.

The various pore sizes present different strengths and weaknesses. It can be noted that this information adds the ability to fine tune the product based on the required application. A lower temperature HTC pre-treatment is more likely to form a more mesoporous AC with greater oxygen surface functionality, under the activation method used. The use of time and temperature can also be used to tailor the pore size range. The impact of this was demonstrated during this experiment. In each of the materials tested, it was seen that as temperature was increased, the loss endured by the material also increased. This was also the case as time was increased. This had a direct impact on the internal structure of the sample, through measurements of pore volume, pore size distribution, and surface area. Higher temperatures led to a faster mass removal. In SP this was recognised by the development in the mesoporous zone. More extreme conditions favoured a larger pore

volume, benefitting the development of the macropore region also. In CG this was acknowledged by a larger increase in micropores, which was significant in the growth of surface area. This was distinguished by ultra-micropores growing into super-micropores. Figure 5.42 and 5.43 demonstrates this knock-on effect by placing the variable of mass loss, which was as a direct result of the conditions, on the x-axis. In Figure 5.42, the pore volume in activated SP and CG continue to rise in an upward fashion. The trend of activated SP is steeper than activated CG, due to the larger mesopores, which usually contribute more to the total pore volume than micropores. The trend continues to rise in these samples. This is as more mass is removed from the bulk and surface, so the pore volume continues to increase. A capitulation was not met with these samples, however there is a turning point in the activated SS trend where the total pore volume falls away. This will be due to pore sizes increasing above the mesoporous range and the complete loss of carbon, as SS was found to be 16 % ash, hence why is falls away so early with respect to mass lost. The growth in pore volume did not have a linear relationship with temperature and would peak and rapidly fall away. This was the case when the fixed carbon fraction was depleted.

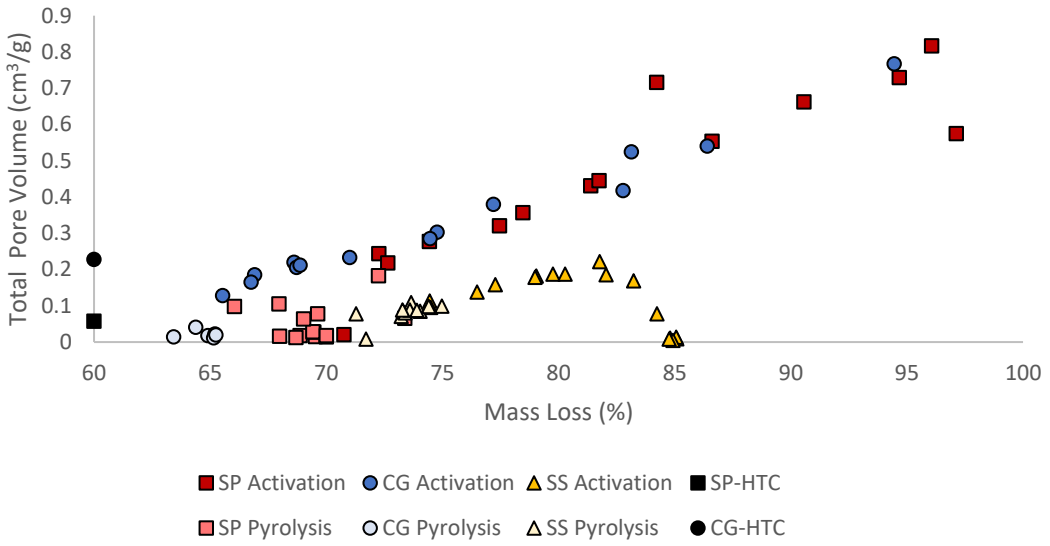

Figure 5.42 Total pore volume against mass loss of all samples. Precursors SP-HTC & CG-HTC have been placed on the chart for an appreciation of pore volume development, the mass loss value is arbitrary

In Figure 5.43, the surface area is displayed as a result of mass loss. Activated CG has the superior surface area characteristics throughout, as the loss is exposed in micropore region, so a lower mass removal is required to develop more pore walls. From the mass loss recorded, there is potential for higher surface areas to be achieved in the future by using more extreme conditions, as CG has proven to be more resistant to loss than SP. The trend of activated SP is down and to the right of the chart, relative to activated CG, as more loss is required to equal a relative surface area, and it does not meet the same peak recorded surface area as activated CG. The trend begins to plateau showing more loss does not always form more surface area. At this point the losses sustained are most likely removing surface area through the widening and connecting of pores. However, the development of new micropores is able to balance the reduction through mass loss. On the other hand, the reverse trend is shown for activated SS, which recorded the highest surface area in the pyrolysis samples and the degradation from activation is too much for the sample.

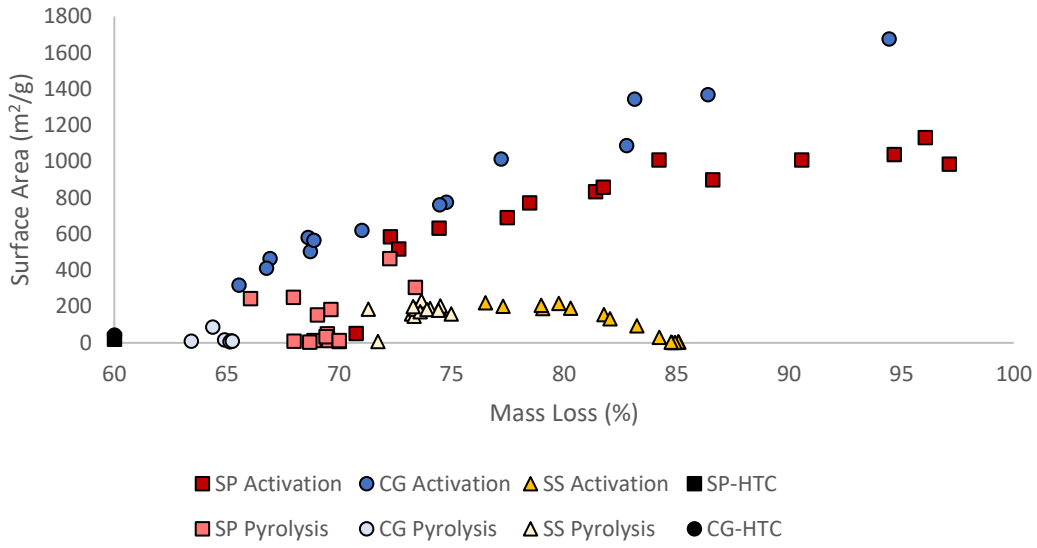

Figure 5.43 Surface area against mass loss for all samples. Precursors SP-HTC & CG-HTC have been placed on the chart for an appreciation of surface area growth, the mass loss value is arbitrary

The shortcomings of SS as an AC are evident to see here when the surface area and pore volume is compared to SP and CG. There are pyrolysis samples which perform better than activated SS. The pyrolysis samples are displayed in the charts to demonstrate that the steam activating agent is the crucial parameter for development. Ultimately the activation conditions of time and temperature have a direct correlation with the mass loss, which in turn, leads to the chain of events which impacts the sample porosity.

Temperature was found to be the biggest influence between the parameters varied. An increased activation duration was also found to increase mass loss, and ultimately improve porosity. It is difficult to judge two parameters with different units, however, each incremental increase did not have the same relative impact on mass loss or pore development as temperature did. The impact of each 50 °C increment on SP activation had steady 1 – 1.4 multiplier on surface area and 1.2 – 1.7 on pore volume, compared to a 30-minute interval which would begin at a similar level but drop off above an hour. In CG activation, a 50 °C increment increased the surface area by 1.2 – 1.4 times and the pore volume by 1.2 – 1.6 times. The multiplier for a 30-minute increment was lower than the impact of temperature initially, and then follows the same trend of falling away at higher timeframes.

The optimum conditions were found to be between 750 – 800 °C for 1 – 2 hours when activating SP. This was different to the optimum conditions for activating CG, which was around 850 °C for between 0.5 – 1 hour. The difference in conditions is representative of the material's varying levels of reactivity. SP was seen to be more suspectable to losses under the activation conditions, hence why the temperature range is lower. The timeframe is longer, but as we have seen, the duration has less impact and becomes less influential as time goes on. For CG, the temperature chosen was due to the material seemingly peaking at this point in key sample characteristics. A sample at above 850 °C for 1 hour was not run, but it would likely incur too much loss, despite any improvements that would most likely be made to the surface area and pore volume. The optimum range was not select based on the material that created the biggest values. This was adjudged by balancing a distribution of favourable results in all parameters measured, and importantly, a high yield. The

relationship between quality and quantity appears inversely proportional and a balance must be struck to retain enough product which is functional. The aspiration of this study used a framework of achieving 15 % yield of a highly carbonaceous material (85 – 95 carbon wt%) with a varied pore size distribution, exuding 800 m^2/g surface area and 0.2 cm^3/g pore volume. Within the range, all these attributes have been met. Being critical of the materials, CG may have too little mesoporosity, which may impact adsorption and transportation within the material. SP suffers too great of a yield loss at 800 °C which creates a large ash fraction, so the optimum temperature is closer to 750 °C than 800°C. This ash fraction is the main inhibitor in activated SP samples from reaching the threshold of 85 % carbon content. This study acts as the first AC made from SP, through the raw experiments and the first through HTC pre-treatment, poising SP as a mesoporous carbon with ash problems. The material has potential, and the technology is a good recycling stream for the waste.

The yield is the single biggest denominator as to whether the process is viable. Losses in the activation are shown to be integral to the development of pores. At various points of the thesis, yield has been presented as hydrochar yield, carbon yield, and activation yield. However, there are carbon losses across the entire process which have not yet been taken into account. Rather than just comparing the raw and hydrochar activation yields, this section investigates the whole life carbon across the project and questions whether those losses can be justified.

The key activation samples for SP and CG have been used as examples in Sankey mass flow diagrams, focussing on the carbon and ash, seen in Figures 5.44 – 5.47. The diagrams flow from left to right. Each graph shows the input of a 100 g raw biomass waste sample. The sum assumes we start with 100 g of product, for ease of comparison, but the yields may fluctuate in a scaled operation*. The black bar represents raw biomass at the beginning of the process, and the brown bars to the right represent the carbon journey through pre-treatment and activation. The top right corner of each graph shows the final carbon weightage. The pink bar also shows the ash contribution throughout, ending bottom right.

The first case studied will be the full treatment of CG-RAW into CG-HTC-ACT-850, displayed in Figure 5.44. The first split in the carbon column, brown, is due to the HTC process and it shows that 45 % of the starting carbon is removed in the process wastewater. This loss has not previously been factored into the activation yield. The upper route shows the carbon retained in CG-HTC. The next split is the losses encountered in the pyrolysis phase, through the removal of volatiles. Continuing along the top pathway, the next split is where the steam activation takes place. From the initial starting mass, 21 % carbon is retained, which is a profound different to the 76 % carbon retention calculated during the activation. Similarly, considering the carbon fraction of the final sample, this represents a 12.8 % overall process yield from CG-RAW, whereas the activation calculation from CG-HTC-ACT-850-0.5 misrepresents the yield as 22.8 %. Figure 5.45 shows the more straightforward transition of the direct activation of the raw sample. By comparing the two charts the difference in carbon retention is now not as large and the pre-treatment method has lost some of its appeal, with the longer process returning an additional 33 %. It does show the impact of HTC on the ash fraction, which is less than 10 % of the non-treated sample. The ash component is seen to have a large removal after the HTC, and beyond that, it remains unaffected by the activation conditions.

*HTC was tested with 60 g, hydrochar activation using 5 g and raw activation using 10 g.

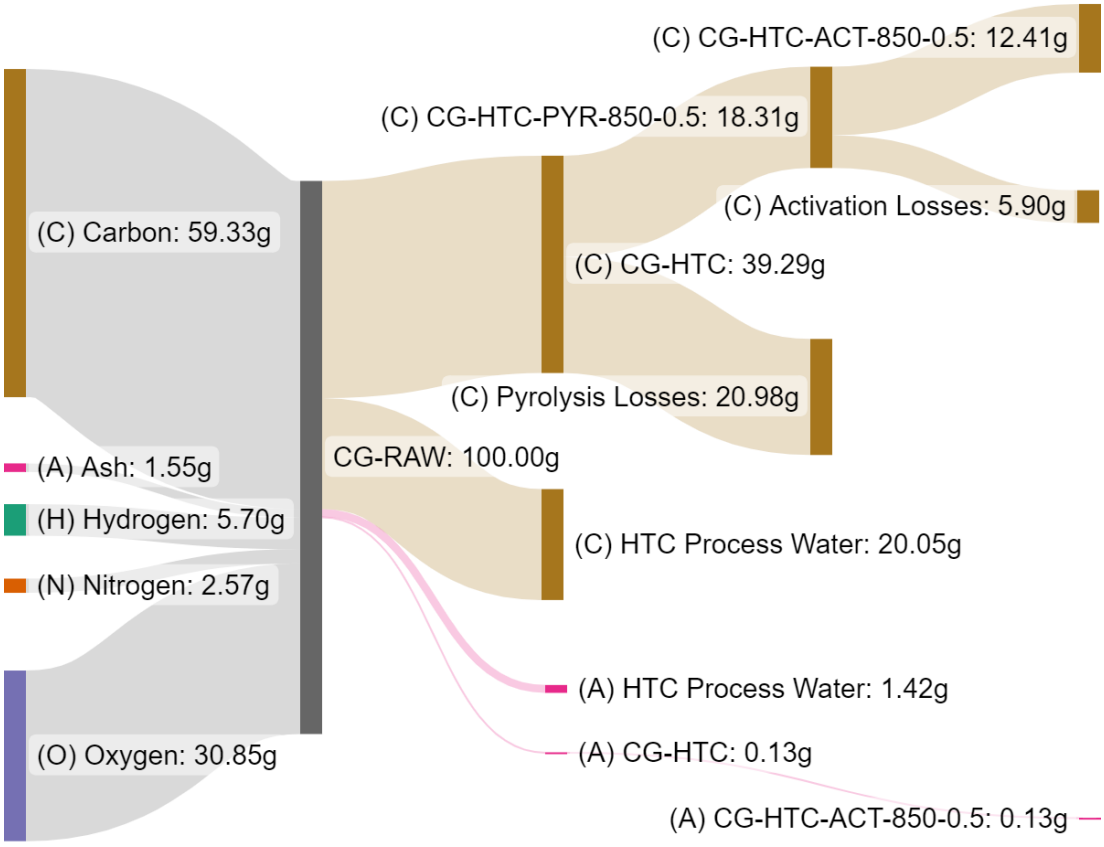

Figure 5.44 Mass flow of CG-HTC-850-0.5 production. Diagram created using SankeyMATIC

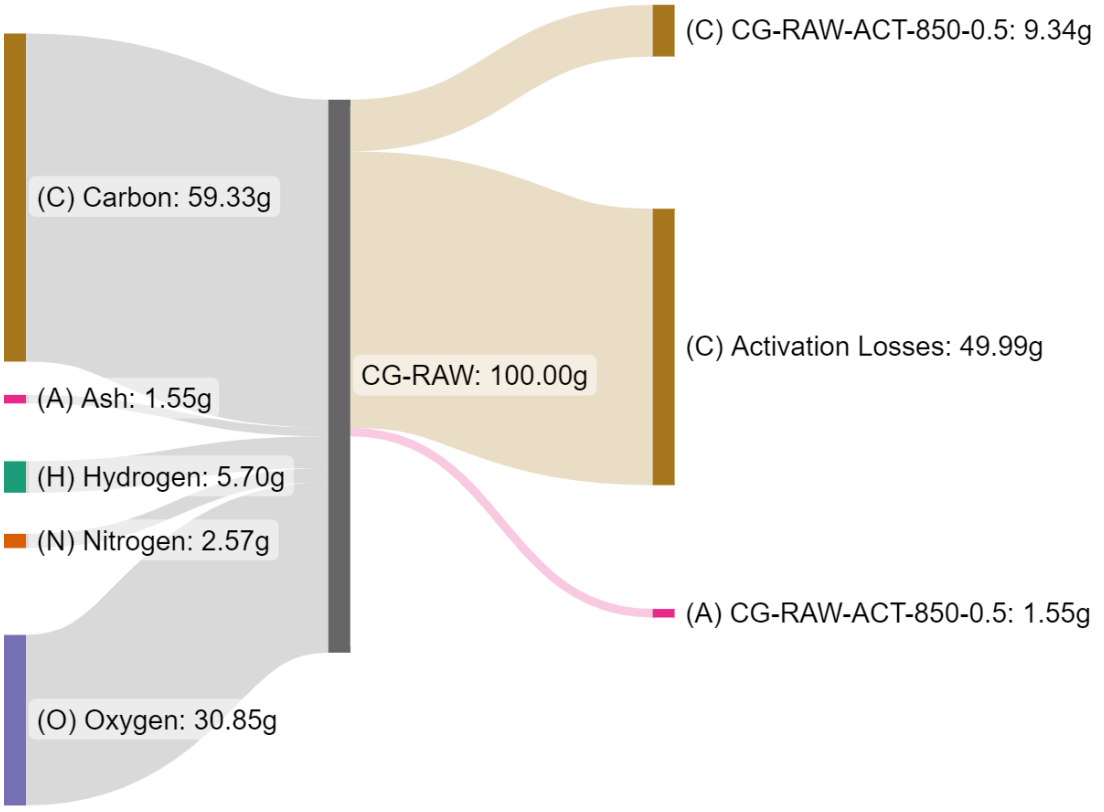

Figure 5.45 Mass flow of CG-RAW-850-0.5 production. Diagram created using SankeyMATIC

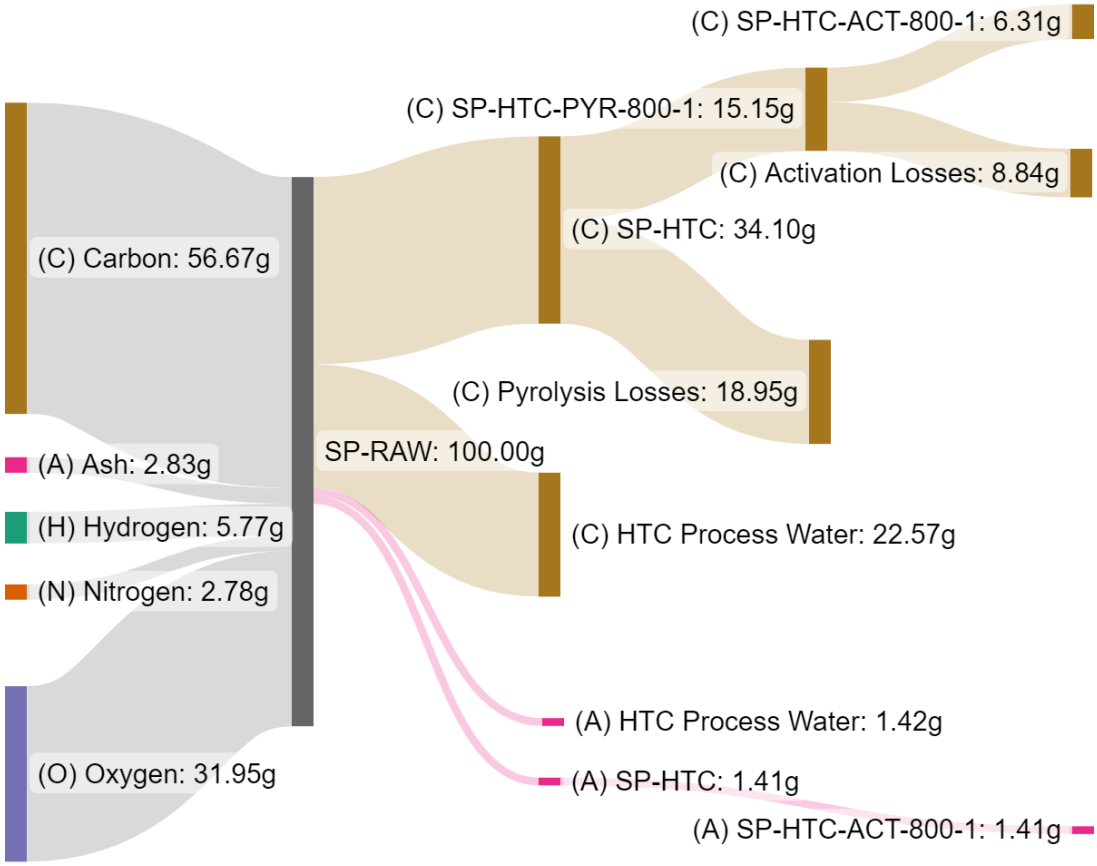

Figure 5.46 Mass flow of SP-HTC-800-1 production. Diagram created using SankeyMATIC

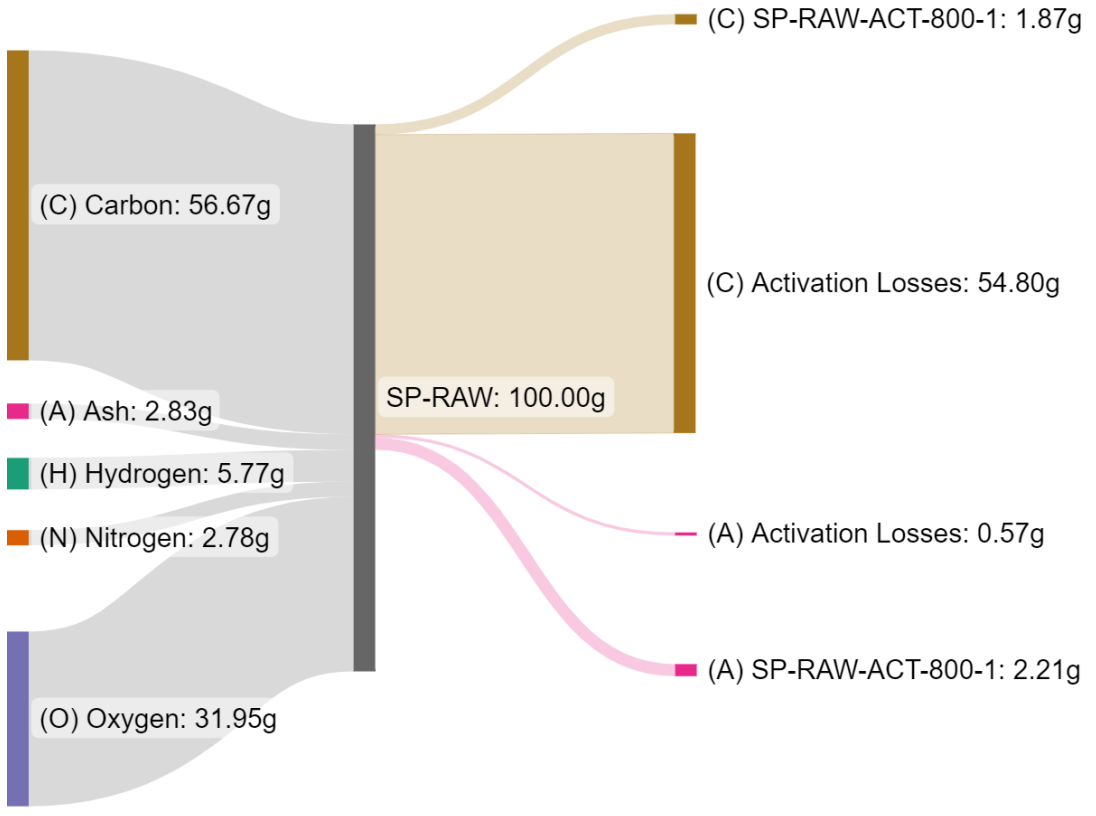

Figure 5.47 Mass flow of SP-RAW-800-1 production. Diagram created using SankeyMATIC

The other hydrochar ACs from the list of key samples have also been listed in Appendix Table 9.22 and 9.23.

In Figure 5.46, the transition from SP-HTC to SP-HTC-ACT-800-1 can be seen. An assumption has been made in the strawberry calculation due to the incomplete mass balance from the industrial processing unit. So, the solid yield from HTC has been assumed to be 55 %, which is equal to that calculated in the coffee sample. Although this most likely is not true, as a less complete reaction took place. The literature suggests higher activation temperatures reduce hydrochar yield, so the value calculated may be a slight underestimation (Congsomjit & Areeprasert, 2020), (Yu et al., 2020), although that is often in samples with a high lignin content (Hoekman et al., 2011), (Kang et al., 2012). The value calculated does not reflect well on the pre-treatment route as the process only returns 6.3 g of carbon. Although this it over three times the amount as the raw sample, it only amounts to an 11 % carbon yield and process yield of 8.5 %. The carbon yield is much lower than the initial calculated value of 38.7 % from the activation test alone. The original hydrochar yield for this sample was low to begin with at 12 %, so the reduction does not appear as stark. On the pink line, the removal of ash through HTC is highlighted. The low removal of ash in the HTC process may be due to the HTC process conditions, or from the starting ash content of SP-RAW compared to CG-RAW, as both processes remove the same mass of ash. The yield of Figure 5.47 is 4.2 %. Comparing these two charts shows the benefits of introducing the pre-treatment, as the raw sample contains more ash than carbon. But the process is limited overall by the high loss factored in across the process. Comparing the activated SP and CG charts, the losses are greater in the SP route, once again pointing out the frailties of the SP material. CG returns twice as much carbon as SP, although the starting concentration is higher. This reiterates that coffee appears better suited for activation.

The results display the advantages of installing the pre-treatment process, including the lower ash, higher carbon retention, greater yield, without going into detail on the vastly improved structure. However, despite the yield improvement, neither material meets 15 % yield target, so these benefits are reduced to marginal gains. The control of yield appears a common issue across the subject (Topcu et al., 2022), (Correa et al, 2017). Congsomjit & Areeprasert (2020) were able to produce hydrochar ACs from sugar cane bagasse using steam activation and reach yields between 14 – 27 % yield. However, the maximum surface area produced was 390 m^2/g, so perhaps the expectations should be tapered when dealing with more delicate waste organics. This research concurs with the findings that hydrochars produced at low HTC temperatures cannot withstand steam activation temperatures higher than 900 °C. Masoumi & Dalai (2020) were able to retain 25 % yield from algae and reach surface areas greater than 2100 m^2/g. This was using a KOH chemical activation. Potentially the mainstream production of AC from waste will not use traditional steam activation. Until the issues surrounding scaling chemical activation can be found, there is little alternative. This would be one way to reduce the losses experienced.

From a result driven research perspective, this project has been successful and a continued study to optimise the parameters is justified. A high-quality specification AC is generated from the CG sample and a functioning wastewater adsorption AC has been proven with the SP sample. But in terms of manufacturing a product from the material, there are many economic barriers in the way. Firstly, gathering the material would be a challenge. The production of SP from food manufacturers is niche and seasonal. The manufacturers will also generate several other waste products so additional tests would have to be conducted by combining multiple sources of waste to see if the product is compatible. In terms of coffee, the grounds are abundant, but distributed as small quantities in homes, offices, and retail stores. A contract with a large coffee multinational would be needed, but CG is

already in use for many other applications so there may be competition. To mass produce hydrochar would require dedicated HTC pilot plants, and as mentioned previously, they are still a rarity. Activation kilns are much more common, but the capital expenditure would be costly. The equipment is an ongoing responsibility and will require staff, maintenance, and a lot of energy to run. It is unlikely that combusting the hydrochar could power the HTC process and an activation plant, because of the temperature requirements for activation. The addition of an HTC process will introduce process water which must be treated to remove the organics and ash which it has been polluted with. In terms of financing the operation, there would most likely be no gate-fee for treating these materials, due to the non-hazardous nature of the material, So, the product must be of a quality to be marketed. The materials presented in this thesis would fit that quota. However, there is no guarantee the quality would remain if scaled from a 5 g test to a multi ton per day assembly line.

Balancing the economics may be challenging, as the whole process yield is 12.8 % for the optimal CG product. ACs can sell for an impressive price because of their functionality, versatility, and the manufacturing costs which factors the losses. The activated SP and CG hydrochar can be compared to some competitor's materials, in Table 5.57. The grading system of activated carbon is wide due to the many parameters which affect performance. The key figures for quality are surface area, pore volume and pore size distribution. Here is a selection of competing activated carbon products, with wastewater treatment in mind.

Table 5.57 Information on activated carbons recommended for wastewater treatment

Name	Type	Range	Surface Area m^2/g	Price / kg	Ash	Raw material
Filtrasorb	GAC	Micro	1050	£2.85	-	Coal
CYCLECARB	GAC	Meso	775 - 900	£0.90 - £1.65	-	Coal
GPP 20	GAC	Meso	725	£0.99	-	Coal
Antaco GAC	GAC	Micro	840	-	-	-
Antaco PAC	PAC	Meso	1120	-	-	-
Norit RB 4W	EAC	-	1100	1-35 euro/kilo	9 %	-
Norit 830W	GAC	-	1150	1-35 euro/kilo	12 %	Coal
Darco Hg	PAC	-	600	1-35 euro/kilo	-	Coal
Norit RK35	GAC	-	875	1-35 euro/kilo	7 %	-

Information received through sales team for respective companies

To surmise the broader project, replicating industrial grade activated carbon would require a process which would subject the material to 750 – 800 °C for approximately an hour. The resulting material should match the specifications of competitor carbon but at present will only account for around 13 % of the mass put in. Based on the research in the table above, the activated hydrochars should assume a minimum sale price of £1000 per ton and the

value of hydrochar commercially as £130/ton, then the production cost of 1 ton of AC must be below £350 in order to make it commercially viable and create a production line. Although if the activated carbon was simply for use within the HTC liquid post process only, then there are additional savings to consider from not outsourcing. So, the matter comes down to the quantity of activated carbon needed for wastewater treatment and whether the > 85 % loss is greater than the total hydrochar produced. An additional concern would be whether the activated carbon could be reactivated easily and effectively on site. This is a field that requires great depth of study, which is not in the scope of this thesis, but it is worth considering. The realisation of this technology is not currently feasible, especially with the current energy climate, but projects such as this can contribute to wider knowledge and help progress the industry.

Based on the results gathered the methodology overall should be considered a success. The activation conditions selected were broad and thorough, acknowledging that 700 °C is too low for real development and 900 °C is un upper boundary due to the associated losses. The use of the physical route and the selection of steam as an activating agent make it possible for the method to be trialled at a larger operating scale. Higher temperatures caused more losses and reduced the yield. However, the losses were liberated from within the material, so the mass loss resulted in greater porosity. As is the nature of research, the method did not always go to plan. The full list of experimental results is available in the Appendix. Table 9.6, 9.11 and 9.18 show the volume of liquid used for the activating agent. Despite using a single speed peristaltic pump and adhering to the timings, the same amount of steam was not always used to activate the samples. The steam was already in excess, so this shouldn't have impacted the process too much, as there were not drastic reductions. Human error could also come into play at times, as the pump was switched on and off manually, which would be timed with a stopwatch. Overall, the framework culminated in two quality ACs and one poor quality AC.

The issues with pre-treatment have been covered already. However, it can be said, based on the results, that the industrial production route is not yet as reliable, or high quality as the batch lab method. This is the case with scaled equipment still undergoing R&D and a risk that was considered. One assumption which was made throughout the thesis is that the pyrolysis sample is representative of the sample directly before the activating agent is introduced. However, these materials were run for the duration of time the activating agent would have been introduced for and then had a cool down period which could take over 6 hours. It was seen that there is little fluctuation between pyrolysis samples, and they reach a plateau of loss, but it is worth considering.

There may have been a degree of bias when selecting the activated hydrochar granules for analysis, such as in the gas adsorption tests, while trying to find the highest surface area that the materials were capable of producing. Only whole remaining granules were selected for the analysis, and powdered ash was not purposely placed into the analysis, unless it was still attached to the sample. The samples selected may not be representative of the complete batch. This may have resulted in the higher temperature samples achieving extremely high results, whereas they may have reduced and trailed off if a randomly distributed sample was used, changing the trend. In other situations, samples had to be broken down to fit into the measuring vessels, which would have reduced surface area compared to the complete sample pellets. The difference between being tested as a powder and as a pellet would have impacted the surface area, and it was not possible to

remain consistent. In terms of gas adsorption, one sample remains puzzling. The pyrolysis sample for both SP and CG produced a large CO_2 adsorption isotherm, despite measuring a minor micropore volume, surface area, and total pore volume. However, on the N_2 adsorption, the samples had no adsorption capacity. The pyrolysis samples were devoid of oxygen and had only been heat treated. The result would appear anomalous, for it not happening in both pyrolysis samples. It is to be noted that the values for CG-RAW and GC-HTC in mass balance of HTC, Table 5.26 in Section 5.2.1, differ to the results presented earlier in that section. The values in this table are worked out through solid TOC measurement, whereas this thesis used a combination of TGA and EA. If the values from this thesis were entered, the solid yield and carbon yield from HTC would have been lower. This shows the difference between analysis methods.

Certain materials did not behave as expected in the reactor. The raw samples had a large mass loss. The samples were high in volatile content, less dense without a pre-treatment and persisted to blow away in the carrier gas. This caused issues and broken apparatus. The apparatus required cleaning after every run to prevent this. The liberation of volatiles, elutriated solids, and the condensing steam could create a tar like substance on the outlet. If that was not removed, there was a risk of a pressure build and the bung would release. This was frequently seen with the CG runs in particular. The raw activation samples created a different challenge due to blockages. As the raw material is a waste organic product, the sample fluctuation can be quite wide. Repeats on SP-HTC-800-1, Table 9.6, shows a wide fluctuation in yield. This pattern was repeated with chemical composition, which detected 57 % carbon in one sample and 79 % in another. Repeatability and reproducibility of prepared samples are important parameters to show the reliability of the measurement methods and the preparation methods. Considering the limited time on facilities, only selected samples for selected facilities were repeated for the purpose of error analysis. The tables containing the standard errors can be found in the Appendix.

5.6 Closing Remarks

It is known that waste disposal is a mounting issue, and a cheap, efficient solution is necessary. In the area of wet waste disposal in particular, challenges arise due to the expensive and energy intensive drying treatments. These need to be performed before most treatment options can be considered. HTC is a valuable technology for these treatment specifications, acting as a faster and more energy efficient alternative technology. Using the hydrochar product for AC production was hypothesised as an ideal destination.

The results provide solid evidence that an HTC pre-treatment creates a vastly superior AC when treating raw organic waste materials. Based on this it can be said that the production of AC from hydrochars shows enormous potential to rival the quality of current market offerings produced from coal. But there is still a large gap between this proof of concept and actually producing the material from a continuous waste stream. The losses endured and energy requirements are a restriction on this method. Based on the method used, this study has been the first to produce ACs from an industrial HTC treatment process.

It was noted that there was a knowledge gap to explore steam activation conditions on activating hydrochars. The method is successful at producing consumer grade AC, with proven adsorption capabilities, and the optimum condition regions have been noted. Despite the quality of product, the quantity produced remains the biggest hurdle. The steam activation technology may be too harsh for the materials studied. Future studies must look at efficiencies and protective measures to prevent such high mass losses without impacting the porosity.

Ultimately, the production of activated carbon from wet biomass waste via HTC would be deemed an ideal route for creating a higher value product from waste if it wasn't for the low yield. This is an emerging field with much potential and an area that could one day thrive.

6 Conclusion

This project aimed to produce activated carbon from hydrochars derived from streams of organic waste. The specific conclusions of this work are as follows:

1) Activated carbon from strawberry pomace hydrochar was found to be highly mesoporous carbons, demonstrating 85 % porosity. The carbon content was recorded to be > 80 % in most samples. The material had an affinity for the chemisorption of oxygen, particularly on the external surface. The optimal steam activation range was found to be 750 – 800 °C for 1 – 2 hours. Here the surface area was recorded at 1039 m^2/g and the total pore volume was 0.729 cm^3/g, favouring mesoporosity. The sample performed better than the commercial GAC comparison at the removal of coloured material and TOC from process wastewater. The presence of pore shielding may inhibit the removal of adsorbate from the material. The material may have some limitations due to the susceptibility of the material to the conditions used, which resulted in a lower yield. This could present itself in the form of a high ash content. Overall, this material is recommended for activation.

2) Activated carbon products from coffee ground hydrochar had a high microporosity. The sample was the most resistant to loss and the yield produced by this sample was the highest, at 12.8 %. The materials remained > 90 % carbon, due to the low ash content, due to an 80 % removal in the HTC pre-treatment. The optimal steam activation range was found to be 850 °C for 0.5 – 1 hour. In this range, the surface area recorded was 1344 m^2/g and the total pore volume was 0.524 cm^3/g, which was 94 % microporous. The narrow pore size eliminated hysteresis and showed a high capacity for gas adsorption with > 100 cm^3/g CO_2. This material performed best throughout the study and is an ideal precursor for activation.

3) Producing activated carbon from sewage sludge hydrochar was unsuccessful. None of the produced samples were categorised as activated carbons due to their low carbon content and relative porosity. The highest carbon content was recorded as 37.7 % at the lowest activation conditions. The major issue was the starting ash content, 16 %, which was retained and recorded 80 % in one activated sample. The pyrolysis tests, without steam activation, produced higher surface areas 232 m^2/g compared to 220 m^2/g, and recorded equal pore volumes, 0.22 cm^3/g. Ultimately, this material is not suitable for activation through this methodology. However, the HTC process is a suitable treatment process for the waste.

4) HTC pre-treatment is necessary when activating the precursors used in this project. Raw activation samples required method adjustments and binders to produce sample. Coffee grounds cannot be reliably activated without first undergoing HTC treatment. Strawberry pomace can be activated as a raw material; however, the sample is more reactive to the activation conditions, resulting in a low yield and a higher than acceptable ash content. Activated carbons produced from raw precursors could not match the quality of those produced from hydrochar. Despite additional carbon losses during the pre-treatment, the whole process carbon retention is higher than the direct raw activation. Hydrochars pre-treated at 200 °C produced more mesoporous activated carbons and hydrochars pre-treated at 220 °C created more microporous carbons.

7 Further Work

7.1 Narrow experimental range for optimisation

Based on the findings of this research, the optimum range has been found for the activation of coffee grounds hydrochar (850 °C for 0.5 – 1 hour) and strawberry pomace hydrochar (750 – 800 °C for 1 – 2 hours). From this the experimental matrix this can be narrowed further to pinpoint the optimum conditions to maximise the potential from the materials. The endurance of the coffee grounds hydrochar also opens it up to testing at more extreme conditions.

7.2 The impact of the HTC pilot plant versus the batch reactor

In this project, the samples processed through the HTC pilot plant were shown to have succumb to greater losses and produced more mesoporous activated carbons when activated. For future work, to assess the merits of the HTC pilot plant, the pilot scale rig would be used to pre-treat coffee grounds and the batch reactor would be used for strawberry pomace. The activation methodology would remain the same, to compare the effects the AC characteristics, and whether they are material specific or due to the equipment. This would provide additional verification of the new continuous large-scale method. One of the conclusions was that using lower HTC temperatures has the potential to increases mesoporosity in the activated carbon, this can be proven through this work.

7.3 HTC pre-treatment temperature adjustment

The HTC conditions used in the HTC pilot plant have raised concerns about the extent of carbonization afflicted on the raw biomass. A more thorough testing matrix introduced in the pre-treatment phase would add an additional dimension to the complete process. The inclusion of hydrochars produced at higher HTC temperatures would offer an insight into how the pre-treatment influences the yield, surface area, porosity, and whether it impacts the optimum activation conditions.

7.4 The role of sample preparation through pelletization

The materials were pelletized using two different methods. One was soon after HTC process in a large-scale pelletizer, the other was applied after drying and storage, where it was pelletised in a hand press. The timescale after the HTC process and the methodology used could have influenced the structure which remains stable after activation.

7.5 Test raw materials at less severe conditions (Chemical Activation)

This study showed the raw SP biomass products were unusable for activation without a pre-treatment step, to avoid extreme losses. The methodology is not fit for the needs of the raw biomass and the discussion pointed out that the mass scale production of ACs from waste material may differ from the current industrial production method of steam activation. Testing the raw material at lower temperatures could give a better idea of the potential, for instance using chemical activation which can be conducted at lower temperatures, such as KOH activation, which has not been trialled on SP before.

8 References

(Achaw, 2012) O.W. Achaw. A Study of the Porosity of Activated Carbons Using the Scanning Electron Microscope. (2012) DOI: 10.5772/36337

(Afolabi et al., 2020) O.O.D. Afolabi, M. Sohail, Y.L. Cheng. Optimisation and characterisation of hydrochar production from spent coffee grounds by hydrothermal carbonisation. Renewable Energy. Volume 147, Part 1, 2020, Pages 1380-1391, https://doi.org/10.1016/j.renene.2019.09.098.

(Agraniotis et al., 2017) M. Agraniotis, C. Bergins, M. Stein-Cichoszewska, E. Kakaras. High-efficiency pulverized coal power generation using low-rank coals. Low-Rank Coals for Power Generation, Fuel and Chemical Production, Pages 95–124. (2017). doi:10.1016/B978-0-08-100895-9.00005-X

(Aghababaei et al., 2021) A. Aghababaei, R. Azargohar, A.K. Dalai, J. Soltan & C.H. Niu. Adsorption of carbamazepine from water by hydrothermally and steam activated agricultural by-products: equilibrium, site energy, and thermodynamic studies, Chemical Engineering Communications, 2021. DOI: 10.1080/00986445.2021.1922893

(Ahlberg et al., 2006) G. Ahlberg, O. Gustafsson, P. Wedel. Leaching of metals from sewage sludge during one year and their relationship to particle size. Environmental Pollution 144 (2006) pages 545-553, doi:10.1016/j.envpol.2006.01.022

(Ahn, Kim & Lee, 2020) H. Ahn, D. Kim, Y. Lee. Combustion characteristics of sewage sludge solid fuels produced by drying and hydrothermal carbonization in a fluidized bed. Renewable Energy, 147, pages 957 – 968, 2020 https://doi.org/10.1016/j.renene.2019.09.057

(Akhtar & Amin, 2012) J. Akhtar, N.S. Amin. *A review on operating parameters for optimum liquid oil yield in biomass pyrolysis.* Renewable and Sustainable Energy Reviews*, Vol 16 (7), pages 5101-5109, 2012.* doi:10.1016/j.rser.2012.05.033

(Albers et al., 2003) P.W. Albers, J. Pietsch, J. Krauter, S.F. Parker. *Investigations of activated carbon catalyst supports from different natural sources. Physical Chemistry Chemical Physics, 5(9), pages 1941–1949, 2003.* doi:10.1039/b212210n

(Alhashimi & Aktas, 2017) H.A. Alhashimi, C.B.Aktas. Life cycle environmental and economic performance of biochar compared with activated carbon: A meta-analysis. Resources, Conservation and Recycling. Volume 118, Pages 13-26 (2017). https://doi.org/10.1016/j.resconrec.2016.11.016

(Alves et al., 2019) Alves, A.C.F., Antero, R.V.P., de Oliveira, S.B. et al. Activated carbon produced from waste coffee grounds for an effective removal of bisphenol-A in aqueous medium. Environ Sci Pollut Res 26, 24850–24862 (2019). https://doi.org/10.1007/s11356-019-05717-7

(Amorós-Pérez et al., 2018) A. Amorós-Pérez, L. Cano-Casanova, M. Ouzzine, M. Rufete-Beneite, A.J. Romero-Anaya, M.Á. Lillo-Ródenas, Á. Linares-Solano. Spherical Activated Carbons with High Mechanical Strength Directly Prepared from Selected Spherical Seeds. Materials (Basel). 2018 May 10;11(5):770. doi: 10.3390/ma11050770

(Anukam & Berghel, 2021) A. Anukam, J. Berghel. Biomass Pretreatment and Characterization: A Review. Biotechnical applications of biomass. (2021) DOI: http://dx.doi.org/10.5772/intechopen.93607

(Antero et al., 2019) R.V.P. Antero, A.C.F. Alves, P.T.F. Sales, S.B. de Oliveira, S.A. Ojala, S.S.Brum. A new approach to obtain mesoporous-activated carbon via hydrothermal carbonization of Brazilian Cerrado biomass combined with physical activation for bisphenol-A removal, Chemical Engineering Communications, 206:11, pages 1498-1514 (2019). DOI: 10.1080/00986445.2019.1601625

(Aragon-Briceno et al., 2021) C.I. Aragon-Briceno, A.K. Pozarlik, E.A. Bramer, L. Niedzwiecki, H. Pawlak-Kruczek, G. Brem. Hydrothermal carbonization of wet biomass from nitrogen andphosphorus approach: A review. Renewable Energy, 171, pages 401 – 415 (2021). https://doi.org/10.1016/j.renene.2021.02.109

(Baccile et al., 2009) N. Baccile, G. Laurent, F. Babonneau, F. Fayon, M.M. Titirici, M. Antonietti. Structural Characterization of Hydrothermal Carbon Spheres by Advanced Solid-State MAS 13C NMR Investigations. J. Phys. Chem. C 2009, 113, 9644–9654. Doi: 10.1021/jp901582x

(Bach & Semiat, 2011) A. Bach, R. Semiat. The role of activated carbon as a catalyst in GAC/iron oxide/H2O2 oxidation process. Desalination, Volume 273, Issue 1, Pages 57-63 (2011). https://doi.org/10.1016/j.desal.2010.04.020

(Baig 7Gul, 2020) MM. Baig, I.H. Gul. Conversion of wheat husk to high surface area activated carbon for energy storage in high-performance supercapacitors. Biomass and Bioenergy, 144, 105909 (2020). https://doi.org/10.1016/j.biombioe.2020.105909

(Bansal & Goyal, 2005) R.C. Bansal, M. Goyal. Activated Carbon Adsorption. Taylor & Francis. (2005).

(Beguin & Frackowiak, 2009) F. Beguin, E. Frackowiak. Carbons for Electrochemical Energy Storage and Conversion Systems. Taylor & Francis. Pages 1 – 61, (2009)

(Bergius, 1913) F. Bergius. Production of hydrogen from water and coal from cellulose at high temperatures and pressures. Journal of the Society of Chemical Industry, Volume 32, Issue 9 page 462-467, 1913. https://doi.org/10.1002/jctb.5000320904

(Bergius, 1932) F. Bergius. Chemical reactions under high pressure. Nobel lectures chemistry, Pages 262-263, 1932.

(Bergna et al., 2020) D. Bergna, T. Hu, H. Prokkola, H. Romar, U. Lassi. Effect of Some Process Parameters on the Main Properties of Activated Carbon Produced from Peat in a Lab-Scale Process. Waste Biomass Valor 11, 2837–2848 (2020). https://doi.org/10.1007/s12649-019-00584-2

(Beri et al., 2021) K.Y.V. Beri, D.P. Barbosa, M. Zbair, S. Ojala, S. Botelho de Oliveira. Adsorption of Estradiol from aqueous solution by hydrothermally carbonized and steam activated palm kernel shells. Energy Nexus, Volume 1, 2021. https://doi.org/10.1016/j.nexus.2021.100009

(Bhatt & Tao, 2020) A.H. Bhatt, L. Tao. Economic Perspectives of Biogas Production via Anaerobic Digestion. Bioengineering, 7, 74 (2020) doi:10.3390/bioengineering7030074

(Bouchenafa-Saïb et al., 2014) N. Bouchenafa-Saïb, A. Mekarzia, B. Bouzid, O. Mohammedi, A. Khelifa, K. Benrachedi & N. Belhaneche. Removal of malathion from polluted water by adsorption onto chemically activated carbons produced from coffee grounds, Desalination and Water Treatment, 52:25-27, 4920-4927, (2014) https://doi.org/10.1080/19443994.2013.808845

(Boudrahem et al., 2011) F. Boudrahem, A. Soualah, and F. Aissani-Benissad. Pb(II) and Cd(II) Removal from Aqueous Solutions Using Activated Carbon Developed from Coffee Residue Activated with Phosphoric Acid and Zinc Chloride. Journal of Chemical & Engineering Data 2011 56 (5), 1946-1955 DOI: 10.1021/je1009569

(Brown & Lard, 1974) S.M. Brown, E.W. Lard. A comparison of nitrogen and mercury pore size distributions of silicas of varying pore volume, Powder Technology, Volume 9, Issue 4, Pages 187-190, 1974. https://doi.org/10.1016/0032-5910(74)80031-8.

(Brown et al., 2020) A.E. Brown, G.L. Finnerty, M.A. Camargo-Valero, A.B. Ross. Valorisation of macroalgae via the integration of hydrothermal carbonisation and anaerobic digestion. Bioresource Technology, 312, 123539 (2020). https://doi.org/10.1016/j.biortech.2020.123539

(Bubanale & Shivashankar, 2017) S. Bubanale, M. Shivashankar. History, Method of Production, Structure and Applications of Activated Carbon. International Journal of Engineering Research & Technology (IJERT). Vol. 6 Issue 06, pages 495 - 498 (2017).

(Bueno et al., 2021) S. Bueno, E. Duran, B. Gamiz, M.C. Hermosín. Formulating low cost modified bentonite with natural binders to remove pesticides in a pilot water filter system. Journal of Environmental Chemical Engineering, 9, 104623 (2021). https://doi.org/10.1016/j.jece.2020.104623

(Campbell, 2022) B. Campbell. The removal and recovery of organic contaminants from hydrothermal carbonisation process water. DOI: https://doi.org/10.15126/thesis.900542

(Castro et al., 2011) C.S. Castro, A.L. Abreu, C.L. T. Silva, M.C. Guerreiro. Phenol adsorption by activated carbon produced from spent coffee grounds. Water Sci Technology 1 November 2011; 64 (10): 2059–2065. doi: https://doi.org/10.2166/wst.2011.786

(Canziani & Spinosa, 2019) R. Canziani, L. Spinosa. Sludge from wastewater treatment plants. Industrial and Municipal Sludge, 2019 doi: 10.1016/B978-0-12-815907-1.00001-5

(Cecen, 2014) F. Cecen. Kirk-Othmer Encyclopedia of Chemical Technology. John Wiley & Sons. Pages 1 – 34 (2014). https://doi.org/10.1002/0471238961.0103200902011105.a01.pub3

(Cervera-Mata et al., 2021) A. Cervera-Mata, L. Lara, A. Fernández-Arteaga, J.A. Rufián-Henares, G. Delgado. Washed hydrochar from spent coffee grounds: A second generation of coffee residues. Evaluation as organic amendment. Waste management, 120, 2021, 322-329. https://doi.org/10.1016/j.wasman.2020.11.041

(Chang, Chang & Tsai, 2000) C.F. Chang, C.Y. Chang, W.T. Tsai. Effects of Burn-off and Activation Temperature on Preparation of Activated Carbon from Corn Cob Agrowaste by

CO2 and Steam. Journal of Colloid and Interface Science. Volume 232, Issue 1, Pages 45-49 (2000). https://doi.org/10.1006/jcis.2000.7171

(Che, 2002) I. Cheyne. THE DEFINITION OF WASTE IN EC LAW. Journal of Environmental Law, Vol. 14, No. 1, pages 61-73 (2002). https://www.jstor.org/stable/44248349

(Chegini, Briens & Pjontek, 2022) G. Chegini, C. Briens, D. Pjontek. Production and characterization of adsorbents from a hydrothermal char by pyrolysis, carbon dioxide and steam activation. *Biomass Conv. Bioref.* (2022). https://doi.org/10.1007/s13399-022-02439-8

(Chen et al., 2017) J. Chen, L. Zhang, G. Yang, Q. Wang, R. Li, L.A. Lucia. Preparation and characterization of activated carbon from hydrochar by phosphoric acid activation and its adsorption performance in prehydrolysis liquor. BioResources 12, pages 5928 – 5941. https://ojs.cnr.ncsu.edu/index.php/BioRes/article/viewFile/BioRes_12_3_5928_Chen_Preparation_Characterization_Activated_Carbon_Hydrochar_Prehydrolysis_Liquor/5403

(Child, 2014) M. Child. INDUSTRIAL-SCALE HYDROTHERMAL CARBONIZATION OF WASTE SLUDGE MATERIALS FOR FUEL PRODUCTION. https://www.researchgate.net/publication/264197007_INDUSTRIAL-SCALE_HYDROTHERMAL_CARBONIZATION_OF_WASTE_SLUDGE_MATERIALS_FOR_FUEL_PRODUCTION

(Ching et al., 2011) S.L. Ching, M.S. Yusoff, H.A. Aziz, M. Umar. Influence of impregnation ratio on coffee ground activated carbon as landfill leachate adsorbent for removal of total iron and orthophosphate. Desalination, Volume 279, Issues 1–3, 2011, Pages 225-234, https://doi.org/10.1016/j.desal.2011.06.011.

(Choe et al., 2019) U. Choe, A.M. Mustafa, H. Lin, J. Xu, K. Sheng. Effect of bamboo hydrochar on anaerobic digestion of fish processing waste for biogas production. Bioresource Technology, 283, pages 340 – 349 (2019). https://doi.org/10.1016/j.biortech.2019.03.084

(Ciftyurek et al., 2018) E. Ciftyurek, D. Bragg, O. Oginni, R. Levelle, K. Singh, L. Sivanandan, E.M. Sabolsky. Performance of Activated Carbons Synthesized from Fruit Dehydration Biowastes for Supercapacitor Applications. Environmental Progress & Sustainable Energy (Vol.38, No.3), 2018. https://doi.org/10.1002/ep.13030

(Congsomjit & Areeprasert, 2020) D. Congsomjit, C. Areeprasert. Hydrochar-derived activated carbon from sugar cane bagasse employing hydrothermal carbonization and steam activation for syrup decolorization. Biomass Conversion and Biorefinery, 2020. https://doi.org/10.1007/s13399-020-00635-y

(Connelly, 2017) https://andyjconnelly.wordpress.com/2017/03/13/bet-surface-area/

(Correa et al, 2017) Influence of the Carbonization Process on Activated Carbon Properties from Lignin and Lignin-Rich Biomasses. C.R. Correa, M. Stollovsky, T. Hehr, Y. Rauscher, B.Rolli, A Kruse. *ACS Sustainable Chemistry & Engineering*, *5* (9), pages 8222-8233, 2017. DOI: 10.1021/acssuschemeng.7b01895

(Crossley et al., 2019) O.P. Crossley, R.B. Thorpe, D. Peus, J. Lee. Phosphorus recovery from process waste water made by the hydrothermal carbonisation of spent coffee grounds.

Bioresource Technology, Volume 301, 2019,
https://doi.org/10.1016/j.biortech.2019.122664

(Cubero-Cardoso et al., 2020) J. Cubero-Cardoso, A. Serrano, Á. Trujillo-Reyes, D.K. Villa-Gómez, R. Borja and F. G. Fermoso. Valorization Options of Strawberry Extrudate Agro-Waste. A Review. Innovation in the Food Sector Through the Valorization of Food and Agro-Food By-Products, (2020).
https://digital.csic.es/bitstream/10261/222387/1/Chapter_ValorizationOptions_2020.pdf

(Cychoz et al., 2016) K.A. Cychosz, R. Guillet-Nicolas, J.G. Martinez, M. Thommes. Recent advances in the textural characterization of hierarchically structured nanoporous materials. Cite this: Chem. Soc. Rev., 46, 389. DOI: 10.1039/c6cs00391e

(Dąbrowski , 2001) A. Dąbrowski. Adsorption — from theory to practice. Advances in Colloid and Interface Science. Volume 93, Issues 1–3, Pages 135-224 (2001).
https://doi.org/10.1016/S0001-8686(00)00082-8

(Dang & Nguyen, 2019) C.H. Dang, T.D. Nguyen. Physicochemical Characterization of Robusta Spent Coffee Ground Oil for Biodiesel Manufacturing. Waste Biomass Valor 10, 2703–2712 (2019). https://doi.org/10.1007/s12649-018-0287-9

(Danish & Ahmad, 2018) M. Danish, T. Ahmad. A review on utilization of wood biomass as a sustainable precursor for activated carbon production and application. Renewable and Sustainable Energy Reviews, 87, pages 1 – 21 (2018).
https://doi.org/10.1016/j.rser.2018.02.003

(Danso-Boateng et al., 2020) E. Danso-Boateng, E. Nyktari, A.D. Wheatley, R.G. Holdich, A.S. Mohammed. Removal of Organic Pollutants from Effluent of Anaerobic Digester Using Hydrochars Produced from Faecal Simulant and Sewage Sludge. Water Air Soil Pollution (2020) 231: 192 https://doi.org/10.1007/s11270-020-04557-3

(de Fatima Salgado et al, 2018) M. de Fatima Salgado, A.M. Abioye, M.M. Junoh, J.A.P. Santos, F.N. Ani. Preparation of activated carbon from babassu endocarpunder microwave radiation by physical activation. 2018 *IOP Conf. Ser.: Earth Environ. Sci.* 105 012116 (2018). doi:10.1088/1755-1315/105/1/012116

(DEFRA, 2020) Department for Environment, Food & Rural Affairs. UK Statistics on Waste, Government Statistic Service (2020).
https://assets.publishing.service.gov.uk/government/uploads/system/uploads/attachment_data/file/918270/UK_Statistics_on_Waste_statistical_notice_March_2020_accessible_FINAL_updated_size_12.pdf

(Demirbas, 2005) A. Demirbas. Potential applications of renewable energy sources, biomass combustion problems in boiler power systems and combustion related environmental issues. Progress in Energy and Combustion Science 31, pages 171–192 (2005).
doi:10.1016/j.pecs.2005.02.002

(Demirbas & Arin, 2010) A. Demirbas, G. Arin. An Overview of Biomass Pyrolysis. Energy Sources 24, pages 471 – 482 (2010). http://dx.doi.org/10.1080/00908310252889979

(Demirbas, 2011) A. Demirbas. Waste management, waste resource facilities and waste conversion processes. Energy Conversion and Management 52, pages 1280 – 1287 (2011).
http://dx.doi.org/10.1016/j.enconman.2010.09.025

(Diaz & Martin-Gullon, 2006) J.A. Mendez-Diaz, I. Martin-Gullon. Types of Carbon Adsorbents and their Production. Activated carbon surfaces in environmental remediation, Interface science and technology series, 7, Pages 1 – 48 (2006). ISBN: 0-12-370536-3

(Dinjus, Kruse & Tröger, 2011) E. Dinjus, A. Kruse, N. Tröger. Hydrothermal Carbonization – 1. Influence of Lignin in Lignocelluloses. Chemical Engineering & Technology Volume 34, Issue 12, pages 2037 – 2043 (2011). https://doi.org/10.1002/ceat.201100487

(Dhyani & Bhaskar, 2018) V. Dhyani, T. Bhaskar. A comprehensive review on the pyrolysis of lignocellulosic biomass. Renewable Energy, 129, pages 695 – 716 (2018). http://dx.doi.org/10.1016/j.renene.2017.04.035

(Dogan et al., 2020) M. Dogan, P. Sabaz, B.K. Kizilduman, Y. Turhan. Activated carbon synthesis from tangerine peel and its use in hydrogen storage. Journal of the Energy Institute, 93, pages 2176 – 2185 (2020). https://doi.org/10.1016/j.joei.2020.05.011

(Donatello, Tyrer & Cheeseman, 2010) S. Donatello, M. Tyrer, C.R. Cheeseman. EU landfill waste acceptance criteria and EU Hazardous Waste Directive compliance testing of incinerated sewage sludge ash. Waste Management 30 (2010) 63–71 doi:10.1016/j.wasman.2009.09.028

(Dubinin, 1989) M.M. Dubinin. Fundamentals of the Theory of Adsorption in Micropores of Carbon Adsorbents: Characteristics of Their Adsorption Properties and Microporous Structures. Carbon, 27, pages 457-467 (1989). https://doi.org/10.1016/0008-6223(89)90078-X

(Eibisch, Schroll & Fuß, 2015) N. Eibisch, R. Schroll, R. Fuß. Effect of pyrochar and hydrochar amendments on the mineralization of the herbicide isoproturon in an agricultural soil. Chemosphere 134, pages 528 – 535, 2015. http://dx.doi.org/10.1016/j.chemosphere.2014.11.074

(Eid et al., 2018) E.M. Eid, S.A. Alrumman, A.F. El-Bebany, K.F. Fawy, M.A. Taher, A.E. Hesham, G.A. El-Shaboury, M.T. Ahmed. The evaluation of sewage sludge application as a fertilizer for broad bean crops. Food and Energy Security, Volume 7, Issue 3, (2015), https://doi.org/10.1002/fes3.142

(Engineering ToolBox, 2010) Standard Grade Coal - Heat Values. [online] Available at: https://www.engineeringtoolbox.com/coal-heating-values-d_1675.html [Accessed 09 February 2023]

(Erdogan et al., 2015) E. Erdogan, B. Atila, J. Mumme, M.T. Reza, A. Toptas, M. Elibol, J. Yanik. Characterization of products from hydrothermal carbonization of orange pomace including anaerobic digestibility of process liquor. Bioresource Technology 196, pages 35 – 42, 2015. http://dx.doi.org/10.1016/j.biortech.2015.06.115

(Escala et al., 2012) M. Escala, T. Zumbühl, C. Koller, R. Junge, R. Krebs. Hydrothermal Carbonization as an Energy-Efficient Alternative to Established Drying Technologies for Sewage Sludge: A Feasibility Study on a Laboratory Scale. Energy Fuels 2013, 27, 454−460, 2012. dx.doi.org/10.1021/ef3015266

(Fan et al., 2020) J. Fan, Y. Li, H. Yu, Y. Li, Q. Yuan, H. Xiao, F. Li, B. Pan. Using sewage sludge with high ash content for biochar production and Cu (II) sorption. Science of Total Environment, 713, 2020. https://doi.org/10.1016/j.scitotenv.2020.136663

(Fang et al., 2015) J. Fang, B. Gao, J. Chen, A.R. Zimmerman. Hydrochars derived from plant biomass under various conditions: Characterization and potential applications and impacts. Chemical Engineering Journal, 267, pages 253 – 259, 2015. http://dx.doi.org/10.1016/j.cej.2015.01.026

(Fang et al., 2017) Minireview of potential applications of hydrochar derived from hydrothermal carbonization of biomass. Journal of Industrial and Engineering Chemistry, 57, pages 15 – 21, 2017. http://dx.doi.org/10.1016/j.jiec.2017.08.026

(Flora et al., 2013) J.F.R. Flora, X. Lu, L. Li, J.R.V. Flora, N.D. Berge. The effects of alkalinity and acidity of process water and hydrochar washing on the adsorption of atrazine on hydrothermally produced hydrochar. Chemosphere, 93, pages 1989 – 1996, 2013. http://dx.doi.org/10.1016/j.chemosphere.2013.07.018

(Fomkin & Petukhova, 2020) A.A. Fomkin, G.A. Petukhova. Features of Gas, Vapor, and Liquid Adsorption by Microporous Adsorbents. Russ. J. Phys. Chem. 94, 516–525 (2020). https://doi.org/10.1134/S0036024420030097

(Franklin, 1951) R.E. Franklin. Acta Cryst., 4, pages 253 - 261 (1951)

(Franklin, 1951) R.E. Franklin. Proc. Royal Society, 209, pages 196 – 218 (1951)

(Fuertes et al., 2010) A.B. Fuertes, M.C. Arbestain, M. Sevilla, J.A. Maciá-Agulló, S. Fiol, R. López, R.J. Smernik, W.P. Aitkenhead, F. Arce, F. Macias. Chemical and structural properties of carbonaceous products obtained by pyrolysis and hydrothermal carbonisation of corn stover. Australian Journal of Soil Research, 2010, 48, 618–626. Doi: 10.1071/SR10010

(Funke & Ziegler, 2010) A. Funke, F. Ziegler. Hydrothermal carbonization of biomass: A summary and discussion of chemical mechanisms for process engineering. Biofuels, Bioprod. Bioref. 4:160–177 (2010) DOI: 10.1002/bbb.198

(Fytili and Zabaniotou, 2008) D. Fytili and A. Zabaniotou. Utilization of sewage sludge in EU application of old and new methods—A review, Renewable and sustainable energy reviews, Vol. 12, Pages 116-140, 2008 doi:10.1016/j.rser.2006.05.014

(Gagic et al, 2018) Gagic, Tanja; Perva-Uzunalić, Amra; Knez, Zeljko; Skerget, Mojca (2018). Hydrothermal degradation of cellulose at temperature from 200 °C to 300 °C. Industrial & Engineering Chemistry Research, 57, 18, pages 6576 – 6584, 2018. doi:10.1021/acs.iecr.8b00332

(Galhena et al., 2018) D.T. L. Galhena, B.C. Bayer, J.C. Meyer, S. Hofmann, G.A. J. Amaratunga. Reduced Graphene Oxide as a Monolithic Multifunctional Conductive Binder for Activated Carbon Supercapacitors. ACS Omega, 3 (8), pages 9246-9255 (2018). DOI: 10.1021/acsomega.8b01075

(Gao et al., 2012) Y. Gao, X.H. Wang, H.P. Yang, H.P. Chen. Characterization of products from hydrothermal treatments of cellulose. Energy, 42, pages 457 – 465, 2012. doi:10.1016/j.energy.2012.03.023

(Gao et al., 2020) Y. Gao, Q. Yue, B. Gao, A. Li. Insight into activated carbon from different kinds of chemical activating agents: A review. Science of The Total Environment, Volume 746, 141094 (2020). https://doi.org/10.1016/j.scitotenv.2020.141094

(Gao et al., 2021) F. Gao, Y. Zang, Y. Wang, C. Guan, J. Qu, M. Wu. A review of the synthesis of carbon materials for energy storage from biomass and coal/heavy oil waste. New Carbon Materials, 36(1), pages 34-48 (2021). DOI: 10.1016/S1872-5805(21)60003-3

(Gascó et al., 2018) G. Gascó, J. Paz-Ferreiro, M.L. Álvarez, A. Saa, A. Méndez. Biochars and hydrochars prepared by pyrolysis and hydrothermal carbonisation of pig manure. Waste management, 79, pages 395 – 403 (2018). https://doi.org/10.1016/j.wasman.2018.08.015

(GIA, 2021) Global Industry Analysts. Global Activated Carbon Industry. (2021) 5112912

(Golea et al., 2020) D.M. Golea, P. Jarvis, B. Jefferson, G. Moore, S. Sutherland, S.A. ParsonsS.J. Judd. Influence of granular activated carbon media properties on natural organic matter and disinfection by-product precursor removal from drinking water. Water Research, 174, 115613 (2020). https://doi.org/10.1016/j.watres.2020.115613

(Gollakota, Kishore & Gu, 2018) A.R.K. Gollakota, N. Kishore, S. Gu. A review on hydrothermal liquefaction of biomass. Renewable and Sustainable Energy Reviews, 81, pages 1378 – 1392 (2018). http://dx.doi.org/10.1016/j.rser.2017.05.178

(Gomez de la Cruz et al., 2015) F.J. Gomez-de la Cruz, F Cruz-Peragon, P.J. Casanova-Pelaez, J.M. Palomar-Carnicero. A vital stage in the large-scale production of biofuels from spent coffee grounds: the drying kinetics. Fuel Process. Technolology, Vol. 130, pages 188–196. (2015). https://doi.org/10.1016/J.FUPROC.2014.10.012

(Gondek et al., 2020) K. Gondek, M. Mierzwa-Hersztek, M. Kopeć, T. Zaleski, S. Bogdal, M. Bieniasz, J. Błaszczyk, E. Kaczmarczyk, B. Kowalczyk, J. Knaga, J. Nawrocki, M. Pniak, R. Jarosz. MINERAL COMPOSITION OF FRUITS AND LEAVES OF SAN ANDREAS® EVERBEARING STRAWBERRY IN SOILLESS CULTIVATION. J. Elem., 25(4): pages 1333-1347 (2020). DOI: 10.5601/jelem.2020.25.2.2013

(González-García, 2017) P. González-García. Activated carbon from lignocellulosics precursors: A review of the synthesis methods, characterization techniques and applications. Renewable and Sustainable Energy Reviews, Volume 82, Part 1, Pages 1393-1414 (2018). https://doi.org/10.1016/j.rser.2017.04.117

(Gottipati, 2012) R. Gottipati. Preparation and Characterization of Microporous Activated Carbon from Biomass and its Application in the Removal of Chromium (VI) from Aqueous Phase. Doctoral thesis. National Institute of Technology, Rourkela. (2012). https://core.ac.uk/download/pdf/53189039.pdf

(Grande et al., 2013) C.A. Grande, R. Blom, A. Möller, J. Möllmer. High-pressure separation of CH4/CO2 using activated carbon. Chemical Engineering Science, Volume 89, Pages 10-20 (2013). https://doi.org/10.1016/j.ces.2012.11.024

(Gravalos et al., 2018) I. Gravalos, T. Gialamas, Z. Koutsoftis, D. Kateris, Z. Tsiropoulos, P. Xyradakis, A. Georgiades. Energetic Study on Animal Fats and Vegetable Oils Using Combustion Bomb Calorimeter. Journal of Agricultural Machinery Science, 4 (1), pages 69 – 74 (2008).

(Gregg & Sing, 1982) S.J. Gregg, K.S.W. Sing. Adsorption, Surface Area and Porosity. 2nd Edition, Academic Press, London. (1982) https://doi.org/10.1002/bbpc.19820861019

(Grobelak & Jaskulak, 2019) A. Grobelak, M. Jaskulak. Sludge multifunction's in a phytobiome—Forest and plantation application including microbial aspects, Industrial and Municipal Sludge, 2019, Pages 323-336 https://doi.org/10.1016/B978-0-12-815907-1.00014-3

(Guillet-Nicholas et al., 2016) R. Guillet-Nicholas, R. Ahmad, K.A. Cychosz, F. Kleitz, M. Thommes. Insights into the pore structure of KIT-6 and SBA-15 ordered mesoporous silica – recent advances by combining physical adsorption with mercury porosimetry. New J. Chem., 40, 4351 (2016). DOI: 10.1039/c5nj03466c

(GVW, 2019) Grand View Research. Activated Carbon Market Size, Share & Trends Analysis Report By Product (Powdered, Granular), By Application (Liquid, Gas), By End Use (Water Treatment, Air Purification), By Region, And Segment Forecasts, 2019 – 2025. 978-1-68038-073-6

(Haile, 2014) M. Haile. Integrated volarization of spent coffee grounds to biofuels. Biofuel Research Journal 2 65-69 (2014)

(He et al., 2012) X. He, R. Li, J. Qiu, K. Xie, P. Ling, M. Yu, X. Zhang, M. Zheng. Synthesis of mesoporous carbons for supercapacitors from coal tar pitch by coupling microwave-assisted KOH activation with a MgO template. Carbon, 50, pages 4911 – 4921 (2012). http://dx.doi.org/10.1016/j.carbon.2012.06.020

(He, Sun & Han, 2013) M. He, Y. Sun, B. Han Green Carbon Science: Scientific Basis for Integrating Carbon Resource Processing, Utilization and Recycling. Angew. Chem. Int. Ed., 52, 9620 – 9633 (2013). DOI: 10.1002/anie.201209384

(He, Giannis & Wang, 2013) C. He, A. Giannis, J.Y. Wang. Conversion of sewage sludge to clean solid fuel using hydrothermal carbonization: Hydrochar fuel characteristics and combustion behaviour. Applied Energy, 111, pages 257 – 266, 2013. http://dx.doi.org/10.1016/j.apenergy.2013.04.084

(He et al., 2015) C. He, K. Wang, A. Giannis, Y. Yang, J.Y. Wang. Products evolution during hydrothermal conversion of dewatered sewage sludge in sub and near-critical water: Effects of reaction conditions and calcium oxide additive. International Journal of Hydrogen Energy, 40, pages 5776 – 5797, 2015. http://dx.doi.org/10.1016/j.ijhydene.2015.03.006

(He et al., 2020) C. He, H. Lin, Leilei Dai, R. Qiu, Y. Tang, Y. Wang, P.G. Duan, Y.S. Ok. Waste shrimp shell-derived hydrochar as an emergent material for methyl orange removal in aqueous solutions. Environment International, 134, 2020. https://doi.org/10.1016/j.envint.2019.105340

(Heidari et al., 2019) M. Heidari, A. Dutta, B. Acharya, S. Mahmud. A review of the current knowledge and challenges of hydrothermal carbonization for biomass conversion. Journal of the Energy Institute, 92, pages 1779 – 1799, 2019. https://doi.org/10.1016/j.joei.2018.12.003

(Heidarinejad et al., 2020) Z. Heidarinejad, M.H. Dehghani, M. Heidari, G. Javedan, I. Ali, M. Sillanpää. Methods for preparation and activation of activated carbon: a review. Environmental Chemistry Letters, 8, pages 393–415 (2020). https://doi.org/10.1007/s10311-019-00955-0

(Hitzl et al., 2015) M. Hitzl, A. Corma, F. Pomares, M. Renz. The hydrothermal carbonization (HTC) plant as a decentral biorefinery for wet biomass. Catalysis Today, 257, pages 154 – 159, 2015. http://dx.doi.org/10.1016/j.cattod.2014.09.024

(Hoekman et al., 2011) S.K. Hoekman, A. Broch, C. Robbins. Hydrothermal Carbonization (HTC) of Lignocellulosic Biomass. *Energy & Fuels*, *25* (4), pages 1802-1810, 2011. DOI: 10.1021/ef101745n

(Hong et al., 2018) W. Hong, L. Wang, K. Liu, X. Han, Y. Zhou, P. Gao, R. Ding, E. Liu. Asymmetric supercapacitor constructed by self-assembled camellia-like BiOCl and activated carbon microspheres derived from sweet potato. Journal of Alloys and Compounds, 746, pages 292 – 300 (2018). https://doi.org/10.1016/j.jallcom.2018.02.231

(Hossain, Zaini & Mahlia, 2017) N. Hossain, J.H. Zaini, T.M.I. Mahlia. A REVIEW OF BIOETHANOL PRODUCTION FROM PLANT-BASED WASTE BIOMASS BY YEAST FERMENTATION. International Journal of Technology, 1, pages 5-18 (2017). ISSN 2086-9614

(Hsu & Teng, 2000) L.Y. Hsu, H. Teng. Influence of different chemical reagents on the preparation of activated carbons from bituminous coal. Fuel Processing Technology, Volume 64, Issues 1–3, Pages 155-166 (2000). https://doi.org/10.1016/S0378-3820(00)00071-0

(Hung et al., 2011) P.C. Hung, W.C. Lo, K.H. Chi, S.H. Chang, M.B. Chang. Reduction of dioxin emission by a multi-layer reactor with bead-shaped activated carbon in simulated gas stream and real flue gas of a sinter plant. Chemosphere, 82, pages 72 – 77 (2011). http://dx.doi.org/10.1016/j.chemosphere.2010.10.004

(Iro, Subramani & Dash, 2016) Z.S. Iro, C. Subramani, S.S. Dash. A Brief Review on Electrode Materials for Supercapacitor. Int. J. Electrochem. Sci., 11, pages 10628 – 10643 (2016). doi: 10.20964/2016.12.50

(Islam et al., 2021) A. Islam, S.H. Limon, M. Romić, A. Islam. Hydrochar-based soil amendments for agriculture: a review of recent progress. Arabian Journal of Geosciences, 14, 2021. https://doi.org/10.1007/s12517-020-06358-8

(Iwanow et al., 2020) M. Iwanow, T. Gärtner, V. Sieber, B. König. Activated carbon as catalyst support: precursors, preparation, modification and characterization. Beilstein J. Org. Chem., 16, pages 1188–1202 (2020). doi:10.3762/bjoc.16.104

(Iwazaki et al., 2009) T. Iwazaki, R. Obinata, W. Sugimoto, Y. Takasu. High oxygen-reduction activity of silk-derived activated carbon. Electrochemistry Communications, 11, pages 376 – 378 (2009). doi:10.1016/j.elecom.2008.11.045

(Jäger et al., 2010) H. Jäger, W. Frohs, G. Collin, F. von Sturm, O. Vohler, G. Nutsch. Ullmann's Encyclopedia of Industrial Chemistry, Carbon, 1. General (2010) https://doi.org/10.1002/14356007.a05_095.pub2

(Jain et al., 2013) A. Jain, V. Aravindan, S. Jayaraman, P.S. Kumar, R. Balasubramanian, S. Ramakrishna, S. Madhavi, M.P. Srinivasan. Activated carbons derived from coconut shells as high energy density cathode material for Li-ion capacitors. SCIENTIFIC REPORTS, 3: 3002, 2013. DOI: 10.1038/srep03002

(Jain, Balasubramanian & Srinivasan, 2015) A. Jain, R. Balasubramanian, M.P. Srinivasan. Tuning hydrochar properties for enhanced mesopore development in activated carbon by hydrothermal carbonization. Microporous and Mesoporous Materials, 203, pages 178 – 185, 2015. http://dx.doi.org/10.1016/j.micromeso.2014.10.036

(Jezowski & Kowalczewski, 2019) P. Jezowski, P.L. Kowalczewski. Starch as a Green Binder for the Formulation of Conducting Glue in Supercapacitors. Polymers, 11, 1648 (2019). doi:10.3390/polym11101648

(Jin-Hong, Qi-Mei & Xiao-Rong, 2014) Z. Jin-Hong, L. Qi-Mei and Z. Xiao-Rong. The Hydrochar Characters of Municipal Sewage Sludge Under Different Hydrothermal Temperatures and Durations. Journal of Integrative Agriculture, 13(3): pages 471-482 (2014). doi: 10.1016/S2095-3119(13)60702-9

(Jorda-Beneyto et al., 2008) M. Jorda-Beneyto, D. Lozano-Castello, F. Suarez-Garcıa, D. Cazorla-Amoros, A. Linares-Solano. Advanced activated carbon monoliths and activated carbons for hydrogen storage. Microporous and Mesoporous Materials 112, 235–242 (2008). doi:10.1016/j.micromeso.2007.09.034

(Jüntgen, 1986) H. Jüntgen. Activated carbon as catalyst support: A review of new research results. Fuel, Volume 65, Issue 10, Pages 1436-1446 (1986). https://doi.org/10.1016/0016-2361(86)90120-1

(Jurkiewicz, Pawlyta & Burian, 2018) K. Jurkiewicz, M. Pawlyta, A. Burian. Structure of Carbon Materials Explored by Local Transmission Electron Microscopy and Global Powder Diffraction Probes. Journal of Carbon Research, 4, 68, (2018). doi:10.3390/c4040068

(Jutakridsada et al., 2016) P. Jutakridsada, C. Prajaksud, L. Kuboonya-Aruk1, S. Theerakulpisut, K. Kamwilaisak. Adsorption characteristics of activated carbon prepared from spent ground coffee. Clean Techn Environ Policy (2016) 18:639–645 DOI 10.1007/s10098-015-1083-x

(Kambo & Dutta, 2015) H.S. Kambo, A. Dutta. A comparative review of biochar and hydrochar in terms of production, physico-chemical properties and applications. Renewable and Sustainable Energy Reviews 45, pages 359 – 378, 2015. http://dx.doi.org/10.1016/j.rser.2015.01.050

(Kaneko et al., 1992) K. Kaneko, C. Ishii, M. Ruike, H., Kuwabara. Origin of superhigh surface area and microcrystalline graphitic structures of activated carbons. Carbon Volume 30, Issue 7, Pages 1075-1088 (1992). https://doi.org/10.1016/0008-6223(92)90139-N

(Kaneko, 1994) K. Kaneko. Determination of pore size and pore size distribution: 1. Adsorbents and catalysts, Journal of Membrane Science, Volume 96, Issues 1-2, Pages 59 – 89 (1994) https://doi.org/10.1016/0376-7388(94)00126-X

(Kang, Bae & Lee, 2005) M. Kang, Y. Bae, C. Lee. Effect of heat treatment of activated carbon supportson the loading and activity of Pt catalyst. Carbon 43, pages 1512–1516 (2005). doi:10.1016/j.carbon.2005.01.035

(Kang et al., 2012) S. Kang, X. Li, J. Fan, J. Chang. **Characterization of Hydrochars Produced by Hydrothermal Carbonization of Lignin, Cellulose, d-Xylose, and Wood Meal**. *Industrial & Engineering Chemistry Research, 51* (26), pages 9023-9031, 2012. DOI: 10.1021/ie300565d

(Kaza et al., 2018) S. Kaza, L. Yao, P. Bhada-Tata, F. Van Woerden. What a Waste 2.0: A Global Snapshot of Solid Waste Management to 2050. World Bank Publications (2018). https://books.google.co.uk/books?hl=en&lr=&id=bnN_DwAAQBAJ&oi=fnd&pg=PP13&dq=waste+prediction+2050&ots=f9NcEtd-Pc&sig=hYcpBlxCecWyZlqUEg7dfwdUkcQ&redir_esc=y#v=snippet&q=2.01&f=false

(Kierzek et al., 2004) K. Kierzek, E. Frackowiak, G. Lota, G. Gryglewicz, J. Machnikowski. Electrochemical capacitors based on highly porous carbons prepared by KOH activation. Electrochimica Acta, Volume 49, Issue 7, pages 1169-1170, (2004). https://doi.org/10.1016/j.electacta.2003.08.026

(Khan et al., 2019) T.A. Khan, A.S. Saud, S.S. Jamari, M.H.A. Rahim, J.W. Park, H.J. Kim. Hydrothermal carbonization of lignocellulosic biomass for carbon rich material preparation: A review. Biomass and Bioenergy, 130, 105384 (2019). https://doi.org/10.1016/j.biombioe.2019.105384

(Khenniche & Aissani, 2009) L. Khenniche & F. Aissani. Characterization and utilization of activated carbons prepared from coffee residue for adsorptive removal of salicylic acid and phenol: Kinetic and isotherm study. Desalination and Water Treatment. Volume 11, 2009 - Issue 1-3 https://www.tandfonline.com/doi/abs/10.5004/dwt.2009.801

(Khok et al., 2020) Y.T. Khok, C.H. Ooi, A. Matsumoto, F.Y. Yeoh. Reactivation of spent activated carbon for glycerine purification. Adsorption, 26, pages 1015–1025 (2020). https://doi.org/10.1007/s10450-020-00210-x

(Kim, Lee & Park, 2014) D. Kim, K. Lee, K.Y. Park. Hydrothermal carbonization of anaerobically digested sludge for solid fuel production and energy recovery. Fuel, 130, pages 120 – 125, 2014. http://dx.doi.org/10.1016/j.fuel.2014.04.030

(Kim, Lee & Park, 2016) D. Kim, K. Lee, K.Y. Park. Upgrading the characteristics of biochar from cellulose, lignin, and xylan for solid biofuel production from biomass by hydrothermal carbonization. Journal of Industrial and Engineering Chemistry, Volume 42, 25 October 2016, Pages 95-100, 2016. doi:10.1016/j.jiec.2016.07.037

(Kondamudi et al., 2008) N. KONDAMUDI, S.K. MOHAPATRA, M. MISRA. Spent Coffee Grounds as a Versatile Source of Green Energy. J. Agric. Food Chem. 2008, 56, 11757–11760.

(Kong et al., 2014) L. Kong, Y. Xiong, L. Sun, S. Tian, X. Xu, C. Zhao, R. Luo, X. Yang, K. Shih, H. Liu. Sorption performance and mechanism of a sludge-derived char as porous carbon-based hybrid adsorbent for benzene derivatives in aqueous solution. Journal of Hazardous Materials, 247, pages 205 – 211, 2014. http://dx.doi.org/10.1016/j.jhazmat.2014.04.014

(Krishnan et al., 2014) D. Krishnan, K. Raidongia, J. Shao, J. Huang. Graphene Oxide Assisted Hydrothermal Carbonization of Carbon Hydrates. ACS Nano, 8, 1, pages 449–457, 2014. https://doi.org/10.1021/nn404805p

(Kruczek, Drygas & Habryka, 2016) M. Kruczek, B. Drygas, C. Habryka. Pomace in fruit industry and their contemporary potential application. World Scientific News, 48, pages 259 – 265, 2016. https://www.researchgate.net/publication/304151790_Pomace_in_fruit_industry_and_their_contemporary_potential_application

(Krylova & Zaitchenko, 2018) A.Y. Krylova, V.M. Zaitchenko. Hydrothermal Carbonization of Biomass: A Review. Solid Fuel Chem., 52, pages 91–103 (2018). https://doi.org/10.3103/S0361521918020076

(Kyotani, 2003) T. Kyotani. Carbon Alloys: Novel Concepts to Develop Carbon Science and Technology, Chapter 7 – Porous Carbon, Pages 109 – 127 (2003). https://doi.org/10.1016/B978-008044163-4/50007-3

(Laksaci et al., 2017) H. Laksaci, A. Khelifi, B. Belhamdi, M. Trari. Valorization of coffee grounds into activated carbon using physic—chemical activation by KOH/CO2. Journal of Environmental Chemical Engineering 5 (2017) https://doi.org/10.1016/j.jece.2017.09.036

(Lam et al., 2017) S.S. Lam, R.K. Liew, M.Y. Wong, E. Azwar, A. Jusoh, R. Wahi. Activated Carbon for Catalyst Support from Microwave Pyrolysis of Orange Peel. Waste Biomass Valor 8:pages 2109–2119 (2017). DOI 10.1007/s12649-016-9804-x

(Lamastra et al., 2018) L. Lamastra, N.A Suciu, M. Trevisan. Sewage sludge for sustainable agriculture: contaminants' contents and potential use as fertilizer. Chem. Biol. Technol. Agric. (2018) 5:10 https://doi.org/10.1186/s40538-018-0122-3

(Lamine et al., 2014) S.M. Lamine, C. Ridha, H.M. Mahfoud, C. Mouad, B. Lotfi, A.H. Al-Dujaili. Chemical Activation of an Activated Carbon Prepared from Coffee Residue. Energy Procedia, Volume 50, 2014, Pages 393-400, https://doi.org/10.1016/j.egypro.2014.06.047

(Lapus, 2007) R.M. Lapus. Activated Charcoal For Paediatric Poisonings: The Universal Antidote? Therapeutics and toxicology. Lippincott Williams & Wilkins. Pages 216 – 222 (2007).

(Lehmann & Joseph, 2009) J. Lehmann, S. Joseph. Biochar applications, Biochar for environmental management: science, technology and implementation. Second edition. Page 207-208 (2009).

(Leicester, 1945) H.M. Leicester. Tobias Lowitz - Discoverer of Basic Laboratory Methods, College of Physicians and Surgeons. Pages 149 – 151 (1945).

(Leimkuehler, 2010) E.P. Leimkuehler. Production, Characterization, and Applications of Activated Carbon. University of Missouri. (2010).

(Li et al., 2019) Y. Li, H. Liu, K. Xiao, X. Liu, H. Hu, X. Li, H. Yao. Correlations between the physicochemical properties of hydrochar and specific components of waste lettuce: Influence of moisture, carbohydrates, proteins and lipids. Bioresource Technology, 272, pages 482 – 488, 2019. https://doi.org/10.1016/j.biortech.2018.10.066

(Li et al., 2021) W. Li, L.A. Stevens, C.N. Uguna, C.H. Vane, W. Meredith, L. Tang, Q. Li, C.E. Snape. Comparison of the impact of moisture on methane adsorption and nanoporosity for over mature shales and their kerogens. International Journal of Coal Geology, Volume 237, 2021. https://doi.org/10.1016/j.coal.2021.103705.

(Libra et al., 2011) J.A. Libra, K.S. Ro, C. Kammann, A. Funke, N.D. Berge, Y. Neubauer, M.M. Titirici, C. Fühner, O. Bens, J. Kern, K.H. Emmerich. Hydrothermal carbonization of biomass residuals: a comparative review of the chemistry, processes and applications of wet and dry pyrolysis. Biofuels (2011) 2(1), 71–106. https://doi.org/10.4155/bfs.10.81

(Linares-Solano et al., 2000) A. Linares-Solano, C.S.M. de Lecea, D. Cazorla-Amorós, I. Martín-Gullón Porosity Development during CO2 and Steam Activation in a Fluidized Bed Reactor. Energy Fuels, 14, 1, 142–149 (2000). https://doi.org/10.1021/ef9900637

(Liu et al., 2016) T. Liu, Z. Liu, Q. Zheng, Q. Lang, Y. Xia, N, Peng, C. Gai. Effect of hydrothermal carbonization on migration and environmental risk of heavy metals in sewage sludge during pyrolysis. Bioresource Technology, 247, pages 828 – 290, 2016. http://dx.doi.org/10.1016/j.biortech.2017.09.090

(Liu, Chmely & Abdoulmoumine, 2017) Q. Liu, S.C. Chmely, N. Abdoulmoumine. Biomass Treatment Strategies for Thermochemical Conversion. Energy Fuels, 31, 3525−3536 (2017). DOI: 10.1021/acs.energyfuels.7b00258

(Lozano-Castello et al., 2002) D. Lozano-Castello, D. Cazorla-Amoros, A. Linares-Solano, D.F. Quinn. Activated carbon monoliths for methane storage: influence of binder. Carbon, 40, pages 2817 – 2825 (2002). PII: S0008-6223(02)00194-X

(Lu & Berge, 2014) X. Lu, N.D. Berge, Influence of feedstock chemical composition on product formation and characteristics derived from the hydrothermal carbonization of mixed feedstocks. Bioresource Technology, 166, 2014. Doi: 10.1016/j.biortech.2014.05.015

(Lua et al., 2004) A.C. Lua, T. Yang, J. Guo. *Effects of pyrolysis conditions on the properties of activated carbons prepared from pistachio-nut shells. Journal of Analytic ad Applied Physics, 72(2), pages 279–287, 2004.* doi:10.1016/j.jaap.2004.08.001

(Ľudmila et al., 2015) H. Ľudmila, J. Michal, Š. Andrea, H. Aleš. LIGNIN, POTENTIAL PRODUCTS AND THEIR MARKET VALUE. WOOD RESEARCH, 60 (6), pages 973-986 (2015).

(Lv et al., 2018) C. Lv, B. Liang, K. Li, Y. Zhao, Hongwen Sun. Boosted activity of graphene encapsulated CoFe alloys by blending withactivated carbon for oxygen reduction reaction. Biosensors and Bioelectronics, 117, pages 802 – 809 (2018). https://doi.org/10.1016/j.bios.2018.07.020

(Ma, & Li, 2013) H. Ma, Z. Li. Realistic Pore Structure of Portland Cement Paste: Experimental Study and Numerical Simulation. Computers and Concrete. 11. Pages 317-336, 2013. 10.12989/cac.2013.11.4.317.

(MacDermid-Watts, Pradhan & Dutta, 2020) K. MacDermid-Watts, R. Pradhan, A. Dutta. Catalytic Hydrothermal Carbonization Treatment of Biomass for Enhanced Activated Carbon: A Review. Waste and Biomass Valorisation (2020). https://doi.org/10.1007/s12649-020-01134-x

(Macías Pérez et al., 1997) M.C. Macías Pérez, C. Salinas Martínez de Lecea, A. Linares Solano. *Platinum supported on activated carbon cloths as catalyst for nitrobenzene hydrogenation. 151(2), pages 461–475, 1997.* doi:10.1016/s0926-860x(96)00303-1

(Masoumi & Dalai, 2020) S. Masoumi, AK. Dalai. Optimized production and characterization of highly porous activated carbon from algal-derived hydrochar, Journal of Cleaner Production, Volume 263, 2020. ISSN 0959-6526, https://doi.org/10.1016/j.jclepro.2020.121427.

(Mäkelä, Fullana & Yoshikawa, 2016) M. Mäkelä, A. Fullana, K. Yoshikawa. Ash behaviour during hydrothermal treatment for solid fuel applications. Part 1: Overview of different

feedstock. Energy Conversion and Management, 121, pages 402 – 408, 2016. http://dx.doi.org/10.1016/j.enconman.2016.05.016

(Marin-Batista et al., 2020) J.D. Marin-Batista, A.F. Mohedano, J.J. Rodríguez, M.A. de la Rubia. Energy and phosphorous recovery through hydrothermal carbonization of digested sewage sludge. Waste Management 105, pages 566 – 574, 2020. https://doi.org/10.1016/j.wasman.2020.03.004

(Marsh & Rodriguez-Reinoso, 2006) H. Marsh, F. Rodriguez-Reinoso. Activated Carbon. Elsevier. Pages 1 – 359 (2006)

(Massaya et al., 2021) J. Massaya, K.H. Chan, B. Mills-Lamptey. et al. Developing a biorefinery from spent coffee grounds using subcritical water and hydrothermal carbonisation. Biomass Conv. Bioref. (2021). https://doi.org/10.1007/s13399-020-01231-w

(Mateo et al., 2020) W. Mateo, H. Lei, E. Villota, M. Qian, Y. Zhao, E. Huo, Q. Zhang, X. Lin, C. Wang, Z. Huang. Synthesis and characterization of sulfonated activated carbon as a catalystfor bio-jet fuel production from biomass and waste plastics. Bioresource Technology, 297, 122411 (2020). https://doi.org/10.1016/j.biortech.2019.122411

(Mateo-Sagasta et al., 2015) J. Mateo-Sagasta, L. Raschid-Sally, A. Thebo. Wastewater: Economic Asset in an Urbanizing World, Chapter 2: Global Wastewater and Sludge Production, Treatment and Use, Pg 15-38 (2015), DOI 10.1007/978-94-017-9545-6

(Mbarki et al., 2019) F. Mbarki, T. Selmi, A. Kesraoui, M. Seffen, P. Gadonneix, A. Celzard, V. Fierro. Hydrothermal pre-treatment, an efficient tool to improve activated carbon performances. Industrial Crops & Products, 140, 2019. https://doi.org/10.1016/j.indcrop.2019.111717

(McNutt & He, 2019) J. McNutt, Q. He. Spent coffee grounds: A review on current utilization. Journal of Industrial and Engineering Chemistry 71 (2019) 78 - 88

(Merzari et al., 2019) F. Merzari, M. Langone, G. Andreottola, L. Fiori. Methane production from process water of sewage sludge hydrothermal carbonization. A review. Valorising sludge through hydrothermal carbonization. CRITICAL REVIEWS IN ENVIRONMENTAL SCIENCE AND TECHNOLOGY. 2019. https://doi.org/10.1080/10643389.2018.1561104

(Mestre et al., 2015) A.S. Mestre, E. Tyszko, M.A. Andrade, M. Galhetas, C. Freireb, A.P. Carvalho. Sustainable activated carbons prepared from a sucrose-derived hydrochar: remarkable adsorbents for pharmaceutical compounds. RSC Adv., 5, 2015. DOI: 10.1039/c4ra14495c

(Micali et al., 2019) F. Micali, B. Mendecka, L. Lombardi, M. Milanese, G. Ferrara, A. de Risi. Experimental Investigation on High-Temperature Hydrothermal Carbonization of Olive Pomace in Batch Reactor. AIP Conference Proceedings 2191, 020112 (2019); https://doi.org/10.1063/1.5138845

(Mohan & Nair, 2020) S. Mohan, V.V. Nair. Comparative Study of Separation of Heavy Metals from Leachate Using Activated Carbon and Fuel Ash. J. Hazard. Toxic Radioact. Waste, 24(4): 04020031 (2020). https://doi.org/10.1061/(ASCE)HZ.2153-5515.0000520

(Molina-Sabio et al., 1996) M. Molina-Sabio, M.T. Gonzalez, F. Rodriguez-Reinoso, A. Sepúlveda-Escribano. *Effect of steam and carbon dioxide activation in the micropore size*

distribution of activated carbon. Carbon, 34(4), pages 505–509, 1996. doi:10.1016/0008-6223(96)00006-1

(Moore et al., 2009) J.J. Moore, M. Blieske, H. Delgado, A. Lerche, C. Alsup, J. Pacheco, M. Bough, D. Byard. Research and Development Needs for Advanced Compression of Large Volumes of Carbon Dioxide. 2009. https://www.nist.gov/system/files/documents/pml/high_megawatt/6_1-Approved-Moore.pdf

(Mu'azu et al., 2017) N.D. Mu'azu, N. Jarrah, M. Zubair, O. Alagha. Removal of Phenolic Compounds from Water Using Sewage Sludge-Based Activated Carbon Adsorption: A Review. International Journal of Environmental Research and Public Health 2017, 14, 1094; doi:10.3390/ijerph14101094

(Mumme et al., 2011) J. Mumme, L. Eckervogt, J. Pielert, M. Diakité, F. Rupp, J. Kern. Hydrothermal carbonization of anaerobically digested maize silage. Bioresource Technology, 102, pages 9255 – 9260, 2011. http://dx.doi.org/10.1016/j.biortech.2011.06.099

(Murray, Horvath & Nelson, 2008) A. Murray, A. Horvath and K.L. Nelson. Hybrid life-cycle environmental and cost inventory of sewage sludge treatment and end-use scenarios: a case study from China. Environ Sci Technol, 42 (2008), pp. 3163-3169 https://doi.org/10.1021/es702256w

(Mussatto et al., 2011) S.I. Mussatto, E.M.S Machado, S. Martins. et al. Production, Composition, and Application of Coffee and Its Industrial Residues. Food Bioprocess Technology 4, 661 (2011). https://doi.org/10.1007/s11947-011-0565-z

(Nabais et al., 2008) J.M.V. Nabais, P. Nunes, P.J.M. Carrott, M.M.L.R. Carrott, A.M. García, M.A. Díaz-Díez. Production of activated carbons from coffee endocarp by CO2 and steam activation. Fuel Processing Technology, Volume 89, Issue 3, Pages 262-268 (2008). https://doi.org/10.1016/j.fuproc.2007.11.030.

(Naisse et al., 2015) C. NAISSE, C. GIRARDIN, R. LEFEVRE, A. POZZI, R. MAAS, A. STARK, C. RUMPEL. Effect of physical weathering on the carbon sequestration potential of biochars and hydrochars in soil. GCB Bioenergy, 7, 488–496, 2015. doi: 10.1111/gcbb.12158

(Namane et al., 2005) A. Namane, A. Mekarzia, K. Benrachedi, N. Belhaneche-Bensemra, A. Hellal. Determination of the adsorption capacity of activated carbon made from coffee grounds by chemical activation with ZnCl2 and H3PO4. Journal of Hazardous Materials, Volume 119, Issues 1–3, 2005, Pages 189-194, https://doi.org/10.1016/j.jhazmat.2004.12.006.

(Narbaitz & Karimi-Jashni, 2012) R.M. Narbaitz, A. Karimi-Jashni. Electrochemical reactivation of granular activated carbon: Impact of reactor configuration. Chemical Engineering Journal, 197, pages 414 – 423 (2012). http://dx.doi.org/10.1016/j.cej.2012.05.049

(Nawirska & Uklańska, 2008) A. Nawirska, C. Uklańska. Waste products from fruit and vegetable processing as potential sources for food enrichment in dietary fibre. Acta Sci. Pol., Technol. Aliment. 7(2) pages 35-42, 2008. https://www.food.actapol.net/pub/3_2_2008.pdf

(Neele et al., 2011) F. Neele, M. Koenen, J.V. Deurzen, A. Seebregts, H. Groenenberg, T. Thielemann. Large-scale CCS transport and storage networks in North-west and Central Europe. Energy Procedia 4, pages 2740–2747, 2011. http://dx.doi.org/10.1016/j.egypro.2011.02.176

(Negara et al., 2019) D.N.K.P. Negara, T.G.T. Nindhia, I.W. Surata, F. Hidajat, M. Sucipta. Nanopore structures, surface morphology, and adsorption capacity of tabah bamboo-activated carbons. Surfaces and Interfaces, Volume 16, Pages 22-28 (2019). https://doi.org/10.1016/j.surfin.2019.04.002

(Nguyen et al., 2021) V.K. Nguyen, D.K. Chaudhary, R.H. Dahal, N.H. Trinh, J. Kim, S.W. Chang, Y. Hong, D.D. La, X.C. Nguyen, H.H. Ngo, W.J. Chung, D.D. Nguyen. Review on pre-treatment techniques to improve anaerobic digestion of sewage sludge. Fuel 285, 2021, doi: https://doi.org/10.1016/j.fuel.2020.119105

(Nieber, 2017) K. Nieber. The Impact of Coffee on Health. Planta Med 2017; 83, pages 1256–1263 (2017) https://doi.org/10.1055/s-0043-115007

(Nizamuddin et al., 2017) S. Nizamuddin, H.A. Baloch, G.J. Griffin, N.M. Mubarak, A.W. Bhutto, R. Abro, S.A. Mazari, B.S. Ali. An overview of effect of process parameters on hydrothermal carbonization of biomass. Renewable and Sustainable Energy Reviews, 73, pages 1289 – 1299. http://dx.doi.org/10.1016/j.rser.2016.12.122

(Noh, Agarwal & Schwarz, 1987) J.S. Noh, R.K. Agarwal, J.A. Schwarz. Hydrogen storage systems using activated carbon. International Journal of Hydrogen Energy. Volume 12, Issue 10, 1987, Pages 693-700 (1987). https://doi.org/10.1016/0360-3199(87)90132-7 [40]

(OEC, 2019) Observatory of Economic Complexity. Coffee. https://oec.world/en/profile/hs92/coffee

(OFWAT, 2015) Water 2020: Regulatory framework for wholesale markets and the 2019 price review, Appendix 1: Sludge treatment, transport and disposal – supporting evidence and design options. (2015) https://www.ofwat.gov.uk/wp-content/uploads/2015/12/pap_tec20151210water2020app1.pdf

(Oh et al., 2009) W.C. Oh, J.G. Kim, H. Kim, M.L. Chen, F.J. Zhang, K. Zhang, Z.D. Meng. Preparation of Spherical Activated Carbon and Their Physicochemical Properties. Journal of the Korean Ceramic Society Vol. 46, No. 6, pages 568~573, 2009 DOI:10.4191/KCERS.2009.46.6.568

(Okada et al., 2003) K. Okada, N. Yamamoto, Y. Kameshima, A. Yasumori. Porous properties of activated carbons from waste newspaper prepared by chemical and physical activation. Journal of Colloid and Interface Science, 262, pages 179–193. (2003). doi:10.1016/S0021-9797(03)00107-3

(Okolie et al., 2020) J.A. Okolie, S. Nanda, A.K. Dalai, J.A. Kozinski. Optimization and modelling of process parameters during hydrothermal gasification of biomass model compounds to generate hydrogen-rich gas products. International Journal of Hydrogen Energy, 45, pages 18275 – 18288 (2020). https://doi.org/10.1016/j.ijhydene.2019.05.132

(O'Kelly, 2005) B.C. O'Kelly. Sewage Sludge to Landfill: Some Pertinent Engineering Properties, Journal of the Air & Waste Management Association, 55:6, 765-771, DOI: 10.1080/10473289.2005.10464670

(Otowa, Tanibata & Itoh, 1993) T. Otowa, R. Tanibata, M. Itoh. Production and adsorption characteristics of MAXSORB: high-surface-area active carbon. Gas Separation & Purification, Vol 7, No 4, Page 245, (1993). https://doi.org/10.1016/0950-4214(93)80024-Q

(Pal et al., 2017) A. Pal, M.S.R. Shahrom, M. Moniruzzaman, C.D. Wilfred, S. Mitra, K. Thu, B.B. Saha. Ionic liquid as a new binder for activated carbon based consolidated composite adsorbents. Chemical Engineering Journal, 326, pages 980 – 986 (2017). http://dx.doi.org/10.1016/j.cej.2017.06.031

(Pallarés, González-Cencerrado & Arauzo, 2018) J. Pallarés, A. González-Cencerrado, I. Arauzo. Production and characterization of activated carbon from barley straw by physical activation with carbon dioxide and steam. Biomass and Bioenergy, Volume 115, Pages 64-73 (2018). https://doi.org/10.1016/j.biombioe.2018.04.015

(Parra et al., 1995) J.B. Parra, J.C. de Sousa, J.J. Pis, J.A. Pajares, R.C. Bansal. Effect of gasification on the porous characteristics of activated carbons from a semianthracite. Carbon, Volume 33, Issue 6, Pages 801-807 (1995). https://doi.org/10.1016/0008-6223(95)00004-W

(Parshetti et al., 2013) G.K. Parshetti, Z. Liu, A. Jain, M.P. Srinivasan, R. Balasubramanian. Hydrothermal carbonization of sewage sludge for energy production with coal. Fuel 111, 2013. 201-210 http://dx.doi.org/10.1016/j.fuel.2013.04.052

(Pauline & Joseph, 2020) Hydrothermal carbonization of organic wastes to carbonaceous solid fuel–A review of mechanisms and process parameters. Fuel 279, 2020. https://doi.org/10.1016/j.fuel.2020.118472

(Pawar et al., 2021) P.R. Pawar, P. Rao, G. Prakash, A.M. Lali. Organic waste streams as feedstock for the production of high volume-low value products. Environ Sci Pollut Res 28, pages 11904–11914 (2021). https://doi.org/10.1007/s11356-020-07985-0

(Pechler & Emig, 1991) N. Pechler, G. Emig. Adsorptive purification of large waste gas streams. Gas Separation & Purification, Volume 5, Issue 4, Pages 247-251 (1991). https://doi.org/10.1016/0950-4214(91)80032-Z

(Peng et al., 2016) C. Peng, Y. Zhai, Y. Zhu, B. Xu, T. Wang, C. Li, G. Zeng. Production of char from sewage sludge employing hydrothermal carbonization: Char properties, combustion behaviour and thermal characteristics. Fuel, 176, pages 110 – 118, 2016. http://dx.doi.org/10.1016/j.fuel.2016.02.068

(Peng, Gai & Peng, 2020) Nana Peng, Chao Gai, Chao Peng. Enhancing hydrogen-rich syngas production and energy recovery efficiency by integrating hydrothermal carbonization pre-treatment with steam gasification. Energy, 210, 118655 (2020). https://doi.org/10.1016/j.energy.2020.118655

(Piai et al., 2020) L. Piai, M. Blokland, A. van der Wal, A. Langenhof. Biodegradation and adsorption of micropollutants by biological activatedcarbon from a drinking water production plant. Journal of Hazardous Materials, 388, 122028 (2020). https://doi.org/10.1016/j.jhazmat.2020.122028

(Pirmoradi et al., 2020) M. Pirmoradi, N. Janulaitis, R.J. Gulotty Jr, J.R. Kastner. Bi-Metal-Supported Activated Carbon Monolith Catalysts for Selective Hydrogenation of Furfural.

Industrial & Engineering Chemistry Research 59 (40), pages 17748-17761, 2020. DOI: 10.1021/acs.iecr.0c02866

(Pinel et al., 1999) C. Pinel, E. Landrivon, H. Lini, P. Gallezot. Effect of the Nature of Carbon Catalysts on Glyphosate Synthesis. Journal of Catalysis, Volume 182, Issue 2, Pages 515-519 (1999). https://doi.org/10.1006/jcat.1998.2374

(Plaza et al., 2012) M.G. Plaza, A.S. González, C. Pevida, J.J. Pis, F. Rubiera. Valorisation of spent coffee grounds as CO2 adsorbents for postcombustion capture applications. Applied Energy, Volume 99, 2012, Pages 272-279, https://doi.org/10.1016/j.apenergy.2012.05.028.

(Pradel, 2019) M. Pradel. Survey data of sewage sludge treatment and disposal routes originated from activated sludgewater treatment in France. Data in Brief 26, 2019 https://doi.org/10.1016/j.dib.2019.104541

(Prauchner & Rodríguez-Reinoso, 2012) M.J. Prauchner, F. Rodríguez-Reinoso. Chemical versus physical activation of coconut shell: A comparative study. Microporous and Mesoporous Materials, Volume 152, Pages 163-171 (2012). https://doi.org/10.1016/j.micromeso.2011.11.040

(Puccini et al., 2017) M. Puccini, E. Stefanelli, M. Hiltz, M. Seggiani, S. Vitolo. Activated Carbon from Hydrochar Produced by Hydrothermal Carbonization of Wastes. Chemical Engineering Transactions, 57, pages 169-174, 2017. DOI: 10.3303/CET1757029

(Rakowski, 2015) D. Rakowski. Renewable Energy: A Development Opportunity for Rural Regions in Poland. Review paper. University of Szczecin, Poland, pages 21 - 25 (2015). http://br.wszia.edu.pl/zeszyty/pdfs/br39_03rakowski.pdf

(RAM, 2020) Research and Markets. Global Activated Carbon Markets 2020-2025: Powdered Activated Carbon Accounts for Approx 60% of the $5.75 Billion Market. (2020)

(Reza et al., 2013) M.T. Reza, J.G. Lynam, M.H. Uddin, C.J. Coronella. Hydrothermal carbonization: Fate of inorganics. Biomass and Bioenergy, Volume 49, Pages 86-94 (2013). https://doi.org/10.1016/j.biombioe.2012.12.004

(Reza et al., 2014) M.T. Reza, M.H. Uddin, J.G. Lynam, S.K. Hoekman, C.J. Coronella. Hydrothermal carbonization of loblolly pine: reaction chemistry and water balance. Biomass Conv. Bioref., 4, pages311–321 (2014). DOI 10.1007/s13399-014-0115-9

(Reza et al., 2016) M.T. Reza, A. Freitas, X. Yang, C.J. Coronella. Wet Air Oxidation of Hydrothermal Carbonization (HTC) Process Liquid. ACS Sustainable Chem. Eng. 2016, 4, 3250−3254. DOI: 10.1021/acssuschemeng.6b00292

(Richards et al., 2021) A.P. Richards, D. Haycock, J. Frandsen, T.H. Fletcher. A review of coal heating value correlations with application to coal char, tar, and other fuels. Fuel, 283, 118942 (2021). https://doi.org/10.1016/j.fuel.2020.118942

(Rizhikovs et al., 2012) J. Rizhikovs, J. Zandersons, B. Spince, G. Dobele, E. Jakab. Preparation of granular activated carbon from hydrothermally treated and pelletized deciduous wood. Journal of Analytical and Applied Pyrolysis, 93, pages 68 – 76, 2012. doi:10.1016/j.jaap.2011.09.009

(Robens, 1994) E. Robens. Some intriguing items in the history of adsorption. Studies in Surface Science and Catalysis. Volume 87, Pages 109-118 (1994). https://doi.org/10.1016/S0167-2991(08)63070-0

(Rodríguez-Reinoso, Molina-Sabio & González, 1995) F. Rodríguez-Reinoso, M. Molina-Sabio, M.T. González. The use of steam and CO2 as activating agents in the preparation of activated carbons. Carbon, Volume 33, Issue 1, Pages 15-23 (1995). https://doi.org/10.1016/0008-6223(94)00100-E

(Rodriguez-Reinoso & Sepulveda-Escribano, 2001) F. Rodriguez-Reinoso, A. Sepulveda-Escribano. Handbook of Surfaces and Interfaces of Materials: Chapter 9: POROUS CARBONS IN ADSORPTION AND CATALYSIS, Pages 309 – 355 (2001). https://doi.org/10.1016/B978-012513910-6/50066-9

(Román et al., 2013) S. Román, J.M.V. Nabais, B. Ledesma, J.F. González, C. Laginhas, M.M. Titirici. Production of low-cost adsorbents with tunable surface chemistry by conjunction of hydrothermal carbonization and activation processes. Microporous and Mesoporous Materials, 165, pages 127 – 133, 2013. http://dx.doi.org/10.1016/j.micromeso.2012.08.006

(Román et al., 2018) S. Román, J. Libra, N. Berge, E. Sabio, K. Ro, L. Li, B. Ledesma, A. Álvarez, S. Bae. Hydrothermal Carbonization: Modelling, Final Properties Design and Applications: A Review. Energies 2018, 11, 216; doi:10.3390/en11010216

(Rouquerol, 1999) F. ROUQUEROL. *Adsorption by Powders and Porous Solids || Assessment of Surface Area, pages 165–189, 1999.* doi:10.1016/B978-012598920-6/50007-5

(Rosiek, 2020) K. Rosiek. Directions and Challenges in the Management of Municipal Sewage Sludge in Poland in the Context of the Circular Economy. Sustainability 2020, 12, 3686 doi:10.3390/su12093686

(Sadish et al., 2019) O. Sadish, S.P. Sebastian, K.S.P. Banu, R. Mahendran. Hydrochar as an Energy Alternative to Coal: Effect of Temperature on Hydrothermal Carbonization of Paper Board Mill Sludge. International Journal of Current Microbiology and Applied Sciences. 8, pages 1668-1675, 2019. 10.20546/ijcmas.2019.806.199.

(Saetea & Tippayawong, 2013) P. Saetea, N. Tippayawong. Characterization of Adsorbent from Hydrothermally Carbonized and Steam Activated Sewage Sludge. Proceedings of the World Congress on Engineering 2013 Vol III. https://www.researchgate.net/publication/286122369_Characterization_of_Adsorbent_from_Hydrothermally_Carbonized_and_Steam_Activated_Sewage_Sludge

(Saidur et al., 2011) R. Saidur, E.A. Abdelaziz, A. Demirbas, M.S. Hossain, S. Mekhilef. A review on biomass as a fuel for boilers. Renewable and Sustainable Energy Reviews, 15, pages 2262 – 2289 (2011). doi:10.1016/j.rser.2011.02.015

(Salvadora & Jiménez, 1996) F. Salvadora, C.S. Jiménez. A new method for regenerating activated carbon by thermal desorption with liquid water under subcritical conditions. Carbon, Volume 34, Issue 4, Pages 511-516 (1996). https://doi.org/10.1016/0008-6223(95)00211-1

(Šaponjac et al., 2015) V.T. Šaponjac, A. Gironés-Vilaplana, S. Djilas, M. Vinčić. Chemical composition and potential bioactivity of strawberry pomace. RSC Advances 5, (7) pages 5397 – 5405, 2015. DOI: 10.1039/c4ra14296a

(Saqib et al., 2017) N.U. Saqib, M. Oh, W. Jo, S. Park, J. Lee. Conversion of dry leaves into hydrochar through hydrothermal carbonization (HTC). J Mater Cycles Waste Management, 19: pages 111–117 (2017). DOI 10.1007/s10163-015-0371-1

(Saqib et al., 2019) N.U. Saqib, H.B. Sharma, S. Baroutian, B. Dubey, A.K. Sarmah, Valorisation of food waste via hydrothermal carbonisation and techno-economic feasibility assessment. Science of the Total Environment, 690, pages 261 – 276, 2019. https://doi.org/10.1016/j.scitotenv.2019.06.484

(Schonvogel et al., 2019) D. Schonvogel, M. Nowotny, T. Worieschеck, H. Multhaupt, P. Wagner, A. Dyck, C. Agert, M. Wark. Hydrothermal Carbonization-Derived Carbon from Waste Biomass as Renewable Pt Support for Fuel Cell Applications: Role of Carbon Activation. Energy Technol. 7, 2019. DOI: 10.1002/ente.201900344

(Sevilla & Fuertes, 2009) M. Sevilla and A.B. Fuertes. Chemical and Structural Properties of Carbonaceous Products Obtained by Hydrothermal Carbonization of Saccharides. Chem - A Eur J, 15 (2009), pp. 4195-4203. Doi: 10.1002/chem.200802097

(Sevilla & Fuertes, 2009) M. Sevilla and A.B. Fuertes. The production of carbon materials by hydrothermal carbonization of cellulose. Carbon, 47, pages 2281 – 2289, 2009. doi:10.1016/j.carbon.2009.04.026

(Sevilla, Fuertes & Mokaya, 2011) M. Sevilla, A.B. Fuertes, R. Mokaya. High density hydrogen storage in superactivated carbons from hydrothermally carbonized renewable organic materials. *Energy Environ. Sci.*, 2011,4, pages 1400-1410, 2011. https://doi.org/10.1039/C0EE00347F

(Sevilla & Fuertes, 2016) M. Sevilla, A.B. Fuertes. *A Green Approach to High-Performance Supercapacitor Electrodes: The Chemical Activation of Hydrochar with Potassium Bicarbonate. ChemSusChem, 2016, 9, pages 1-10.* doi:10.1002/cssc.201600426

(Sevilla & Mokaya, 2014) M. Sevilla, R. Mokaya. Energy storage applications of activated carbons: supercapacitors and hydrogen storage. Energy & Environmental Science. Issue 4, Page 1250-1280 (2014). https://doi.org/10.1039/C3EE43525C

(Shafie, Al-atta & Zainal, 2018) S.A. Shafie, K.A. Al-atta, Z.A. Zainal. Effect of hydrothermal and vapothermal carbonization of wet biomass waste on bound moisture removal and combustion characteristics. Applied Thermal Engineering, 139, pages 187 – 195 (2018). https://doi.org/10.1016/j.applthermaleng.2018.02.073

(Shahrivar & Gharabaghi, 2020) J. Shahrivar, M. Gharabaghi. Separation of $AuCN_2^-$ by activated carbon and functionalized graphene/activated carbon composite. Advanced Powder Technology, Volume 31, Issue 12, Pages 4648-4656 (2020). https://doi.org/10.1016/j.apt.2020.10.005

(Sharma et al., 2020) R. Sharma, K. Jasrotia, N. Singh, P. Ghosh, S. Srivastava, N.R. Sharma, J. Singh, R. Kanwar, A. Kumar. A Comprehensive Review on Hydrothermal Carbonization of Biomass and its Applications. Chemistry Africa (2020) 3:1–19 https://doi.org/10.1007/s42250-019-00098-3

(Shen, 2020) Y. Shen. A review on hydrothermal carbonization of biomass and plastic wastes to energy products. Biomass and Bioenergy, 134, 2020. https://doi.org/10.1016/j.biombioe.2020.105479

(Shokry, Elkady & Salama, 2020) H. Shokry, M. Elkady, E. Salama. Eco-friendly magnetic activated carbon nano-hybrid for facile oil spills separation. Nature Scientific Reports, 10:10265 (2020). https://doi.org/10.1038/s41598-020-67231-y

(Silva, 1998) M.A. Silva, S.A. Nebra, M.J Machado-Silva, & C.G Sanchez. (1998). The use of biomass residues in the Brazilian soluble coffee industry. Biomass and Bioenergy, 14, 457–467. https://doi.org/10.1016/S0961-9534(97)10034-4

(Simsir, Eltugral & Karagoz, 2017) H. Simsir, N. Eltugral, S. Karagoz. Hydrothermal carbonization for the preparation of hydrochars fromglucose, cellulose, chitin, chitosan and wood chips via low-temperatureand their characterization. Bioresource Technology, 246, pages 82 – 87, 2017. http://dx.doi.org/10.1016/j.biortech.2017.07.018

(Sing & Williams, 2004) K.S.W. Sing, R.T. Williams. Physisorption Hysteresis Loops and the Characterization of Nanoporous Materials. Review, Adsorption Science & Technology Vol. 22 No. 10, pages 773 – 782 (2004).

(Singh et al., 2014) J. Singh, R. Laurenti, R. Sinha and B. Frostell. Progress and challenges to the global waste management system. Waste Management & Research, Vol. 32(9), pages 800–812 (2014). DOI: 10.1177/0734242X14537868

(Sircar, Golden & Rao, 1996) S. Sircar, T.C. Golden, M.B. Rao. Activated carbon for gas separation and storage. Carbon, Volume 34, Issue 1, Pages 1-12 (1996). https://doi.org/10.1016/0008-6223(95)00128-X

(Smith et al., 2018) A.M. Smith, C. Whittaker, I. Shield, A.B. Ross. The potential for production of high-quality bio-coal from early harvested Miscanthus by hydrothermal carbonisation. Fuel, 220, pages 546 – 557 (2018). https://doi.org/10.1016/j.fuel.2018.01.143

(Soares et al., 2008) O.S.G.P. Soares, J.J.M. Órfão, M.F.R. Pereira. Activated Carbon Supported Metal Catalysts for Nitrate and Nitrite Reduction in Water. *Catal Lett* 126, pages 253–260 (2008). https://doi.org/10.1007/s10562-008-9612-4

(Sterling, 2019) R.J. Sterling. An investigation into the impact of hydrothermal carbonisation on the suitability of biomass for fuel switching. Thesis, University of Nottingham (2019). http://eprints.nottingham.ac.uk/57021/

(Stevenson, Leckie & Eliassen, 1972) Michael K. Stevenson, James O. Leckie, Rolf Eliassen. Preparation and Evaluation of Activated Carbon Produced from Municipal Waste. EPA Technical Report No.157. Pages 1 – 30 (1972).

(Stranges, 2000) A. Stranges. Germany's synthetic fuel industry, 1927–1945. In: Lesch J.E. (eds) The German Chemical Industry in the Twentieth Century. Chemists and Chemistry, vol 18. Springer, Dordrecht. 2000. https://doi.org/10.1007/978-94-015-9377-9_7

(Steurer & Ardissone, 2015) E. Steurer, G. Ardissone. Hydrothermal Carbonization and Gasification Technology for Electricity Production using Biomass. Energy Procedia, 79, pages 47 – 54 (2015). doi: 10.1016/j.egypro.2015.11.473

(Struhsaker, Cooney, Siex, 1997) T.T. Struhsaker, D.O. Cooney, K.S. Siex. Charcoal Consumption by Zanzibar Red Colobus Monkeys: Its Function and Its Ecological and

Demographic Consequences. International Journal of Primatology 18, 61–72 (1997). https://doi.org/10.1023/A:1026341207045

(Stüber et al., 2011) F. Stüber, K.M. Smith, M.B. Mendoza, R.R.N. Marques, A. Fabregat, C. Bengoa, J. Font, A. Fortuny, S. Pullket, G.D. Fowler, N.J.D. Graham. Applied Catalysis B: Environmental, 110, pages 81 – 89, 2011. doi:10.1016/j.apcatb.2011.08.029

(Su, 2020) Y. Su. Multi-agent evolutionary game in the recycling utilization of construction waste. Science of the Total Environment, 738, 139826 (2020). https://doi.org/10.1016/j.scitotenv.2020.139826

(Su et al., 2020) Y. Su, L. Liu, D. Xu, H. Du, Y. Xie, Y. Xiong, S. Zhang. Syngas production at low temperature via the combination of hydrothermal pre-treatment and activated carbon catalyst along with value-added utilization of tar and bio-char. Energy Conversion and Management, 205, 112382 (2020). https://doi.org/10.1016/j.enconman.2019.112382

(Suidan, Snoeyink & Schmitz, 1977) M.T. Suidan, V.L. Snoeyink, R.A. Schmitz. Reduction of Aqueous Free Chlorine with Granular Activated Carbon—pH and Temperature Effects. Environ. Sci. Technol. Volume 11, Number 8, 785 – 789 (1977).

(Sultana et al., 2022) A.I. Sultana, C. Chambers, M.M.N. Ahmed, P. Pathirathna, T. Reza. Multifunctional Loblolly Pine-Derived Superactivated Hydrochar: Effect of Hydrothermal Carbonization on Hydrogen and Electron Storage with Carbon Dioxide and Dye Removal. *Nanomaterials* 2022, *12*, 3575. https://doi.org/10.3390/nano12203575

(Tang et al., 2020) L. Tang, X.Y. Ma, Y. Wang, S. Zhang, K. Zheng, X.C. Wang, Y. Lin. Removal of trace organic pollutants (pharmaceuticals and pesticides) and reduction of biological effects from secondary effluent by typical granular activated carbon. Science of the Total Environment, 749, 141611 (2020). https://doi.org/10.1016/j.scitotenv.2020.141611

(Telesca et al., 2013) A. Telesca, M. Marroccoli, D. Calabrese, G.L. Valenti, F. Montagnaro. Flue gas desulfurization gypsum and coal fly ash as basic components of prefabricated building materials. Waste Management, 33, pages 628 – 633 (2013). http://dx.doi.org/10.1016/j.wasman.2012.10.022

(Tessmer, Vidic & Uranowski, 1997) C.H. Tessmer, R.D. Vidic, L.J. Uranowski. Impact of Oxygen-Containing Surface Functional Groups on Activated Carbon Adsorption of Phenols. Environ. Sci. Technol., 31, pages 1872-1878 (1997). DOI: S0013-936X(96)00474-9

(Thommes et al., 2015) M. Thommes, K. Kaneko, A.V. Neimark, J.P. Olivier, F. Rodriguez-Reinoso, J. Rouquerol, K.S.W. Sing. Physisorption of gases, with special reference to the evaluation of surface area and pore size distribution (IUPAC Technical Report). Pure Appl. Chem.; 87(9-10), pages 1051–1069 (2015). DOI 10.1515/pac-2014-1117

(Tian & Wu, 2018) Y. Tian, J. Wu. A Comprehensive Analysis of the BET Area for Nanoporous Materials. AIChE Journal, Vol. 64, No.1, pages 286 – 293 (2018) DOI 10.1002/aic.15880

(Titirici et al., 2007) Maria M. Titirici, A. Thomas, S.H. Yu, J.O. Müller, M. Antonietti. A Direct Synthesis of Mesoporous Carbons with Bicontinuous Pore Morphology from Crude Plant Material by Hydrothermal Carbonization. Chem. Mater., 19, 17, page 4205–4212, 2007. https://doi.org/10.1021/cm0707408

(Titirici, Thomas & Antonietti, 2007) M.M. Titirici, A. Thomas, M. Antonietti. Back in the black: hydrothermal carbonization of plant material as an efficient chemical process to treat the CO2 problem? New J. Chem., 31, page 787–789, 2007. DOI: 10.1039/b616045j

(Topcu et al., 2022) N.S. Topcu, G. Duman, H. Olgun, J. Yanik. Evaluation of Poultry Manure: Combination of Phosphorus Recovery and Activated Carbon Production. *ACS Omega*, *7* (24), pages 20710-20718, 2022. DOI: 10.1021/acsomega.2c00975

(Travlou et al., 2016) N.A. Travlou, C. Ushay, M. Seredych, E. Rodríguez-Castellon, T.J. Bandosz. Nitrogen-Doped Activated Carbon-Based Ammonia Sensors: Effect of Specific Surface Functional Groups on Carbon Electronic Properties. ACS Sens., 1, pages 591−599 (2016). DOI: 10.1021/acssensors.6b00093

(Tursi, 2019) A review on biomass: importance, chemistry, classification, and conversion. Biofuel Research Journal 22, pages 962-979 (2019). DOI: 10.18331/BRJ2019.6.2.3

(Trunschke, 2013) A. Trunschke. Surface Area and Pore Size Determination. ACFHI, Modern Methods in Heterogeneous Catalysis Research. (2013). https://www.iitk.ac.in/che/pdf/resources/BET-TPX-Chemi-reading-material.pdf

(Ukanwa et al., 2019) K.S. Ukanwa, K. Patchigolla, R. Sakrabani, E. Anthony, S. Mandavgane. A Review of Chemicals to Produce Activated Carbon from Agricultural Waste Biomass. Sustainability, 11, 6204 (2019). doi:10.3390/su11226204

(Urbanowska et al., 2020) A. Urbanowska, M. Kabsch-Korbutowicz, M. Wnukowski, P. Seruga, Marcin Baranowski, H. Pawlak-Kruczek, M. Serafin-Tkaczuk, K. Krochmalny, L. Niedzwiecki. Treatment of Liquid By-Products of Hydrothermal Carbonization (HTC) of Agricultural Digestate Using Membrane Separation. Energies 2020, 13, 262; doi:10.3390/en13010262

(Urdang, 1942) G. Urdang. Pictorial Life History of the Apothecary Chemist Carl Wilhelm Scheele, Page 61 (1942).

(Van der Stelt et al., 2011) M.J.C. van der Stelt, H. Gerhauser, J.H.A. Kiel, K.J. Ptasinski. Biomass upgrading by torrefaction for the production of biofuels: A review. Biomass & Bioenergy, 24, pages 3748 – 3762 (2011). http://dx.doi.org/10.1016/j.biombioe.2011.06.023

(Van Ewijk & Stegemann, 2020) S. van Ewijk, J.A. Stegemann. Recognising waste use potential to achieve a circular economy. Waste Management, 105, pages 1 – 7 (2020). https://doi.org/10.1016/j.wasman.2020.01.019

(Volpe & Fiori, 2017) M. Volpe, L. Fiori. From olive waste to solid biofuel through hydrothermal carbonisation: The role of temperature and solid load on secondary char formation and hydrochar energy properties. Journal of Analytical and Applied Pyrolysis, 124, pages 63 – 72 (2017) http://dx.doi.org/10.1016/j.jaap.2017.02.022

(Wang et al., 2018) T. Wang, Y. Zhai, Y. Zhu, C. Li, G. Zeng. A review of the hydrothermal carbonization of biomass waste for hydrochar formation: Process conditions, fundamentals, and physicochemical properties. Renewable and Sustainable Energy Reviews, 90, pages 223 – 247, 2018. https://doi.org/10.1016/j.rser.2018.03.071

(Wang, Chang & Li, 2019) L. Wang, Y. Chang, A. Li. Hydrothermal carbonization for energy-efficient processing of sewage sludge: A review. Renewable Energy Reviews 108 (2019) Pages 423 – 440 https://doi.org/10.1016/j.rser.2019.04.011

(Ward, Lewis & Green, 2014) Anaerobic digestion of algae biomass: A review. Algal Research, 5, pages 204 – 214 (2014). http://dx.doi.org/10.1016/j.algal.2014.02.001

(Webb & Orr, 1997) P.A. Webb, C. Orr. Analytical Methods in Fine Particle Technology. Micromeritics Instrument Corporation, pages 53 – 271 (1997).

(Wegiel, 2016) http://wegiel-aktywny.pl/o-firmie/

(Westermarck, 2000) S. Westermarck. USE OF MERCURY POROSIMETRY AND NITROGEN ADSORPTION IN CHARACTERISATION OF THE PORE STRUCTURE OF MANNITOL AND MICROCRYSTALLINE CELLULOSE POWDERS, GRANULES AND TABLETS. Academic Dissertation, University of Helsinki, 2000) ISBN 952-91-2535-6

(Wickramaratne & Jaroniec, 2013) N.P. Wickramaratne, M. Jaroniec. Activated Carbon Spheres for CO2 Adsorption. ACS Appl. Mater. Interfaces, 5, 5, 1849–1855 (2013). https://doi.org/10.1021/am400112m

(Wilk et al., 2019) M. Wilk, A. Magdziarz, K. Jayaraman, M. Szymańska-Chargot, I. Gökalp. Hydrothermal carbonization characteristics of sewage sludge and lignocellulosic biomass. A comparative study. Biomass and Bioenergy, 120, pages 166 – 175, 2019. https://doi.org/10.1016/j.biombioe.2018.11.016

(Won et al., 2020) J.S. Won, H.R. Lee, M.J. Lee, M.H. Jeon, S.G. Lee, Y.L. Joo. Fabrication of Activated Carbon Fibers with Sheath-Core, Hollow, or Porous Structures via Conjugated Melt Spinning of Polyethylene Precursor. Polymers (Basel). 2020 Dec 3;12(12):2895. doi: 10.3390/polym12122895.

(Wu et al., 2014) L. Wu, X. Zhang, D. Liu, H. Peng. T. Long. Activated Carbons Derived from Livestock Sewage Sludge and their Absorption Ability for the Livestock Sewage, IERI Procedia, Vol. 9, Pages 33-42, 2014 doi: 10.1016/j.ieri.2014.09.037

(Xia et al., 2019) Y. Xia, H. Liu, Y. Guo, Z. Liu, W. Jiao. Immobilization of heavy metals in contaminated soils by modified hydrochar: Efficiency, risk assessment and potential mechanisms. Science of the Total Environment, 685, pages 1201 – 1208, 2019. https://doi.org/10.1016/j.scitotenv.2019.06.288

(Xin, Li & son, 2020) W. Xin, X. Li, Y. Song. Sludge-based mesoporous activated carbon: the effect of hydrothermal pretreatment on material preparation and adsorption of bisphenol A. Journal of Chemical Technology & Biotechnology, Volume 95, Issue 6 p. 1666-1674, 2020. https://doi.org/10.1002/jctb.6358

(Xu et al., 2020) Z.X. Xu, H. Song, P.J. Li, Z.X. He, Q. Wang, K. Wang, P.G. Duan. Hydrothermal carbonization of sewage sludge: Effect of aqueous phase recycling. Chemical Engineering Journal, 387, 2020. https://doi.org/10.1016/j.cej.2019.123410

(Xue et al., 2018) Y. Xue, C. Du, Z. Wu, L. Zhang. Relationship of cellulose and lignin contents in biomass to the structure and RB-19 adsorption behaviour of activated carbon. New J. Chem., 42, pages 16493—16502 (2018). DOI: 10.1039/c8nj03007c

(Yang et al., 2016) L. Yang, Lin, T. Huang, X. Jiang, W. Jiang. *Effect of steam and CO2 activation on characteristics and desulfurization performance of pyrolusite modified activated carbon. Adsorption, 22(8), pages 1099–1107, 2016.* doi:10.1007/s10450-016-9832-7

(Yang et al., 2020) Surface modification on semi-coke-based activated carbon for enhanced separation of CH4/N2. Chemical Engineering Research and Design, 161, pages 312 – 321 (2020). https://doi.org/10.1016/j.cherd.2020.07.025

(Yu et al., 2020) F. Yu, X. Zhu, W. Jin, J. Fan, J.H. Clark, S. Zhang. Optimized synthesis of granular fuel and granular activated carbonfrom sawdust hydrochar without binder. Journal of Cleaner Production, 276, 2020. https://doi.org/10.1016/j.jclepro.2020.122711

(Yu et al., 2023) H. Yu, X. Yang, Q Li, Y. Zhang, H. Zhou. Breaking the temperature limit of hydrothermal carbonization of lignocellulosic biomass by decoupling temperature and pressure, Green Energy & Environment, 2023. https://doi.org/10.1016/j.gee.2023.01.001.

(Yue et al., 2017) L. Yue, L. Rao, L. Wang, L. Wang, J. Wu, X. Hu, H. DaCosta, J. Yang, M. Fan. Efficient CO2 Capture by Nitrogen-Doped Biocarbons Derived from Rotten Strawberries. Industrial & Engineering Chemistry Research 2017 56 (47), 14115-14122 DOI: 10.1021/acs.iecr.7b02692

(Zdravkov et al., 2007) B.D. Zdravkov, J.J. Cermak, M. Sefara, J. Janku. Pore classification in the characterization of porous materials: A perspective. Central European Journal of Chemistry. (2007) DOI: 10.2478/s11532-007-0017-9

(Zetterberg & Chen, 2015) L. Zetterberg, D. Chen. The time aspect of bioenergy – climate impacts of solid biofuels due to carbon dynamics. GCB Bioenergy, 7, pages 785–796, 2015. https://doi.org/10.1111/gcbb.12174

(Zhai et al., 2017) Y. Zhai, C. Peng, B. Xu, T. Wang, C. Li, G. Zeng, Y. Zhu. Hydrothermal carbonisation of sewage sludge for char production with different waste biomass: Effects of reaction temperature and energy recycling. Energy, 127, pages 167 – 174 (2017). http://dx.doi.org/10.1016/j.energy.2017.03.116

(Zhai et al., 2020) Y. Zhai, X. Liu, Y. Zhu, C. Peng, T. Wang, L. Zhu, C. Li, G. Zeng. carbonization of sewage sludge: The effect of feed-water pH on fate and risk of heavy metals in hydrochars. Bioresource Technology 217, pages 183 – 188, 2016. http://dx.doi.org/10.1016/j.biortech.2016.06.085

(Zhang et al., 2018) B. Zhang, M. Heidar, B. Regmi, S. Salaudeen, P. Arku, M. Thimmannagari, A. Dutta. Hydrothermal Carbonization of Fruit Wastes: A Promising Technique for Generating Hydrochar. Energies 2018, 11, 2022; doi:10.3390/en11082022

(Zhang et al., 2019) J. Zhang, J. Sun, T.A. Shifa, D. Wang, X. Wu, Y. Cui. Hierarchical MnO2/activated carbon cloth electrode prepared by synchronized electrochemical activation and oxidation for flexible asymmetric supercapacitors. Chemical Engineering Journal, 372, pages 1047 – 1055 (2019). https://doi.org/10.1016/j.cej.2019.04.202

(Zhang et al., 2020a) J. Zhang, I. Jones, Z. Isabelle, Z. Mingming; Z. Zhang, J. Preciado-Hernandez, D. Zhang. *Pore Development During CO2 and Steam Activation of a Spent Tyre Pyrolysis Char. Waste and Biomass Valorization, 2020. do*i:10.1007/s12649-020-01165-4

(Zhang et al., 2020b) X. Zhang, Y. Zhang, H.H. Ngo, W. Guo, H. Wen, D. Zhang, C. Li, L. Qi. Characterization and sulfonamide antibiotics adsorption capacity of spent coffee grounds based biochar and hydrochar. Science of The Total Environment, Volume 716, 2020 https://doi.org/10.1016/j.scitotenv.2020.137015

(Zhao et al., 2014) P. Zhao, Y. Shen, S. Ge, K. Yoshikawa. Energy recycling from sewage sludge by producing solid biofuel with hydrothermal carbonization. Energy Conversion and Management, 78, 2014, pages 815 – 821 http://dx.doi.org/10.1016/j.enconman.2013.11.026

(Zheng et al., 2020) X. Zheng, Z. Jiang, Z. Yinga, J. Song, W. Chen, B. Wang. Role of feedstock properties and hydrothermal carbonization conditions on fuel properties of sewage sludge-derived hydrochar using multiple linear regression technique. Fuel, 271, 117609 (2020). https://doi.org/10.1016/j.fuel.2020.117609

(Zhou et al., 2017) L. Zhou, Q. Yu, Y. Cui, F. Xie, W. Li, Y. Li, M. Chen. Adsorption properties of activated carbon from reed with a high adsorption capacity. Ecological Engineering, 102, pages 443 – 450 (2017). http://dx.doi.org/10.1016/j.ecoleng.2017.02.036

(Zhu et al., 2015) X. Zhu, Y. Liu, F. Qian, C. Zhou, S. Zhang, J. Chen. Role of Hydrochar Properties on the Porosity of Hydrochar-based Porous Carbon for Their Sustainable Application. ACS Sustainable Chem. Eng., 3, pages 833−840, 2015. DOI: 10.1021/acssuschemeng.5b00153

(Zhu et al., 2019) G. Zhu, L. Yang, Y. Gao, J. Xu, H. Chen, Y. Zhu, Y. Wang, C. Liao, C. Lu, C. Zhu. Characterization and pelletization of cotton stalk hydrochar from HTC and combustion kinetics of hydrochar pellets by TGA. Fuel, 244, pages 479 – 491. https://doi.org/10.1016/j.fuel.2019.02.039

9 Appendix

Table 9.1 Sample identification key

Material	Key	Pre-treatment	Key	Process	Key	Temp.	Key	Time	Key
Coffee Grounds	CG	No pre-treatment	RAW	Pyrolysis	PYR	X °C	X	X hours	X
Sewage Sludge	SS	Hydrothermal carbonization	HTC	Activation	ACT	i.e. 700°C	700	i.e. 1 hour	1
Strawberry Pomace	SP	-	-	-	-	-	-	-	-

Table 9.2 HTC CG experiments: conditions and results

Sample	DS	DS CG mass	Temp set point	Reaction time	RHP	pH	DS product	Solid yield	Moisture content
	wt%	g	°C	h	bar		g	%	g
CG007	10	60	220	5	1.8	4.00	33.2	55.3	83.3
CG008	10	60	220	5	3.7	3.95	33.61	56.0	81.2
CG009	10	60	220	5.5	2.6	3.94	33.52	55.9	85.3
CG010	10	60	220	5	2.5	3.99	34.14	56.9	81.5
CG011	10	60	220	5	4.1	3.99	34.3	57.2	81.5
CG012	10	60	220	5	2.2	4.04	35.22	58.7	84.5
CG014	10	60	220	5	2.1	4.00	33.18	55.3	81.5
CG015	10	60	220	5	2.8	3.99	33.62	56.0	86.9

CG029	10	60	200	5	2.5	3.99	32.0	53.3	83.5

Residual Head Pressure (RHP).

Table 9.3 HTF SP pyrolysis experiments: conditions and results

Sample	Temp.	Time	N_2 Flowrate	Ramp Rate	Mass In	Mass Out	Yield	Carbon Yield
	°C	h	l/min	°C/min	g	g	%	%
SP-HTC-PYR-700-0.5	700	0.5	1	10	5.0183	1.6333	32.54	119.35
SP-HTC-PYR-750-0.5	750	0.5	1	10	5.0411	1.5312	30.37	109.44
SP-HTC-PYR-800-0.5	800	0.5	1	10	5.0586	1.5744	31.12	111.82
SP-HTC-PYR-850-0.5	850	0.5	1	10	5.0424	1.5366	30.47	111.19
SP-HTC-PYR-900-0.5	900	0.5	1	10	5.0344	1.5105	30.00	112.14
SP-HTC-PYR-950-0.5	950	0.5	1	10	5.0773	1.5234	30.00	109.46
SP-HTC-PYR-700-1	700	1	1	10	4.9981	1.6970	33.95	120.60
SP-HTC-PYR-750-1	750	1	1	10	5.0207	1.5328	30.53	107.09
SP-HTC-PYR-800-1	800	1	1	10	5.0194	1.5351	30.58	111.36
SP-HTC-PYR-850-1	850	1	1	10	5.0099	1.6035	32.01	120.24
SP-HTC-PYR-900-1	900	1	1	10	5.0239	1.5073	30.00	115.05
SP-HTC-PYR-700-2	700	2	1	10	5.0105	1.6050	32.03	113.31
SP-HTC-PYR-750-2	750	2	1	10	5.0337	1.5593	30.98	114.84

SP-HTC-PYR-800-2	800	2	1	10	4.9971	1.3866	27.75	99.93
SP-HTC-PYR-750-6	750	6	1	10	5.0934	1.5946	31.31	-
Standard Error (±)	-	-	-	-	0.0001	0.0001	1.31	5.36

Standard error from the instrument or calculated through sample standard deviation of repeat SP-HTC-ACT-800-1 activation samples

Table 9.4 HTF SP activation experiments: conditions and results

Sample	**Temp.**	**Time**	**N_2 Flowrate**	**Ramp Rate**	**Activating Agent**	**Mass In**	**Mass Out**	**Yield**	**Carbon Yield**
	°C	h	l/min	°C/min	ml	g	g	%	%
SP-HTC-ACT-700-0.5	700	0.5	1	10	46	5.0426	1.4748	29.25	105.64
SP-HTC-ACT-750-0.5	750	0.5	1	10	47	5.0771	1.4080	27.73	97.63
SP-HTC-ACT-800-0.5	800	0.5	1	10	50	5.0385	0.9376	18.61	64.85
SP-HTC-ACT-850-0.5	850	0.5	1	10	59	5.0323	0.6737	13.39	42.42
SP-HTC-ACT-900-0.5	900	0.5	1	10	51	5.0605	0.4776	9.44	28.00
SP-HTC-ACT-950-0.5	950	0.5	1	10	54	5.0321	0.1982	3.94	12.32
SP-HTC-ACT-700-1	700	1	1	10	110	5.0022	1.3682	27.35	97.94
SP-HTC-ACT-750-1	750	1	1	10	108	5.0034	1.1276	22.54	78.30
SP-HTC-ACT-800-1	800	1	1	10	101	5.0135	0.7912	12.04	38.74
SP-HTC-ACT-850-1	850	1	1	10	106	5.0558	0.1456	2.88	7.76

SP-HTC-ACT-700-2	700	2	1	10	206	5.0525	1.2916	25.56	92.59
SP-HTC-ACT-750-2	750	2	1	10	198	5.0706	0.9260	18.26	62.36
SP-HTC-ACT-800-2	800	2	1	10	200	4.9964	0.2661	5.33	12.72
SP-HTC-ACT-850-2	850	2	1	10	204	5.0024	0.1256	2.51	75.35
SP-HTC-ACT-700-4	700	4	1	10	405	5.0701	1.0920	21.54	-
Standard Error (±)	-	-	0.1	-	2	0.0001	0.0001	1.31	5.4

Standard error from the instrument or calculated through sample standard deviation of repeat SP-HTC-ACT-800-1 activation samples

Table 9.5 HTF SP raw activation experiments: conditions and results

Sample	Temp.	Time	N_2 Flowrate	Ramp Rate	Activating Agent	Mass In	Mass Out	Yield
	°C	h	l/min	°C/min	ml	g	g	%
SP-RAW-ACT-750-0.5	750	0.5	0.5	10	54	5.2188	1.1293	21.64
SP-RAW-ACT-800-0.5	800	0.5	0.5	10	51	5.208	0.6872	13.20
SP-RAW-ACT-850-0.5	850	0.5	0.5	10	59	5.0844	0.3328	6.55
SP-RAW-ACT-900-0.5	900	1	0.5	10	55	5.1858	0.1469	2.83
SP-RAW-ACT-750-1	750	1	0.5	10	105	5.4018	0.8920	16.51
SP-RAW-ACT-800-1	800	1	0.5	10	113	5.2455	0.2178	4.15
SP-RAW-ACT-850-1	850	1	0.5	10	50	5.107	0.2014	3.94

SP-RAW-ACT-700-2	700	2	0.5	10	199	5.1915	1.0689	20.59
SP-RAW-ACT-750-2	750	2	0.5	10	177	5.0258	0.6620	13.17
SP-RAW-ACT-800-2	800	2	0.5	10	202	4.5485	0.0923	2.03
Standard Error (±)	-	-	0.1	-	2	0.0001	0.0001	1.31

Standard error from the instrument or calculated through sample standard deviation of repeat SP-HTC-ACT-800-1 activation samples

Table 9.6 HTF SP-HTC-ACT-800-1 repeat experiments: conditions and results

Sample	**Temp.**	**Time**	**N_2 Flowrate**	**Ramp Rate**	**Activating Agent**	**Mass In**	**Mass Out**	**Yield**
	°C	h	l/min	°C/min	ml	g	g	%
SP-HTC-ACT-800-1	800	1	1	10	101	5.0135	0.7912	15.78
SP-HTC-ACT-800-1-RX1	800	1	1	10	84	5.3743	0.5004	9.31
SP-HTC-ACT-800-1-RX2	800	1	1	10	96	5.1193	0.3675	7.18
SP-HTC-ACT-800-1-RX3	800	1	1	10	92	5.5710	0.8454	15.18
SP-HTC-ACT-800-1-RX4	800	1	1	10	94	5.6068	0.8649	15.43
SP-HTC-ACT-800-1-RX5	800	1	1	10	90	5.1911	0.5020	9.67
SP-HTC-ACT-800-1-RX6	800	1	1	10	103	5.0118	0.5885	11.74
Standard Error (±)	-	-	0.1	-	2	0.0001	0.0001	1.31

Standard error from the instrument or calculated through sample standard deviation

Table 9.7 SP-HTC-ACT-800-1 TGA repeats

Sample	Moisture	Volatiles	Fixed Carbon	Ash
	%	%	%	%
SP-HTC-ACT-800-1 R1	4.78	9.91	64.42	20.89
SP-HTC-ACT-800-1 R2	4.90	7.23	70.77	17.10
SP-HTC-ACT-800-1 R3	4.72	8.65	67.85	18.78
SP-HTC-ACT-800-1 R4	7.07	7.35	72.24	13.34
SP-HTC-ACT-800-1 R5	4.89	8.65	68.34	18.12
SP-HTC-ACT-800-1 R6	5.27	8.38	69.43	16.92
Standard Error (±)	0.37	0.40	1.10	1.02

Standard error calculated through sample standard deviation

Table 9.8 SP-HTC-ACT-800-1 ultimate analysis repeats

Sample	Carbon	Hydrogen	Nitrogen	Oxygen	Ash	H/C	O/C
	Wt.%	Wt.%	Wt.%	Wt.% BD	Wt.%	Atomic Ratio	Atomic Ratio
SP-HTC-ACT-800-1	69.77	0	1.27	14.53	14.42	0	0.16
SP-HTC-ACT-800-1 R1	57.44	0.84	1.11	18.66	21.94	0.18	0.24
SP-HTC-ACT-800-1 R2	76.82	0.71	1.45	1.30	19.71	0.11	0.01
SP-HTC-ACT-800-1 R3	79.59	1.02	1.56	3.48	14.35	0.15	0.03
SP-HTC-ACT-800-1 R4	74.09	1.01	1.18	4.67	19.05	0.16	0.05

SP-HTC-ACT-800-1 R5	66.49	1.13	1.19	9.25	21.94	0.20	0.10
SP-HTC-ACT-800-1 R6	78.98	0.81	1.29	0.93	17.98	0.12	0.01
Standard Error (±)	3.01	0.14	0.06	2.59	1.19	0.13	0.09

Ash content from proximate analysis, moisture content from proximate analysis used for dry hydrogen weight, oxygen calculated by difference (BD). Standard error calculated through sample standard deviation

Table 9.9 SP-HTC-ACT-800-1 adsorption repeats

Sample	BET Surface Area	Microporous Volume	Mesoporous Volume	Total Volume	Average Pore Diameter	Microporosity	Mesoporosity
	m^2/g	cm^3/g	cm^3/g	cm^3/g	nm	%	%
SP-HTC-ACT-800-1	964	0.325	0.299	0.631	2.62	52	47
SP-HTC-ACT-800-1 R1	1071	0.330	0.530	0.873	3.26	38	61
SP-HTC-ACT-800-1 R2	1011	0.322	0.429	0.764	3.02	42	56
SP-HTC-ACT-800-1 R3	913	0.288	0.254	0.548	2.40	53	46
SP-HTC-ACT-800-1 R4	965	0.301	0.300	0.607	2.52	49	49
SP-HTC-ACT-800-1 R5	1106	0.349	0.500	0.860	3.11	41	58
SP-HTC-ACT-800-1 R6	1026	0.307	0.416	0.731	2.85	42	57
Standard Error (±)	23	0.007	0.037	0.044	0.113	2.06	2.00

Standard error calculated through sample standard deviation

Table 9.10 HTF CG pyrolysis experiments: conditions and results

Sample	Temp.	Time	N_2 Flowrate	Ramp Rate	Mass In	Mass Out	Yield	Carbon Yield
	°C	h	l/min	°C/min	g	g	%	%
CG-HTC-PYR-700-0.5	700	0.5	1	10	5.0128	1.8323	36.55	-
CG-HTC-PYR-750-0.5	750	0.5	1	10	5.0098	1.7587	35.11	-
CG-HTC-PYR-800-0.5	800	0.5	1	10	5.0545	1.8209	36.03	-
CG-HTC-PYR-850-0.5	850	0.5	1	10	5.0248	1.7742	35.31	-
CG-HTC-PYR-900-0.5	900	0.5	1	10	5.0122	1.7471	34.86	118.99
CG-HTC-PYR-950-0.5	950	0.5	1	10	5.0415	1.7630	34.97	-
CG-HTC-PYR-700-1	700	1	1	10	5.0338	1.7933	35.63	-
CG-HTC-PYR-750-1	750	1	1	10	5.0331	1.7665	35.10	119.35
CG-HTC-PYR-800-1	800	1	1	10	5.0011	1.8293	36.58	123.22
CG-HTC-PYR-850-1	850	1	1	10	5.0113	1.7439	34.80	115.96
CG-HTC-PYR-900-1	900	1	1	10	5.0098	1.7580	35.10	-
CG-HTC-PYR-700-2	700	2	1	10	4.997	1.7623	35.27	-
CG-HTC-PYR-750-2	750	2	1	10	5.0682	1.7662	34.85	-
CG-HTC-PYR-800-2	800	2	1	10	5.0338	1.7495	34.76	117.67

Standard Error (±)	-	-	0.1	-	0.0001	0.0001	1.70	5.67

Standard error from the instrument or calculated through sample standard deviation of repeat CG-HTC-ACT-850-0.5 R200 *activation samples*

Table 9.11 HTF CG activation experiments: conditions and results

Sample	Temp.	Time	N_2 Flowrate	Ramp Rate	Activating Agent	Mass In	Mass Out	Yield	Carbon Yield
	°C	h	l/min	°C/min	ml	g	g	%	%
CG-HTC-ACT-700-0.5	700	0.5	1	10	50	5.0312	1.734	34.46	115.11
CG-HTC-ACT-750-0.5	750	0.5	1	10	50	5.0241	1.6622	33.08	111.56
CG-HTC-ACT-800-0.5	800	0.5	1	10	46	5.0217	1.4556	28.99	99.57
CG-HTC-ACT-850-0.5	850	0.5	1	10	53	5.0968	1.1547	17.47	57.10
CG-HTC-ACT-900-0.5	900	0.5	1	10	50	5.0065	0.6809	13.60	45.51
CG-HTC-ACT-950-0.5	950	0.5	1	10	48	5.0309	0.2793	5.55	18.40
CG-HTC-ACT-700-1	700	1	1	10	100	5.0135	1.6662	33.23	109.22
CG-HTC-ACT-750-1	750	1	1	10	103	5.0173	1.5747	31.39	106.23
CG-HTC-ACT-800-1	800	1	1	10	102	5.0594	1.2765	25.23	82.90
CG-HTC-ACT-850-1	850	1	1	10	100	5.0189	0.8466	16.87	56.58
CG-HTC-ACT-700-2	700	2	1	10	205	5.0389	1.5765	31.29	102.78
CG-HTC-ACT-750-2	750	2	1	10	208	5.0303	1.2845	25.54	84.42

CG-HTC-ACT-800-2	800	2	1	10	206	5.0446	0.8688	17.22	56.42
CG-HTC-ACT-700-4	700	4	1	10	398	5.0073	1.5584	31.12	104.30
Standard Error (±)	-	-	0.1	-	-	0.0001	0.0001	1.70	5.67

Standard error from the instrument or calculated through sample standard deviation of repeat CG-HTC-ACT-850-0.5 R200 *activation samples*

Table 9.12 HTF CG raw activation experiments: conditions and results

Sample	**Temp.**	**Time**	**N_2 Flowrate**	**Ramp Rate**	**Activating Agent**	**Mass In**	**Mass Out**	**Yield**	**Carbon Yield**
	°C	h	l/min	°C/min	ml	g	g	%	%
CG-RAW-ACT-700-0.5	700	0.5	0.5	10	38	8.784	1.66	18.90	48.91
CG-RAW-ACT-750-0.5	750	0.5	0.5	10	40	8.9032	0.2427	2.73	70.55
CG-RAW-ACT-800-0.5	800	0.5	0.5	10	46	10.4118	1.3330	12.80	33.13
CG-RAW-ACT-850-0.5	850	0.5	0.5	10	52	11.9308	1.3320	11.16	28.89
CG-RAW-ACT-900-0.5	900	0.5	0.5	10	55	10.3894	0.1409	1.36	-
CG-RAW-ACT-700-1	700	1	0.5	10	71	11.5461	1.4010	12.13	31.40
CG-RAW-ACT-750-1	750	1	0.5	10	78	9.0689	0.1020	1.12	2.91
CG-RAW-ACT-800-1	800	1	0.5	10	84	10.6738	0.0415	0.39	-
CG-RAW-ACT-850-1	850	1	0.5	10	76	11.0316	0.0847	0.77	-
Standard Error (±)	-	-	0.1	-	-	0.0001	0.0001	1.70	5.67

Standard error from the instrument or calculated through sample standard deviation of repeat CG-HTC-ACT-850-0.5 *R200 activation samples*

Table 9.13 HTF CG-HTC-ACT-850-0.5 R200 repeat experiments: conditions and results

Sample	Temp.	Time	N_2 Flowrate	Ramp Rate	Activating Agent	Mass In	Mass Out	Yield	Carbon Yield
	°C	h	l/min	°C/min	ml	g	g	%	%
CG-HTC-ACT-850-0.5	850	0.5	1	10	52	5.0804	1.2044	23.71	79.37
CG-HTC-ACT-850-0.5 RX1	850	0.5	1	10	37	5.0298	1.1050	21.97	73.20
CG-HTC-ACT-850-0.5-RX2	850	0.5	1	10	58	5.0987	1.1000	21.57	69.71
CG-HTC-ACT-850-0.5-RX3	850	0.5	1	10	53	5.0968	0.7577	14.87	47.65
CG-HTC-ACT-850-0.5-RX4	850	0.5	1	10	51	4.9716	0.8955	18.01	58.88
CG-HTC-ACT-850-0.5-RX5	850	0.5	1	10	52	5.0674	0.5268	10.40	33.93
CG-HTC-ACT-850-0.5-RX6	850	0.5	1	10	54	5.1026	0.5995	11.75	36.92
Standard Error (±)	-	-	0.1	-	-	0.0001	0.0001	1.70	5.67

Standard error calculated through sample standard deviation

Table 9.14 CG-HTC-ACT-850-0.5 R200 TGA repeats

Sample	Moisture	Volatiles	Fixed Carbon	Ash
	%	%	%	%
CG-HTC-ACT-850-0.5 R1	13.50	5.78	77.72	3.00
CG-HTC-ACT-850-0.5 R2	14.55	6.04	76.16	3.26
CG-HTC-ACT-850-0.5 R3	11.79	5.29	80.17	2.75

CG-HTC-ACT-850-0.5 R4	10.68	7.53	78.41	3.38
CG-HTC-ACT-850-0.5 R5	11.62	7.27	77.23	3.88
Standard Error (±)	0.70	0.43	0.67	0.19

Standard error calculated through sample standard deviation

Table 9.15 CG-HTC-ACT-850-0.5 R200 ultimate analysis repeats

Sample	**Carbon**	**Hydrogen**	**Nitrogen**	**Oxygen**	**Ash**	**H/C**	**O/C**
	Wt.%	Wt.%	Wt.%	Wt.% BD	Wt.%	Atomic Ratio	Atomic Ratio
CG-HTC-ACT-850-0.5 R1	94.3	0.0	2.2	0.0	3.4	0.00	0.00
CG-HTC-ACT-850-0.5 R2	80.5	0.0	1.6	14.3	3.4	0.00	0.18
CG-HTC-ACT-850-0.5 R3	93.4	0.03	1.9	1.5	3.1	0.00	0.02
CG-HTC-ACT-850-0.5 R4	88.8	0.81	2.0	7.1	1.3	0.01	0.08
CG-HTC-ACT-850-0.5 R5	93.6	0.0	2.0	0.0	4.4	0.00	0.00
CG-HTC-ACT-850-0.5 R6	94.0	0.0	2.2	0.0	3.8	0.00	0.00
Standard Error (±)	2.02	0.12	0.07	2.18	0.40	0.01	0.03

Ash content from proximate analysis, moisture content from proximate analysis used for dry hydrogen weight, oxygen calculated by difference (BD). Standard error calculated through sample standard deviation

Table 9.16 CG-HTC-ACT-850-0.5 R200 adsorption repeats

Sample	BET Surface Area	Microporous Volume	Mesoporous Volume	Total Volume	Average Pore Diameter	Microporosity	Mesoporosity
	m^2/g	cm^3/g	cm^3/g	cm^3/g	nm	%	%
CG-HTC-ACT-850-0.5 R1	1208	0.423	0.150	0.577	1.91	73	26
CG-HTC-ACT-850-0.5 R2	1174	0.402	0.143	0.549	1.87	73	26
CG-HTC-ACT-850-0.5 R3	924	0.314	0.073	0.390	1.69	80	19
CG-HTC-ACT-850-0.5 R4	1175	0.412	0.137	0.552	1.88	75	25
CG-HTC-ACT-850-0.5 R5	1281	0.440	0.168	0.612	1.91	72	28
Standard Error (±)	54	0.020	0.014	0.034	0.03	1.36	1.37

Standard error calculated through sample standard deviation

Table 9.17 HTF SS pyrolysis experiments: conditions and results

Sample	Temp.	Time	N_2 Flowrate	Ramp Rate	Activating Agent	Mass In	Mass Out	Yield
	°C	h	l/min	°C/min	ml	g	g	%
SS-HTC-PYR-700-0.5	700	0.5	1	10	-	5.0418	1.4261	28.29
SS-HTC-PYR-750-0.5	750	0.5	1	10	-	5.0235	1.34529	26.78
SS-HTC-PYR-800-0.5	800	0.5	1	10	-	5.0127	1.3239	26.41
SS-HTC-PYR-850-0.5	850	0.5	1	10	-	5.1003	1.3012	25.51
SS-HTC-PYR-900-0.5	900	0.5	1	10	-	5.031	1.3421	26.68

SS-HTC-PYR-950-0.5	950	0.5	1	10	-	4.9947	1.2449	24.92
SS-HTC-PYR-700-1	700	1	1	10	-	5.0141	1.4398	28.72
SS-HTC-PYR-750-1	750	1	1	10	-	5.0038	1.3315	26.61
SS-HTC-PYR-800-1	800	1	1	10	-	5.0333	1.3258	26.34
SS-HTC-PYR-850-1	850	1	1	10	-	5.051	1.3335	26.40
SS-HTC-PYR-900-1	900	1	1	10	-	4.9951	1.2497	25.02
SS-HTC-PYR-950-1	950	1	1	10	-	5.021	1.2129	24.16
SS-HTC-PYR-700-2	700	2	1	10	-	5.056	1.3507	26.71
SS-HTC-PYR-750-2	750	2	1	10	-	5.0042	1.2988	25.95
SS-HTC-PYR-800-2	800	2	1	10	-	5.0565	1.3198	26.10
SS-HTC-PYR-850-2	850	2	1	10	-	4.9309	1.2618	25.59
Standard Error (±)	-	-	0.1	-	-	0.0001	0.0001	1.31

Standard error from the instrument or calculated through sample standard deviation of repeat SP-HTC-ACT-800-1 activation samples

Table 9.18 HTF SS activation experiments: conditions and results

Sample	Temp.	Time	N_2 Flowrate	Ramp Rate	Activating Agent	Mass In	Mass Out	Yield
	°C	h	l/min	°C/min	ml	g	g	%
SS-HTC-ACT-700-0.5	700	0.5	1	10	44	5.0551	1.2911	25.54

SS-HTC-ACT-750-0.5	750	0.5	1	10	46	5.0162	1.1395	22.72
SS-HTC-ACT-800-0.5	800	0.5	1	10	48	5.0368	1.0194	20.24
SS-HTC-ACT-850-0.5	850	0.5	1	10	46	5.0326	0.8438	16.77
SS-HTC-ACT-900-0.5	900	0.5	1	10	47	5.0777	0.7569	14.91
SS-HTC-ACT-950-0.5	950	0.5	1	10	45	5.0873	0.7729	15.19
SS-HTC-ACT-700-1	700	1	1	10	92	5.085	1.1951	23.50
SS-HTC-ACT-750-1	750	1	1	10	95	5.0484	1.058	20.96
SS-HTC-ACT-800-1	800	1	1	10	85	5.0395	0.9187	18.23
SS-HTC-ACT-850-1	850	1	1	10	95	5.0425	0.7528	14.93
SS-HTC-ACT-900-1	900	1	1	10	95	5.0243	0.7575	15.08
SS-HTC-ACT-700-2	700	2	1	10	187	4.9622	1.0429	21.02
SS-HTC-ACT-750-2	750	2	1	10	187	5.0073	0.8993	17.96
SS-HTC-ACT-800-2	800	2	1	10	183	5.065	0.7986	15.77
SS-HTC-ACT-850-2	850	2	1	10	186	5.0241	0.7658	15.24
SS-HTC-ACT-700-4	700	4	1	10	389	5.0273	0.9909	19.71
Standard Error (±)	-	-	0.1	-	-	0.0001	0.0001	1.31

Standard error from the instrument or calculated through sample standard deviation of repeat SP-HTC-ACT-800-1 activation samples

Table 9.19 Digested SP Ash Composition

Element	Concentration	Intensity	Concentration	Concentration	Intensity	Intensity	Average Concentration Replicate	Average Intensity Replicate
	ppm		SD	% RSD	SD	% RSD		
Ca 210.324	55.08	27603	0.06	0.11	28	0.1	55.0	27603
Ca 318.127	55.19	319554	0.14	0.25	767	0.2	55.2	319554
Cd 214.439	Uncal	15	-	-	10	66.0	Uncal	15
Co 238.892	-0.01	8	0	7.75	4	49.3	0.0	8
Cr 267.716	0.05	2677	0	0.68	17	0.6	0.1	2677
Cu 324.754	0.13	6818	0	0.2	12	0.2	0.1	6818
Fe 238.204	7.43	223746	0	0.06	134	0.1	7.4	223746
Fe 370.792	7.33	331	0.43	5.87	18	5.5	7.3	331
K 404.721	14.78	253	0.1	0.66	2	0.8	14.8	253
K 766.491	12.99	700762	0.04	0.33	2326	0.3	13.0	700762
K 769.897	9.32	519172	0.03	0.35	1707	0.3	9.3	519172
Mg 202.582	3.42	2267	0.03	0.75	17	0.8	3.4	2267
Mg 278.142	3.81	1910	0.04	1.01	19	1.0	3.8	1910
Mn 257.610	Uncal	82056	-	-	244	0.3	Uncal	82056

Na 330.237	2.41	105	0.04	1.82	3	2.9	2.4	105
Na 568.821	2.36	1089	0.26	10.93	142	13.0	2.4	1089
Na 589.592	0.95	164638	0.02	2.22	3634	2.2	1.0	164638
Na 615.423	Uncal	158	-	-	28	17.5	Uncal	158
Ni 231.604	0.01	89	0	21.09	8	8.5	0.0	89
P 213.618	9.23	14054	0.07	0.72	101	0.7	9.2	14054
P 215.407	9.27	892	0.16	1.73	15	1.7	9.3	892
Pb 220.353	0.02	82	0	2.53	1	1.3	0.0	82
Zn 213.857	3.47	126150	0	0.09	113	0.1	3.5	126151

Table 9.20 Application Tests Raw Results

Sample	**SP-HTC**	**SP-HTC-ACT-850-0.5**	**SP-HTC-ACT-800-1**	**SP-HTC-ACT-750-2**	**CG-HTC**	**CG-HTC-ACT-850-0.5**	**CG-HTC-ACT-800-2**	**GAC**	**Initial**
470 (AU)	1.09	0.01	0.02	1.59	1.08	0.81	0.10	0.40	2.10
TOC (mg/L C)	8683	4374	4149	5832	8296	3958	3242	4125	8540

Table 9.21 X-Ray Photoelectron Spectroscopy of Coffee Grounds Atomic Compositions

Sample	C	O	N	P	Mg
	%	%	%	%	%
CG-RAW	87.18	12.83	-	-	-
CG-HTC	82.79	15.40	1.81	-	-
CG-HTC-PYR-850-1	92.27	6.40	1.34	-	-
CG-HTC-ACT-850-0.5 R200	95.59	3.05	1.38	-	-
CG-HTC-ACT-850-1	97.29	1.62	1.09	-	-
CG-RAW-ACT-850-0.5	95.09	3.98	0.37	0.24	0.32

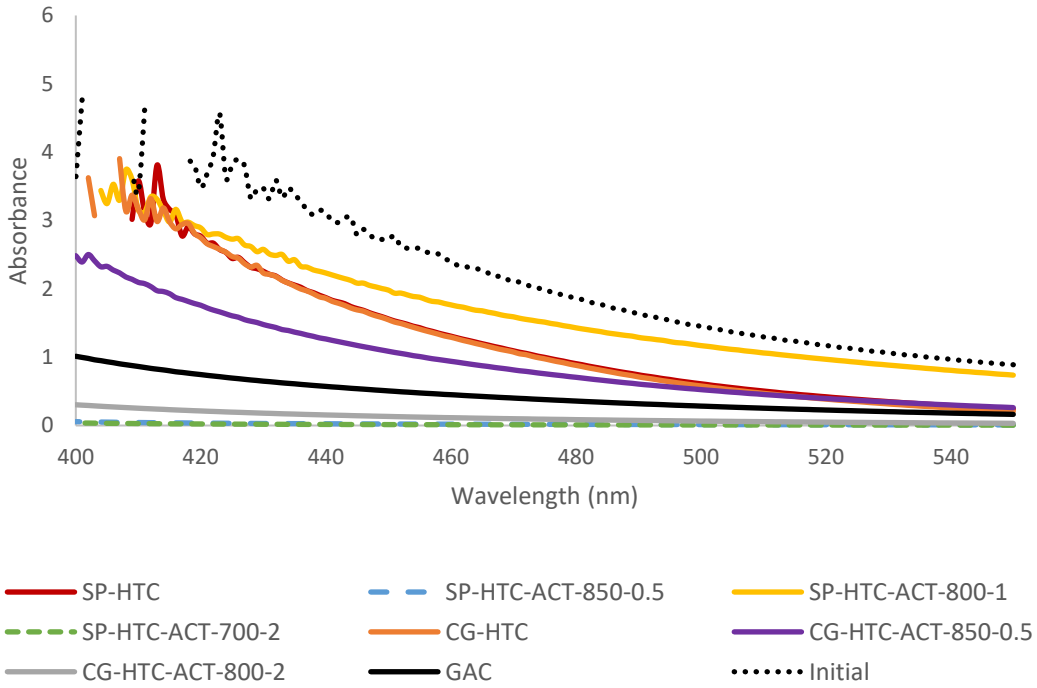

Figure 9.1 Absorbance spectrum for application test

Table 9.22 Whole process yield CG-HTC-ACT-850-1

CG Activation @ 850-1	Yield	Carbon	Ash	Total
CG-Raw	100.00	59.33	1.55	
Mass (g)		59.33	1.55	100.00
CG-HTC	55.67	70.56	0.23	
Mass (g)		39.28	0.13	55.67
CG-HTC-PYR-850-1	28.99	94.40	0.61	
Mass (g)		15.23	0.10	16.14

CG-HTC-ACT-850-1	48.55	95.86	1.41	
Mass (g)		7.51	0.11	7.83

Table 9.23 Whole process yield SP-HTC-ACT-750-2

SP Activation @ 750-2	**Yield**	**Carbon**	**Ash**	**Total**
SP-Raw	100.00	56.67	2.83	
Mass (g)		56.67	2.83	100.00
SP-HTC	55.67	61.26	2.54	
Mass (g)		34.10	1.41	55.67
SP-HTC-PYR-750-2	17.24	89.85	6.48	
Mass (g)		17.24	1.12	17.24
SP-HTC-ACT-750-2	10.24	85.35	9.06	
Mass (g)		8.74	0.93	10.24